Flexible Universal Branch Model for Steady State Operational Analysis and Optimisation of Hybrid AC/DC Grids

ALVAREZ-BUSTOS, ABRAHAM

Flexible Universal Branch Model for Steady State Operational Analysis and Optimisation of Hybrid AC/DC Grids

Abraham Alvarez-Bustos

A Thesis presented for the degree of
Doctor of Philosophy

Department of Engineering
Durham Energy Institute
University of Durham
England

December 2020

Dedicated to

God

Who gave me life, health, intelligence and strength to always pursue my dreams

My Parents

Abraham Alvarez Batres and Margarita Bustos Plascencia

With a lot of love, affection and respect, because they gave me even the impossible in the hardest times, so that I could achieve my dreams without having any limitations or worries

My Supervisors

Dr Behzad Kazemtabrizi and Dr Mahmoud Shahbazi

Who guide me, support me and were always with me from the beginning to the end of this work

And my Siblings, Family and Friends

Who encouraged me day by day in this journey

Diego Alvarez Bustos and Raquel Alvarez Bustos

Carlos Jesus Ferrandón Cervantes and Max Joshua Rodríguez Clavel

Michaela Buerdsell

Abstract

This thesis presents a new Flexible Universal Branch Model (FUBM) formulation for solving Power Flows, Optimal Power Flow (OPF) and Security Constrained Optimal Power Flow (SCOPF) for hybrid AC/DC grids. The prowess of the new formulation is that it (i) provides a direct link between AC and DC parts of the grid allowing for solving the entire network within a unified frame of reference (not sequentially) and (ii) can realistically model any element within the AC/DC power grid, ranging from conventional AC transmission lines to multiple types of AC/DC interface devices such as Voltage Source Converter (VSC) by introducing additional control variables. The model is formulated in such a way that it does not make a distinction, from a mathematical perspective, between AC and DC elements. Therefore, traditional AC power balance equations can be used to solve a complete AC/DC grid. Moreover, the physical attributes and optional independent variables of the FUBM encapsulate the characteristics and controls of other complex elements in the electrical power grid allowing a flexible analysis of a fully controllable AC/DC grid allowing the formulation to achieve operating points which will be infeasible otherwise. Detailed description of the FUBM is presented and compared to the traditional approaches. In comparison, traditional approaches require several model libraries and specific power balance equations per element as well as the type of grid to achieve the same results as the ones presented with the FUBM. Power flow formulation using FUBM also allows for the introduction of extra levels of control that may be available in a hybrid AC/DC grid. Similarly, the flexible OPF formulation takes advantage of the FUBM multiple control options to properly simulate flexibility of operation in these grids. Finally, the FUBM is implemented for the SCOPF to allow for corrective actions following contingencies for even more flexibility of operation. Post-contingency corrective actions include fast controls available to the VSCs that are used to adjust the system operating point to withstand even the most severe contingencies. Throughout the thesis, the model was tested against several test systems and solvers. The results clearly show that the FUBM is not only on a par with existing models for steady state analysis but surpasses them in solution accuracy, computational efficiency and scalability for larger system sizes.

Declaration

The work in this thesis is based on research carried out at the Power Systems Research Group, the Department of Engineering, Durham University, England. No part of this thesis has been submitted elsewhere for any other degree or qualification and it is all my own work unless referenced to the contrary in the text.

Acknowledgements

At the end of such a hard and difficult work, it is immediately clear that, for me to achieve it, would have been impossible without the participation of people and institutions that have supported and encouraged me. Therefore, it is my pleasure to use this space to express my thanks.

To God, for having accompanied and guided me throughout my career, for being my strength in moments of weakness and for giving me a life full of learning, experiences and especially full of happiness next to my loved ones.

To my family, that without their support, collaboration and inspiration it would have been impossible to carry out this hard work; mainly to my parents, Margarita and Abraham, for all the values and affection they have given me. My family this thesis is for them and to them.

I thank in a special and sincere way to Dr Behzad Kazemtabrizi and Dr Mahmoud Shahbazi for their support and confidence in my work and their ability to guide it with knowledge.

For those who have shared their friendship with me. Specially my good friends Carlos Ferrandón, Max Joshua, and Erick Alonso, with whom even the slightest conversation leaves you something helpful. I have always received their words of encouragement, in good and bad we will always be together.

Finally, I must thank to Durham University and the Department of Engineering for providing me with a place of study and teaching in addition to invaluable knowledge.

This work was done in part thanks to the financial support of Durham University UK in collaboration with Consejo Nacional de Ciencia y Tecnología (CONACyT) and Secretaría de Energía (SENER), Mexico.

Contents

List of Figures

List of Tables

Nomenclature

α	VSC Loss Coefficient
β	VSC Loss Coefficient
ϵ	Convergence Tolerance
γ	VSC Loss Coefficient
λ	Lagrangian multiplier equality constraints
$\mathcal{I}$	Indices
$\mathcal{L}$	Lagrangian Function
μ	Lagrangian multiplier inequality constraints
θ_{sh}	Shift Angle
b_c	Shunt Susceptance
B_{eq}	Variable Susceptance
f	Objective Function
$g(x)$	Equality Constraints
$g_{G_{sw}}$	VSC Power Loss Correction
g_{P_b}	Active Power Balance Equations
g_{P_f}	Active Power "From" Control Constraints
$g_{P_{dp}}$	Droop Control Constraints

g_{Q_b}	Reactive Power Balance Equations
g_{Q_t}	Reactive Power "To" Control Constraints
g_{Q_z}	Reactive Power Zero Constraints
g_{S_b}	Complex Balance Equations
G_{sw}	Converter Switching losses
g_{V_f}	DC Voltage "From" Control Constraints
g_{V_t}	AC Voltage "To" Control Constraints
H	Hessian Matrix
$h(x)$	Inequality Constraints
$h_{S_f^2}$	Loadability Constraint
i_f	Current "From"
i_t	Current "To"
$I_{b_{inj}}$	Current Bus Injections
I_{br}	Branch Current
I_{dc}	VSC Current DC side
i_{sw}	VSC Switching current
J	Jacobian Matrix
k_2	Converter Constant
k_{dp}	Voltage Droop Control Slope
L_l	Operational Limits Long Term
L_m	Operational Limits Medium Term
L_s	Operational Limits Short Term

$L_{S_L^2}$	Squared Power Transmission Limits
m_a	Tap Changer/modulation amplitude
N	Complex Tap Changer
N_k	Maximum number of corrective actions
P_f	Active Power "From"
P_t	Active Power "To"
P_{ci}	VSC Active power at the Compensator node
P_{dc}	VSC Active Power DC side
P_{loss}	VSC Switching losses
Q_f	Reactive Power "From"
Q_t	Reactive Power "To"
Q_{ci}	VSC Reactive Power Compensator
r_s	Series Resistance
S_d	Apparent Power Demand
S_f	Apparent Power "From"
S_g	Generation Injections
s_k	Status of the Corrective Action
S_t	Apparent Power "To"
$S_{b_{inj}}$	Apparent Power Bus Injections
S_{br}	Branch Apparent Power
T_k	Interval of time available for corrective actions
u	Control Variables

V	Nodal Complex Voltage
V_a	Nodal Voltage Angle
v_f	Voltage "From"
V_m	Nodal Voltage Magnitude
v_t	Voltage "To"
v_{ac}	Voltage AC side
V_{br}	Branch Voltage
v_{dc}	Voltage DC side
x	Optimisation Variables
x_s	Series Reactance
y_s	Series Admittance
Y_{br}	Branch Admittance Matrix
Y_{bus}	Bus Admittance Matrix
Y_{ff}	Branch Admittance "From" - "From" Vector
Y_{ft}	Branch Admittance "From" - "To" Vector
Y_{tf}	Branch Admittance "To" - "From" Vector
Y_{tt}	Branch Admittance "To" - "To" Vector
z_k	Slack Variables

List of Acronyms

AC	Alternate Current
CF	Contingency Filter
CTPST	Controlled Tap Phase Shifter Transformer
CTT	Controlled Tap-Changing Transformers
DC	Direct Current
ED	Economic Dispatch
ENTSO-E	European Network of Transmission System Operators for Electricity
EPS	Electrical Power System
FACTS	Flexible AC Transmission System
FPFA	Flexible Power Flow Algorithm
FPFA	Flexible AC/DC Power Flow Algorithm
FSCOPF	Flexible Security constrained Optimal Power Flow
FUBM	Flexible Universal Branch Model
HVDC	High Voltage Direct Current
KVL	kirchhoff's Current Law
KVL	kirchhoff's Voltage Law
LP	Linear Programming

MTDC Multi-Terminal DC

NDC Non-Dominated Contingency

NERC North American Electric Reliability Corporation

NLP Non Linear Programming

NREL National Renewable Energy Laboratory

OPF Optimal Power Flow

PI Performance Index

PR Power Router

PST Phase Shifter Transformer

RC Research Challenge

RES Renewable Energy Source

RPI Reliability Performance Index

RTS-GMLC Reliability Test System of the Grid Modernization Laboratory Consortium

SCOPF Security Constrained Optimal Power Flow

SI Severity Index

SSSA Steady-State Classical Power Flow Security Analysis

STATCOM Static Compensator

TSA Transmission System Analyst

TSO Transmission System Operator

TYNDP Ten-Year Network Development Plan

UC Unit Commitment

UNFCCC United Nations Framework Convention on Climate Change

UPFC Unified Power Flow Controller

VSC Voltage Source Converter

Chapter 1

Introduction

1.1 Problem Statement

Throughout the last fifteen years, Power Systems have been undergoing significant and unprecedented transformations which have brought about new challenges for their secure and efficient operation [1]. In 2015, parties to the United Nations Framework Convention on Climate Change (UNFCCC) reached a landmark agreement to combat climate change [2, 3, 4]. However, the electrical network in its current state is not prepared to deal with a fully decarbonised and sustainable electricity system by 2050. Therefore, the Ten-Year Network Development Plan (TYNDP) 2020, by the European Network of Transmission System Operators for Electricity (ENTSO-E), includes approximately 80% of grid development projects related to the integration of Renewable Energy Sources (RESs) as well as the modernisation of the transmission network [5]. Similarly in the UK, the Future Energy Scenarios report by National Grid includes the integration of at least 40GW of renewable generation to the grid as well as a huge emphasis on improving the flexibility of the power grid at all voltage levels [6]. With these projects, ENTSO-E aims to alleviate the existing problem of power flow congestion and improve the levels of operational security, as well as maximising the operational flexibility and reliability of the Pan-European Transmission Grid. [7, 8, 9].

The modernisation projects aim to create a completely controllable hybrid AC/DC power grid where Transmission System Operators (TSOs) can adjust the settings

of one or multiple control devices to redirect the power flow through less congested transmission lines, whilst maintaining the transmission voltage within secure operational limits. This is achieved by overlaying a multi-terminal Voltage Source Converter (VSC)-based HVDC network on top of an existing AC Electrical Power System (EPS) in coordination with multiple control elements, for example, PSTs, and CTTs within the meshed AC grid itself [5, 9, 10]. Such hybrid networks are inherently more flexible largely due to the additional control features of the VSCs [10, 11, 12].

Notwithstanding the operational benefits of hybrid AC/DC grids, these networks are more complex and therefore there is a need for proper operational planning procedures in place to ensure a continuous, safe and reliable operation of the network at all times and under all operating conditions [13, 14]. It goes without saying that any power system operational planning framework should be contingent on not only obtaining the secure operating states but also the operating states that are most economical [15]. Consequently, TSOs carry out numerous steady state studies such as Unit Commitment (UC), Economic Dispatch (ED), Optimal Power Flow OPF and the Security Constrained Optimal Power Flow (SCOPF) analysis as part of the operational planning of the network [16, 17, 18, 19, 20]. The Power System operational planning time-line, seen in Fig. 1.1, illustrates the planning time-scale for which each planning study is typically relevant.

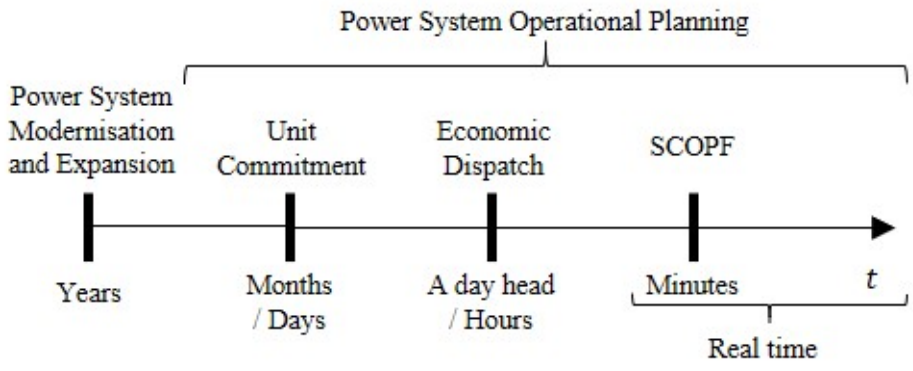

Figure 1.1: Power System Planning Time-line

Since the majority of the consumed energy is generated in real time, and the

energy consumption changes throughout the day, UC must be planned in advance to ensure that enough generation is always available to satisfy the demands of the system. To "Commit a generating unit" is to start, synchronise, and connect a generator to the system in order to successfully deliver the power. The UC problem is an optimisation problem that essentially aims to minimise generation costs, while satisfying the system generation constraints (e.g. minimum up- and downtime, unit capability limits, generation, and reserve constraints), by finding the best realistic combination of generation units to satisfy a demand estimate for a certain period of time. On the other hand, ED problem uses the already selected generation units specified by the solution of the UC problem. The aim of ED is to minimise the generation operating cost of the whole system by determining the power output of each generating unit under the constrained condition of the system load demands. In other words, ED, finds the lowest-cost generation dispatch for a set of generators that equals the total load plus losses. However, it ignores the effect that the selected generation dispatch has on the transmission lines thermal limits or the effect of delivered reactive power to the grid. The OPF as the name implies, couples the ED calculation with a power flow calculation so that the ED and the power flow are solved simultaneously [15, 21]. Mathematically, in the OPF problem a chosen objective function (normally the total generation cost) is solved towards its optimum operating point subject to realistic techno-economic and security constraints of the power system [14, 15, 22]. More generally, the OPF problem is basically a constrained, non-linear, non-convex, optimisation problem which for an actual EPS can contain a large number of non-linear constraints representing the physical limitations of the actual system as well as the economic boundaries within which the system needs to operate [14]. TSOs have relied on an evolution of the OPF tool, the SCOPF, for the adequate planning and operational planning of the power grid since 1987 [23]. In contrast to OPF, it takes into account system operational constraints under a set of postulated contingencies (i.e. disturbance events which could lead to a deviation of the nominal steady-state operating point in the system), and thus it is an effective way to determine the best operating conditions when subjected to credible operations restrictions, such as thermal or stability limits. As a conse-

quence, the SCOPF, when compared to the base-case OPF, is a considerably more complicated optimisation problem, since each contingency requires the same number of constraints and variables as one OPF scenario, thus the problem is expanded drastically since each element in the EPS can be a possible critical contingency. Moreover, the complexity and the growth of the number of constraints and contingencies is only increasing in the context of a hybrid AC/DC EPS such as the Pan-European Transmission Grid.

From an analysis perspective, Power Flow, OPF and the SCOPF should be computationally tractable and at the same time scalable (i.e. provide solutions to larger systems without significantly sacrificing computational time). In practice, the existing analysis tools that are able to solve them are mostly limited to solving AC systems with minimal capabilities to accommodate realistic network element representation and/or model libraries required for fast and accurate solutions of hybrid AC/DC networks [24, 25, 26, 27, 28]. Moreover, many of these tools simplify the problem by using approximations of the actual system, and in real power systems operational planning any solution for a hybrid network should be able to properly reflect the intricacies of the converters' interactions and capture enough detail to be a realistic representation of the actual system. Existing solution methods for hybrid AC/DC grids normally employ a sequential method for solving the AC and DC parts of the network in sequence [29, 30, 31]. As a result, the equations per model and grid vary accordingly. Meanwhile, there are two open source non linear AC/DC OPF formulations presented in [32] and [33] to solve the AC and DC grids simultaneously. The first one is an extension of the 'PowerModels.jl' package, and the second one is a Python-based framework. However, both approaches still have to model each electrical element individually. Thus, regardless of the approach taken, an extensive model library to selectively be able to incorporate various EPS elements and accommodate different network types (AC or DC) is normally needed. Furthermore, the power and voltage control of these tools are limited to the VSC variables without considering other control elements in the grid. Such limitations make it even harder to build flexibility and adaptability into the typical commercial power systems analysis tools that Transmission System Analysts (TSAs) use on a

daily basis.

Thus far, the closest approach to a compact model has been done by linking the traditional π branch model in series with an ideal transformer such as the one presented in [24]. This is very effective for the analysis of AC-only grids, however for hybrid AC/DC grids, the model is rather limited. This thesis therefore presents a new Flexible Universal Branch Model (FUBM) for the Steady State Operational Analysis and Optimisation of Hybrid AC/DC grids. The proposed model is capable of seamlessly modeling an array of network elements ranging from conventional AC and DC branches, CTT, PST, Static Compensators (STATCOMs) and VSCs. Meanwhile, additional combined elements (e.g. Universal Power Flow Controller [UPFC]) can also be modelled using these fundamental network elements. Additionally, distinction between the AC and DC grid is not required thanks to the flexibility and high versatility of the model. Therefore, conventional AC Power Flow, OPF and SCOPF equations are used to solve hybrid AC/DC grids. In other words, using the FUBM the entire network can be solved on one single frame of reference thereby eliminating the need for solving the DC and AC parts of the network in sequence. One of the main advantages of the FUBM formulation is that it is highly adaptable to any network topology with any degree of complexity and hosting a variety of control elements. To this end, the model may accommodate any control variables associated with any control elements that are active over the course of the solution by extending the vector of state variables accordingly. Similarly, the vector of constraints may be extended to accommodate any specific controls on power (e.g. scheduled power output of converters in a multi-terminal VSC-HVDC link) or on voltage (e.g. voltage control set points for an STATCOM) if deemed appropriate. As a result, the operation of a flexible and fully controllable AC/DC grid can be simulated without adding extra burden to the optimization problem or any computational effort. Thus, the FUBM for AC/DC OPF will maintain all the advantages and characteristics of the individual traditional models in a simpler, more compact, and flexible form.

Even though the FUBM is designed to seamlessly model several elements of the Electrical Power System, it is not currently designed to model the Current Source

Converter (CSC). The reasons for selection the VSC over the CSC for this first stage of the model are the following:

- Theoretically, FACTS controllers, HVDC links and Multi Terminal DC Grids (MTDC) can be realized by either a VSC or a CSC [14].
- Even though the VSC and the CSC are designed to perform similar tasks, the CSC is more complex than a VSC in both power and control circuits. Filter capacitors are used at the ac terminals of a CSC to improve the quality of the output ac current waveforms. This adds to the overall cost of the converter. Furthermore, filter capacitors resonate with the ac-side inductances. As a result, some of the harmonic components present in the output current might be amplified, causing high harmonic distortion in the ac-side current. Besides, conventional bi-level switching scheme cannot be used in CSC.
- Due to the elevated cost of the CSC, in Europe all the power system projects from entso-e in the TYNDP include only VSCs as their main linker for FACTS and DC grids for the next 10 years [5].
- Unless a switch of sufficient reverse voltage withstanding capability such as Gate-Turn-Off Thyristor (GTO) is used, a diode has to be placed in series with each of the switches in CSC. This almost doubles the conduction losses compared with the case of VSC.
- The dc-side energy-storage element in CSC topology is an inductor, whereas that in VSC topology is a capacitor. The power loss of an inductor is expected to be larger than that of a capacitor. Thus, the efficiency of a CSC is expected to be lower than that of a VSC.

As a result the implementation of the CSC for the FUBM is not considered for this research. However, since the CSC are a mature and well-established technology used to convert electric power from AC to DC or vice versa, their inclusion for the FUBM has been considered for future work.

1.2 State of the Art

In order to research the development of a compact model for steady state operational analysis and optimisation of Hybrid AC/DC Grids, acknowledgement of the SCOPF challenges and knowledge over the existing AC/DC power system analysis tools needs to be included. Thus, the state of the art of this thesis is divided in three sections, the SCOPF state of the art, the existing AC/DC Software State of the art, and the Compact Hybrid models state of the art. Notice that the state of the art of the SCOPF implicitly involves the Power flow and OPF state of the art since they could be considered as sub problems of the SCOPF.

1.2.1 SCOPF state of the art

The efficient and optimum economic operation and planning of the electric power generation systems has always occupied an important position in the electric power industry. Due to high energy costs, knowing the optimum operation point in the power grid is desirable [15]. The first introduction to OPF was in 1962 by Carpentier [34]. Since then, a series of advancements has been made to this original idea. Challenges to OPF formulation are presented in [35, 36]. The first approach to SCOPF was made by Monticelli, which illustrated the solution of the economic dispatch problem with security constraints whilst taking into account the system corrective capabilities following contingencies [23]. Meanwhile, in [22], there is no distinction in the terminology between OPF and SCOPF further signifying the fact that SCOPF is basically an extension to the OPF. Unlike the OPF, the SCOPF takes into consideration not only any constraints that are binding during the normal operation (i.e. the base or pre-contingency state) but also those that become binding following a contingency. As per the definition by the North American Electric Reliability Corporation (NERC), a contingency is defined as the unexpected failure or outage of a system component, such as a generator, transmission line, circuit breaker, switch or other electrical element [37]. In practice, all optimisation problems consider security constraints and at least $n-1$ contingencies. The $n-1$ *contingency criterion* therefore refers to the condition in which the system should be able to

withstand the outage in any one single element. This contingency criterion is a standard condition for practical security-constrained operational planning carried out by TSOs.

The reason for including such reliability criteria for planning the short-term operation of the system is that the system operator knows in advance of the conditions that are led following a contingency and ensure system operational security is maintained at all times even following any outage of any number of elements. Nevertheless operational security in the system cannot be guaranteed 100 % of time due to the unpredictability nature of contingencies and the inherent complexity of the power system. Following the occurrence of a contingency, only a limited number of control actions may be available to the TSO. Typically corrective actions are previously analysed and listed to be taken if necessary (Human operators reactions to contingencies is still unsolved [36, 38]). Unfortunately, uncertainty (wind, load, generation, system, Timescale)is presented in the actual power system and it is increasing day by day. The way to tackle this is by running stochastic scenarios and using robust optimisation TSOs have to create several different scenarios in order to tackle this and create a list of possible effective corrective actions to deal with a certain contingency (based on the analysis of the results). This technique has a lot of disadvantages. Not only is time consuming but also may lead to a sub-optimal results that will end up in a higher cost [39].

There are several challenges to SCOPF computation and formulation [39]. One main challenge is the selection of the corrective actions to be used for each contingency [38]. Some papers have been written in this area. An experimental method, in which a linear penalty function on each control variable is imposed, is described in [40]. Algorithms are proposed to identify the most effective subset of control actions and minimising controller movements for real-time voltage/reactive power control in [41]. Since in OPF, each control variable participates in minimising the objective function as well as in enforcing constraints, based on fuzzy theory, OPF problem is converted to a crisp optimisation problem in [42]. A reformulation of OPF as a mathematical program with equilibrium constraints, in which no more than a pre-specified number of controls are allowed to move, is presented in [43]. A

way to limit the number of corrective actions used in post-contingency states has been reported in [39].

Reduction of the contingencies for SCOPF problem is a major issue. In practice, it is well known that certain contingencies do not constrain the optimal solution. Those contingencies should not be included in the list of contingencies to be tested when solving SCOPF. Full and simplified post-contingency models to reduce the size of SCOPF are presented in [44].

The full model for post contingency states is an iterative approach divided in four stages. It aims to obtain the smallest set of contingencies that provides the optimal objective value. The four iterative stages considering a full post-contingency states model include: a SCOPF considering only potentially binding contingencies, a Steady-State Classical Power Flow Security Analysis (SSSA), a Contingency Filter (CF), and a post-contingency OPF to identify which contingencies can be secured by corrective actions [45, 46, 47]. So far, most CF techniques rank contingencies using a Severity Index (SI), rely on Lagrange multipliers of a relaxed preventive SCOPF solution or or use the Non-Dominated Contingency (NDC) technique [47, 48]. Papers [47] and [46] show that NDC approach has better results than SI techniques and Benders approach. However, this approach cannot be applied if computer memory sources are limited [39].

Handling of discrete variables in OPF has been a widely revised challenging problem [22, 36]. Small step variables are typically handled by using the round-off strategy in combination with an approach that guarantee the feasibility of the solution. Several approaches have been proposed. These ones include either the use of penalty functions within Non Linear Programming (NLP) or Linear Programming (LP) solvers [49], ordinal optimisation [50], interior point cutting plane [51], consideration of the sensitivities of the objective function and inequality constraints with respect to discrete variables change [52], global optimisation methods [53, 54, 55].

Most techniques to handle discrete variables have been tested for OPF formulation. Therefore they can be applied to solve SCOPF where the number of discrete variables is significantly larger. Nevertheless their performance needs to be tested.

An extension to the conventional SCOPF that involves Power Router technology (or Energy Router Device) to increase flexibility and control over the transmission grid is addressed in [56]. They present what they called Flexible Security constrained Optimal Power Flow (FSCOPF). It utilises fast power router control in the post contingency time frame. In the paper an increase in flexibility is achieved by modifying the constraints used for optimisation. An expansion of this idea to include all the elements that conform to the future Flexible AC/DC network, such as PST, CTT, Controlled Tap Phase Shifter Transformer (CTPST), Power Router (PR), Flexible AC Transmission Systems (FACTSs), and HVDC lines is necessary. It is therefore appropriate to focus on developing formulations for solving SCOPF and OPF for such hybrid flexible AC/DC networks which is one of the main pillars of this thesis.

1.2.2 AC/DC Software and Analysis Tools

Since a new generation of Flexible AC/DC analysis tools is needed, in recent years, commercial power system software companies like PSS®E, DIgSILENT© - Power Factory and PowerWorld© have started to add the ability to simulate hybrid AC/DC networks to their existent AC tools [26, 27, 57]. However, their functionality is still very limited, and fully flexible controls over each one of the their elements is not available. Moreover, a main issue is that these commercial packages have a considerable high cost and since the models are closed, little modifications can be done to achieve a fully flexible functionality. As an alternative to commercial programs, open-source power system tools have been reported in the literature such as PowerModels.jl©, GridCal, and the wolrd famous MATPOWER© [58, 59, 60]. The three of them are open source software packages for the analysis of EPSs. Even though they have proven to be powerful EPSs analysis software packages, their formulation is still an AC based tool, therefore using traditional approaches, major modifications to the software need to be done to implement a fully controllable AC/DC Hybrid Grid.

The main core of the Power Flow analysis, OPF and SCOPF of AC/DC Power Flow is the formulation of the non-linear power balance equations and power flow

equations. Two different strategies have been suggested for their solution, namely the Sequential and the Unified approach [61, 62]. Sequential methods rely on building blocks to solve the dc network as well as the ac network iteratively. Once the DC grid is solved iteratively and the converter losses are calculated, the AC power flow solution of the initial loop changes. Consequently, apart from these internal loop iterations for the DC and AC grid, an external iteration loop is also required to ensure the overall convergence of the algorithm [63]. As an advantage, sequential methods can be implemented into an existing AC power flow program. However, sequential methods have only first order convergence rate, resulting in computational inefficiency. Moreover, such complexities make sequential methods rather unreliable mainly due to the fact that the convergence of external loop would be affected if any internal loop failed to converge [64]. On the other hand, unified methods employ a better approach by solving the entire VSC, AC grid, and DC grid equations simultaneously. Unified approaches have quadratic convergence thereby achieving faster and more accurate solutions [62, 65]. The main disadvantage of unified approaches is that they cannot be added to existing AC-only computational tools without making major modifications to the original code [66].

Implementation of both approaches have been done for commercial and open source analysis tools. Modifications to the mentioned open source software tools have been reported in the literature. The first modification was done by Jef Beerten and Ronnie Belmans to MATPOWER allowing to study the steady-state interactions between multiple non-synchronised AC grids and DC systems based on VSC HVDC technology, it is an open source code named MATACDC [25]. By being a sequential approach, MATACDC does not modify MATPOWER's original code. However, the approach is very limited since no controls have been added and it is therefore only available for simple power flow analysis. Moreover, this approach is now out of date and is no longer compatible with the newest version of MATPOWER. On the other hand a recent unified approach to modify PowerModels.jl was presented in [32], where the formulation, convex relaxation and linear approximation of OPFs for AC/DC Grids was presented. A similar approach is done by the software Hynet presented in [33] which is a Python-based framework.

All reported approaches still have to model each electrical element individually. Thus, regardless of the approach taken, an extensive model library to selectively be able to incorporate various EPSs elements and accommodate different network types (AC or DC) is normally needed. Moreover, the VSC model used for their implementation requires a full reformulation of the existing AC tools to achieve an accurate unified solution. Furthermore, the power and voltage control of these tools are still limited to the VSC variables without considering other control elements.

1.2.3 Flexible AC/DC Universal Models

To the author's knowledge no hybrid AC/DC models have been reported in the literature, and as mentioned above, so far the closest approach to a compact model is the one presented in MATPOWER for AC grids, where the traditional π model of the branch is merged with an ideal fixed transformer. This model only includes two elements and no compatibility with DC grids [24].

1.3 Research Aims and Objectives

Even though nowadays there are analysis tools to solve AC/DC grids, they require an extensive model library in which additional controls from network elements may not necessarily be facilitated. Moreover, the majority of these tools are developed as commercial products. Therefore, as expected, the details of their models and solvers are not available for the wider research community who may not be able to procure the commercial licences. Thus, modifications to the models and software are very limited. As a result, modifications that could be used to analyse system flexibility for hybrid AC/DC networks are not at least widely available through commercial licensed software packages. These modifications include but are not limited to: adding extra control variables to the power system elements, combining existing models to create a new model, optimising current and extra control variables inside the models, create model related power and voltage control constraints, or consider fast action corrective actions of VSCs for post contingency cases.

Moreover, as stated previously, with the ever increasing penetration of converter-

connected renewable resources, as well as integration of flexible demand technologies (e.g. Electric Vehicles), the electric power system of the future will be a hybrid AC/DC network in almost all voltage level. It is therefore necessary to be able to properly analyse the operation of the system properly and make use of the extra levels of control and flexibility available in these systems.

Therefore, one of the objectives in this project has been to develop a Flexible Universal Branch Model (FUBM) formulation for steady state operational analysis and optimisation of fully controllable hybrid AC/DC grids through which, the global impact of the control actions of the system elements (hence its flexibility) can be thoroughly investigated. This work therefore entails the development and implementation of a new model formulation to represent realistically, several power system elements both for AC and DC sides of a hybrid grid and their associated couplings. Meanwhile, the FUBM aims to provide a physical link between the AC and DC grids allowing for solving the entire hybrid EPS within a unified frame of reference. Furthermore, the model aims to realistically model almost any element within the AC/DC power grid, ranging from conventional AC transmission lines to multiple and controllable AC/DC interface devices such as the VSC. To achieve this, the model includes extra optional control variables and control constraints which represent the extra degrees of flexibility that may exist in a hybrid AC/DC grid. For example, for a voltage source control representation, the extra control variables/constraints would represent the converter's AC voltage control and independent active and reactive power flow controls in the converter. To this end, the FUBM is therefore a *universal* model with which one can represent an entire system simply by including a set of variables and constraints associated with the operation of each element within the system.

From a purely mathematical perspective, the FUBM is a universal model formulation in that it combines several element representations within one model. In this way, model representation within the Power Flows, OPF and SCOPF analysis of hybrid AC/DC grids becomes more streamlined as the problems are formulated as mathematical programmes and there is virtually no distinction between AC and DC sides of the network. This means, that the whole system can be solved in its entirety

with one set of equations pertaining to both AC and DC sides whilst at the same time respecting the coupling constraints (i.e. power balances) between AC and DC sides. As a result, existing AC analysis tools which require an upgrade to simulate fully controllable AC/DC hybrid grids will not require major modifications in their formulations. Moreover, the extra control will allow to find an operating point which may be infeasible otherwise. Meanwhile, the structure of the formulation of FUBM allows for the ensuing steady-state analysis problems (e.g. OPF, and SCOPF) to be formulated and solved using general-purpose model-based solvers such as AIMMS which has been used extensively in this work. The AIMMS implementation of FUBM for both OPF and SCOPF has been used with a variety of non-linear gradient-based solvers for both small-scale and large-scale systems. This capability and universality of the model further allows a more streamlined and better integration and customisation of models for steady-state analysis problems that are often featured in power systems short-term operational planning studies.

Furthermore, any new model formulations should not sacrifice computational tractability for accuracy of representation. It is therefore appropriate that the universal model formulation presented in this thesis stays computationally tractable for medium to large-scale systems.

Moreover, the FUBM should also be integrated within existing open-source power system specialist software. For this thesis, the software of choice has been MATPOWER. Since MATPOWER is an internationally acknowledged and proved tool for AC power system analysis, the new FUBM and the formulation for power flows and OPF of hybrid AC/DC grids has been implemented as an upgraded version of the existing software.

In summary, the main objectives of this research can be identified as distinct research challenges outlined in the next section.

1.4 Research Challenges

This work attempts to address four main Research Challenges (RCs):

RC1. Development of the FUBM: To develop a novel flexible universal AC/DC model formulation to represent and realistically simulate a wide variety of power system elements and their controls for purposes of steady-state analysis - The FUBM model formulation is presented in Chapter 3.

RC2. Flexible Steady State Formulation using FUBM: To develop a flexible formulation for Power Flows, OPF and SCOPF using the FUBM for simulating the operation of fully controllable, flexible AC/DC power systems thereby allowing for evaluating the impact of operational flexibility and security for these networks. - The formulation of a fully flexible Power Flow problem is featured in 4, whereas formulations for OPF and SCOPF are addressed in Chapters 5 and 6.

RC3. Implementation of the FUBM: To integrate the FUBM and the ensuing flexible formulation in both an existing AC steady state analysis tool (MATPOWER), and a general-purpose mathematical optimisation software tool (AIMMS) for developing next generation analysis tools for solving hybrid AC/DC grids. To this end, the model should be adaptable to a diverse pool of solvers, and stays tractable for medium and larger size systems - the integration of FUBM in MATPOWER and AIMMS has been illustrated in Chapters 4, 5 and 6. The computational efficiency of the model is illustrated through comparisons to already prominently used power system analysis packages in Chapter 5.

RC4. Flexibility of the System: To use the implementation of the FUBM in MATPOWER and AIMMS, to evaluate the system flexibility, and operational security for future hybrid AC/DC networks - this challenge has been addressed through system simulations in chapters 4 - 6, with chapter 6 solely focusing on SCOPF solutions.

1.5 Publications

Table 1.1 is used to summarise the research publications throughout the study period and beyond. It includes published papers, software releases and future publications. Parts of this thesis (in particular, Chapters 3, 4, and 5) are based on the below papers that have already been published, and parts of the thesis are currently being planned to be developed into further publications (Chapter 6).

Table 1.1: List of Publications

Publication	Status
"Flexible General Branch Model Unified Power Flow Algorithm for Future Flexible AC/DC Published Networks", (2018), IEEE International Conference of Electrical Engineering 2018 for Energy systems in Europe (EEEIC/I&CPS Europe). DOI: 10.1109/EEEIC.2018.8493705	Published
"Universal Branch Model for the Solution of Optimal Power Flows in Hybrid AC/DC Grids", (2020), International Journal of Electrical Power Energy Systems - ElSevier, DOI: 10.1016/j.ijepes.2020.106543.	Published
"MATPOWER-FUBM: Flexible Universal Branch Model, Steady-State Operations, Power Control, Optimal Power Flows and Analysis Tools for Hybrid AC/DC Power Systems Research", (2020), Software Release, Technical Note and Quick Guide, Open Source Code, Platform: MATLAB, at MATPOWER Development, Available at: https://github.com/AbrahamAlvarezB/matpower-fubm	Published
"MATPOWER-FUBM: Steady-State Analysis, Control and Operational Planning Tools for Hybrid AC/DC Power Systems Research" at IEEE Transactions on Power Systems.	Under Development
"Fast Acting Corrective Actions on the SCOPF for Post-contingency Stages using the FUBM in Hybrid AC/DC Grids" at IEEE Transactions on Power Systems.	Under Development

1.6 Future Research Collaborations

Due to the interest garnered from the publications from the power systems research community, the author and supervisors of this thesis have been contacted to collaborate in the development of the next generation universal analysis tools. Table 1.2 summarises the projects that are currently planned to be spun out of this thesis.

Table 1.2: Future Research Collaborations

Project:	MATPOWER MP Element-FUBM
Lead Researcher:	Ray Zimmerman
Development of the next generation of the worldwide known tool MATPOWER. This project combines the ideas developed in the FUBM with the MPelement to create a unique and fully controllable class element to simulate all the elements of the power system for generation, transmission and distribution systems for hybrid AC/DC grids and Smart Grids. This MPelement-FUBM will require a novel formulation to solve the transmission positive sequence equations and the unbalanced distribution three phase equations will be developed in a unified approach.	
Project:	GridCal-FUBM
Lead Developer:	Santiago Peñate Vera
GridCal is an open source power systems calculation software with a well developed graphical user interface (GUI). The project aims to include the FUBM and its formulation to Gridcal. This project will be mainly developed in Python. At the end of the project a new version of the software (GridCal-FUBM) will be released.	
Project:	AIMMS-FUBM
Lead Developer:	AIMMS Optimisation Software Company
Writing a Book and designing video tutorials for the power/energy research community of advanced optimisation of AC/DC hybrid grids in AIMMS e-learning platform.	

Chapter 2

Literature Review

The main aim of this thesis is the develop a fully controllable, and flexible universal model formulation for operational planning optimisation of hybrid AC/DC power systems. To this end, this chapter begins with the introduction of general concepts as well as the formulation of mathematical problems that are commonly used to evaluate the steady-state operation of power systems; namely, Power Flows, Optimal Power Flows and Security-constrained Optimal Power Flows. Furthermore, this chapter also includes a comprehensive review of the methods to formulate and solve mathematical optimisation problems both for unconstrained and constrained problems, including linear and/or nonlinear constraints, followed by a review of some of the most widely-used solution algorithms and computational tools, which are employed to solve OPF and SCOPF problems. The concepts, mathematical formulation and the optimisation algorithms will be referenced and used throughout this thesis.

2.1 Power Flow Analysis

Over the last fifty years, Newton's method has proven to be a superior algorithm for solving power flow problem [67]. The basic problem involves the iterative solution of a system of non-linear equations as in (2.1.1), where $\mathbf{F}$ represents a set of n non-linear equations, and $\mathbf{x}$ is the vector of n unknown state variables [68].

$$\mathbf{F}(\mathbf{x}) = \mathbf{0} \quad \text{or} \quad \begin{cases} f_1(x_1, x_2, \ldots, x_n) = 0, \\ f_2(x_1, x_2, \ldots, x_n) = 0, \\ \vdots \\ f_n(x_1, x_2, \ldots, x_n) = 0, \end{cases} \tag{2.1.1}$$

According to Newton's Method, the vector of state variables $\mathbf{x}$ will be determined by performing a Taylor series expansion of $\mathbf{F}(\mathbf{x})$ about an initial estimate $\mathbf{x_0}$:

$$\mathbf{F}(\mathbf{x}) = \mathbf{F}(\mathbf{x_0}) + \mathbf{J}(\mathbf{x_0})(\mathbf{x} - \mathbf{x_0}) + \text{higher-order terms} \tag{2.1.2}$$

where $\mathbf{J}(\mathbf{x_0})$ is a matrix of first order partial derivatives of $\mathbf{F}(\mathbf{x})$ with respect to $\mathbf{x}$, termed the Jacobian, and it is evaluated at $\mathbf{x} = \mathbf{x_0}$.

This expansion lends itself to a suitable formulation for calculating the vector of state variables $\mathbf{x}$ by assuming that $\mathbf{x} = \mathbf{x_1}$, where $\mathbf{x_1}$ is the value computed by the algorithm at the iteration 1 and that this value is sufficiently close to the initial estimate $\mathbf{x} = \mathbf{x_0}$. Based on this premise, all high-order derivative terms in (2.1.2) may be neglected [69].

Hence the iterative solution,

$$\mathbf{\Delta x} = -\mathbf{F}/\mathbf{J} \tag{2.1.3}$$

$$\begin{bmatrix} x_{1i} - x_{1(i-1)} \\ x_{2i} - x_{2(i-1)} \\ \vdots \\ x_{3i} - x_{3(i-1)} \end{bmatrix} = - \begin{bmatrix} f_1(\mathbf{x}_{(i-1)}) \\ f_2(\mathbf{x}_{(i-1)}) \\ \vdots \\ f_n(\mathbf{x}_{(i-1)}) \end{bmatrix} * \begin{bmatrix} \frac{\partial f_1(\mathbf{x}_{(i-1)})}{\partial x_1} & \frac{\partial f_1(\mathbf{x}_{(i-1)})}{\partial x_2} & \cdots & \frac{\partial f_1(\mathbf{x}_{(i-1)})}{\partial x_n} \\ \frac{\partial f_2(\mathbf{X}_{(i-1)})}{\partial x_1} & \frac{\partial f_2(\mathbf{x}_{(i-1)})}{\partial x_2} & \cdots & \frac{\partial f_2(\mathbf{x}_{(i-1)})}{\partial x_n} \\ \vdots & \vdots & \ddots & \vdots \\ \frac{\partial f_n(\mathbf{X}_{(i-1)})}{\partial x_1} & \frac{\partial f_n(\mathbf{x}_{(i-1)})}{\partial x_2} & \cdots & \frac{\partial f_n(\mathbf{x}_{(i-1)})}{\partial x_n} \end{bmatrix}^{-1} \tag{2.1.4}$$

In order to get accurate results the evaluated functions $\mathbf{F}(\mathbf{x_i})$ must meet a specified tolerance until convergence. A typical value for this tolerance is shown in (2.1.5).

$$\varepsilon = 1e^{-8} \tag{2.1.5}$$

2.1.1 Network Modelling and Power Flow Equations

In Power Flow Analysis, the nodal bus injections are matched to the injections from loads and generators to form the AC nodal power balance equations. Thus, Kirchoff's laws are satisfied at each node. These equations are expressed in (2.1.6) as a function of the complex bus voltages and generator injections in complex matrix form [24]. Graphically the power balance equations are shown in Fig. 2.1. Newton's Method is used to solve these non-linear equations.

$$\mathbf{g_{S_b}}(\mathbf{V}, \mathbf{S_g}) = \mathbf{S_{bus}}(\mathbf{V}) + \mathbf{S_d} - \mathbf{S_g} = \mathbf{0} \tag{2.1.6}$$

Where,

$$\mathbf{S_{bus}}(\mathbf{V}) = [\mathbf{V}]\mathbf{I_{bus}}^* = [\mathbf{V}]\mathbf{Y_{bus}}^*\mathbf{V}^* \tag{2.1.7}$$

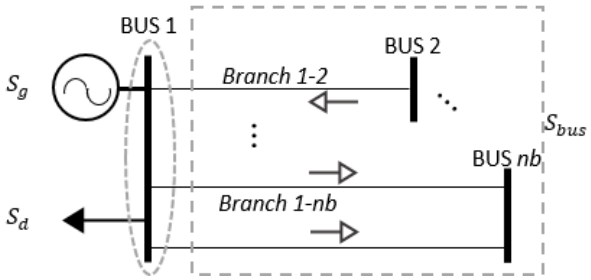

Figure 2.1: Nodal Power Balance Equations

In the traditional Power Flow analysis, the mismatch equations given by (2.1.6) are separated in active power balance equations and reactive power balance equations as presented in (2.1.8), where the voltage angle V_a and the magnitude, V_m are the state variables [68]. Furthermore, in power flows, all the buses in the power system are divided in three categories. The *slack bus* is required to provide the mismatch between scheduled generation, the total system load (including losses) and total generation. The slack bus is commonly considered as the reference bus because both voltage magnitude and angle are specified; therefore, it is also called

the swing bus. The rest of generator buses are called regulated or PV buses because the net real power is known and voltage magnitude is regulated. Most of the buses in practical power systems are load buses. Load buses are called PQ buses because both net real and reactive power loads are specified.

For PQ buses, both voltage magnitudes and angles are unknown, whereas for PV buses, only the voltage angle is unknown. As both voltage magnitude and angle are specified for the *slack bus*, there are no variables that must be solved for. As such, in a system with nb buses and ng generators, there are $2(nb-1)+(ng-1)$ unknowns. To solve these unknowns, the real and reactive power balance equations in (2.1.6) and (2.1.7) are used.

$$\begin{bmatrix} \Delta V_a \\ \Delta V_m \end{bmatrix} = - \begin{bmatrix} Real(\mathbf{g_{S_b}}(\mathbf{V_a}, \mathbf{V_m})) \\ Imag(\mathbf{g_{S_b}}(\mathbf{V_a}, \mathbf{V_m})) \end{bmatrix} * \begin{bmatrix} Real(\frac{\partial \mathbf{g_{S_b}}}{\partial \mathbf{V_a}}) & Real(\frac{\partial \mathbf{g_{S_b}}}{\partial \mathbf{V_m}}) \\ Imag(\frac{\partial \mathbf{g_{S_b}}}{\partial \mathbf{V_a}}) & Imag(\frac{\partial \mathbf{g_{S_b}}}{\partial \mathbf{V_m}}) \end{bmatrix}^{-1} \tag{2.1.8}$$

Firstly, in order to calculate the complex power injections, and solving the power balance equations using Newton's Methods as presented in (2.1.8), obtaining the admittance matrix Y_{bus} is necessary. There are several approaches for the calculation of Y_{bus}. However, in this thesis MATPOWER's basic formulation will be used.

MATPOWER uses a general transmission line model; transformers and phase shifters are modelled with a common branch model, consisting of a standard π transmission line model, with series impedance [24]. In order to simulate the Phase Shifter as well as the Tap changer, the transformer in the π model is modelled with a complex tap N as seen in (2.1.9). Thus, the complete branch admittance matrix is presented in (2.1.10) and the model is shown in Fig. 2.2.

$$N = \tau e^{j\theta_{\text{shift}}} \tag{2.1.9}$$

$$\mathbf{Y_{br}} = \begin{bmatrix} (y_s + j\frac{b_c}{2})\frac{1}{\tau^2} & -y_s\frac{1}{\tau e^{-j\theta_{\text{shift}}}} \\ -y_s\frac{1}{\tau e^{j\theta_{\text{shift}}}} & y_s + j\frac{b_c}{2} \end{bmatrix} \tag{2.1.10}$$

The four elements of this matrix for branch i are labelled as follows:

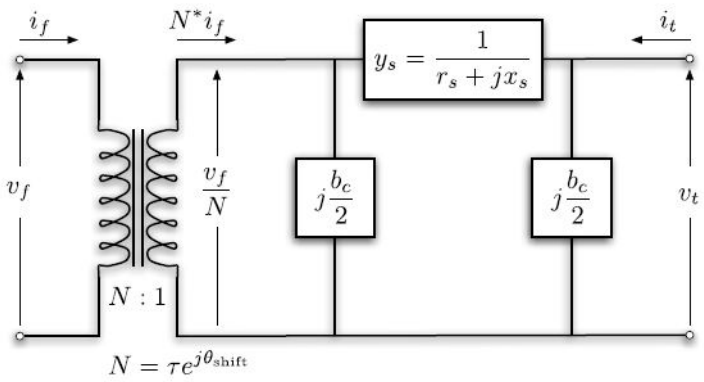

Figure 2.2: MATPOWER Branch Model[24]

$$\mathbf{Y_{br}}^{\mathbf{i}} = \begin{bmatrix} {y_{ff}}^i & {y_{ft}}^i \\ {y_{tf}}^i & {y_{tt}}^i \end{bmatrix} \tag{2.1.11}$$

For a network with nl branches, the $nl \times nb$ system branch admittance matrices Y_f and Y_t relate the bus voltages to the $nl \times 1$ vectors I_f and I_t of branch currents at the from and to ends of all branches, respectively.

$$\mathbf{I_f} = \mathbf{Y_f V} \tag{2.1.12}$$

$$\mathbf{I_t} = \mathbf{Y_t V} \tag{2.1.13}$$

The system admittance matrices can be formed as follows [24]:

$$\mathbf{Y_f} = [\mathbf{Y_{ff}}]\mathbf{C_f} + [\mathbf{Y_{ft}}]\mathbf{C_t} \tag{2.1.14}$$

$$\mathbf{Y_t} = [\mathbf{Y_{tf}}]\mathbf{C_f} + [\mathbf{Y_{tt}}]\mathbf{C_t} \tag{2.1.15}$$

$$\mathbf{Y_{bus}} = {\mathbf{C_f}}^\top \mathbf{Y_f} + {\mathbf{C_t}}^\top \mathbf{Y_t} + [\mathbf{Y_{sh}}] \tag{2.1.16}$$

Connection matrices $\mathbf{C_f}$ and $\mathbf{C_t}$, used in building the system admittance matrices, contain identifiers to relate between which nodes a branch is connected. Each connection matrix has a size of $[n_l \times n_b]$, and contains an indicator with the value of 1 where the branch element "from" or "to" side connects with the bus. All the non nodal incidences of C_f and C_t are zero. [24]. Up to this point, it can be appreciated

that the only variables during the Newton iterative process are the $\mathbf{V}_a$ and the $\mathbf{V}_m$. Therefore, $\mathbf{Y_{bus}}$ and $N = \tau e^{j\theta_{\text{shift}}}$ remain constant.

The classic formulation of Power Flow problem presented above is useful for solving most conventional AC-only power systems. However, in order to model and solve a fully flexible and controllable AC/DC power system, the AC and DC sides of the network should be coupled using an appropriate coupling equation that respects the balance of power between AC and DC. Moreover, additional control variables may be introduced into the problem formulation to represent extra controls that may exist in an AC/DC power system (e.g. power flow control exerted by a Voltage Source Converter). It is therefore necessary to modify the classic formulation of the Power Flow problem to accommodate these additional capabilities in order to be able to solve a fully flexible and controllable AC/DC power system. Meanwhile, a modified (so called flexible) power flow problem formulation is required to initialise the Optimal Power Flow problem for hybrid AC/DC power systems.

2.2 OPF & SCOPF

The formulation of the Optimal Power Flow and the Security Constrained Optimal Power Flow are very similar to each other. In fact the SCOPF problem could be considered as a generalisation of the OPF problem that considers not only the system pre-contingency (i.e. normal operation) binding constraints but also post-contingency (i.e. post disturbance) constraints that become binding following a contingency (i.e. disturbance in the system). Both problems can be formulated as non-linear mathematical optimisation (mathematical programming) problems. The goal of the OPF problem is essentially to determine the state variables for the system with which a certain objective (e.g. cost of active power dispatch by the generators) is at its minimum when subject to the system realistic operational boundaries defined in form of equality and inequality constraints. The SCOPF generalises this definition by including any additional constraints that may be binding for post-contingency (i.e. following a disturbance) states. Equations (2.2.17), (2.2.18) and (2.2.19) correspond to the classical OPF formulation corresponding to its objective

function as well as the equality and inequality constraints respectively. Equations (2.2.17) to (2.2.25) correspond to the formulation of the SCOPF.

$$\begin{aligned} &min \qquad f_0(\mathbf{x}_0, \mathbf{u}_0) \\ &\mathbf{x}_0, \ldots, \mathbf{x}_c \\ &\mathbf{u}_0, \ldots, \mathbf{u}_c \end{aligned} \tag{2.2.17}$$

subject to:

$$\mathbf{g}_0(\mathbf{x}_0, \mathbf{u}_0) = \mathbf{0} \tag{2.2.18}$$

$$\mathbf{h}_0(\mathbf{x}_0, \mathbf{u}_0) \leq \mathbf{L_l} \tag{2.2.19}$$

$$\mathbf{g}_k{}^s(\mathbf{x}_k{}^s, \mathbf{u}_0) = \mathbf{0} \quad k = 1, \ldots, c \tag{2.2.20}$$

$$\mathbf{h}_k{}^s(\mathbf{x}_k{}^s, \mathbf{u}_0) \leq \mathbf{L_s} \quad k = 1, \ldots, c \tag{2.2.21}$$

$$\mathbf{g}_k(\mathbf{x}_k, \mathbf{u}_k) = \mathbf{0} \quad k = 1, \ldots, c \tag{2.2.22}$$

$$\mathbf{h}_k(\mathbf{x}_k, \mathbf{u}_k) \leq \mathbf{L_m} \quad k = 1, \ldots, c \tag{2.2.23}$$

$$|\mathbf{u}_k - \mathbf{u}_0| \leq \overline{\Delta \mathbf{u}_k} \quad k = 1, \ldots, c \tag{2.2.24}$$

$$\overline{\Delta \mathbf{u}_k} = T_k \tfrac{d\mathbf{u}_k}{dt} \tag{2.2.25}$$

The objective function in (2.2.17) depends on the aims of the study. Traditionally, the total generation cost is the summation of the polynomial cost functions (typically quadratic, but can be of other forms, e.g. piece-wise linear) for each generator. Equality and inequality constraints introduced in (2.2.18) and (2.2.19) correspond to constraints for the pre-contingency state respectively. Similarly, vectors $\mathbf{x_0}$ and $\mathbf{u_0}$ pertain to the state and control variables for the pre-contingency state. Post-contingency constraints given in equations (2.2.20) to (2.2.23), are defined for the k^{th} contingency with k ranging from 1 to the number of contingencies c, pertaining to each post-contingency state. Likewise, vectors $\mathbf{x}_k$ and $\mathbf{u}_k$ correspond to the state and control variables for post-contingency states. For classical AC only formulation, state variables correspond to the nodal voltages phase angles and magnitudes. Post-contingency control variables may include actions pertaining to generators active power dispatch, tap ratios of on-load tap-changing transformers, variable reactance for shunt elements, phase shifter transformer angles and etc.

The post-contingency state can either be preventive secure or corrective secure. If no control actions are allowed (or available) following a contingency, the ensuing post-contingency states determined by the SCOPF are said to be of a preventive secure type, whereas if control actions are allowed the ensuing post-contingency states are of the corrective secure type. It follows that preventive secure states are more conservative than corrective secure states. However, with the additional fast action control elements present in a hybrid AC/DC power system, it is highly likely that any SCOPF formulation for such systems include post-contingency corrective actions. Superscript s in (2.2.20) and (2.2.21) indicates "short term time" relating to the time in which TSO cannot modify any control variable following a contingency. For corrective actions, equation (2.2.24) represents the maximum amount of adjustments to the control variables between the base case (i.e. $k = 0$) and the k^{th} post-contingency state. T_k is the interval of time available for corrective actions to ensure the feasibility of the post-contingency state and $d\mathbf{u}_k/dt$ is the rate of change of the control variables in response to a contingency. Finally $\mathbf{L}_s$, $\mathbf{L}_m$, and, $\mathbf{L}_l$ denote respectively the short-term (emergency), medium-term, and the long-term (normal) operating limits [39, 70].

Power balance equations are the equality constraints shown in (2.2.18), (2.2.20) and (2.2.22). On the other hand, inequality constraints, shown in (2.2.19), (2.2.21), and (2.2.23), refer to actual operational limits in the system (e.g. transmission lines thermal limits, limits on the ratios of on-load tap-changing transformers, as well as operational limits on the branch currents and voltage magnitudes). In order to meet the constraints with "realistic" values, (2.2.24) will be limiting the adjustments over the control variables.

Meanwhile, a set of constraints limiting the number of corrective actions allowed in each post-contingency state (i.e. for post contingency state variables) can be included [39]. The formulation is the following:

$$-\mathbf{s}_k\overline{\Delta\mathbf{u}_k} \leq \mathbf{u}_k - \mathbf{u}_0 \leq \mathbf{s}_k\overline{\Delta\mathbf{u}_k} \quad k = 1, \ldots, c \tag{2.2.26}$$

$$\mathbf{1}^T\mathbf{s}_k \leq N_k \quad k = 1, \ldots, c \tag{2.2.27}$$

$$\mathbf{s}_k \in \{0, 1\} \quad k = 1, \ldots, c \tag{2.2.28}$$

If the status of the corrective action u_{k_j} of the j^{th} element is equal to 1, it means that this action is allowed. Alternatively, as seen in (2.2.29), constraint in (2.2.27) can be expressed in terms of time needed for controls implementation, where t_k is the vector of times needed to implement the control actions.

$$\mathbf{s}_k{}^T \mathbf{t}_k \leq T_k \quad k = 1, \ldots, c \tag{2.2.29}$$

EPS have fast response actions and slow response actions. While transformer tap changers and angles of phase shifter transformers are some examples of a faster response variables, network switching, connection of non-dispatched generators, and connection or disconnection of shunt compensation, are some examples of slower response variables. For this thesis only fast response actions will be considered.

It is also worth mentioning that the formulation presented above is the general formulation for snapshot solutions of OPF and SCOPF problems. In the context of short-term optimum planning of network operation there may be a need for running multiple instances of the relevant optimisation problems for a specific planning horizon. The so-called multi-period formulation of OPF and SCOPF will involve successive runs of these problems for each time-period within the planning horizon. There may also be the need for temporal coupling constraints between each time period in this case (for example, when one of the decision variables is the level of energy available in energy storage devices). Whilst the focus of this thesis has been the single-period formulations these can be easily expanded to encompass multi-periods without any changes to the core formulations of the OPF and SCOPF problems.

2.2.1 Lagrangian Function and Slack Variables

Both OPF and SCOPF, at their cores, are formulated as non-linear constrained optimisation problems. In general, in an optimisation problem, the goal is to find an $\mathbf{x}$ vector of choice (or decision) variables x which minimises (or extermises) $f(\mathbf{x})$ subject to, $\mathbf{g} = 0$, equality and, $\mathbf{h} \leq \mathbf{L}$, inequality constraints [71]. Normally, for solving a constrained non-linear optimisation problem such as the OPF or the SCOPF, all inequality constraints should first be converted to equality constraints. In order to do so, an appropriate, yet unknown, non-negative slack variable, ${z_i}^2$,

per inequality constraint is added [71]. In the context of the OPF and SCOPF formulation given in (2.2.17) to (2.2.25), once transferring $\mathbf{L_s}$, $\mathbf{L_m}$ and $\mathbf{L_l}$ to the left-hand side, the inequality constraints from (2.2.19), (2.2.21), and (2.2.23) can be transformed to (2.2.30), in which $k = 0$ will be the pre-contingency state.

$$h_{ik}(\mathbf{x}_k, \mathbf{u}_k, \mathbf{z}_k) = h_{ik}(\mathbf{x}_k, \mathbf{u}_k) - L_{lik} + {z_i}^2{}_k = 0 \quad \forall \quad k \in \{0, 1, \ldots, c\} \tag{2.2.30}$$

Which can be written in a vector form as seen in (2.2.31):

$$\mathbf{h}_k(\mathbf{x}_k, \mathbf{u}_k, \mathbf{z}) = \mathbf{h}_k(\mathbf{x}_k, \mathbf{u}_k) + \mathbf{z}_k = 0 \quad \forall \quad k \in \{0, 1, \ldots, c\} \tag{2.2.31}$$

Where $\mathbf{z}$ is an ni vector associated with ni inequalities given by:

$$\mathbf{z} = \begin{pmatrix} {z_1}^2 \\ {z_2}^2 \\ \vdots \\ {z_{ni}}^2 \end{pmatrix} \tag{2.2.32}$$

To solve either the OPF, in (2.2.17) to (2.2.19), or the SCOPF problem shown in (2.2.17) to (2.2.25), the Lagrangian function, seen in (2.2.33), must be minimised.

$$\mathcal{L}(\mathbf{x}_k, \mathbf{u}_k, \mathbf{z}_k, \lambda_k, \mu_k) = f(\mathbf{x}_0, \mathbf{u}_0) +$$
$$\sum_{i=0}^{ne} \lambda_{ki} g_{ki}(\mathbf{x}_k, \mathbf{u}_k) + \sum_{j=0}^{ni} \mu_{kj} h_{kj}(\mathbf{x}_k, \mathbf{u}_k, \mathbf{z}_k) \quad \forall \quad k \in \{0, 1, \ldots, c\} \tag{2.2.33}$$

Where λ and μ vectors are the Lagrange multipliers for the ne and ni equality and inequality constraints respectively (including contingencies) [72].

Necessary conditions, seen in (2.2.34) to (2.2.37), need to be satisfied for minimising $\mathcal{L}(\mathbf{x}_k, \mathbf{u}_k, \mathbf{z}_k, \lambda_k, \mu_k)$ in (2.2.33).

$$\frac{\partial \mathcal{L}(\mathbf{x}_k, \mathbf{u}_k, \mathbf{z}_k, \lambda_k, \mu_k)}{\partial x_{j_k}} = \frac{\partial f(\mathbf{x}_k, \mathbf{u}_k)}{\partial x_{j_k}} +$$
$$\sum_{i=1}^{ne} \lambda_{ki} \frac{\partial g_{ki}(\mathbf{x}_k, \mathbf{u}_k)}{\partial x_{j_k}} + \sum_{j=1}^{ni} \mu_{ki} \frac{\partial h_{ki}(\mathbf{x}_k, \mathbf{u}_k, \mathbf{z}_k)}{\partial x_{j_k}} = 0,$$
$$\forall j = 1, 2, \cdots, nx \quad (nx \text{ optimisation variables}) \tag{2.2.34}$$

$$\frac{\partial \mathcal{L}(\mathbf{x}_k, \mathbf{u}_k, \mathbf{z}_k, \lambda_k, \mu_k)}{\partial \lambda_{j_k}} = \frac{\partial f(\mathbf{x}_k, \mathbf{u}_k)}{\partial \lambda_{j_k}} + \sum_{i=1}^{ne} g_{ki}(\mathbf{x}_k, \mathbf{u}_k) = 0$$

$$\forall j = 1, 2, \cdots, ne \quad (ne \text{ equations}) \tag{2.2.35}$$

$$\frac{\partial \mathcal{L}(\mathbf{x}_k, \mathbf{u}_k, \mathbf{z}_k, \lambda_k, \mu_k)}{\partial \mu_{j_k}} = \frac{\partial f(\mathbf{x}_k, \mathbf{u}_k)}{\partial \mu_{j_k}} + \sum_{i=1}^{ni} h_{ki}(\mathbf{x}_k, \mathbf{u}_k, \mathbf{z}_k) = 0$$

$$\forall j = 1, 2, \cdots, ni \quad (ni \text{ equations}) \tag{2.2.36}$$

$$\frac{\partial \mathcal{L}(\mathbf{x}_k, \mathbf{u}_k, \mathbf{z}_k, \lambda_k, \mu_k)}{\partial z_{j_k}} = 2 z_{j_k} \mu_{j_k} = 0$$

$$\forall j = 1, 2, \cdots, ni \quad (ni \text{ equations}) \tag{2.2.37}$$

Equation (2.2.37) is satisfied when either z_{j_k} is zero, or if μ_{j_k} is zero. These relations are called transversality conditions. If μ_{i_k} is zero, it means that z_{j_k} is non-zero, and hence the value of h_{kj} is less than L_{lkj}; in (2.2.19). Consequently the constraint is said to be non-binding or inactive. On the other hand, if $z_{j_k} = 0$, the constraint is active and binding. Of the ni inequality constraints of (2.2.19), let a represent the number of active constraints. Since $z_{j_k} = 0$ when constraints are active, we ignore them in binding constraints.

Therefore:

$$-\nabla f_k(\mathbf{x}_k, \mathbf{u}_k) = \sum_{i=1}^{a_\lambda} \lambda_{ik} \nabla g_{ik}(\mathbf{x}_k, \mathbf{u}_k) + \sum_{i=1}^{a_\mu} \mu_{ik} \nabla h_{ik}(\mathbf{x}_k, \mathbf{u}_k) \tag{2.2.38}$$

Equation (2.2.38) indicates that the negative gradient of the objective function can be expressed as a linear combination of the gradients of active constraints.

2.2.2 Karush-Kuhn-Tucker conditions

Since active or binding constraints are not known from the beginning, a general way of writing the above conditions, called the Karush-Kuhn-Tucker (KKT), is as follows: If all ni inequalities are transformed to equalities and included with ne equalities of the problem, the KKT conditions are:

$$\nabla f(\mathbf{x}_k, \mathbf{u}_k) + \sum_{i=1}^{a_{ne}} \lambda_{ik} \nabla g_{ik}(\mathbf{x}_k, \mathbf{u}_k) + \sum_{i=1}^{a_{ni}} \mu_{ik} \nabla h_{ik}(\mathbf{x}_k, \mathbf{u}_k) = 0 \tag{2.2.39}$$

$$g_{ik} = 0, \quad i = 1, 2, \cdots, a_{ne} \tag{2.2.40}$$

$$\lambda_{ik} \neq 0, \quad i = 1, 2, \cdots, a_{ne} \tag{2.2.41}$$

$$h_{ki} \leq 0, \quad i = 1, 2, \cdots, a_{ni} \tag{2.2.42}$$

$$\mu_{ik} h_{ki} = 0, \quad i = 1, 2, \cdots, a_{ni} \tag{2.2.43}$$

$$\mu_{ik} \geq 0, \quad i = 1, 2, \cdots, a_{ni} \tag{2.2.44}$$

Kuhn-Tucker conditions are necessary conditions to ensure a relative minimum (or maximum) for convex programming problems [15, 21, 38, 71, 72].

It is observed from the KKT Complementary Slackness Condition, seen in (2.2.43) and (2.2.44), that: If μ_{ik} equals zero, h_{ki} is non zero. Therefore, the constraint, as said before, is not binding (The solution is within the feasible region). On the other hand, if μ_{ik} is non zero, the constraint is binding (The solution point is on the constraint). Then, the value of h_{ki} is zero. The Lagrangian Multiplier also indicates the sensitivity of the Lagrangian function (and hence the objective function) to changes in the respectively constraint [15, 71].

In order to minimise the Lagrangian function in (2.2.33) whilst satisfying KKT conditions, optimisation methods need to be applied.

2.3 Optimisation Methods for Power Systems

Optimisation problems can be divided in a variety of distinct categories based on their formulations and the types of the objective functions, state variables, and constraints. Deterministic optimisation problems are categorised by their type of

variables: (i) Continuous (ii) Discrete (iii) Mixed integer variables [73]. The OPF problem generally contains only continuous variables but can also contain mixed integer variables (e.g. if the objective function is a piece-wise cost function or in case of transformer tap changer ratios). However, these integer variables and their ensuing discrete functions can be approximated as continuous during the solution process [74]. Thus, the ensuing optimisation problem can be solved considering only continuous functions and variables. Note that once the optimal point has been found, discrete variables must be adjusted to their closest step that meet the constraints.

In general, optimisation methods for power systems are classified in two basic groups [21, 75, 76, 77]:

1. Conventional optimisation methods
    (a) Unconstrained optimisation approaches
    (b) Linear programming (LP)
    (c) Network flow programming (NFP)
    (d) Nonlinear programming (NLP)
    (e) Quadratic programming (QP)
    (f) Newton's Method - Hessian
    (g) Mixed integer programming (MIP)
    (h) Interior point (IP) methods.
2. Intelligence search methods
    (a) Neural network (NN)
    (b) Evolutionary algorithms (EAs)
    (c) Tabu search (TS)
    (d) Particle swarm optimisation (PSO).

This section aims to show the wide variety of powerful methods for solving OPF and SCOPF. However, it is worth to highlight that choosing a solution method depends on the type of the problem. Since the OPF and SCOPF in general and

specifically for Hybrid AC/DC grids correspond to a non-convex, non-linear optimisation problem, not all the methods from the list above are equally applicable without any approximation and simplifications. One of the goals of this thesis is to solve the OPF and SCOPF problems in their general form and therefore, subsections 2.3.1 and 2.3.2 are only a general description of the methods in the list above for the sake of completeness, whereas subsections 2.4.1, 2.4.2 and 2.4.3 describe in more detail the specific computational resources and solvers employed in this thesis to solve the nonlinear OPF (and SCOPF) problem with continuous variables.

2.3.1 Conventional Methods

Unconstrained optimisation Approaches

Unconstrained optimisation approaches are the ones whose aim is to minimise or maximise an objective function, but they are not subject to any equality or inequality constraints. These types of problems are the basis of the constrained optimisation algorithms. In particular, most of the constrained optimisation problems in power system operation can be converted into unconstrained optimisation problems. The major unconstrained optimisation approaches that are used in power system operation are the gradient method, line search, Lagrange multiplier method, Newton-Raphson optimisation, trust-region optimisation, quasi-Newton method, double dog-leg optimisation and conjugate gradient optimisation [15, 21, 71].

Linear Programming

Non-linear power system optimisation problems use Linear programming (LP)-based techniques to linearise their objective functions and constraints. The simplex method is known to be quite effective for solving LP problems. Several advantages have been seen when LP approach is used. Firstly, it is reliable, especially in regard to the convergence properties. Secondly, it can quickly identify infeasibility. Thirdly, it accommodates a large variety of power system operating limits, including the very important contingency constraints. On the other hand, some disadvantages of LP techniques are: An inaccurate evaluation of system losses and insufficient ability to

find an exact solution compared with an accurate non-linear power system model. However, a large number of practical applications have shown that LP-based solutions generally meet the requirements of engineering precision [21, 71]. Thus, LP is widely used to solve power system operation problems such as security-constrained economic dispatch, optimal power flow and steady-state security Regions [15].

Network Flow Programming

Network flow programming (NFP) is a special form of LP. NFP was first applied to solve optimisation problems in power systems in the 1980s. The early applications of NFP were mainly on a linear model. Recently, nonlinear convex NFP has been used in power system optimisation problems. NFP-based algorithms have the features of fast speed and simple calculation. These methods are efficient for solving simplified OPF problems such as security-constrained economic dispatch, multiarea systems economic dispatch, and optimal reconfiguration of an electric distribution network. However, by being an LP algorithm they still suffer from the same disadvantages as traditional LP techniques [15, 21, 75, 76, 77].

Nonlinear Programming

Nonlinear programming (NLP)-based techniques can easily handle power system operation problems such as the OPF problem with their non-linear objective and constraint functions. Firstly, the direction of the iterative search towards the solution is obtained by getting the first partial derivatives of the equations. Therefore, these methods are referred to as first-order methods, an example being the generalised reduced gradient (GRG) method. Higher accuracy, regardless of the initial search point, is a characteristic of NLP methods compared to LP-based approach. Nevertheless, a slow convergent rate may occur because of zigzagging in the search direction.[15, 21, 71, 77]

Quadratic Programming

NLP include Quadratic programming (QP) methods. The main difference between LP and QP optimisation problems is made by the definition of the objective function

formulation: LP can handle only linear objective functions, while in QP the objective function is quadratic and the constraints are in linear form. The LP objective function can be seen as a simplification of the QP objective function. Therefore, any QP formulation can easily be transformed into an LP formulation. However, the actual solution processes for both LP and QP are distinctly different. Just like NLP, one main advantage of QP over LP approaches is a higher accuracy. Since the most-used objective function in power system optimisation is the generator cost function, which generally is a quadratic, QP has a special mention in this classification. Thus, there is no simplification for such an objective function for power system optimisation problem solved by QP [21, 77].

Newton's Method - Hessian

The Newton–Raphson optimisation is also called Hessian matrix method. Using the second order Taylor series expansion, the objective function can be approximated. Therefore, it requires the computation of the second-order partial derivatives of the power-flow equations and other constraints (i.e. the Hessian matrix). For this method, KKT conditions are the necessary to achieve optimality. As one convergence advantage, the Hessian matrix $H(x)$ will be constant if the original non-linear objective function and their constraints are quadratic functions (e.g. Typical cost function). The disadvantage is that it needs to compute the inverse of the Hessian matrix, which leads to expensive memory and calculation burden. If suitable approximations to the Hessian can be found, quadratic and linear methods can be quite powerful [21, 77].

The (dual) quasi-Newton method uses the gradient, and does not need to compute second-order derivatives because they are approximated. Newton-type methods (as opposed to quasi-Newton methods) calculate the Hessian directly and proceed in a direction of descent to locate the minimum after a number of iterations. Calculating $H(x)$ numerically involves a large amount of computations. It works well for medium to moderately large optimisation problems where the objective function and the gradient are much faster to compute than the Hessian [78].

Mixed Integer Programming

The OPF and SCOPF can also be formulated as a mixed-integer programming (MIP) optimisation problem with integer variables such as shunt reactors or capacitors, step transformer tap ratios, and generation units on or off status. MIP is extremely demanding of computer resources and the number of discrete variables is an important indicator of how difficult an MIP will be to solve. MIP methods that are used to solve OPF and SCOPF problems include the recursive MIP technique using an approximation method and the branch-and-bound (B&B) method, which is a typical method for integer programming. A decomposition technique is generally adopted to decompose the MIP problem into a continuous problem and an integer problem. Decomposition methods such as Benders decomposition method (BDM) can greatly improve the efficiency in solving a large-scale network by reducing the dimensions of the individual subproblems. The results show a significant reduction in the number of iterations, required computation time, and memory space. In addition, decomposition allows the application of a separate method for the solution of each subproblem, which makes the approach very attractive. MIP can be used to solve the unit commitment, OPF, as well as optimal reconfiguration of the electric distribution network. One mayor drawback of MIP is the convergence, if the problem is highly non linear and there are too many integer variables, the solution may not converge. Therefore, the MIP is mostly used for Unit Commitment and DC OPF [15, 21, 75, 76, 77].

Interior Point Methods

The interior point (IP) method was originally used to solve LP problems. It is faster and is perhaps better than the conventional simplex algorithm in LP. However, basic IP methods, in general, suffer from bad initial conditions, termination, and optimality criteria and, in most cases, are unable to solve non-linear and quadratic objective functions. The extended quadratic interior point (EQIP) method can handle quadratic objective functions subject to linear and non-linear constraints. The improved quadratic interior point (IQIP) method features a general starting point (rather than a good point as in the former EQIP as well as general IP methods)

that is even faster than the EQIP optimisation scheme. Currently IP methods have improved drastically and are one of the most widely used methods for solving OPF and SCOPF. Some of their improvements offer great speed, accuracy, and convergence in solving multi-objective and multi-constraint optimisation problems. Depending on the size and non-linearity of the problem, new methods are also capable of finding a global solution of an interconnected system and a partitioned system for local optimisation [21, 77].

2.3.2 Intelligent Search Methods

Neural Network

The optimisation neural network (ONN) was first used to solve LP problems in 1986. Recently, ONN was extended to solve NLP problems. ONN is completely different from traditional optimisation methods. It changes the solution of an optimisation problem into an equilibrium point (or equilibrium state) of a nonlinear dynamic system, and changes the optimal criterion into energy functions for dynamic systems. This method is well known for working with a parallel computational structure [15, 21, 75, 76, 77].

Evolutionary Algorithms

Natural evolution is a population-based optimisation process. The evolutionary algorithms (EAs) are different from the conventional optimisation methods, and they do not need to differentiate cost function and constraints. Theoretically, similarly to simulated annealing, EAs converge to the global optimum solution. EAs, including evolutionary programming (EP), evolutionary strategy (ES), and GA, are artificial intelligence methods for optimisation based on the mechanics of natural selection, such as mutation, recombination, reproduction, crossover, selection, and so on. Since EAs require all information to be included in the fitness function, it is very difficult to consider all OPF constraints. Thus, EAs are generally used to solve the classic economic dispatch and simplified versions of the OPF and SCOPF problem, as well as optimal reconfiguration of an electric distribution network[15, 21, 75, 76, 77].

Tabu Search

The Tabu search (TS) algorithm is mainly used for solving combinatorial optimisation problems. It is an iterative search algorithm, characterised by the use of a flexible memory. It is able to eliminate local minima and to search areas beyond a local minimum. The TS method is also mainly used to solve simplified OPF problems such as the unit commitment and reactive optimisation problems [79].

Particle Swarm optimisation

Particle swarm optimisation (PSO) is a swarm intelligence algorithm, inspired by the social dynamics and an emergent behaviour that arises in socially organised colonies. The PSO algorithm exploits a population of individuals to probe promising regions of the search space. In recent years, various PSO algorithms have been successfully applied in many power-engineering problems including OPF, however it is a very uncommon algorithm to be used in for electrical power systems [21, 77].

2.4 Computational Tools and Solvers for Power Systems Optimisation

Currently there are many software options for power system optimisation which contain one or more of the described Optimisation Methods from section 2.3. In this thesis the FubM will be implemented in Matpower, a software tool specifically designed for Power Systems Steady State Analysis and Optimisation, and to Aimms, a mathematical modelling tool for optimisation in general. Both software tools are widely known by researchers and the industry. Subsections 2.4.1 and 2.4.2 will briefly describe the software tools and then subsections 2.4.3, 2.4.4, 2.4.5 and 2.4.6 will describe their optimisation algorithms in detail.

2.4.1 Matpower and MIPS Method

Matpower is a software tool built in Matlab language for solving Power Flow and Optimal Power Flow problems. It is intended as a simulation tool for researchers,

educators and the industry. By being an open source code software tool, modifications to the algorithms and models can be done. Currently MATPOWER's director, lead developer and researcher is Professor Ray D. Zimmerman. The most updated version of the software can be found in [60] or at https://matpower.org [24].

Table 2.1 contains the optimisation algorithms that MATPOWER is able to use for the solution of AC OPF. Solvers marked with an asterisk presented their best performance in MATPOWER,and therefore the FUBM will be implemented for them.

Table 2.1: MATPOWER's Optimisation Solvers for AC OPF

Name	Description
MIPS*	MATPOWER's Interior Point Solver (Primal/Dual)
FMINCON*	MATLAB's Optimisation Toolbox
IPOPT* 3.11	Interior Point Method
KNITRO* 12.0	Artelys Knitro Optimisation Package
MINOPF	MINOS-based solver
PDIPM	Primal/Dual Interior Point Method
SDPOPF	Solver based on Semi-definite relaxation
TRALM	Trust Region Based Augmented Lagrangian Method

*Best performance solvers in MATPOWER

2.4.2 AIMMS Optimisation Software

AIMMS is a general-purpose modelling tool with an Integrated Development Environment (IDE) for formulating and solving optimisation problems as mathematical programming problems. It integrates a state of the art modelling language with a series of world class numerical solvers for linear, mixed-integer, and nonlinear programming such as baron, cplex, conopt, gurobi, knitro, path, snopt and xa. One of the most useful features of AIMMS is the capability of specifying and solving linear and nonlinear constraint-based optimization models. In addition, AIMMS is able to manage stochastic programming and robust optimization to include data uncertainty [80].

AIMMS environment allows to define the full optimisation problem using a com-

pact and rich notation available for procedural statements and symbolic constraints. AIMMS transforms the model to match with the selected solver structure. Furthermore, AIMMS also builds the Hessian and the Jacobian of the problem [81].

Table 2.2 contains the optimisation algorithms that AIMMS is able to use for the solution of NLP optimisation problems. Solvers marked with an asterisk presented their best performance in AIMMS, and therefore the FUBM will be implemented for them.

Table 2.2: AIMMS's NLP Optimisation Solvers

Name	Description
CONOPT* 4.0	Reduced Gradient Optimisation
IPOPT* 3.11	Interior Point Method
KNITRO* 12.0	Artelys Knitro Optimisation Package
MINOPF	MINOS-based solver
SNOPT	Sparse Nonlinear OPTimizer

*Best performance solvers in AIMMS

2.4.3 MATPOWER's MIPS Method

MATPOWER's Power System Analysis tool includes its own primal-dual interior point method implemented in pure-MATLAB code called MIPS (MATPOWER Interior Point Solver). MIPS has proven to be suitable for large scale systems with a high level of non-linearity. Currently it is used as MATPOWER's default solver for AC and DC OPF problems [24]. Before getting into details of MIPS formulation, it is worth to highlight that MATPOWER uses a specific notation for the calculation of partial derivatives of functions. For simplicity this notation is specified below and will be used later for the description of MIPS Algorithm.

MATPOWER's Notation

The following section covers MATPOWER's notation which is used as the main mathematical notation for formulating models and relevant optimisation problems in this thesis.

The First derivatives for a scalar function $f : \mathbb{R}^n \to \mathbb{R}$ of a real vector $\mathbf{x} = [x_1 \quad x_2 \quad \dots \quad x_n]^\top$ are expressed as (2.4.45).

$$f_{\mathbf{x}} = \frac{\partial f}{\partial \mathbf{x}} = \begin{bmatrix} \frac{\partial f}{\partial x_1} & \frac{\partial f}{\partial x_2} & \dots & \frac{\partial f}{\partial x_n} \end{bmatrix} \tag{2.4.45}$$

And similarly for the second partial derivatives the Hessian of f, is shown in (2.4.49).

$$f_{\mathbf{xx}} = \frac{\partial^2 f}{\partial \mathbf{x}^2} = \frac{\partial}{\partial \mathbf{x}} \left(\frac{\partial f}{\partial \mathbf{x}} \right)^\top = \begin{bmatrix} \frac{\partial^2 f}{\partial x_1^2} & \dots & \frac{\partial^2 f}{\partial x_1 x_n} \\ \vdots & \dots & \vdots \\ \frac{\partial^2 f}{\partial x_n x_1} & \dots & \frac{\partial^2 f}{\partial x_n^2} \end{bmatrix} \tag{2.4.46}$$

For a vector function $\mathbf{f} : \mathbb{R}^n \to \mathbb{R}^m$ of a vector $\mathbf{x}$, where

$$\mathbf{f}(\mathbf{x}) = [f_1(\mathbf{x}) \quad f_2(\mathbf{x}) \quad \dots \quad f_m(\mathbf{x})]^\top \tag{2.4.47}$$

the first derivatives form the Jacobian matrix, where row i is the transpose of the gradient of f_i are:

$$\mathbf{f}_{\mathbf{x}} = \frac{\partial \mathbf{f}}{\partial \mathbf{x}} = \begin{bmatrix} \frac{\partial f_1}{\partial x_1} & \dots & \frac{\partial f_1}{\partial x_n} \\ \vdots & \dots & \vdots \\ \frac{\partial f_n}{\partial x_1} & \dots & \frac{\partial f_n}{\partial x_n} \end{bmatrix} \tag{2.4.48}$$

In these derivations, the 3-dimensional set of second partial derivatives of the set of functions $\mathbf{f}$ will not be computed. Instead a matrix of partial derivatives will be formed by multiplying transposed of the Jacobian Matrix of the vector function by a vector of Lagrange multipliers $\boldsymbol{\lambda}$. Thus the Hessian notation will be as shown in (2.4.49)

$$\mathbf{f}_{\mathbf{xx}}(\boldsymbol{\lambda}) = \frac{\partial}{\partial \mathbf{x}} \left(\mathbf{f}_{\mathbf{x}}{}^\top \boldsymbol{\lambda} \right) \tag{2.4.49}$$

Since the entire formulation will be presented in matrix form, please note that $[\mathbf{A}]$ is used to denote a diagonal matrix with vector $\mathbf{A}$ on the diagonal and $\mathbf{e}$ is a vector of all ones.

MIPS Method

The deterministic solution of the OPF using MIPS can be achieved by following the optimisation theory presented in this chapter. For this approach, all the n_i inequality constraints are transformed into equality constraints using the barrier method from appendix A. In the method, all the boundaries from the inequality constraints are represented by a set of logarithmic functions times a perturbation parameter ζ, and a positive vector of slack variables $\mathbf{z}$. After this transformation the optimisation problem can be expressed as in (2.4.50) to (2.4.53)

$$\min_{\mathbf{x}} \quad f(\mathbf{x}) - \zeta \sum_{m=1}^{n_i} \ln(z_m) \tag{2.4.50}$$

subject to:

$$\mathbf{g}(\mathbf{x}) = \mathbf{0} \tag{2.4.51}$$

$$\mathbf{h}(\mathbf{x}) + \mathbf{z} = \mathbf{0} \tag{2.4.52}$$

$$\mathbf{z} > \mathbf{0} \tag{2.4.53}$$

As the parameter of perturbation ζ approaches zero, the solution to this problem approaches that of the original problem.

Thus, for a given value of ζ, the Lagrangian of the problem in equations (2.4.50) to (2.4.53) is expressed as in (2.4.54).

$$\mathcal{L}^{\zeta}(\mathbf{x}, \boldsymbol{\lambda}, \boldsymbol{\mu}, \mathbf{z}) = f(\mathbf{x}) + \boldsymbol{\lambda}^{\top}\mathbf{g}(\mathbf{x}) + \boldsymbol{\mu}^{\top}\mathbf{h}(\mathbf{x} + \mathbf{z}) - \zeta \sum_{m=1}^{n_i} \ln(z_m) \tag{2.4.54}$$

The partial derivatives of the Lagrangian with respect to each one of the variables are presented in (2.4.55) to (2.4.58).

$$\mathcal{L}^{\zeta}_{\mathbf{x}}(\mathbf{x}, \boldsymbol{\lambda}, \boldsymbol{\mu}, \mathbf{z}) = f_{\mathbf{x}} + \boldsymbol{\lambda}^{\top}\mathbf{g}_{\mathbf{x}} + \boldsymbol{\mu}^{\top}\mathbf{h}_{\mathbf{x}} \tag{2.4.55}$$

$$\mathcal{L}^{\zeta}_{\mathbf{z}}(\mathbf{x}, \boldsymbol{\lambda}, \boldsymbol{\mu}, \mathbf{z}) = \boldsymbol{\mu}^{\top} - \zeta {1_z}^{\top}[Z]^{-1} \tag{2.4.56}$$

$$\mathcal{L}^{\zeta}_{\boldsymbol{\lambda}}(\mathbf{x}, \boldsymbol{\lambda}, \boldsymbol{\mu}, \mathbf{z}) = \mathbf{g}^{\top}(\mathbf{x}) \tag{2.4.57}$$

$$\mathcal{L}^{\zeta}_{\boldsymbol{\mu}}(\mathbf{x}, \boldsymbol{\lambda}, \boldsymbol{\mu}, \mathbf{z}) = \mathbf{h}^{\top}(\mathbf{x}) + \mathbf{z}^{\top} \tag{2.4.58}$$

And the Hessian of the Lagrangian with respect to $\mathbf{x}$ in (2.4.59).

$$\mathcal{L}^{\zeta}_{\mathbf{xx}}\left(\mathbf{x}, \boldsymbol{\lambda}, \boldsymbol{\mu}, \mathbf{z}\right) = f_{\mathbf{xx}} + \mathbf{g}_{\mathbf{xx}}(\boldsymbol{\lambda}) + \mathbf{h}_{\mathbf{xx}}(\boldsymbol{\mu}) \tag{2.4.59}$$

MIPS First Order Optimality Conditions

As seen in subsection 2.2.2, in order to reach an optimum the Karush-Kuhn-Tucker optimality conditions need to be satisfied. The first order condition is satisfied by setting the first partial derivatives of the Lagrangian above to zero as shown in (2.4.60).

$$\mathbf{F}\left(\mathbf{x}, \boldsymbol{\lambda}, \boldsymbol{\mu}, \mathbf{z}\right) = 0 \tag{2.4.60}$$

$$\mathbf{z} > 0 \tag{2.4.61}$$

$$\boldsymbol{\mu} > 0 \tag{2.4.62}$$

where:

$$\mathbf{F}\left(\mathbf{x}, \boldsymbol{\lambda}, \boldsymbol{\mu}, \mathbf{z}\right) = \begin{bmatrix} \mathcal{L}^{\zeta}_{\mathbf{x}}{}^{\top} \\ [\boldsymbol{\mu}]\mathbf{z} - \zeta \mathbf{1}_{\mathbf{z}} \\ \mathbf{g}(\mathbf{x}) \\ \mathbf{h}(\mathbf{x}) + \mathbf{z} \end{bmatrix} = \begin{bmatrix} f_{\mathbf{x}}{}^{\top} + \mathbf{g}_{\mathbf{x}}{}^{\top}\boldsymbol{\lambda} + \mathbf{h}_{\mathbf{x}}{}^{\top}\boldsymbol{\mu} \\ [\boldsymbol{\mu}]\mathbf{z} - \zeta \mathbf{1}_{\mathbf{z}} \\ \mathbf{g}(\mathbf{x}) \\ \mathbf{h}(\mathbf{x}) + \mathbf{z} \end{bmatrix} \tag{2.4.63}$$

MIPS Newton Step

The MIPS method solves the Karush-Khun-Tucker first order optimality conditions using Newton's method. Where the changes in $\mathbf{x}$, $\mathbf{z}$, $\boldsymbol{\lambda}$ and $\boldsymbol{\mu}$ are calculated as presented in equations (2.4.64) and expanded in (2.4.65).

$$\begin{bmatrix} \mathbf{F}_{\mathbf{x}} & \mathbf{F}_{\mathbf{z}} & \mathbf{F}_{\lambda} & \mathbf{F}_{\mu} \end{bmatrix} \begin{bmatrix} \Delta\mathbf{x} \\ \Delta\mathbf{z} \\ \Delta\boldsymbol{\lambda} \\ \Delta\boldsymbol{\mu} \end{bmatrix} = -\mathbf{F}\left(\mathbf{x}, \boldsymbol{\lambda}, \boldsymbol{\mu}, \mathbf{z}\right) \tag{2.4.64}$$

$$\begin{bmatrix} \mathcal{L}^{\zeta}_{\mathbf{xx}} & 0 & \mathbf{g_x}^{\top} & \mathbf{h_x}^{\top} \\ 0 & [\boldsymbol{\mu}] & 0 & [\mathbf{z}] \\ \mathbf{g_x} & 0 & 0 & 0 \\ \mathbf{h_x} & I & 0 & 0 \end{bmatrix} \begin{bmatrix} \Delta\mathbf{x} \\ \Delta\mathbf{z} \\ \Delta\boldsymbol{\lambda} \\ \Delta\boldsymbol{\mu} \end{bmatrix} = - \begin{bmatrix} \mathcal{L}^{\zeta}_{\mathbf{x}}{}^{\top} \\ [\boldsymbol{\mu}]\mathbf{z} - \zeta\mathbf{1_z} \\ \mathbf{g}(\mathbf{x}) \\ \mathbf{h}(\mathbf{x}) + \mathbf{z} \end{bmatrix} \tag{2.4.65}$$

The set of equations in (2.4.65) can be simplified and reduced to a smaller set of equations by solving explicitly for $\Delta\mu$ in terms of Δz and for $\Delta\mathbf{z}$ in terms of $\Delta\mathbf{x}$. Equations (2.4.66) to (2.4.68) take the 2^{nd} row of (2.4.65) and solve for $\Delta\mu$.

$$[\boldsymbol{\mu}]\Delta\mathbf{z} + [\mathbf{z}]\Delta\boldsymbol{\mu} = -[\boldsymbol{\mu}]\mathbf{z} + \zeta\mathbf{1_z} \tag{2.4.66}$$

$$[\mathbf{z}]\Delta\boldsymbol{\mu} = -[\mathbf{z}]\boldsymbol{\mu} + \zeta\mathbf{1_z} - [\boldsymbol{\mu}]\Delta\mathbf{z} \tag{2.4.67}$$

$$\Delta\boldsymbol{\mu} = -\boldsymbol{\mu} + [\mathbf{z}]^{-1}\left(\zeta\mathbf{1_z} - [\boldsymbol{\mu}]\Delta\mathbf{z}\right) \tag{2.4.68}$$

Similarly, solving the 4^{th} row of (2.4.65) for $\Delta\mathbf{z}$ yields

$$\mathbf{h_x}\Delta\mathbf{x} + \Delta\mathbf{z} = -\mathbf{h}(\mathbf{x}) - \mathbf{z} \tag{2.4.69}$$

$$\Delta\mathbf{z} = -\mathbf{h}(\mathbf{x}) - \mathbf{z} - \mathbf{h_x}\Delta\mathbf{x} \tag{2.4.70}$$

Then, substituting (2.4.68) and (2.4.70) into the 1^{st} row of (2.4.65) results in:

$$\mathcal{L}^{\zeta}_{\mathbf{xx}}\Delta\mathbf{x} + \mathbf{g_x}^{\top}\Delta\boldsymbol{\lambda} + \mathbf{h_x}^{\top}\Delta\boldsymbol{\mu} = -\mathcal{L}^{\zeta}_{\mathbf{x}}{}^{\top} \tag{2.4.71}$$

$$\mathcal{L}^{\zeta}_{\mathbf{xx}}\Delta\mathbf{x} + \mathbf{g_x}^{\top}\Delta\boldsymbol{\lambda} + \mathbf{h_x}^{\top}\left(-\boldsymbol{\mu} + [\mathbf{z}]^{-1}\left(\zeta\mathbf{1_z} - [\boldsymbol{\mu}]\Delta\mathbf{z}\right)\right) = -\mathcal{L}^{\zeta}_{\mathbf{x}}{}^{\top} \tag{2.4.72}$$

$$\begin{aligned} &\mathcal{L}^{\zeta}_{\mathbf{xx}}\Delta\mathbf{x} + \mathbf{g_x}^{\top}\Delta\boldsymbol{\lambda} + \\ &\mathbf{h_x}^{\top}\left(-\boldsymbol{\mu} + [\mathbf{z}]^{-1}\left(\zeta\mathbf{1_z} - [\boldsymbol{\mu}]\left(-\mathbf{h}(\mathbf{x}) - \mathbf{z} - \mathbf{h_x}\Delta\mathbf{x}\right)\right)\right) = -\mathcal{L}^{\zeta}_{\mathbf{x}}{}^{\top} \end{aligned} \tag{2.4.73}$$

$$\begin{aligned} &\mathcal{L}^{\zeta}_{\mathbf{xx}}\Delta\mathbf{x} + \mathbf{g_x}^{\top}\Delta\boldsymbol{\lambda} - \mathbf{h_x}^{\top}\boldsymbol{\mu} + \mathbf{h_x}^{\top}[\mathbf{z}]^{-1}\zeta\mathbf{1_z} + \\ &\mathbf{h_x}^{\top}[\mathbf{z}]^{-1}[\boldsymbol{\mu}]\mathbf{h}(\mathbf{x}) + \mathbf{h_x}^{\top}[\mathbf{z}]^{-1}[\mathbf{z}]\boldsymbol{\mu} + \mathbf{h_x}^{\top}\mathbf{z}^{-1}[\boldsymbol{\mu}]\mathbf{h_x}\Delta\mathbf{x} = -\mathcal{L}^{\zeta}_{\mathbf{x}}{}^{\top} \end{aligned} \tag{2.4.74}$$

$$\begin{aligned} &\left(\mathcal{L}^{\zeta}_{\mathbf{xx}} + \mathbf{h_x}^{\top}[\mathbf{z}]^{-1}[\boldsymbol{\mu}]\mathbf{h_x}\right)\Delta\mathbf{x} + \mathbf{g_x}^{\top}\Delta\boldsymbol{\lambda} + \\ &\mathbf{h_x}^{\top}[\mathbf{z}]^{-1}\left(\zeta\mathbf{1_z} + [\boldsymbol{\mu}]\mathbf{h}(\mathbf{x})\right) = -\mathcal{L}^{\zeta}_{\mathbf{x}}{}^{\top} \end{aligned} \tag{2.4.75}$$

$$\mathbf{Mm}\Delta\mathbf{x} + \mathbf{g_x}^{\top}\Delta\boldsymbol{\lambda} = -\mathbf{Nn} \tag{2.4.76}$$

Where:

$$\mathbf{M_m} \equiv \mathcal{L}^{\zeta}_{\mathbf{xx}} + \mathbf{h_x}^{\top}[\mathbf{z}]^{-1}[\boldsymbol{\mu}]\mathbf{h_x} \tag{2.4.77}$$

and

$$\mathbf{N_n} \equiv \mathcal{L}^{\zeta}_{\mathbf{x}}{}^{\top} + \mathbf{h_x}^{\top}\mathbf{z}^{-1}\left(\zeta\mathbf{1_z} + [\boldsymbol{\mu}]\mathbf{h}(\mathbf{x})\right) \tag{2.4.78}$$

Combining (2.4.76) and the 3^{rd} row of (2.4.65) results in a system of equations of reduced size as shown in (2.4.79).

$$\begin{bmatrix} \mathbf{M_m} & \mathbf{g_x}^{\top} \\ \mathbf{g_x} & 0 \end{bmatrix} \begin{bmatrix} \Delta\mathbf{x} \\ \Delta\boldsymbol{\lambda} \end{bmatrix} = \begin{bmatrix} -\mathbf{N_n} \\ -\mathbf{g}(\mathbf{x}) \end{bmatrix} \tag{2.4.79}$$

The following steps are used by MIPS to complete the Newton update.

- Compute $\Delta\mathbf{X}$ and $\Delta\boldsymbol{\lambda}$ from (2.4.79).
- Compute $\Delta\boldsymbol{z}$ from (2.4.70).
- Compute $\Delta\boldsymbol{\mu}$ from (2.4.68).

Strict feasibility is maintained during the newton calculation by scaling the primal and dual variables by α_p and α_d respectively. Where these scale factors are computed as follows:

$$\alpha_p = min\left(\xi \min_{\Delta z_m < 0}\left(-\frac{z_m}{\Delta z_m}\right), 1\right) \tag{2.4.80}$$

$$\alpha_d = min\left(\xi \min_{\Delta \mu_m < 0}\left(-\frac{\mu_m}{\Delta \mu_m}\right), 1\right) \tag{2.4.81}$$

Thus, the updated variables are as follows:

$$\mathbf{x} \leftarrow \mathbf{x} + \alpha_p\Delta\mathbf{x} \tag{2.4.82}$$

$$\mathbf{z} \leftarrow \mathbf{z} + \alpha_p\Delta\mathbf{z} \tag{2.4.83}$$

$$\boldsymbol{\lambda} \leftarrow \boldsymbol{\lambda} + \alpha_p\Delta\boldsymbol{\lambda} \tag{2.4.84}$$

$$\boldsymbol{\mu} \leftarrow \boldsymbol{\mu} + \alpha_p\Delta\boldsymbol{\mu} \tag{2.4.85}$$

The parameter ξ is a constant scalar with a value slightly less than one. In MIPS, ξ is set to 0.99995. During the Newton iterations, the perturbation parameter ζ

must converge to zero in order to satisfy the first order optimality conditions of the original problem. After updating $\mathbf{z}$ and $\boldsymbol{\mu}$, MIPS updates ζ at each iteration as shown in (2.4.86). Where σ has a value between 0 to 1 and in MIPS it is set to 0.1.

$$\zeta \leftarrow \sigma \frac{\mathbf{z}^{\top}\boldsymbol{\mu}}{n_i} \tag{2.4.86}$$

2.4.4 Conopt v4.0

CONOPT is a solver for large-scale nonlinear optimisation (NLP) developed and maintained by ARKI Consulting and Development A/S in Bagsvaerd, Denmark. The solver uses a widely extended version of the already well known Generalised Reduced Gradient (GRG) method to achieve greater reliability and speed for models that present a large degree of non-linearity.

Within CONOPT's extensions to the GRG method, pre-processing phases, linear mode iterations, sequential linear programming and a sequential quadratic programming component makes CONOPT also efficient on simpler and mildly nonlinear models as well. CONOPT has a built-in logic to dynamically select the most appropriate method depending on the characteristics of the problem.

CONOPT formulation assumes that all variables are continuous and all constraints are smooth with smooth first derivatives. In addition, the solver considers a sparse Jacobian matrix. The Local optimum is obtained once CONOPT finds a local optimum which satisfies the traditional Karush-Kuhn-Tucker optimality conditions. The Hessian Matrix is needed for models with many degrees of freedom for an efficient solution since they can only be solved efficiently if second-order partial derivatives are available.

CONOPT strategy relies on finding a first feasible solution (particularly well suited for models with fewer degrees of freedom) and then find the local optimal operating point.

Algorithm Overview

CONOPT is designed to solve an optimisation problem of the form below (2.4.87).

$$\min_{\mathbf{x}} \quad f(\mathbf{x}) \tag{2.4.87}$$

subject to:

$$\mathbf{g}(\mathbf{x}) = \mathbf{L} \tag{2.4.88}$$

$$\mathbf{x}_{min} < \mathbf{x} < \mathbf{x}_{max} \tag{2.4.89}$$

where $\mathbf{x}$ is the vector of optimisation variables and $\mathbf{L}$ is a vector containing the equality and inequality right sides. Equation (2.4.88) contains the equality and inequality constraints. In AIMMS, the inequalities are converted into equalities, and therefore properly bounded slack variables $\mathbf{z}$ are added to the optimisation vector $\mathbf{x}$. In this case $\mathbf{g}$ represents the non-constant terms of the equality and inequality constraints. It follows that constant terms on the left hand side are moved to the right forming $\mathbf{L}$.

CONOPT modifications to the GRG algorithm are very extensive, therefore only a brief description of CONOPT's general algorithm is presented below. A much more dense description of it can be found in [82] and [83]. The key steps in CONOPT-GRG algorithm are:

1. Initialise and Find a feasible solution.
2. Compute the Jacobian of the constraints, $\mathbf{J}$.
3. Select a set of n basic variables $\mathbf{x}_b$, such that $\mathbf{B}$, the sub-matrix of basic column from the Jacobian $\mathbf{J}$, is non-singular. Factorize $\mathbf{B}$, and the remaining variables $\mathbf{x}_n$, are the nonbasic variables.
4. Solve $\mathbf{B}^\top \lambda = \partial f / \partial \mathbf{x}_b$ for the λ multipliers.
5. Compute the reduced gradient, $\mathbf{r} = \partial f / \partial \mathbf{x} - \mathbf{J}^\top \lambda$. By definition, $\mathbf{r}$ will be zero for the basic variables.
6. If $\mathbf{r}$ projected on the bounds is small, then stop. The current point is close to optimal.

7. Select the set of super basic variables $\mathbf{x}_s$, as a subset of the nonbasic variables that profitably can be changed, and find a search direction, $\mathbf{d}_s$, for the super basic variables based on $\mathbf{r}_s$ and possibly on some second order information.

8. Perform a line search along the direction $\mathbf{d}$. For each step, $\mathbf{x}_s$ is changed in the direction $\mathbf{d}_s$ and $\mathbf{x}_b$ is subsequently adjusted to satisfy $\mathbf{g}(\mathbf{x}_b, \mathbf{x_s}) = \mathbf{L}$ in a pseudo-Newton process using the factored $\mathbf{B}$ from step 3.

9. Repeat from step 2 until the optimal is achieved.

2.4.5 Knitro v12.0

Knitro is a C-package for solving nonlinear large scale optimisation problems. Knitro implements four state-of-the-art interior-point and active-set methods. Each algorithm possesses strong convergence properties and is coded for maximum efficiency and robustness. A general outline of the algorithms implemented in Knitro is shown below. Full description of them is described in [84].

Interior/Direct algorithm

The interior-point method replaces the nonlinear programming problem by a series of barrier subproblems controlled by a barrier parameter. Interior-point methods perform one or more minimisation steps on each barrier subproblem, then decrease the barrier parameter and repeat the process until the original problem has been solved to the desired accuracy. The Interior/Direct method computes iterations by solving the primal-dual KKT matrix using direct linear algebra. In order to obtain global convergence in the presence of non-convexity and Hessian or Jacobian singularities, the primary step may be replaced, under certain circumstances, by a safeguarding trust region step. If the method encounters difficulties, it may temporarily switch to the Interior/CG algorithm, described below.

Interior/CG algorithm

This method is related to the Interior/Direct algorithm. Contrary to the traditional interior-point approaches proposed in the literature, the primal-dual KKT system of

this algorithm is solved using a projected conjugate gradient iteration. A projection matrix is factorized and the conjugate gradient method is applied to approximately minimize a quadratic model of the barrier problem. The use of conjugate gradients on large-scale problems allows Knitro to utilise exact second derivatives without explicitly forming or storing the Hessian matrix. An incomplete Cholesky preconditioning matrix factorisation can be computed and applied during the conjugate gradient iterations for problems with equality and inequality constraints. This generally results in improved performances in terms of number of conjugate gradient iterations and CPU time [85, 86] .

Active Set algorithm

Active set methods take a quadratic model of the original problem and separate it in a sequence of subproblems to be solved. In contrast with interior-point methods, the algorithm seeks active inequalities and follows a more exterior path to the solution. A sequential linear-quadratic programming (SLQP) algorithm is implemented by Knitro, similar in nature to a sequential quadratic programming method but using linear programming subproblems to estimate the active set. This method may be preferable to interior-point algorithms when a cinitial point close to the solution can be provided; for example, when solving a sequence of related problems. Knitro can also "crossover" from an interior-point method and apply this method to provide highly accurate active set and sensitivity information[85].

Sequential Quadratic Programming (SQP) algorithm

The SQP method in Knitro is an active-set method that solves a sequence of quadratic programming (QP) subproblems to solve the problem. This method is primarily designed for small to medium scale problems with expensive function evaluations – for example, problems where the function evaluations involve performing expensive black-box simulations and/or derivatives are computed via finite-differencing. The SQP iteration is expensive since it involves solving a QP subproblem. However, it often converges in the fewest number of function/gradient evaluations, which is why this method is often preferable for situations where the

evaluations are the dominant cost of solving the model[85].

2.4.6 IPOPT v3.11

Interior Point Optimiser (IPOPT) is an open source software package for large-scale nonlinear optimisation. It can be used to solve general nonlinear programming problems as expressed as in equations (2.4.90) to (2.4.92).

$$\min_{\mathbf{x}} \quad f(\mathbf{x}) \tag{2.4.90}$$

subject to:

$$\mathbf{g}_L(\mathbf{x}) \leq \mathbf{g}(\mathbf{x}) \leq \mathbf{g}_U(\mathbf{x}) \tag{2.4.91}$$

$$\mathbf{x}_{min} \leq \mathbf{x} \leq \mathbf{x}_{max} \tag{2.4.92}$$

where $\mathbf{x}$ are the optimisation variables, f is the objective function, and $\mathbf{g}$ are the general nonlinear constraints with their respective upper and lower boundaries g_L and g_U respectively. Note that equality constraints of the form $\mathbf{g}(\mathbf{x}) = \mathbf{L}$ can be specified by setting $\mathbf{g_L} = \mathbf{L}$ and $\mathbf{g_U} = \mathbf{L}$.

The IPOPT algorithm is based on the primal-dual barrier method, solving a sequence of barrier problems. Thus, using the general barrier method from appendix A it transforms the inequality constraints of the problem presented in equations (2.4.90) to (2.4.92), into a set of equality constraints with their respective slack variables as shown in equations (2.4.93) to (2.4.96).

$$\min_{\mathbf{x}} \quad f(\mathbf{x}) - \zeta \sum_{m=1}^{n_i} \ln(z_m) \tag{2.4.93}$$

subject to:

$$\mathbf{g}(\mathbf{x}) = \mathbf{0} \tag{2.4.94}$$

$$\mathbf{h}(\mathbf{x}) + \mathbf{z} = \mathbf{0} \tag{2.4.95}$$

$$\mathbf{z} > \mathbf{0} \tag{2.4.96}$$

With a parameter of perturbation $\zeta > 0$, a local solution $\mathbf{x}^*_\zeta$ of this approximated problem can be found. As $\zeta \to 0$ the approximated solution may converge to the

optimal local solution $\mathbf{x}^*$ of the original problem. Thus, IPOPT solves a sequence of sub-optimisation problems where the tolerance ϵ^i is relaxed for an i^{th} iteration. Then, the sub-optimal solution $\mathbf{x}_\zeta^{*\{i\}}$ is used as a starting point for the next $i+1$ sub-problem. As the iterations continue, the sub-problem tolerance $\epsilon^i \to \epsilon$, and thus the original problem is solved.

For the primal dual approach in IPOPT, the KKT conditions are as shown in (2.4.97) to (2.4.98).

$$\Delta f(\mathbf{x}) + \Delta \mathbf{g}(\mathbf{x})\lambda - \mathbf{d_l} = 0 \tag{2.4.97}$$

$$\mathbf{g}(\mathbf{x}) = 0 \tag{2.4.98}$$

$$x d_l - \zeta = 0 \tag{2.4.99}$$

Where each dual variable d_l is defined as in (2.4.100).

$$d_l := \frac{\zeta}{x} \tag{2.4.100}$$

These KKT conditions will be the same conditions of the original problem when:

$$\zeta = 0, \quad \mathbf{x} \geq 0 \quad \text{and} \quad \frac{\zeta}{\mathbf{x}} \geq 0 \tag{2.4.101}$$

Then, the dual variables correspond to the multipliers for the bound constraints. The method is solved using Newton's approach. For $\zeta > 0$, $\mathbf{x}$ and $\mathbf{d_l}$ must satisfy the inequalities from (2.4.102)

$$\mathbf{x} > 0 \quad \text{and} \quad \mathbf{d_l} > 0 \tag{2.4.102}$$

Thus, they can only approach to zero as $\zeta \to 0$.

The IPOPT algorithm then can be described in the following general steps. The detailed IPOPT algorithm can be found in [87].

1. Choose a starting point for $(\mathbf{x}^0, \mathbf{d_l}^0, \boldsymbol{\lambda}^0)$ and ζ^0

2. Initialise the outer iteration counter $i \leftarrow 0$.

3. Determine the error tolerance ϵ_i

4. Obtain the approximate solution $(\mathbf{x}_\zeta^{*\{i\}}, \mathbf{d}_{\mathbf{l}_\zeta}^{*\{i\}}, \boldsymbol{\lambda}_\zeta^{*\{i\}})$.

5. Set the approximate solution as the new starting point.

6. Update the barrier parameter ζ and increase the counter $i = i + 1$.

7. Repeat from Step 3 until $\epsilon_i = \epsilon$ and $\zeta \approx 0$.

2.5 Reliability Contingency Ranking

From subsection 1.2.1 it is clear that the SCOPF shows a strong dependence of a reliable Contingency Filter (CF). As seen from [48] and [47] most CF techniques rank the EPS contingencies using a Severity Index (SI), or they rely on Lagrange multipliers for a relaxed preventive SCOPF solution. Even though the severity of the contingency is one of the main considerations for a reliable Contingency Filter, the probability of occurrence (of contingencies) is another important factor to consider. Thereby a contingency filter which ranks the contingency both by the order of their severity and by their respective probabilities of occurrence will be more reliable than a filter which only relies on severity indices. In [88], a Contingency Ranking method which considers both Reliability rates and the Severity Indices of the contingencies for the system is presented. This method preserves all the advantages of the traditional contingency ranking via SI whilst considering the probability of the contingency occurrence using the transmission lines reliability rates. The method is described in this section.

In [88], to rank the contingencies the *Reliability Performance Index* (RPI) is defined as a product of the Severity Index (or Performance Index) and the Probability of occurrence of a contingency. It is essentially the severity index weighted by the probability of occurrence of each contingency. The contingencies can be ranked for Thermal Limits violations which correspond to the loadability of the transmission lines, and for voltage violations. In this thesis, this specific contingency filter is used for SCOPF problems and therefore it is appropriate to describe the methodology for

calculating the RPIs in the subsequent sections by first defining the severity indices for thermal limit and voltage violations.

2.5.1 Performance Index: Loadability Limits

The performance index for branch loadability limits will indicate the severity of a k contingency based on the distributed power of the branch k over all the remaining $nl-1$ branches of the system during the post-contingency state [89, 90, 91]. Mathematically this index is expressed as in (2.5.103).

$$PI_{L_k}(P_{f_1}, P_{f_2}, \ldots, P_{f_{nl}}) = \sum_{i \in lines} w_i \left(\frac{P_{f_i}}{L_i}\right)^{\alpha} \tag{2.5.103}$$

where

- i is the line or branch number
- k is the line with contingency
- $w_i \in [0, 1]$ is the weight factor for the i line
- P_{f_i} is the active power flowing through the line i (post-contingency)
- L_i is the practical operational limit of the branch
- $\alpha > 1$.

For each k contingency scenario, equation (2.5.103) is calculated. Thus, for a system with nl number of lines there will be nl contingency scenarios, and each k line will have their corresponding PI_{L_k} Loadability Performance Index. The weight factor is selected according to the operational requirements of the grid. The use of α helps to avoid the so called masking effect in contingency ranking. This effect consists of wrongly ranking contingencies above ones that should be in the top of the rank [92].

2.5.2 Performance Index: Bus Voltage violations

The performance index for voltage violations yields a measure on the severity of a k contingency over the bus voltages limits (the voltage is out of bounds) [93]. For a

system with nb buses, this index is calculated as in (2.5.104):

$$PI_{v_k} = \sum_{b \in nb} w_{v_b} \left(\frac{|V_b^k| - |V_b^0|}{V_{b_{max}} - V_{b_{min}}} \right)^{\alpha} \tag{2.5.104}$$

where

- b is the bus number,
- $w_{v_b} \in [0, 1]$ weight factor for each bus,
- V_b^k voltage magnitude of bus b in post-contingency state,
- V_b^0 voltage magnitude of bus b in the pre-contingency state,
- $V_{b_{max}}$ & $V_{b_{min}}$ voltage upper and lower limits

Similarly there will be a PI_{v_k} for each contingency scenario.

2.5.3 Branch Probability States

Each branch in the power system has a probability to be connected (state up or 1) and a probability to be out of service (state down or 0), the transition between these states is known as the failure rate F_R and the Repair Rate R_R. Where a change from an up state to a down state is represented by F_R and the transition from a down state to an up state is represented by R_R [94]. According to [88], the probability state for a branch k to be on service is defined as in (2.5.105) and the probability of a branch to be out of service is defined as in (2.5.106). These steady state probabilities expressions are applicable irrespective of whether the system starts in the pre-contingency state (up) or the post-contingency state (down).

$$P_{1_k} = \frac{R_R}{R_R + F_R} \tag{2.5.105}$$

$$P_{0_k} = \frac{F_R}{F_R + R_R} \tag{2.5.106}$$

The branch probability state for a k contingency is defined as in (2.5.107)

$$P_{S_k} = P_{0_k} \prod_{\substack{i=1 \\ i \neq k}}^{nl} P_{1_i} \tag{2.5.107}$$

2.5.4 Reliability Performance Index

Considering the calculated state probabilities and performance indices for the *nl-1* states, the reliability performance indices are calculated as in (2.5.108) for thermal Violations, and in (2.5.109) for voltage violations. Thus both indices are encircling the severity of a contingency, whilst considering the reliability of the elements in the EPS.

$$RPI_{L_i} = P_{S_i} \times PI_{L_i} \quad \forall i \in lines \tag{2.5.108}$$

$$RPI_{v_i} = P_{S_i} \times PI_{v_i} \quad \forall i \in lines \tag{2.5.109}$$

Chapter Summary

This Chapter has introduced general concepts and theory of modelling electrical power systems for purposes of steady state analysis, and operational optimisation. First the Power Flow Problem was presented in section 2.1 which was shown it can be solved using Newton's Method for solving a system of non-linear equations iteratively. Meanwhile, traditional modelling of power balance equations, and branch power flows which are used to model the network is covered in detail. Modelling of MATPOWER's compact branch model is also described. Moreover, in section 2.2 the classic OPF and SCOPF problem formulations are as constrained non-linear optimisation problems. It is shown that the OPF problem formulation can be solved by converting the constrained problem into an equivalent non-constrained formulation by way of slack variables and constructing a Lagrangian function. This section is then followed by a comprehensive overview of optimisation methods applied to power systems covering both conventional as well as intelligent based approaches. Moreover, the specific power systems computational tools and solvers applied in this thesis are covered in the latter part of this chapter.

While MATPOWER's compact branch model is used later to explain the developed FUBM in Chapter 3, section 2.1 is used as a starting point to develop the Flexible Power Flow Algorithm in Chapter 4. Results from Chapters 3 and 4 in combination with sections 2.2, 2.2.1, and 2.3 are used as a benchmark to develop

the Flexible OPF for AC/DC Hybrid Grids, which is later presented in Chapter 5, where detailed description of the formulation as well as a comparison against the traditional approaches of OPF is shown. Similarly, in Chapter 6 the results from chapter 5 in combination with sections 2.2 and 2.5 are combined to develop the Flexible SCOPF for hybrid AC/DC grids. Thus it can be appreciated that all the theory covered in this chapter is addressed and referenced throughout this thesis.

Chapter 3

The Flexible Universal Branch Model

As discussed in subsection 1.2.3, there are two approaches for the solution of AC/DC grids, (i) the sequential approach, which normally relies on separating the AC and the DC grids and employ a sequential method for solving the AC and DC parts in a non simultaneous form (solving one after the other using internal loops), and (ii) the unified approach, which solves all equations simultaneously for fast and accurate results. Even though sequential methods can be easily integrated into existing AC analysis tools, their loops and linear convergence formulation reduces the calculation accuracy and computational efficiency. On the other hand, unified methods consider a quadratic convergence presenting better and faster results, however major modifications to existing AC analysis tools are required for their implementation for purposes of solving AC/DC grids. Additionally, regardless of the selected approach, if the traditional VSC model is used to represent the interface between the AC and the DC grids, both approaches separate the grid physically and additional coupling equations (i.e. to satisfy power balance between AC and DC sides of the interface) are needed. Moreover, all the different elements in the EPS have different features and there is a different model for each one of them for AC and DC grids. As a result, the equations per model and per grid (AC or DC) scale up according to the complexity of the system and the number of elements presented. Thus, for example, any power system analysis tool normally includes an extensive model library to

selectively be able to incorporate various EPS elements and accommodate different network types (AC or DC).

This Chapter presents a new Flexible Universal Branch Model (FUBM) formulation for solving steady state analysis of hybrid AC/DC grids[1]. The prowess of the new formulation is that it (i) provides a direct link between AC and DC parts of the grid allowing for solving the entire network within a unified frame of reference (not sequentially) and (ii) can realistically model any element within the AC/DC power grid, ranging from conventional AC and DC branches, Controlled Tap Transformers (CTT), Phase Shifter Transformers (PST), Static Compensators (STATCOM) and the Voltage Source Converter (VSC) by introducing additional control variables. Additionally, distinction between the AC and DC grid is not required thanks to the flexibility and high versatility of the model. Therefore, conventional AC-only Power Flow and OPF (and SCOPF) equations are used to solve hybrid AC/DC grids modelled based on FUBM. In other words, the ensuing problem formulation solves the entire network on one single frame of reference using the unified approach, thereby eliminating the need for solving the DC and AC parts of the network in sequence and without requiring major modifications for its implementation in existing AC analysis tools. One of the main advantages of the FUBM formulation is that it is highly adaptable to any network topology with any degree of complexity and hosting a variety of control elements. To this end, the model may accommodate any control variables associated with any control elements that are active over the course of the solution by extending the vector of state variables accordingly. Otherwise they will remain as fixed parameters. Thus, the new FUBM will maintain all the advantages and characteristics of the individual traditional models in a simpler, more compact, yet more flexible form.

The remainder of this Chapter is structured as follows: Section 3.1 introduces the FUBM model in detail. Subsection 3.1.1 illustrates how the model is able to simulate a wide variety of power system elements and additionally it shows the theoretical

[1]The FUBM model presented in this chapter have been published in the International Journal of Electrical Power and Energy Systems - ElSevier by the author of this thesis and his supervisors [28].

comparison between the VSC traditional model and FUBM approach when used to interface AC and DC nodes in an AC/DC hybrid grid. Furthermore, subsection 3.1.2 presents the detailed mathematical model for FUBM and modelling of hybrid EPS when using the FUBM approach is discussed in section 3.2. It particularly describes in detail the link between the AC and the DC grid. Additionally, subsection 3.2.1 introduces various modes of control for the FUBM and VSCs asserting a high degree of flexibility in the model.

3.1 The Flexible Universal Branch Model

The FUBM takes the classic π branch model in series with an ideal transformer, and merges it with the VSC model developed in [69]. The proposed FUBM model is shown in Fig. 3.1. With this arrangement, a wide variety of elements can be simulated to represent the versatile and flexible EPS of the future, not only in AC but also in DC networks. This results in a simple but powerful universal model that interacts seamlessly with all network elements and is also capable of simulating AC/DC networks in one single frame of reference. As stated above, the benefit of this particular seamless way of modelling would be both in versatility of the ensuing formulation in accommodating a variety of network elements both for AC and DC parts of the hybrid grid and as shall be seen later in scalability of the model. The FUBM formulation is capable of solving large-scale hybrid networks in any complexity and with a variety of different control elements to properly simulate the operation of such grids for purposes of operational planning and when an accurate estimation of network operational security is needed.

The FUBM thus provides a formidable tool for both power system analysts aiming for simulating the operation of hybrid AC/DC networks as well as developers of power system analysis software packages, and the wider power systems research community, for its relative simplicity as the FUBM formulation is based on AC network equations and does not require developing separate model libraries for several network elements.

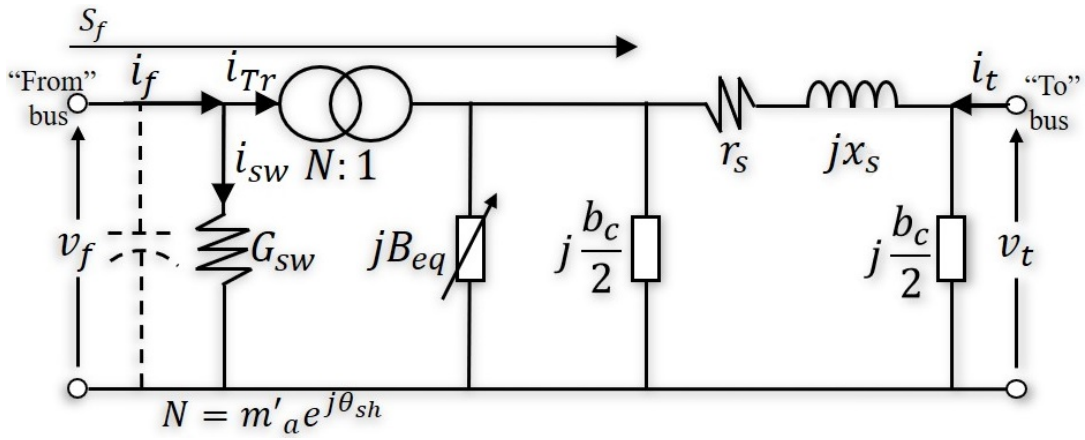

Figure 3.1: Flexible Hybrid AC/DC Universal Branch Model, adapted from[24]

3.1.1 Elements and In-Modelling

The FUBM contains one internal model (in-model) per transmission element of the EPS (one element at a time). These *in-models* share the internal components of the FUBM with each other, and therefore have distinct purposes depending on the desired element to be modeled. As such, the FUBM is capable of modelling a series of elements ranging from standard AC transmission lines to more complex control elements such as the CTT, PST, or VSC-based elements such as the STATCOM all within one single model.

AC and DC Branch in-model

At the most basic level and with no control elements present, the AC π *Branch in-model* uses three internal components namely, the series resistance r_s, and x_s representing the series reactance and b_c representing the standard capacitive charging of the AC transmission lines. On the other hand, if a *DC Branch in-model* is required, the reactive elements of the *Branch in-model* will simply be set to a value of "zero" and the r_s will be the resistance of the DC line.

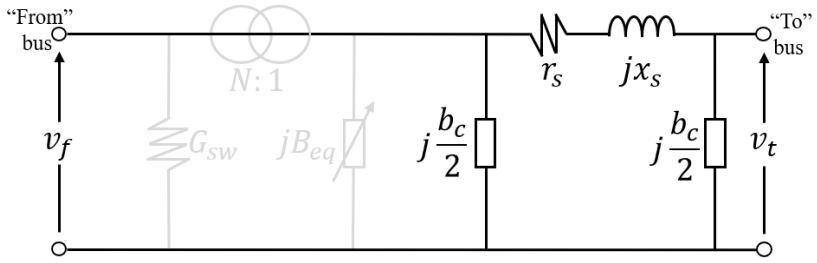

Figure 3.2: AC Branch in-model

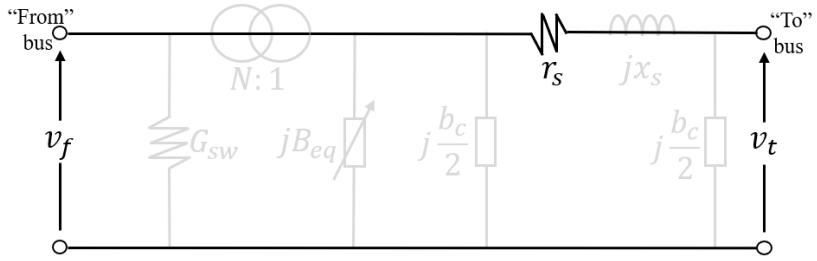

Figure 3.3: DC Branch in-model

Transformer in-model

For the *Transformer in-model*, the fixed parameters r_s and x_s represent its resistance and inductance respectively. The transformer's tap is defined by a complex tap ratio, N, which can be used to model CTT and PST as appropriate. The complex tap ratio is shown in (3.1.1), and in (3.1.2) KVL is applied to the in-model. For both elements, the variable m'_a will represent the magnitude of the complex tap ratio which is meant to represent the tap changer ratio of the CTTs. Similarly, if the *Transformer in-model* is meant to model a PSTs, θ_s represents the phase shifter angle of the PSTs. For a conventional AC EPS with no active control elements other than the synchronous generators (i.e. no CTTs or PSTs) only the *Branch in-model* is sufficient to model the entire EPS. However, if the AC EPS otherwise contains any control elements such as the PST and CTTs, they can be incorporated by activating the m'_a and θ_{sh} as optional control variables as deemed appropriate. Using these optional control variables within the OPF formulation would also provide the means to enforce realistic operational boundaries for the PST and CTT elements in form of limits on the variables and any constraints should a power flow control be needed.

$$N = m'_a e^{j\theta_{\text{sh}}} = k_2 m_a e^{j\theta_{\text{sh}}} \tag{3.1.1}$$

$$-v_t + (r_s + jx_s)\, i_t + \frac{v_f}{N} = 0 \tag{3.1.2}$$

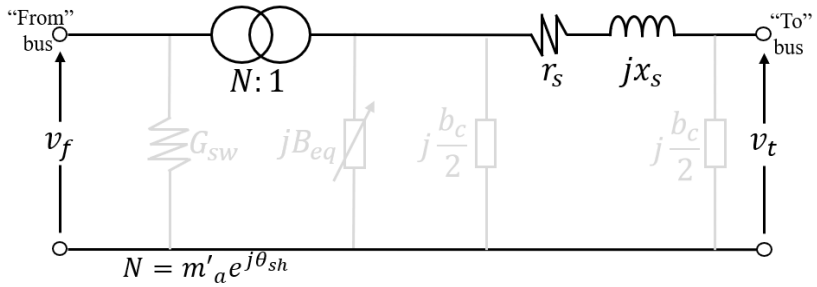

Figure 3.4: Transformer in-model

VSC in-model

The FUBM is designed to be as simple and universal as possible. Hence, it is desired that all the *in-models* share some characteristics with each other (either parameters or variables). For this reason, the usage of the traditional VSC model is not entirely suitable for this specific case. Instead, the *VSC in-model* within the FUBM is designed to be an advanced version of the VSC model presented and validated in [69], where the VSC was represented by a complex tap-changing transformer and a variable shunt susceptance. In the same vein, in the FUBM *VSC in-model* the variables of the complex tap, m'_a and θ_{sh} are meant to model the amplitude modulation index and the phase shifter action of the PWM control of the actual VSC, thereby modelling the independent active and reactive power control capabilities of the actual VSC. The main difference between the *VSC in-model* and the model developed in [69], is that the FUBM approach calculates the losses of the *VSC in-model* according to the detailed model (as stated in the IEC 62751-2 standard), and the model of the VSC presented in [69] makes an approximation of them. As a result, the *VSC in-model* of the FUBM maintains all the advantages of the traditional VSC model, while encompassing almost all of the variables and parameters that are shared between the other *in-models*.

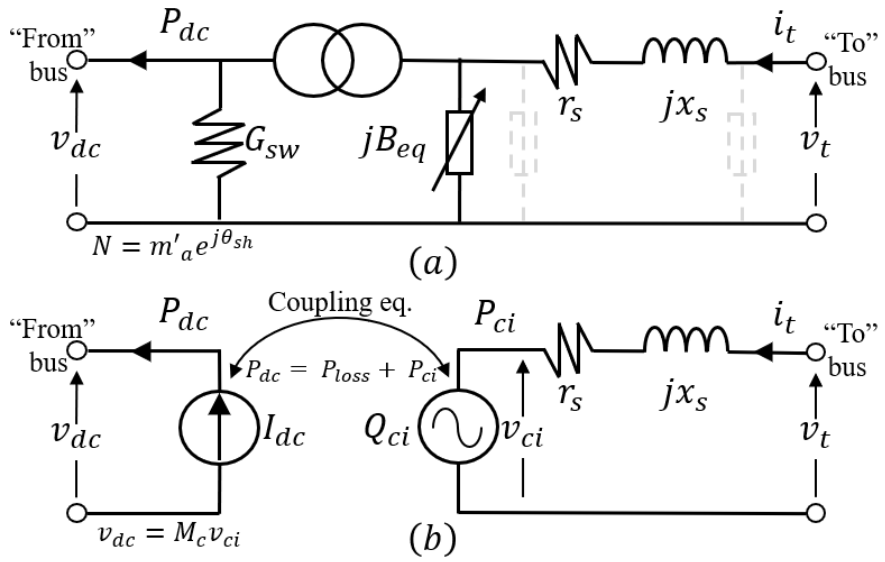

Figure 3.5: (a) FUBM VSC in-model, (b) Traditional VSC model

Figure 3.5 illustrates the comparison between the traditional VSC approach and the *VSC in-model* in terms of the model structure. It is noticeable that for both models, the inductive reactance jx_s and the series resistance r_s represent the magnetic interface and ohmic losses of the converter respectively. Moreover, table 3.1 summarises the control variables (and functions) that are used to model VSC operation for each model formulation. It is seen from Table 3.1 that both models essentially represent the VSC operation in equal detail albeit they are different in implementation, most noticeably, the link between AC and DC sides of the converter in the *VSC in-model* is an actual physical link whereas this link is represented through a power balance coupling equation in the Traditional model.

Table 3.1: FUBM VSC in-model and Traditional VSC model comparison

Function	FUBM VSC	Traditional VSC
Active Power Control	θ_{sh}	I_{dc}
AC side Reactive Control	m_a	M_c
DC side Voltage Control*b	B_{eq}	v_{dc}
Compensate AC Reactive Power*a	B_{eq}	Q_{ci}
VSC Switching losses	G_{sw}	P_{loss}
Interaction between AC and DC side	Physical link	Coupling equation

*a: Only Converters Type I [20, 62]

*b: Only Converters Type II and III [20, 62]

Moreover, as seen it Table 3.1, control over the active power flow is a shared feature between the *VSC in-model* and the traditional VSC model. The latter defines a current source I_{dc} as a variable to control the active power flow. The *VSC in-model*, on the other hand, uses the variable θ_{sh} for this action (just like it is done by the "PST in-model").

VSCs are also well known for their AC side reactive power control capabilities. For both approaches, this is done by modifying the modulation coefficient amplitude m_a. For the *VSC in-model*, just as in the *transformers in-model*, if reactive power control is required, the *VSC in-model* has the option to set either the AC side voltage (i.e. direct voltage control) or an AC side reactive power (i.e. direct reactive power control) to be controlled to a pre-specified value. In the latter case for direct reactive power control, this is done by introducing an additional constraint in the Power Flow (or OPF) formulation.

One of the most important applications of VSCs, especially in the context of modern power systems, is to provide a connection of two (or more) asynchronously operating and otherwise autonomous AC grids via a common DC link (or a multi-terminal DC link). The traditional VSC model represents this by separating the grids and using controlled power sources and coupling equations to simulate an

active power exchange between the AC grids through the common DC link. As seen in Fig. 3.5 (b), the compensation of the reactive power of the AC side "to" bus is realised by adding a small power balance constraint in the *ci* node, and Q_{ci} will adjust to meet the requirements of the system. In a similar way, the FUBM *VSC in-model* compensates the reactive power by using the shunt suceptance B_{eq}. In this case, instead of adding a power balance constraint in the *ci* node, the reactive power flow is monitored, and B_{eq} will be automatically adjusted within the OPF solution process to maintain zero reactive power injection to the DC link. In this thesis, this reactive power compensation at the DC node will be called the "*Zero Constraint*". Thus, just like in the traditional approach, the FUBM simulates the isolation of the AC and DC grids while maintaining the active power exchange.

In relation to calculating the converter's switching losses, the IEC 62751-2 standard recommends modelling the switching losses as a quadratic polynomial function of the VSC AC current [95]. Both the traditional and the FUBM model follow this recommendation. For the traditional model, the losses are calculated as shown in (3.1.3). On the other hand, the *VSC in-model* models the switching losses by introducing a variable in the model namely, G_{sw} which correspond to the switching losses of the VSC for a specified DC voltage (i.e. v_{dc}). This is shown in equation (3.1.4).

Knowing that in essence both models should calculate the same amount of switching losses, the loss model for the *VSC in-model* can be expressed by equation (3.1.3) and (3.1.4) to give (3.1.5).

$$-P_{loss} + \gamma i_t^2 + \beta i_t + \alpha = 0 \tag{3.1.3}$$

$$P_{loss} = v_{dc} i_{sw} = v_{dc}^2 G_{sw} \tag{3.1.4}$$

$$-v_{dc}^2 G_{sw} + \gamma i_t^2 + \beta i_t + \alpha = 0 \tag{3.1.5}$$

As can be seen from both, the power loss equations above, and the Fig 3.5, the interface between the AC side and the DC side is modelled by either adding a coupling equation for the traditional model, or through a physical link for the *VSC in-model* in the FUBM. From the perspective of the FUBM, the balance between AC and DC sides of the converter is maintained automatically since the

nodal active power injection at node "from" (in this case representing the DC side of the converter) in Fig 3.5(a) will simply be the the active power from the AC network minus the converter losses, which matches the coupling equation used by the traditional model seen in (3.1.6). This is why mathematically there is virtually no distinction between AC and DC sides of the converter when modelled using FUBM as the reactive power exchange is maintained at zero at the DC side by satisfying the *Zero constraint* and as seen above the active power exchange is also satisfied automatically.

$$P_{dc} = P_{ci} - P_{loss} \tag{3.1.6}$$

There are mainly three operational limits for any VSC as seen in Figure 3.6, which represent the constraints that both the Traditional VSC and the *VSC in-model* in FUBM should satisfy.

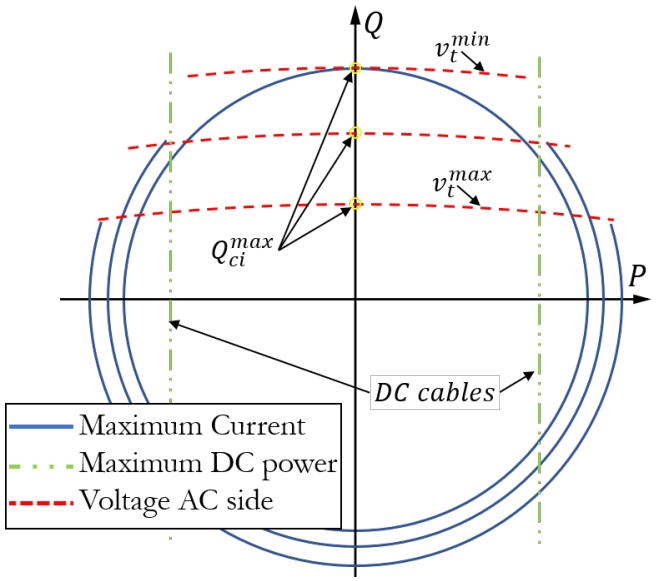

Figure 3.6: VSC Operational Limits, Modified from [96]

The first constraint is the maximum current through the switching devices (i.e. IGBTs). It can be appreciated in Fig 3.6 as an MVA circle in the power plane where maximum current and actual AC voltage are multiplied. If the AC voltage decreases so will the MVA capability [96]. The constraint is expressed mathematically in (3.1.7).

$$P_t^2 + Q_t^2 \leq (v_t i_t^{max})^2 \tag{3.1.7}$$

The second constraint is the reactive power compensation limit Q_{ci} which is mainly dependent on the voltage difference between the AC and the DC voltage. From Figure 3.6, it is noticeable that the maximum reactive power is not a fixed value, therefore its limit is expressed as a constraint in (3.1.8) for the traditional model, and in (3.1.9) for the *VSC in-model* [96][97]. In (3.1.9), B_{eq}^{max} is calculated as shown in (3.1.10). Since, x_s is essentially a constant parameter, both equations (3.1.8) and (3.1.10) essentially show that Q_{ci}^{max} and B_{eq}^{max} represent the same maximum reactive power operational limit in their respective models. Additionally in Fig. 3.6, it is clear that lower limit for the reactive power is automatically constrained by (3.1.7).

$$Q_{ci}^{max} = \frac{v_{ci}|v_t| - |v_t|^2}{x_s} \quad \text{Where:} \quad v_{ci} = \frac{v_{dc}}{k_2 M_c} \tag{3.1.8}$$

$$Q_{B_{eq}}^{max} = v_{ci}^2 B_{eq}^{max} = \frac{v_{ci}|v_t| - |v_t|^2}{x_s} \tag{3.1.9}$$

$$B_{eq}^{max} = \frac{v_{ci}|v_t| - |v_t|^2}{v_{ci}^2 x_s} \quad \text{Where:} \quad v_{ci} = \frac{v_{dc}}{k_2 m_a} \tag{3.1.10}$$

The third constraint is the maximum DC current through the DC cable. If the rate of the cable is smaller than the rate of the VSC it may limit the maximum active power transfer to the DC grid. This constraint is automatically added to the optimisation problem by adding the thermal limits of the DC lines.

After the theoretical comparison between the VSC Traditional model and the *VSC in-model* in the FUBM it is clear that both approaches keep the same amount of variables and constraints and as a result, the latter does not introduce any additional computational burden when simulating VSCs. It is also clear that in the FUBM approach, there is the advantage of modelling the VSC through a unified frame of reference as there is not need for introducing the additional power balance coupling constraints to model the balance between AC and DC sides of the converter.

STATCOM in-model

The FUBM is also capable of modelling STATCOMs explicitly. Unlike other simpler approaches which model the STATCOM as a controllable voltage source, the *STATCOMs in-model* is a more accurate representation of the device. This is achieved by making use of the *VSC in-model* with a fixed DC voltage as shown in Fig. 3.7. This STATCOM model was presented separately in an earlier publication [98] and is now brought together within the FUBM for the sake of completeness.

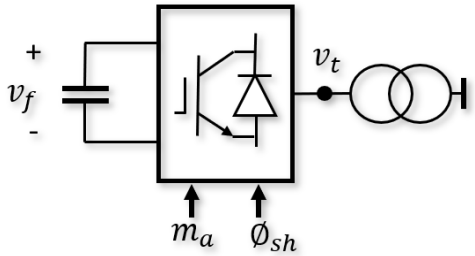

Figure 3.7: STATCOM in-model schematic representation using VSC

In this section, the theoretical underpinnings of all the *in-models* within the FUBM have been described. The selection of a specific *in-model*, and whether any of them are used to exert any control actions within the EPS, is done automatically by activating the appropriate state and control variables (i.e. the *in-model* settings) pertaining to the specific in-models as shown in table 3.2. Notice that the k_2 parameter will depend on the type of the VSC to model - this variable can be used to accommodate any VSC type from normal two-level converters to modular multi-level converters if needs be. For a two-level VSC, the k_2 value will be $\sqrt{3}/2$.

Combined *in-models*

Additional various elements in the EPS may also be modelled using different combinations of the described *in-models* above. In this section, as representative examples, two distinct controller elements are modelled using the FUBM in-models. It goes without saying that other components may also be modelled by combining the appropriate in-models. The first component to be modelled as a combination of in-models is the UPFC from [99], which can be easily modelled by setting two

Table 3.2: Settings for the desired in-Model

Parameter	Branch		CTT	PST	VSC	STATCOM
or Variable	DC	AC				
G_{sw}	0	0	0	0	$*^b$	$*^b$
B_{eq}	0	0	0	0	$*^b$	$*^b$
θ_{sh}	0	0	0	$*^b$	$*^b$	$*^b$
k_2	1	1	1	1	$*^a$	$*^a$
m_a	1	1	$*^b$	1	$*^b$	$*^b$
b_c	0	$*^a$	0	0	0	0
r_s	$*^a$	$*^a$	$*^a$	$*^a$	$*^a$	$*^a$
x_s	0	$*^a$	$*^a$	$*^a$	$*^a$	$*^a$
v_f	free	free	free	free	free	fixed

$*^a$: *in-model* parameter $*^b$: *in-model* active optimization variable

VSC in-models in a back to back configuration with a branch in parallel as shown in figure 3.8. Controls in each one of the *in-models* can be individually adjusted to accurately simulate the controllable reactive and active power of the UPFC as needed [100]. This approach will also simulate the switching losses of theVSCs in the UPFC taking advantage of the explicit VSC loss model, which was presented previously. Table 3.3 presents the settings each one of the in-models to accurately simulate the UPFC.

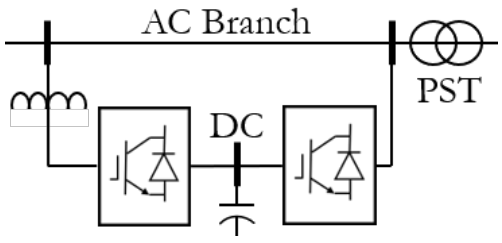

Figure 3.8: UPFC schematic representation using *in-models*

Meanwhile, since the FUBM does not create a distinction between the AC and the DC grid, combinations inside the DC grid could also be created. For example, the Bidirectional DC Converter from [101], could be represented as shown in Fig.

3.9. Where two *VSC in-models* are set in a back to back configuration, and each one is connected to a Low and High Voltage DC circuit. The controls over the B_{eq} and θ_{sh} are deactivated as shown in Table 3.3. Only both m_a are used for voltage control in both sides. This configuration allows to accurately represent the switching losses inside the Bidirectional DC converter using G_{sw} for both VSCs.

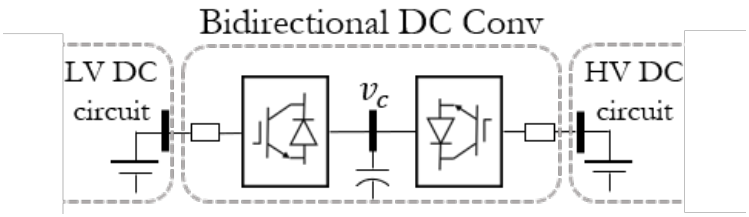

Figure 3.9: Bidirectional DC Converter schematic representation using *in-models*

Table 3.3: Combined in-Models Settings

Parameter	UPFC				Bidirectional DC Conv	
or Variable	AC branch	VSC 1	VSC 2	PST	VSC 1	VSC2
G_{sw}	0	$*^b$	$*^b$	0	$*^b$	$*^b$
B_{eq}	0	$*^b$	$*^b$	0	0	0
θ_{sh}	0	$*^b$	$*^b$	$*^b$	0	0
k_2	1	$*^a$	$*^a$	$*^a$	$*^a$	$*^a$
m_a	1	$*^b$	$*^b$	$*^b$	$*^b$	$*^b$
b_c	0	0	0	0	0	0
r_s	$*^a$	$*^a$	$*^a$	$*^a$	$*^a$	$*^a$
x_s	$*^a$	$*^a$	$*^a$	$*^a$	$*^a$	$*^a$
v_f	free	free	free	free	free	free

$*^a$: in-model parameter, $*^b$: in-model optimization variable

3.1.2 FUBM Nodal Power Equation

In this section, the power balance equations and nodal power injections for the FUBM model are expressed explicitly following MATPOWER's convention which can be found in [24]. However it is worth highlighting that the equations presented

in this section are explicitly defined for the FUBM as a new model following this convention.

By applying Kirchhoff's Law to the FUBM model in Fig. 3.1, the $[2 \times 2]$ model's admittance matrix Y_{br} can be obtained. This is shown in (3.1.11), (3.1.12) and (3.1.13). Notice that the sub index f and t in (3.1.12), represent the connection bus "from" and "to" respectively; e.g. y_{ff} will contain the sum of all the admittance elements connected to "from" bus. Also observe that for the *VSC in-model*, the v_f represents the DC voltage side v_{dc} and hence, the v_t represents the AC voltage side v_{ac}.

$$[I_{br}] = [Y_{br}] \times [V_{br}] \tag{3.1.11}$$

$$\begin{bmatrix} i_f \\ i_t \end{bmatrix} = \begin{bmatrix} y_{ff} & y_{ft} \\ y_{tf} & y_{tt} \end{bmatrix} \begin{bmatrix} v_f \\ v_t \end{bmatrix} = \begin{bmatrix} Y_{br} \end{bmatrix} \begin{bmatrix} v_f \\ v_t \end{bmatrix} \tag{3.1.12}$$

$$Y_{br} = \begin{bmatrix} G_{sw} + (y_s + j\frac{b_c}{2} + jB_{eq})\frac{1}{{m'_a}^2} & \frac{-y_s}{m'_a e^{-j\theta_{\text{sh}}}} \\ \frac{-y_s}{m'_a e^{j\theta_{\text{sh}}}} & y_s + j\frac{b_c}{2} \end{bmatrix} \tag{3.1.13}$$

Complex power flow though the FUBM can be calculated as in (3.1.14) in compact matrix form, which in turn would prodcue the nodal complex power injections in either sides of the FUBM shown in (3.1.15) and (3.1.16).

$$[S_{br}] = [V_{br}] \times [I^*_{br}] \tag{3.1.14}$$

$$S_f = [v_f][i^*_f] = [v_f][y_{ff}v_f + y_{ft}v_t]^* \tag{3.1.15}$$

$$S_t = [v_t][i^*_t] = [v_t][y_{ft}v_f + y_{tt}v_t]^* \tag{3.1.16}$$

From (3.1.15) and (3.1.16) the nodal active and reactive power injections are given for the FUBM in Fig. 3.1.

$$\begin{aligned} P_f &= Real\,(S_f) = Real\,([v_f][y_{ff}v_f + y_{ft}v_t]^*) \\ P_t &= Real\,(S_t) = Real\,([v_t][y_{ft}v_f + y_{tt}v_t]^*) \\ Q_f &= Imag\,(S_f) = Imag\,([v_f][y_{ff}v_f + y_{ft}v_t]^*) \\ Q_t &= Imag\,(S_t) = Imag\,([v_t][y_{ft}v_f + y_{tt}v_t]^*) \end{aligned} \tag{3.1.17}$$

3.2 Modelling Hybrid AC/DC EPS using FUBM

The most fundamental AC/DC grid is the point-to-point VSC -HVDC Transmission Link, shown schematically in Fig. 3.10(a). When incorporating this widely used configuration in conventional power flow formulations (as well as optimal power flow formulations) using the Traditional VSC model, the AC and an DC sides of the network inevitably would be separate as illustrated in Fig. 3.10(b). As a result, three sets of system equations have to be solved individually in order to find a solution for the whole AC/DC Grid, one for the AC side, one for the DC side and one for the interface between them (as the set of coupling equations representing the active power exchange between the AC and the DC grid for the two VSCs). Steady State analyses of AC grids are solved using vectors since the voltages are expressed as complex numbers. Furthermore, AC voltage angles are calculated with regards to one reference bus angle per isolated grid. DC grids on the other hand are analysed using scalars since only the voltage magnitude is relevant for their calculations. It follows that from a purely mathematical perspective, when modelling a hybrid AC/DC EPS using the traditional approach, the AC and DC counterparts are essentially modelled distinctly and also interfaced using the set of coupling equations to be able to simulate the power exchange in the HVDC link.

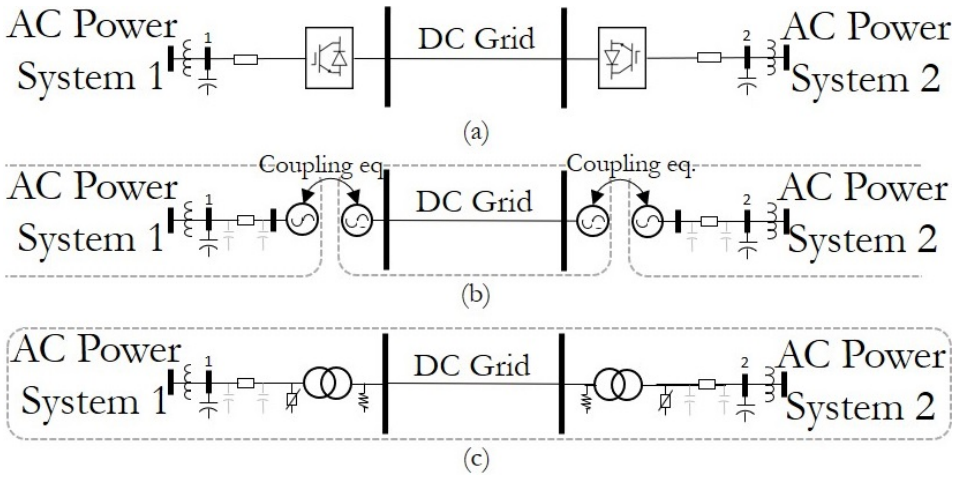

Figure 3.10: (a) Classic VSC-HVDC link, (b) Old-fashioned Link Searated grids generator representation, (c) New Unified Hybrid Grids Link with FUBM

Alternatively, as shown in Fig. 3.10(c), the whole hybrid AC/DC grid can be solved on one single frame of reference when modelled using the FUBM approach. As explained in Section 3.1.1, the *VSC in-model* compensates the reactive power of the AC side while seamlessly keeping the physical link between the AC and DC side. Thus, by taking advantage of the reactive power compensation from the *Zero Constraint*, only active power is exchanged though the DC link. For this reason, there is no need for any additional coupling equations to maintain power balance in the DC link, thereby removing the need for making any distinction between AC and DC counterparts nor for solving the AC and DC parts sequentially.

It follows from above that since FUBM models all elements in one single frame of reference both AC and DC variables are mathematically represented as complex phasors. Thus, essentially the scalar DC voltage magnitude can be represented as a complex phasor with "zero" imaginary part, or in other words with a voltage phase angle of "Zero" as shown in Fig. 3.11 (b). In this unified approach, just as in an any AC system, one reference bus phase angle is needed per isolated grid relative to which all the other nodal phase angles are calculated. Since the voltages in the AC side do have an imaginary part, and do not in the DC side, it is recommended to use a DC node as reference, as in Fig. 3.11 (c). Nevertheless, it should be noted that the reference angle, as the name implies, is only a reference. What really matters is the angular difference between the AC nodes that are interconnected with each other, because this angular difference will have an impact over the AC power flow. If the interconnected nodes have the same voltage angle or a voltage angle of zero, like in the DC side, it means that the DC power flow is purely dictated by the nodal voltage magnitude different in the DC side of the network. Consequently, if the reference angle is chosen in the AC side, it is possible that the DC voltage angles do have a non zero constant angle, as seen in 3.11 (d), which is maintained trough the entire DC grid (hence preserving the DC side characteristics).

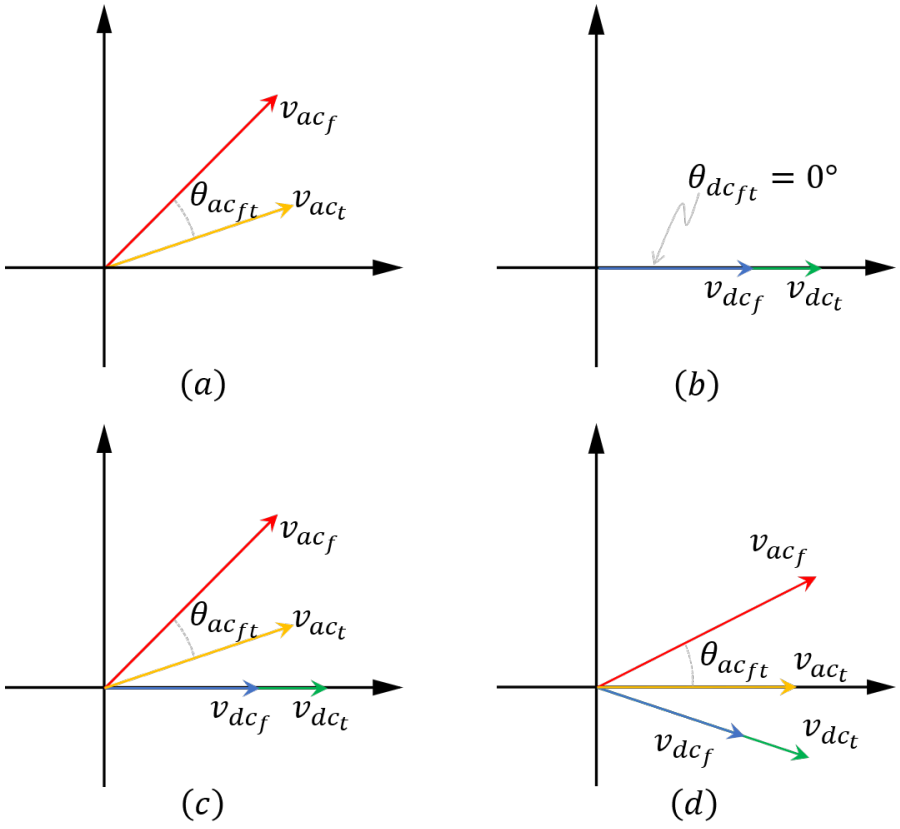

Figure 3.11: (a) AC Phasors, (b) DC Phasors, (c) AC/DC Phasors (V_{dc} as angle reference), (d) AC/DC Phasors (V_{ac_t} as angle reference)

To show mathematically a fully voltage dependence for power transfer in the FUBM for DC grids, first let the power flow "from" side and "to" side of the FUBM be developed as shown in the Appendix B.1, where the power can be expressed as:

$$\begin{aligned} S_f &= P_f + jQ_f \\ S_t &= P_t + jQ_t \end{aligned} \tag{3.2.18}$$

And after substituting (B.1.13), (B.1.14), (B.1.15) and (B.1.16) from the Appendix B.1 in (3.2.18), the power flow "from" side and "to" side can be expressed in rectangular form as such:

$$\begin{aligned} S_f =& R_{y_{ff}} v_{m_f}^2 + jI_{y_{ff}} v_{m_f}^2 + \\ & R_{y_{ft}} v_{m_f} v_{m_t} \cos\left(v_{a_f} - v_{a_t}\right) + I_{y_{ft}} v_{m_f} v_{m_t} \sin\left(v_{a_f} - v_{a_t}\right) + \\ & - jI_{y_{ft}} v_{m_f} v_{m_t} \cos\left(v_{a_f} - v_{a_t}\right) + jR_{y_{ft}} v_{m_f} v_{m_t} \sin\left(v_{a_f} - v_{a_t}\right) \end{aligned} \tag{3.2.19}$$

$$\begin{aligned} S_t =& R_{y_{tt}} v_{m_t}^2 - jI_{y_{tt}} v_{m_t}^2 + \\ & R_{y_{tf}} v_{m_t} v_{m_f} \cos\left(v_{a_t} - v_{a_f}\right) + I_{y_{tf}} v_{m_t} v_{m_f} \sin\left(v_{a_t} - v_{a_f}\right) \\ & - jI_{y_{tf}} v_{m_t} v_{m_f} \cos\left(v_{a_t} - v_{a_f}\right) + jR_{y_{tf}} v_{m_t} v_{m_f} \sin\left(v_{a_t} - v_{a_f}\right) \end{aligned} \tag{3.2.20}$$

Since in a DC grid, the DC voltage angles are the same and the DC branch admittance does not have any imaginary part, then the DC grid equations are simplified to:

$$S_f = R_{y_{ff}} v_{m_f}^2 + R_{y_{ft}} v_{m_f} v_{m_t} \tag{3.2.21}$$

$$S_t = R_{y_{tt}} v_{m_t}^2 + R_{y_{tf}} v_{m_t} v_{m_f} \tag{3.2.22}$$

As it can be appreciated from (3.2.21) and (3.2.22), when an DC element is modelled with the FUBM, the power transfer automatically becomes fully dependant on the voltage magnitude. Therefore, mathematically, the FUBM can be treated as a normal AC element, and accordingly AC power flow and AC OPF equations can be used to solve the hybrid AC/DC power grid.

3.2.1 VSC Control Modes in FUBM

Depending on the operational and control requirements of the hybrid EPS, the VSCs can be set to control the voltage, active and reactive power or all or a combination of both power and voltage control. This section presents different control settings/modes for the VSC that are commonly used in the industry and how the these control actions are mathematically incorporated in the FUBM.

In practice,VSCs have seven different control modes depending on their role in the hybrid EPS, they can be seen in Table 3.4 [62, 63].

Table 3.4: VSC Control Modes

Control Mode	Constraint 1	Constraint 2	VSC Control Type
1	θ_{sh}	v_{ac}	I
2	P_f	Q_{ac}	
3	P_f	v_{ac}	
4	v_{dc}	Q_{ac}	II
5	v_{dc}	v_{ac}	
6	v_{dc} droop	Q_{ac}	III
7	v_{dc} droop	v_{ac}	

TheVSCs are divided to three types and each one has a specific set of control modes. Moreover, there are two active control constraints per VSC control mode. Each constraint combination maintains either a constant power, a constant voltage, voltage droop characteristic or a combination of them. Each individual control constraint has a direct impact over the system feasible region. Consequently, a set of rules have to be followed to avoid any numerical ill-conditioning when implementing Multi-Terminal DC (MTDC) grids or HVDC-Links. In the interest of keeping the voltage of the DC grid within certain limits, there must be at least one VSC type #II or type #III for voltage regulation. If the VSC type #II is selected, there should not be more than one of them in each DC network, and all remaining converters in it must be type #I. Similarly, in an MTDC grid where nVSCs type #III are set, the remaining mVSCs must be type #I. Additionally, all VSC type #III require the addition of the voltage droop characteristic to the formulation of the VSC in-model. Figure 3.12 shows a couple of examples where a linear Power-Voltage control, a non-linear Power-Voltage control, and a linear Current-Voltage control are presented. Finally, when connecting wind farms, photovoltaic power plants, energy storage devices or passive networks via VSC , type #I converter must be used [62, 102]. Regardless of what type of VSC model is being used (either the traditional or the FUBM approach), both must follow the described rules.

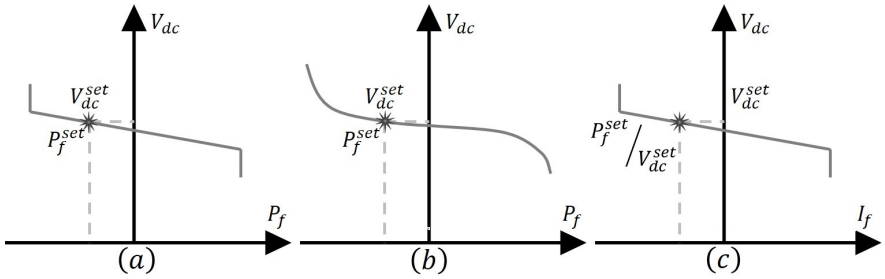

Figure 3.12: (a) $v_{dc} - P_f$ droop. (b) Adaptive droop. (c) $v_{dc} - i_f$ droop

As it was described in Section 3.1.1, Both VSC approaches (traditional and FUBM) should compensate the AC side reactive power of the grid. For an MTDC link with h VSC terminals, using the traditional modelling approach, all VSC models must do this compensation for all VSC terminals. On the other hand, using FUBM *VSC in-model* the *zero constraint* should only be met for $h-1$ VSC terminals. It follows that there will be no reactive power in the DC side of the remaining VSC terminal without the need for activating the *zero constraint* for that terminal. This mathematical advantage over the traditional VSC modelling approach is possible thanks to the unique physical link that the FUBM provides between the AC and the DC sides of the EPS.

The FUBM uses the converter types as identifiers to easily use this advantage. Thus, for MTDC links where one converter type #II has been selected for voltage regulation, only the remaining converters type #I will use the suceptance B_{eq} to compensate the reactive power and thus meet the *zero constraint*. Similarly, for MTDC links with n VSC type #III and m type #I, all m VSC type #I have to meet the *zero constraint*, but only $n-1$ VSC type #III have to meet this constraint. Again the last one will be automatically compensated without the need of any activation. Table 3.5 summarises the voltage regulation structure.

Table 3.5: VSCs structure on a MTDC Grid

MTDC Voltage Regulation Type	Max Number of VSC for Voltage Regulation	Min number of VSC for Zero Contraint	Max number of VSC in the MTDC Grid
Constant Voltage	1 VSC type #II	m VSC type #I	m+1
Voltage Droop Control	n VSC type #III	m VSC type #I and n-1 VSC type #III	m+n

Relating to the control modes, the FUBM is designed to incorporate each one of the aforementioned VSC control constraints individually as it is described in Section 3.1.1. As a result, the *VSC in-model* is not restricted by the pair of control constraints of each VSC control mode of Table 3.4. Therefore, it has the option to activate or deactivate the desired control over the modelled element depending on the operational requirements of the EPS and the specific requirements of the study.

Chapter Summary

In this Chapter, a the new FUBM for the steady state solution of hybrid AC/DC EPS has been presented. As seen in subsection 3.1.1, the proposed FUBM model is capable of seamlessly model a wide variety of network elements as *in-models*. Thanks to this unique ability, there is no need to analyse the system equations model by model and thereby avoiding the inclusion of separate model libraries for each elements for the AC and DC grids. All *in-models* share variables and parameters that, depending on the model type and desired behaviour, may or may not be activated. Meanwhile, as shown in section 3.2 when modelling AC/DC grids using the FUBM, there is no need for introducing additional coupling constraints to maintain power balance between the AC and DC side of the grid. From a purely mathematical perspective, there is no distinction between AC and DC counterparts. Thus, when using the FUBM same AC Power Flow equations can be used to solve the entire hybrid EPS while adding extra control and flexibility to it. In the next chapter, the FUBM is used to solve controlled Power Flows for AC/DC grids.

Chapter 4

Controlled Power Flow Analysis using FUBM

As discussed in Chapters 1 and 2, the core component of any steady state analysis problem formulation such as the OPF or the SCOPF for EPS is the formulation of the Power Flow problem. In Chapter 2 the two suggested strategies for the solution of the non-linear equations of hybrid AC/DC EPS, namely the Sequential and the Unified Power Flow, were presented in detail. While the unified approach solves the the AC and DC equations at the same time, in the sequential approach, the AC and DC systems are solved in a successive fashion.

Sequential methods are normally solved in three loop stages. The first internal loop solves the DC grid, with the second internal loop solving the AC grid, and then an external coupling loop matches the results. The full process is repeated until convergence is achieved. Even though sequential methods can be added as an extension of existing power flow software, they normally suffer from convergence problems simply because lack of convergence in one loop could lead to a knock-on effect on all the other loops. Meanwhile, they normally need a large number of loops to solve the problem due to their linear convergence, which is computationally inherently slow. Moreover their first order convergence feature reduces accuracy in their calculations. Unlike, sequential algorithms, unified power flow algorithms are considerably faster as they maintain a quadratic convergence and avoid having to solve internal iterative loops [62, 65]. The main disadvantage of the unified

algorithms in their current form comes from their implementation. Most existing power flow solvers used for solving the network in steady-state are based on solving AC-only EPS. It is therefore necessary to modify existing software to include power balance equations for the DC network as well as any models explicitly defined for AC/DC interface elements (e.g. converters such as VSC), and DC network elements to be able to solve AC/DC grids using a unified algorithm.

This chapter therefore uses the new FUBM developed in Chapter 3 for solving steady-state power flow problem for a hybrid AC/DC grid[1]. As seen in the previous chapter, since at its core, the FUBM, mathematically is inherently seen as an AC model, the same AC power balance equations can be used to formulate and solve the power flow problem for any hybrid AC/DC EPS. Moreover, using FUBM, the unified power flow algorithm can be used without the need to modifying existing AC-only simulation software to define explicitly DC-only and AC/DC interface elements since FUBM is capable of modelling these elements through implementation of its unique in-model formulation. Formulating and solving a hybrid AC/DC EPS using the FUBM will therefore allows for simple implementation of unified algorithms without major modifications of the core components of an AC-only simulation software, and at the same time preserves the superior quadratic convergence characteristics of unified methods.

Additionally, this Chapter introduces a new Flexible AC/DC Power Flow Algorithm (FPFA). It is based on the unified approach and is solved using Newton's Method. It is worth noticing that, even with the traditional *uncontrolled* power flow algorithm, hybrid AC/DC grids can still be solved if the FUBM is implemented, and the parameters of B_{eq} to meet the zero constraint are known. However, traditional Power Flow Analysis normally does not include any extra variables for either voltage or power control.

Normally in the conventional *uncontrolled* AC Power Flow problem, the phase shifter angle, θ_{sh}, of a Phase Shifter Transformer (PST), for instance, is treated as

[1]The Power Flow formulation using FUBM as well as the some of the test cases presented in this chapter have been published in the IEEE Industrial and Commercial Power Systems Europe (EEEIC / I&CPS Europe) by the author of this thesis and his supervisors [103].

simply a constant parameter (and not an additional state variable for the problem). Similarly, the tap changer ratio, m_a or N, of a Controlled Tap-Changing Transformers (CTT) may be treated as a fixed parameter. There are provisions for changing these parameters as initial conditions of the problem, which will undoubtedly produce different results for the same system, however since these are not treated as decision variables in the problem, there are no provisions for exerting active power regulation nor direct nodal voltage control through either element in a conventional *uncontrolled* AC power flow problem formulation. This limitation remains true even if these elements are modelled through FUBM but in the associated *in-models* for the PST and CTT the corresponding phase shfiter angle and tap changer ratios are still treated as fixed parameters - see table 3.2. Provisions of control requires additional state variables with which certain controls can be exerted as additional constraints.

Consequently, the new FPFA is designed to take advantage of the full control capabilities (in voltage and power) of the FUBM which were illustrated in detail in Chapter 3. Therefore, the proposed FPFA described in this chapter includes a flexible control where all the control variables of the FUBM introduced in the previous chapter, are added to the power flow formulation with which additional control on both power and voltage may be exerted in the system through power flow control elements such as the PSTs and CTTs as well as VSCs. It follows that in the FPFA formulation, the Jacobian matrix containing the first partial derivatives of the nodal power balance equations with respect to the state variables is extended to accommodate the additional control variables and the partial derivatives of their associated nodal mismatch equations when solving the system using Newton's method. In summary, the FPFA has a combination of fixed and variable controls to provide maximum flexibility for the solution.

The remainder of this Chapter is structured as follows: Section 4.1 describes the new FPFA in detail. Subsection 4.1.4 describes the implementation of the control features of the FUBM in the FPFA. Then Subsection 4.1.6 presents the extended Jacobian Matrix for Newton's method. A flowchart shows each step inside the FPFA, including the power losses correction of the VSC when they are used. Section

4.2 presents the test cases and their respective power flow simulations. Finally simulation results are discussed at the end of this chapter.

4.1 Flexible Power Flow Algorithm

4.1.1 Traditional AC Power Flow

From Section 2.1, in the traditional AC Power Flow Analysis, for each node, the sum of all nodal bus power injections $S_{b_{inj}}$ should be equal to the algebraic sum of the nodal loads S_d and generators power injections S_g. This is expressed in form of the nodal power balance equation g_{S_b} which is expressed as a function of the complex bus voltages V as shown in (4.1.1). Where the voltage angle V_a and the V_m are the state variables. In an EPS of nb buses, there are as many power balance equations , forming a system of complex non-linear equations as shown in (4.1.4). Where $\mathbf{g}_{S_b}$ represents a set of nb complex non-linear equations, and $\mathbf{V}$ is the vector of nb unknown complex state variables.

$$g_{S_b}(V) = S_{b_{inj}}(V) + S_d - S_g = 0 \tag{4.1.1}$$

$$\text{Where,} \qquad V = V_m e^{V_a} \tag{4.1.2}$$

$$\tag{4.1.3}$$

$$\mathbf{g}_{S_b}(\mathbf{V}) = 0 \quad \text{or} \quad \begin{cases} g_{S_{b1}}(V_{a_1}, V_{m_1}, \ldots, V_{a_{nb}}, V_{m_{nb}}) = 0, \\ g_{S_{b2}}(V_{a_1}, V_{m_1}, \ldots, V_{a_{nb}}, V_{m_{nb}}) = 0, \\ \vdots \\ g_{S_{bnb}}(V_{a_1}, V_{m_1}, \ldots, V_{a_{nb}}, V_{m_{nb}}) = 0, \end{cases} \tag{4.1.4}$$

The basic power flow problem involves the iterative solution of the system of non-linear equations shown in (4.1.4). As discussed in 2.1, Newton's Method is a highly used powerful method to solve these non-linear power balance equations.

4.1.2 FPFA Bus Categories

As seen in Section 2.1, for ease of formulating the power flow problem, it is typically the case that nodes (buses) are divided into different categories, depending on what initial conditions are known for each node. Such categorisation of nodes will then inform how the system of non-linear power balance equations, shown in (4.1.4) are constructed for the system. Similarly, for the FPFA the buses are divided into three distinct categories, however in this case, the PV nodes are for those nodes in which nodal voltage regulation (control) is available by the action of generators as well as any power controller elements modelled through FUBM that have voltage control capability, ie. the VSCs and the transformers with automatic taps (CTTs). Therefore, the bus categories in the FPFA can be divided as follows:

- **PQ**: These correspond to the conventional load (demand) buses. They do not have voltage regulation. For these nodes at the initiation of the power flow problem the nodal active and reactive power injections are known and as such their associated state variables are the are the nodal voltage magnitude, V_m, and the phase angle, V_a.

- **PV**: The nodal voltage magnitude, V_m is regulated to a pre-defined set-point by either a generator or a FUBM control element. For these types of nodes, the nodal active power is typically known and the nodal voltage magnitude is a known parameter rather than a state variable. The unknown variables are the voltage phase angle, V_a and the nodal reactive power injection (compensation), which is balanced by either a generator, or a FUBM element connected to the node).

- **Slack**: One bus in each electrical island is chosen as the island slack bus. This bus has a fixed voltage magnitude V_m and a set voltage phase angle, V_a, which will be used as a reference for all the nodal voltage phase angles in the island, hereby is also known as the reference bus. The unknown variables at this bus are then the nodal real and reactive power injections, which are then used to assign the real and reactive power at the slack generator.

The different bus types by their corresponding known and unknown variables are shown in table 4.1.

Table 4.1: FPFA Bus Categories

	P	Q	V_m	V_a
PQ	Known	Known	Unkown	Unkown
PV	Known	Unkown	Known	Unkown
Slack	Unkown	Unkown	Known	Known

4.1.3 Extended State Variables

As previously mentioned, the FPFA formulation is extended by FUBM *in-model* control variables as optional state variables, in order to model those categories of devices that can exert control over the system operation. In general, a non-linear equation system with fewer equations than unknowns is called underdetermined as it has infinitely many solutions, but it may also have no solution. In a balanced system of equations, each additional unknown variable provides an available degree of freedom, and each additional equation in the system restricts one degree of freedom. The critical case occurs when the number of equations and the number of state variables are equal. Therefore, in the FPFA for every optional control variable giving a degree of freedom, there exists a corresponding constraint removing a degree of freedom. Thus the expanded set of state variables, denoted by $\mathbf{x}$, and their corresponding non-linear mismatch constraints are showed in (4.1.5).

$$\mathbf{g}(\mathbf{x}) = \begin{bmatrix} \mathbf{g}_{P_b}^{\{i\}}(\mathbf{x}) = 0 \\ \mathbf{g}_{Q_b}^{\{i\}}(\mathbf{x}) = 0 \\ \mathbf{g}_{P_f}^{\{i\}}(\mathbf{x}) = 0 \\ \mathbf{g}_{Q_z}^{\{i\}}(\mathbf{x}) = 0 \\ \mathbf{g}_{V_f}^{\{i\}}(\mathbf{x}) = 0 \\ \mathbf{g}_{Q_t}^{\{i\}}(\mathbf{x}) = 0 \\ \mathbf{g}_{V_t}^{\{i\}}(\mathbf{x}) = 0 \\ \mathbf{g}_{P_{dp}}^{\{i\}}(\mathbf{x}) = 0 \end{bmatrix}, \mathbf{x} = \begin{bmatrix} \mathbf{V_a}^{\{i\}} & \forall i \in \boldsymbol{\mathcal{I}}_{pv} \cup \boldsymbol{\mathcal{I}}_{pq} \\ \mathbf{V_m}^{\{i\}} & \forall i \in \boldsymbol{\mathcal{I}}_{pq} \\ \boldsymbol{\theta}_{\mathbf{sh}}{}^{\{i\}} & \forall i \in \boldsymbol{\mathcal{I}}_{sh} \\ \mathbf{B_{eq}}^{\{i\}} & \forall i \in \boldsymbol{\mathcal{I}}_{Q_z} \\ \mathbf{B_{eq}}^{\{i\}} & \forall i \in \boldsymbol{\mathcal{I}}_{vscII} \\ \mathbf{m_a}^{\{i\}} & \forall i \in \boldsymbol{\mathcal{I}}_{V_t} \\ \mathbf{m_a}^{\{i\}} & \forall i \in \boldsymbol{\mathcal{I}}_{Q_t} \\ \boldsymbol{\theta}_{\mathbf{sh}}{}^{\{i\}} & \forall i \in \boldsymbol{\mathcal{I}}_{vscIII} \end{bmatrix} \tag{4.1.5}$$

Where $\mathbf{g}$ represents the full set of mismatch constraints - these are essentially used to extend the vector of nodal balance equations shown in (4.1.4. Additionally, the sets of bus indices $\boldsymbol{\mathcal{I}}_{ref}$, $\boldsymbol{\mathcal{I}}_{pv}$, $\boldsymbol{\mathcal{I}}_{pq}$ denote the reference, PV and PQ buses, respectively. The sets of element indices $\boldsymbol{\mathcal{I}}_{sh}$, $\boldsymbol{\mathcal{I}}_{Q_z}$, $\boldsymbol{\mathcal{I}}_{vscII}$, $\boldsymbol{\mathcal{I}}_{vscIII}$, $\boldsymbol{\mathcal{I}}_{V_t}$, $\boldsymbol{\mathcal{I}}_{Q_t}$, indicate the FUBM elements for active power control, zero constraint control, FUBM VSCs type #II for V_{dc} fixed control, FUBM VSC type #III for $V_{dc} - P_f$ droop control, FUBM elements for V_t nodal control and FUBM elements for Q_t power control.

4.1.4 Extended Mismatch Equations

This subsection describes in detail each one of the non-linear mismatch equations from (4.1.5) for the FPFA extended formulation. Mismatch equations $\mathbf{g}_{P_b}$, and $\mathbf{g}_{P_b}$ are basically the conventional nodal power balance equations which are required to solve any AC system - these equations are core to the traditional uncontrolled power flow problem. In addition to these, the FPFA contains additional constraints. The Zero Constraint Mismatch equation $\mathbf{g}_{Q_z}$ allows the algorithm to solve AC/DC systems. Finally, mismatch equations $\mathbf{g}_{P_f}$, $\mathbf{g}_{V_f}$, $\mathbf{g}_{Q_t}$, $\mathbf{g}_{V_t}$, and $\mathbf{g}_{P_{dp}}$, allow the system to be fully controllable in terms of power and voltage. Apart from the nodal power balance mismatch equations all the other constraints are optional and their activation will depend on the type of the EPS (i.e. whether it is purely AC, or AC/DC hybrid) and the types of elements included. In the sections following, all additional

constraints in form of mismatch equations are formulated for the FUBM in-models which were described in detail in the previous chapter.

Power Balance Mismatch Equation

The power balance equation system from (4.1.4) has been separated into its real and imaginary parts, as shown in (4.1.6) and (4.1.7), to have one real power balance equation for each unknown voltage phase angle V_a, and one imaginary power balance equation for each unknown nodal voltage magnitude V_m.

$$\mathbf{g}_{P_b}^{\{i\}} = Real\left(\mathbf{g}_{Sb}^{\{i\}}\right) \quad \forall i \in \boldsymbol{\mathcal{I}}_{pv} \cup \boldsymbol{\mathcal{I}}_{pq} \tag{4.1.6}$$

$$\mathbf{g}_{Q_b}^{\{i\}} = Imag\left(\mathbf{g}_{Sb}^{\{i\}}\right) \quad \forall i \in \boldsymbol{\mathcal{I}}_{pq} \tag{4.1.7}$$

In equations (4.1.6) and (4.1.7), the complex nodal power balance equations of (4.1.4) can be defined as the function of the vector of state variables $\mathbf{x}$, which can be written in matrix form as shown in (4.1.8):

$$\mathbf{g}_{Sb}(\mathbf{x}) = \mathbf{S}_{bus}(\mathbf{x}) + \mathbf{S}_d - \mathbf{S}_g = 0 \tag{4.1.8}$$

The complex power injections are represented by $\mathbf{S}_{bus}$ for all the buses in the entire EPS, and it is also calculated in matrix form as in (4.1.9). In which $[\ \ ]$ is used to denote an operator that takes an $n \times 1$ vector and creates the corresponding $n \times n$ diagonal matrix with the vector elements on the diagonal.

$$\mathbf{S}_{bus}(\mathbf{x}) = [\mathbf{V}]\mathbf{I}_{bus}{}^{*} = [\mathbf{V}]\mathbf{Y}_{bus}{}^{*}\mathbf{V}^{*} \tag{4.1.9}$$

The nodal admittance matrix $\mathbf{Y}_{bus}$ has a size of $nb \times nb$. And, the Y_{ii} elements in its diagonal contain the short circuit admittances, and are obtained as the sum of admittances for all the branch elements connected to the bus i, including the shunt elements. The Y_{ij} off-diagonal elements represent the mutual admittances in between nodes i and j, and are the negative of the admittances connecting them. Furthermore, for a network of nl branches, the $nl \times nb$ sparse connection matrices C_f and C_t that are used in building the system admittance matrices can be defined

as follows. The $(i,\ j)$th element of C_f and the $(i,\ k)$th element of Ct are equal to 1 for each branch i, where equal to 1 for each branch i, where branch i connects from bus j to bus k. All other elements of C_f and C_t are zero. Thus, by using the connection matrices, the nodal admittance matrix can be easily calculated as in (4.1.10).

$$\mathbf{Y}_{bus} = \mathbf{C}_f{}^{\top}\mathbf{Y}_f + \mathbf{C}_t{}^{\top}\mathbf{Y}_t + [\mathbf{Y}_{shunt}] \tag{4.1.10}$$

Where the $nl \times nb$ system branch admittance matrices $\mathbf{Y}_f$ and $\mathbf{Y}_t$ are also constructed by using the described connection matrices and the branch admittance components from (3.1.13). for all the nl branch elements of the EPS in vector form as shown in (4.1.11) and (4.1.12) respectively.

$$\mathbf{Y}_f = [\mathbf{Y}_{ff}]\mathbf{C}_f + [\mathbf{Y}_{ft}]\mathbf{C}_t \tag{4.1.11}$$

$$\mathbf{Y}_t = [\mathbf{Y}_{tf}]\mathbf{C}_f + [\mathbf{Y}_{tt}]\mathbf{C}_t \tag{4.1.12}$$

Real Power Control Mismatch Equation

Active power control regulation to a set-point can be provided by *PST* and *VSC in-models*. The $\mathbf{g}_{sh}$ constraint ensures that the active power flow though the FUBM element meets a specified set-point value of P_f^{set}. Power regulation is provided at the "from" side of the branch, and the steady state control variable that is associated with this constraint is θ_{sh}. Thus, the full active power control constraint is shown in matrix form in (4.1.13).

$$\mathbf{g}_{P_f}^{\{i\}}(\mathbf{x}) = Real\left(\mathbf{S}_f^{\{i\}}(\mathbf{x})\right) - \mathbf{P}_f^{set\{i\}} \quad \forall i \in \boldsymbol{\mathcal{I}}_{sh} \tag{4.1.13}$$

Where, with the reference to the FUBM model, the complex power injection "from" side S_f is given by (4.1.14), and similarly obtained for the "to" side S_t in (4.1.15):

$$\mathbf{S}_f^{\{i\}} = [\mathbf{C}_f\mathbf{V}]\left(\mathbf{Y}_f^{\{i\}}\mathbf{V}\right)^* \tag{4.1.14}$$

$$\mathbf{S}_t^{\{i\}} = [\mathbf{C}_t\mathbf{V}]\left(\mathbf{Y}_t^{\{i\}}\mathbf{V}\right)^* \tag{4.1.15}$$

Reactive Power Control Mismatch Equation

Regarding the reactive power control of the "to" side of the *CTT in-models* and AC side for the *VSC in-models*, control constraint in (4.1.16) is set to meet the reactive power reference value $\mathbf{Q}_t^{set}$ by comparing it with the imaginary part of the apparent power from (4.1.15). The steady state variable associated with this constraint is the m_a, which as explained in Subsection 3.1.1, it represents the tap changer for the automatic CTTs and the modulation amplitude index for the selected VSCs.

$$\mathbf{g}_{Q_t}^{\{i\}}(\mathbf{x}) = Imag\left(\mathbf{S}_t^{\{i\}}(\mathbf{x})\right) - \mathbf{Q}_t^{set\{i\}} \quad \forall i \in \boldsymbol{\mathcal{I}}_{Q_t} \tag{4.1.16}$$

Zero Constraint Mismatch Equation

As explained in Subsection 3.1.1, the reactive power compensation inside the *VSC in-model* is represented by the *"Zero constraint"*. This specific control constraint balances the reactive power of the "from" side of the FUBM and thus, it ensures that there is *zero* reactive power flow into the DC network. Similar to the reactive power control, the zero constraint mismatch constraint also tries to balance the reactive power - this time with the "from" side of the FUBM, and it adjusts the value of B_{eq} until the constraint is met. Thus, B_{eq} is the associated state variable of this equation. This mismatch is shown in (4.1.17).

$$\mathbf{g}_{Q_z}^{\{i\}}(\mathbf{x}) = Imag\left(\mathbf{S_f}^{\{i\}}(x)\right) - \mathbf{zero} \quad \forall i \in \mathcal{I}_{Q_z} \tag{4.1.17}$$

AC Voltage Control Mismatch Equation

AC voltage can be controlled at the "to" side bus of the FUBM elements. In the traditional Power Flow problem, only the buses that are directly connected to a generator are considered as PV nodes. This is because in the traditional power flow only generators can compensate the reactive power at their terminals and thus maintaining a set voltage.

On the other hand, when using the FPFA in combination with the FUBM model, not only the generators can compensate the reactive power, but transformers with controllable taps and VSCs can also exert voltage regulation. This is achieved by

varying the m_a and thus varying the reactive power until the actual voltage in terminals meets a set-point. Mathematically, the voltage magnitude V_m is thus considered a constant value (i.e. a pre-set parameter) equal to a specified setting $\mathbf{V}_t^{set}$. Therefore when voltage regulation is implemented the bus type of the node changes from traditionally being a PQ node to a PV node just as it was described in Subsection 4.1.2. This means that the reactive power balance equation that was used for the calculation of the voltage magnitude is not needed anymore for those buses with nodal voltage regulation active. Instead, that same equation is now used for the calculation of the required m_a, where now the voltage magnitude V_m is the constant set-point and the m_a is the new associated state variable to this nodal equation. As a result, the AC Voltage control mismatch equation can be expressed as in (4.1.18). It follows that, the state variable m_a when used to model voltage regulation in the VSC *in-model* corresponds to the amplitude modulation index that exists as a result of PWM control of the converter. For the CTT *in-model*, this variable simply corresponds to the controllable tap ratio of the CTT.

$$\mathbf{g}_{V_t}^{\{i\}} = Imag\left(\mathbf{g}_{Sb}^{\{i\}}\right) \quad \forall i \in \boldsymbol{\mathcal{I}}_{V_t} \tag{4.1.18}$$

DC Voltage Control Mismatch Equation

One of the most commonly used features of the VSCs is the DC voltage regulation. As explained in Section 3.2, MTDC grids can either maintain a fixed DC voltage or a droop control voltage. Mismatch equation $\mathbf{g}_{V_f}$ in (4.1.5) focuses on the fixed voltage regulation and it is provided by the selected VSCs type # II. In a similar way as the AC voltage control is achieved, the fixed DC voltage regulation considers the voltage magnitude V_m as a constant, and thus the "from" side bus is now considered a PV node. As a result, the power balance equation that was used for the calculation of the voltage magnitude in the node is now used for the calculation of the B_{eq} inside the VSCs type # II. Thus, the mismatch equation is defined as (4.1.19).

$$\mathbf{g}_{V_f}^{\{i\}} = Imag\left(\mathbf{g}_{Sb}^{\{i\}}\right) \quad \forall i \in \boldsymbol{\mathcal{I}}_{V_{vscII}} \tag{4.1.19}$$

It is worth to highlight that the B_{eq} of the VSCs type # I and type # II play

a different role. As mentioned in Section 3.2, in a MTDC grid with fixed voltage regulation, all the B_{eq} of the VSCs type #I are set to meet the *Zero Constraint*, which means that the remaining B_{eq} of the VSC type # II remains unused, and thus, this variable is free to regulate the voltage in the DC side of the grid.

Droop Control Mismatch Equation

When Voltage droop control is implemented by the VSCs type #III, the power injected to the DC grid is the function of the nodal DC voltage at the "from" side terminal of the FUBM. This means that the amount of power P_f flowing though the VSCs is determined by the voltage magnitude at its"from" side V_{m_f}. Consequently, the Voltage magnitude at the DC side is still a variable, and thus, it needs to be calculated using the nodal power balance equation. Therefore when using Voltage droop control, the "from" side bus is set as a PQ node. Furthermore, the droop equation will vary depending on the control type as it was shown in Subsection 3.2.1. Equation (4.1.20) presents the traditional voltage-power $v_{dc} - P_f$ standard droop control equation from Fig. 3.12, where the parameter k_{dp} represents the slope for the $v_{dc} - P_f$ control. Additionally, $\mathbf{P}_f^{\{i\}\,set}$, and $\mathbf{Q}_t^{\{i\}\,set}$ are the desired active and reactive power control reference settings. It is a common practice to choose the $V_{m_f}^{set}$ as the expected average DC voltage, and the P_f^{set} will be the corresponding power injection. This equation is used as the Droop Control mismatch equation, and the associated variable with this control constraint will be θ_{sh}.

$$\mathbf{g}_{P_{dp}}^{\{i\}}(\mathbf{x}) = -Real\left(\mathbf{S}_f^{\{i\}}(\mathbf{x})\right) + \mathbf{P}_f^{set^{\{i\}}} - k_{dp}\left(\mathbf{V}_{m_f}^{\{i\}} - \mathbf{V}_{m_f}^{set^{\{i\}}}\right) \quad \forall i \in \boldsymbol{\mathcal{I}}_{vscIII} \quad (4.1.20)$$

4.1.5 VSC Losses Correction

A typical loss model takes every component of a VSC HVDC station into account. The loss model determines the converter station losses as a function of the active and reactive power exchanged between converter and AC network. The IEC 62751-2 standard [95] recommends using a quadratic fitting curve based on the electromagnetic transient simulation results to correct and obtain the exact converter losses.

Accordingly, for the FUBM, the converter loss model is formulated as a second order polynomial function of the converter AC-side current I_t as shown in (4.1.21), in which, depending on the values of α, β, and γ the losses can be broken down into: no-load losses, constant losses, linearly dependant losses and quadratic losses.

$$\mathbf{g}_{G_{sw}}^{\{i\}}(\mathbf{x}) = -\mathbf{V}_{m_f}^{\{i\}\,2}\mathbf{G}_{sw}^{\{i\}} + \gamma\left|\mathbf{i}_t^{\{i\}}\right|^2 + \beta\left|\mathbf{i}_t^{\{i\}}\right| + \alpha \quad \forall i \in \boldsymbol{\mathcal{I}}_{vsc} \tag{4.1.21}$$

4.1.6 NR Method and Extended Jacobian

The main task of all Power Flow Algorithms is to find a solution for the system of non-linear equations of the EPS. For the FPFA this system of mismatch equations is represented by $\mathbf{g}(\mathbf{x}) = \mathbf{0}$ in (4.1.5) and it is solved for all $\mathbf{x}$ state variables. According to Newton's Method, the vector of state variables $\mathbf{x}$ that satisfies the mismatch equations of the system can be approximated by performing a Taylor series expansion of $\mathbf{g}(\mathbf{x})$ as in (4.1.22).

$$\mathbf{g}(\mathbf{x}) \cong \mathbf{g}(\mathbf{x}^{(\mathbf{0})}) + \mathbf{J}(\mathbf{x}^{(\mathbf{0})})(\mathbf{x} - \mathbf{x}^{(\mathbf{0})}) + \text{higher-order terms} \tag{4.1.22}$$

Where the vector $\mathbf{x}^{(\mathbf{0})}$ is an initial estimate of the solution, and $\mathbf{J}$ is the Jacobian matrix containing the first order partial derivatives of $\mathbf{g}(\mathbf{x})$ with respect to $\mathbf{x}$. From Section 2.1, we know that the linear approximation of Taylor series is sufficiently accurate to the functions if the initial condition $\mathbf{x}^{(\mathbf{0})}$ is close enough to the solution values of $\mathbf{x}$, in which case, the higher order terms can be neglected. In numerical analysis, the Newton-Raphson method produces successively better approximations to the roots (or zeroes) of a real-valued function. Thus, at a start point in $\mathbf{x}^{\mathbf{0}}$, the iterative corrections to find the solution of the system of mismatch equations in 4.1.5 are calculated as in (4.1.23), or in its compact form in (4.1.24). Consequently, $\mathbf{x}^{i+1}$ is a better approximation for the solution than $\mathbf{x}^i$ at iteration i.

$$\mathbf{x}^{i+1} - \mathbf{x}^i = -\mathbf{g}(\mathbf{x}^i) \cdot \left(\mathbf{J}(\mathbf{x}^i)\right)^{-1} \tag{4.1.23}$$

$$\Delta\mathbf{x} = -\mathbf{g}(\mathbf{x}) \cdot \mathbf{J}^{-1} \tag{4.1.24}$$

In the Traditional Power Flow algorithm, the Jacobian matrix is generated by calculating only the partial derivatives of the power balance equations with respect to the voltage variables (nodal magnitude and phase angles). Since for the FUBM model, the number of equations and state variables have been extended to include all the extra available controls in the model, the Jacobian matrix $\mathbf{J}$ is also expanded accordingly. Thus, the iterative corrections for the state variables with an expanded Jacobian structure is shown in (4.1.25).

$$\begin{bmatrix} \Delta\mathbf{V_a} \\ \Delta\mathbf{V_m} \\ \Delta\boldsymbol{\theta}_{\mathbf{sh}} \\ \Delta\mathbf{B_{eq}} \\ \Delta\mathbf{B_{eq}} \\ \Delta\mathbf{m_a} \\ \Delta\mathbf{m_a} \\ \Delta\boldsymbol{\theta}_{\mathbf{sh}} \end{bmatrix} = - \begin{bmatrix} \mathbf{g}_{P_b}(\mathbf{x}) \\ \mathbf{g}_{Q_b}(\mathbf{x}) \\ \mathbf{g}_{P_f}(\mathbf{x}) \\ \mathbf{g}_{Q_z}(\mathbf{x}) \\ \mathbf{g}_{V_f}(\mathbf{x}) \\ \mathbf{g}_{Q_t}(\mathbf{x}) \\ \mathbf{g}_{V_t}(\mathbf{x}) \\ \mathbf{g}_{P_{dp}}(\mathbf{x}) \end{bmatrix} / \begin{bmatrix} \frac{\partial \mathbf{g}_{P_b}}{\partial \mathbf{V_a}} & \frac{\partial \mathbf{g}_{P_b}}{\partial \mathbf{V_m}} & \frac{\partial \mathbf{g}_{P_b}}{\partial \boldsymbol{\theta}_{\mathbf{sh}}} & \frac{\partial \mathbf{g}_{P_b}}{\partial \mathbf{B_{eq}}} & \frac{\partial \mathbf{g}_{P_b}}{\partial \mathbf{B_{eq}}} & \frac{\partial \mathbf{g}_{P_b}}{\partial \mathbf{m_a}} & \frac{\partial \mathbf{g}_{P_b}}{\partial \mathbf{m_a}} & \frac{\partial \mathbf{g}_{P_b}}{\partial \boldsymbol{\theta}_{\mathbf{sh}}} \\ \frac{\partial \mathbf{g}_{Q_b}}{\partial \mathbf{V_a}} & \frac{\partial \mathbf{g}_{Q_b}}{\partial \mathbf{V_m}} & \frac{\partial \mathbf{g}_{Q_b}}{\partial \boldsymbol{\theta}_{\mathbf{sh}}} & \frac{\partial \mathbf{g}_{Q_b}}{\partial \mathbf{B_{eq}}} & \frac{\partial \mathbf{g}_{Q_b}}{\partial \mathbf{B_{eq}}} & \frac{\partial \mathbf{g}_{Q_b}}{\partial \mathbf{m_a}} & \frac{\partial \mathbf{g}_{Q_b}}{\partial \mathbf{m_a}} & \frac{\partial \mathbf{g}_{Q_b}}{\partial \boldsymbol{\theta}_{\mathbf{sh}}} \\ \frac{\partial \mathbf{g}_{P_f}}{\partial \mathbf{V_a}} & \frac{\partial \mathbf{g}_{P_f}}{\partial \mathbf{V_m}} & \frac{\partial \mathbf{g}_{P_f}}{\partial \boldsymbol{\theta}_{\mathbf{sh}}} & \frac{\partial \mathbf{g}_{P_f}}{\partial \mathbf{B_{eq}}} & \frac{\partial \mathbf{g}_{P_f}}{\partial \mathbf{B_{eq}}} & \frac{\partial \mathbf{g}_{P_f}}{\partial \mathbf{m_a}} & \frac{\partial \mathbf{g}_{P_f}}{\partial \mathbf{m_a}} & \frac{\partial \mathbf{g}_{P_f}}{\partial \boldsymbol{\theta}_{\mathbf{sh}}} \\ \frac{\partial \mathbf{g}_{Q_z}}{\partial \mathbf{V_a}} & \frac{\partial \mathbf{g}_{Q_z}}{\partial \mathbf{V_m}} & \frac{\partial \mathbf{g}_{Q_z}}{\partial \boldsymbol{\theta}_{\mathbf{sh}}} & \frac{\partial \mathbf{g}_{Q_z}}{\partial \mathbf{B_{eq}}} & \frac{\partial \mathbf{g}_{Q_z}}{\partial \mathbf{B_{eq}}} & \frac{\partial \mathbf{g}_{Q_z}}{\partial \mathbf{m_a}} & \frac{\partial \mathbf{g}_{Q_z}}{\partial \mathbf{m_a}} & \frac{\partial \mathbf{g}_{Q_z}}{\partial \boldsymbol{\theta}_{\mathbf{sh}}} \\ \frac{\partial \mathbf{g}_{V_f}}{\partial \mathbf{V_a}} & \frac{\partial \mathbf{g}_{V_f}}{\partial \mathbf{V_m}} & \frac{\partial \mathbf{g}_{V_f}}{\partial \boldsymbol{\theta}_{\mathbf{sh}}} & \frac{\partial \mathbf{g}_{V_f}}{\partial \mathbf{B_{eq}}} & \frac{\partial \mathbf{g}_{V_f}}{\partial \mathbf{B_{eq}}} & \frac{\partial \mathbf{g}_{V_f}}{\partial \mathbf{m_a}} & \frac{\partial \mathbf{g}_{V_f}}{\partial \mathbf{m_a}} & \frac{\partial \mathbf{g}_{V_f}}{\partial \boldsymbol{\theta}_{\mathbf{sh}}} \\ \frac{\partial \mathbf{g}_{Q_t}}{\partial \mathbf{V_a}} & \frac{\partial \mathbf{g}_{Q_t}}{\partial \mathbf{V_m}} & \frac{\partial \mathbf{g}_{Q_t}}{\partial \boldsymbol{\theta}_{\mathbf{sh}}} & \frac{\partial \mathbf{g}_{Q_t}}{\partial \mathbf{B_{eq}}} & \frac{\partial \mathbf{g}_{Q_t}}{\partial \mathbf{B_{eq}}} & \frac{\partial \mathbf{g}_{Q_t}}{\partial \mathbf{m_a}} & \frac{\partial \mathbf{g}_{Q_t}}{\partial \mathbf{m_a}} & \frac{\partial \mathbf{g}_{Q_t}}{\partial \boldsymbol{\theta}_{\mathbf{sh}}} \\ \frac{\partial \mathbf{g}_{V_t}}{\partial \mathbf{V_a}} & \frac{\partial \mathbf{g}_{V_t}}{\partial \mathbf{V_m}} & \frac{\partial \mathbf{g}_{V_t}}{\partial \boldsymbol{\theta}_{\mathbf{sh}}} & \frac{\partial \mathbf{g}_{V_t}}{\partial \mathbf{B_{eq}}} & \frac{\partial \mathbf{g}_{V_t}}{\partial \mathbf{B_{eq}}} & \frac{\partial \mathbf{g}_{V_t}}{\partial \mathbf{m_a}} & \frac{\partial \mathbf{g}_{V_t}}{\partial \mathbf{m_a}} & \frac{\partial \mathbf{g}_{V_t}}{\partial \boldsymbol{\theta}_{\mathbf{sh}}} \\ \frac{\partial \mathbf{g}_{P_{dp}}}{\partial \mathbf{V_a}} & \frac{\partial \mathbf{g}_{P_{dp}}}{\partial \mathbf{V_m}} & \frac{\partial \mathbf{g}_{P_{dp}}}{\partial \boldsymbol{\theta}_{\mathbf{sh}}} & \frac{\partial \mathbf{g}_{P_{dp}}}{\partial \mathbf{B_{eq}}} & \frac{\partial \mathbf{g}_{P_{dp}}}{\partial \mathbf{B_{eq}}} & \frac{\partial \mathbf{g}_{P_{dp}}}{\partial \mathbf{m_a}} & \frac{\partial \mathbf{g}_{P_{dp}}}{\partial \mathbf{m_a}} & \frac{\partial \mathbf{g}_{P_{dp}}}{\partial \boldsymbol{\theta}_{\mathbf{sh}}} \end{bmatrix} \tag{4.1.25}$$

Each partial derivative inside the Jacobian is a matrix that contains the partial derivatives of the stated equation with respect to each individual variable. For example, the matrix $\frac{\partial \mathbf{g}_{P_b}}{\partial \mathbf{V_a}}$ contains the partial derivatives of each individual active power balance equation in $\mathbf{g}_{P_b}$ with respect to the voltage angle V_a for each PV and PQ node in the EPS. Thus, the size of the matrix $\frac{\partial \mathbf{g}_{P_b}}{\partial \mathbf{V_a}}$ is $[nb-1, nb-1]$. The detailed development and final equations for each matrix of partial derivatives inside the extended Jacobian can be found in the Appendix C.

It is also worth to highlight that the extended Jacobian in (4.1.25) is re-sizable, which means that depending on the case and the active controls, it will contain only the necessary partial derivatives of the extended mismatch equations presented in Subsection 4.1.4 and their associated state variables. Thus, the Jacobian could be as simple as the traditional power flow Jacobian of Section 2.1, or as complex as the one shown in (4.1.25).

4.1.7 FPFA Flowchart

This subsection presents a Flowchart of the FPFA and a detailed explanation for each one of the steps contained in the flowchart. The flowchart is shown in Fig. 4.1(a).

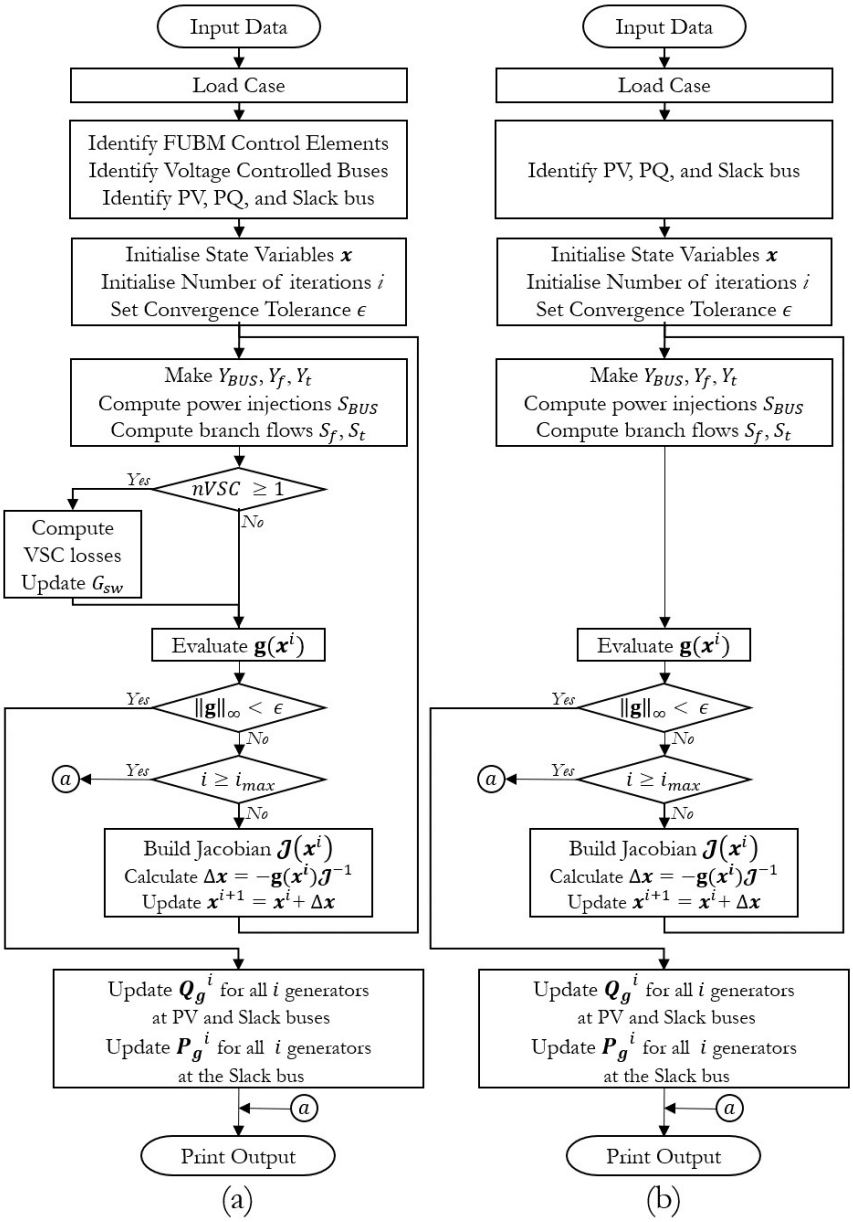

Figure 4.1: (a) FPFA Flowchart (b) AC Power Flow Flowchart

By comparing the flowcharts of the AC Power Flow algorithm and the FPFA using FUBM of Fig. 4.1(b) and Fig. 4.1(a) respectively, it is clear the main structure

of the FPFA using the FUBM is very similar to the general unified approach for the power flow solution of AC power grids. From an implementation perspective, it can therefore be appreciated that by using the FUBM and with only minor modifications to the core formulation of the unified approach, it is possible to simulate a fully controllable AC/DC power EPS with all available controls.

The implementation of FPFA using FUBM is quite simple, after loading the case (here case refers to the system to be solved and can be either AC-only or a hybrid AC/DC EPS), identification of the *in-models* and control elements is carried out by analysing the input parameters (just as explained in Subsection 3.1.1). Here is where identifiers $\boldsymbol{\mathcal{I}}$ for the in-models, controls, and nodes are created. Then, with the initialised state variables, the admittance matrices $\mathbf{Y}_{bus}$, $\mathbf{Y}_f$ and $\mathbf{Y}_t$ are calculated, and they are used to calculate the initial complex nodal power injections and branch power flows. Moreover, depending if the case is an hybrid power grid (AC/DC) or just an AC grid, the losses of the VSCs have to be corrected as explained in Section 4.1.5. Then, the mismatch equations in 4.1.5 are evaluated using the initial condition of the state variables $\mathbf{x}$. To verify if the mismatch equations are satisfied, the largest mismatch is compared against a set tolerance ϵ. This is achieved by calculating the infinity norm of the vector of mismatch equations $\mathbf{g}$ by using the *p-norm*, where p tends to ∞, and is calculated as shown in (4.1.26).

$$||\mathbf{g}||_\infty = \left[\sum_{k=1}^{nx} |\mathbf{g}_k|^\infty\right]^{\frac{1}{\infty}} = \max_k(|\mathbf{g}_k|) \tag{4.1.26}$$

If the mismatch equations have not met the tolerance, then the Jacobian of (4.1.25) is built, and the corrections of the state variables for the next iteration $\mathbf{x}^{i+1}$ are calculated. The process is repeated iteratively until the mismatch equations reach the set tolerance ϵ (convergence), or the maximum number of iterations i_{max} surpassed (divergence).

If convergence is achieved, the reactive power compensation from the Generators $\mathbf{Q}_g$ and the Active Power compensation of the generator(s) connected to the slack bus is calculated. Finally the results are printed.

4.2 MATPOWER-FUBM Power Flow Solution

As it was mentioned in the introduction of this Chapter, unified algorithms are a superior approach for solving the AC Power Flow problem. Nevertheless solving the power flow problem in this way for an AC/DC networks requires major modifications to the core AC-only power flow solvers. Moreover, ideally, any power flow solver should also be able to model the controls available in a hybrid AC/DC system (e.g. VSC voltage and power control) to be able to accurately estimate the operational flexibility of such systems. This feat is absent from most standard AC-only power flow solvers. However, as seen in Section 4.1, by using the FUBM in combination with the FPFA, hybrid AC/DC networks can be modelled and solved efficiently and with minor modifications to AC-only power flow solvers, and at the same time, impacts of operational flexibility promised by these additional controls can be estimated.

MATPOWER Software is a package of free, open-source Matlab-language M-files for solving steady-state power system simulation and optimisation problems. It is very effective for the analysis of AC grids and is widely used worldwide by researchers and the industry alike. Regardless of its success, for new hybrid AC/DC grids, the software is rather limited. To showcase the multiple benefits of the FUBM and the simplicity of its implementation, this section presents the results of the implementation of the FPFA using FUBM to the existing software tool MATPOWER. The original software of MATPOWER can be downloaded in [60] and the modified version of it which can solve hybrid AC/DC grids using the FUBM can be downloaded in [104].

The remainder of this section presents three main case studies and their simulation results. All simulations were carried out using an extension to the MATPOWER AC-only power flow solver which includes the FUBM to model all network elements and the FPFA to solve the ensuing power flow problem. This implementation is called MATPOWER-FUBM power flow solver in this thesis. The first test case is used to validate the FUBM model. The second one presents a test case with multiple control features to showcase the flexibility of the FUBM in modelling a variety of controls. Finally, the last case study is used as a demonstration of the effec-

tiveness of the FUBM model implementation in conjunction with FPFA for solving large-scale systems without sacrificing computational efficiency. All cases have been solved using a PC with CPU Intel Core i7, 2.2GHz and 16GB RAM memory. The FPFA algorithm is set within the tolerance shown in (4.2.27).

$$\epsilon = 1e10^{-12} \tag{4.2.27}$$

4.2.1 Case Study IEEE 57 - IEEE 14

In order to verify the accuracy of the FUBM and the proposed algorithm for power flows, the simulation is performed for the same test system reported in [62]. The test system consists of two asynchronous AC grids interconnected trough two MTDC grids. The first AC grid is the IEEE 57 bus system consisting of 7 generators, 80 transmission lines and 42 loads. The second AC grid corresponds to the IEEE 14 bus system, supplying 11 loads through 20 lines with 5 generators. Regarding the MTDC grids, the first DC grid consists of 3 DC buses which are connected using a ring topology. On the other hand, the second DC grid consists on 7 bipolar buses, five of which are connected to a VSC and the remaining two are pure DC buses. Additionally, Bus 9 has a constant photovoltaic injection of 30 MVA and a pure DC load of 10 MW. Figure 4.2, shows the diagram of the described test system.

Parameters for all VSCs and AC-side transformers are given in Table 4.2. The coefficients for the VSCs polynomial loss model are set to get the converter power loss equal to approximately 1% of its rated power. Table 4.3 summarises the branch parameters for each DC grid.

Table 4.2: IEEE 57-14 VSC Parameters

VSC	Rate	Transformer	Filter	Reactor	Loss Coefficients		
No.	[MVA]	Z_{TR} [pu]	B_f [pu]	Z_s [pu]	γ	β	α
1	200	0.0010+j0.0033	0	0.05	0.001	0.004	0.008
2,3	100	0.0015+j0.0500	0	0.075	0.002	0.004	0.004
4	200	0.0010+j0.0033	0	0.05	0.001	0.004	0.008
5,6,7,8	100	0.0015+j0.0500	0	0.075	0.002	0.004	0.004

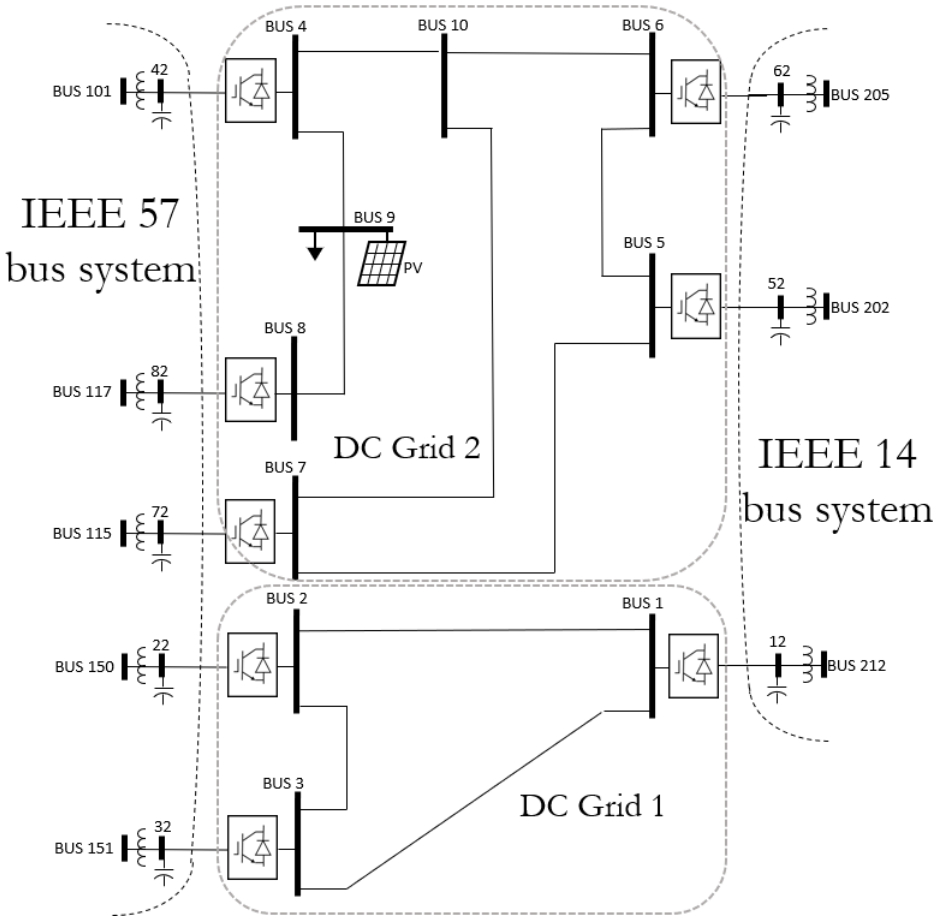

Figure 4.2: IEEE 57 - IEEE 14 MTDC Link

Voltage regulation is provided for both DC grid by employing one VSC type # II per DC grid. The remaining VSCs are set as type # I to control the active power. Furthermore reactive power control and voltage regulation in the AC side is also implemented. Details in the control settings are presented in Table 4.4, where the same control modes presented in Subsection 3.2.1 is used. Notice that for active power control, in each DC area at least one VSC remains free to account for the active power loss though the DC lines.

Simulation Results and Discussion

The proposed MATPOWER-FUBM power flow solver has been used to solve this system. The ensuing power flow problem converged in 0.27 seconds after 11 iterations. All the results match with the ones presented in [62]. Even though the MATPOWER-

Table 4.3: IEEE 57-14 DC Grid Parameters

MTDC Grid 1			MTDC Grid 2		
From Bus	To Bus	r_s [p.u.]	From Bus	To Bus	r_s [p.u.]
1	2	0.010	4	9	0.010 0
2	3	0.010	4	10	0.005 0
3	1	0.020	5	6	0.015 0
			5	7	0.015 0
			6	10	0.010 0
			7	10	0.015 0
			8	9	0.015 0

Table 4.4: IEEE 57-14 VSCs Control Settings

DC Grid	VSC No.	Control Mode	Zero Constraint	V_{dc} [pu]	P_f [MW]	V_t [pu]	Q_t [MVAr]
1	1	5	Free	1	***	1.06	***
	2	3	Active	***	-50	0.99	***
	3	3	Active	***	-50	1.03	***
2	4	4	Free	0.995	***	***	0
	5	2	Active	***	-50	***	0
	6	2	Active	***	-50	***	10
	7	3	Active	***	90	1.001	***
	8	3	Active	***	-60	1	***

FUBM solver is capable of solving the entire network with a single reference bus, this case was simulated using two of them only for comparison purposes. Both reference angles are set in the first bus of each AC grid. Table 4.6 summarises the results for VSC control and Table 4.5 presents the power flows and voltages of each DC grid.

Table 4.5: IEEE57-14 DC Power Flow

MTDC Grid 1				MTDC Grid 2			
From	to	Pf	Pt	From	to	Pf	Pt
1	2	62.93	-62.53	4	9	40.73	-40.56
2	3	12.53	-12.52	4	10	10.86	-10.85
3	1	-37.48	37.77	5	6	6.16	-6.16
				5	7	-56.16	56.65
				6	10	-43.84	44.04
				7	10	33.35	-33.19
				8	9	-60	60.56

Table 4.6: IEEE 57-14 VSCs Control Results

VSC No.	Control Mode	B_{eq} [pu]	V_{dc} [pu]	P_f [MW]	V_t [pu]	Q_t [MVAr]	θ_{sh} [deg]	m_a [pu]
1	5	0.9463	1.000	-100.70	1.060	-95.74	0.0000	0.7859
2	3	-0.4026	0.994	-50.00	0.990	42.75	-43.4876	0.8067
3	3	-0.1045	0.992	-50.00	1.030	12.89	-41.7281	0.7647
4	4	0.0086	0.995	-51.58	1.040	0.00	0.0000	0.8014
5	2	0.0090	0.991	-50.00	1.045	0.00	3.4812	0.7490
6	2	-0.0834	0.990	-50.00	0.996	10.00	9.0110	0.7865
7	3	1.1885	0.999	90.00	1.001	-102.55	14.9765	0.8343
8	3	-0.3612	0.982	-60.00	1.000	40.25	-1.9949	0.7827

Control results from the *VSC in-model* match with the Traditional VSC model presented in [62]. All VSC type # I present zero reactive power injection to the DC grid, which shows that the zero constraint has been achieved. From Table 4.6, it is noticeable that active power has been fully controlled by both MTDC.

Furthermore, the value of θ_{sh} has been obtained for all active power controlled elements. The algorithm has calculated successfully the modulation coefficient and the required value of B_{eq} for both converters types #I and #II. Therefore, both reactive power and voltage control have met the set values within the tolerance. DC grids 1 and 2 present a voltage angle of $V_a = -46.226°$ and $V_a = -0.966°$ for all their buses respectively. It should be noticed that even though the voltage angle in the DC grid has a value, it remains constant throughout the DC network. Thus, as it was demonstrated mathematically in Section 3.2, and in Appendix B.1, there is no reactive power through the DC link, hence the DC power flow is purely dependent on the DC nodal voltages. The fact that the algorithm is obtaining V_a in the DC areas is a solid proof that the algorithm is not creating any distinction between AC and DC elements. It is clear that the FUBM does create a connection between grids and therefore the effects of this interaction result in a more realistic and flexible way of simulating hybrid AC/DC power grids.

4.2.2 Case Study Modified IEEE 30 Bus System

In this case study, the proposed MATPOWER-FUBM solver is used to solve a modified version of the IEEE 30-bus system that was presented in [105]. This widely modified test case combines fixed, and automatic controls to represent diversity of control elements in a typical EPS. All branch and control elements are modelled using the FUBM to show all the described *in-models* working seamlessly all at once. Fig 4.3 shows the test system diagram.

Within the modifications to the case, a MTDC grid with three VSCs in ring topology is included. To integrate two offshore wind farms, a second MTDC grid is also added. For reactive power control, a well-located STATCOM in node B124 has been connected with a fixed DC voltage of 1.1 V. Furthermore a VSC-HVDC link between the node B123 and B108 is added. Additionally, the lines between buses B110-B120 and B112-B114 have been changed to be PSTs for active power control. Similarly for the lines between buses B106-B110 and B116-B117 also are changed to be CTTs for reactive power control and voltage control respectively.

Tables 4.7 summarise the parameters of the VSCs and their respective transform-

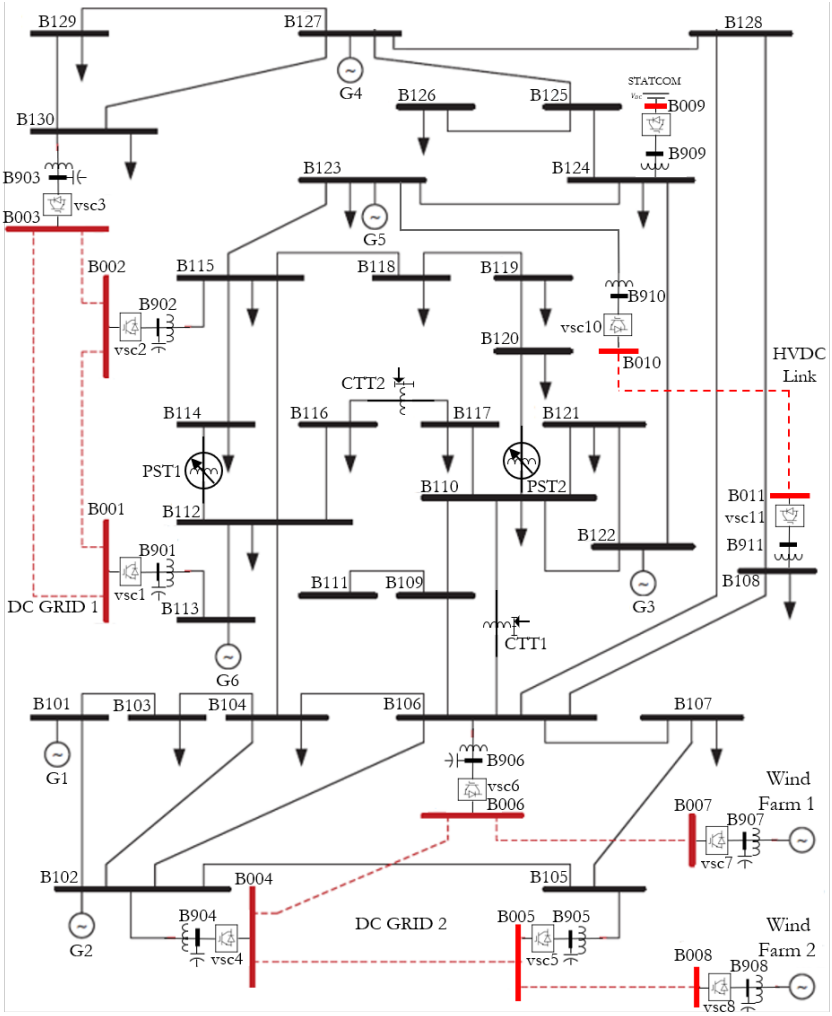

Figure 4.3: Modified IEEE 30 - 2 MTDC grids

ers. The value of the series resistance r_s for all DC lines is 0.05 [pu]. AC system data can be found in MATPOWER's free database [24].

While MTDC Grid 1 regulates the voltage using Voltage Droop Control, voltage regulation is provided to MTDC Grid 2 by employing one VSC type # II. The voltage over the HVDC link is regulated though the VSC 10 that is set up with voltage droop control strategy. Details in the control settings are presented in Table 4.8, again the same control code presented in Subsection 3.2.1 is used. The control settings for the PSTs and CTTs can be found in Table 4.9.

Table 4.7: Modified IEEE 30 VSC Parameters

Rate	Transformer	Filter	Reactor	Loss Coefficients		
MVA	Z_{TR} [pu]	B_f [pu]	Z_s [pu]	γ	β	α
200	0.0015+j0.1121	0.0887	0.0001+j0.1643	0.0001	0.015	0.2

Table 4.8: Modified IEEE 30 VSCs Control Settings

DC Grid	VSC No.	VSC Type	Control Mode	Zero Constraint	V_{dc}^{set} [pu]	P_f^{set} [MW]	V_t^{set} [pu]	Q_t^{set} [MVAr]	k_{dp} [pu]
1	1	III	7	Free	1.1	-3.5	***	***	-0.1
	2	I	2	Active	***	***	***	-25.0	***
	3	III	6	Active	1.1	-2.35	***	***	-0.05
2	4	I	1	Active	***	***	***	***	***
	5	I	3	Active	***	***	1.05	***	***
	6	II	5	Free	1.07	-15	***	***	***
STATCOM	9	II	4	Active	1.1	***	***	***	***
HVDC	10	III	7	Free	1.0	2.0	***	***	-0.05
	11	I	2	Active	***	***	***	***	***

Table 4.9: Modified IEEE 30 PSTs and CTTs Control Settings

Transformer Type	Element No.	P_f^{set} [MW]	V_t^{set} [pu]	Q_t^{set} [MVAr]
PST	1	3.5	***	***
	2	7.5	***	***
CTT	1	***	***	3.0
	2	***	1.01	***

Simulation Results and Discussion

The presented FPFA formulation for the FUBM has been successfully solved in 11 iterations and 0.52 seconds. The system was initialised with flat start. Figure 4.4 shows the convergence in each iteration of the FPFA for all the mismatch equations of the EPS. It is noticeable that from iteration number 3 the mismatch equations have practically converged. The rest of the iterations are just to match with the minimum tolerance ϵ.

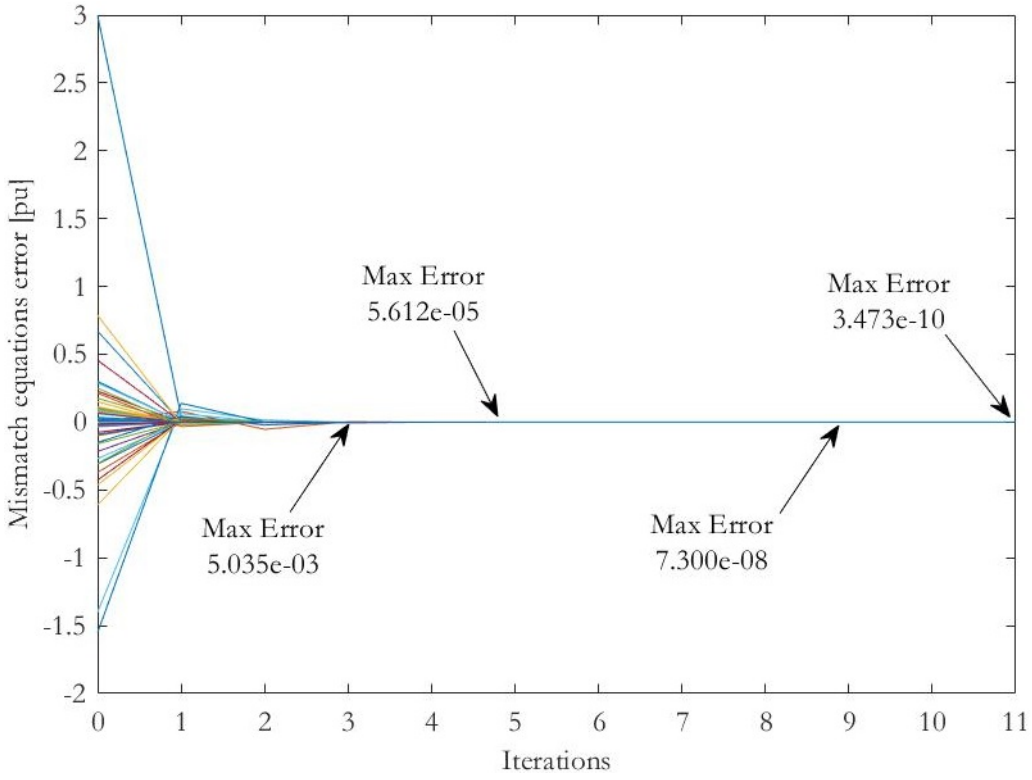

Figure 4.4: Modified IEEE 30 Convergence for all State Variables

Tables 4.10 and 4.11 present the DC grid voltages and the solution of the VSCs controls respectively. It can be appreciated that all the controls meet their target. Also, VSCs 1,3 and 10 have follow the $P_f - V_{dc}$ Droop Control. The control values for the state variables B_{eq}, θ_{sh} and m_a were obtained. Furthermore, the *Zero Constraint* was meet in all the VSC that have the setting as active, but also it can be appreciated that the remaining ones meet this constraint naturally. Even though all DC nodes present voltage angles, they remain the same through-out each isolated DC grid.

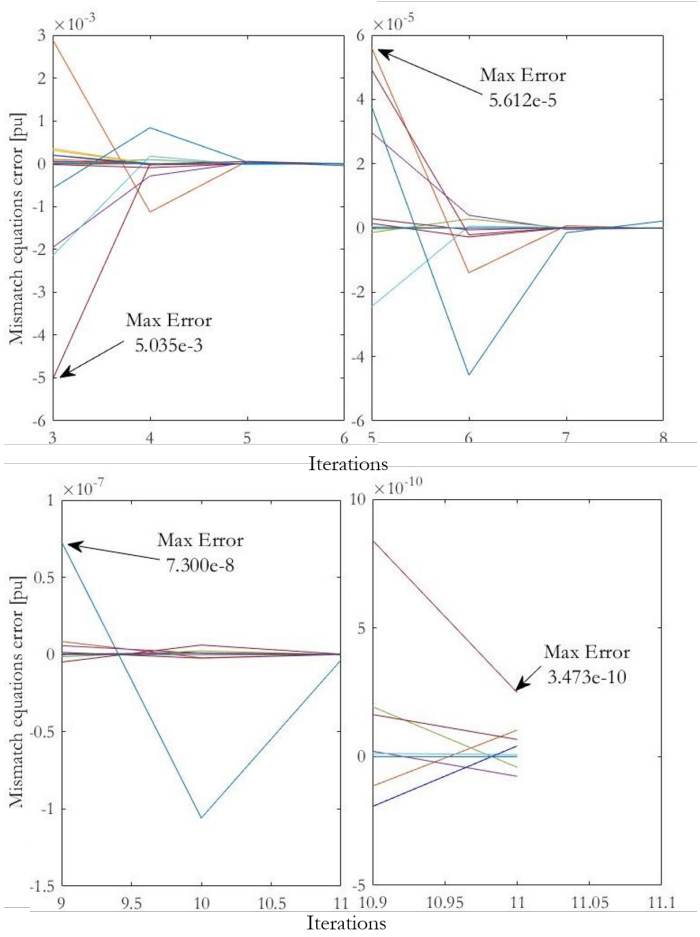

Figure 4.5: Modified IEEE 30 Convergence for all State Variables (Zoom)

Thus, the power flow though the DC Grid is solely dictated by the Voltage magnitude as explained in Section 3.2. Finally in Table 4.12 the results from the PSTs and CTTs are presented.

From Fig. 4.6 and Fig. 4.7 it can be appreciated that from iteration 3 the modulation amplitude has almost reach convergence for Voltage control and Reactive power control in the AC side.

Overall, with this simulation it is clear that the FUBM is capable to model several elements of the power system without sacrificing computational effort. Moreover the entire grid was calculated using just one reference angle in bus B101. All the controls worked as expected. The FPFA has a fast convergence regardless of the amount of controls applied.

Table 4.10: Modified IEEE 30 DC Grids Voltages Results

Bus ID	Vm [pu]	Va [deg]	Bus ID	Vm [pu]	Va [deg]	Bus ID	Vm [pu]	Va [deg]
B001	1.041	-2.277	B005	1.070	-0.467	B009	1.100	-0.100
B002	1.039	-2.277	B006	1.070	-0.467	B0010	1.000	-2.820
B003	1.040	-2.277	B007	1.077	-0.467	B0011	1.001	-2.820
B004	1.070	-0.467	B008	1.075	-0.467			

Table 4.11: Modified IEEE 30 VSC Control Results

VSC ID	P_f [MW]	Q_f [MVAr]	Q_t [MVAr]	θ_{sh} [deg]	B_{eq} [pu]	m_a [tap]
1	-2.91	0	0.01	-2.1581	0	1
2	4.95	0	-25.00	0	0.2298	0.9770
3	-2.05	0	-12.46	2.9197	0.1174	1
4	0.26	0	-26.03	0	0.2366	1
5	9.59	0	-26.07	0	0.2284	0.9811
6	15.00	0	-26.88	-0.4213	0.2469	1
9	0.00	0	-37.65	0	0.3290	1
10	2.00	0	0.01	-1.8995	0	1
11	-2.00	0	-5.32	0	0.0536	1

Table 4.12: Modified IEEE 30 PSTs and CTTs Control Results

Transformer Type	Element No.	P_f [MW]	θ_{sh} [deg]	V_t [pu]	Q_t [MVAr]	m_a [tap]
PST	1	3.5	-0.0402	0.983	1.93	1
	2	7.5	0.2427	0.984	-3.52	1
CTT	1	2.63	0	0.999	3.0	1.0155
	2	11.43	0	1.01	-19.23	0.8717

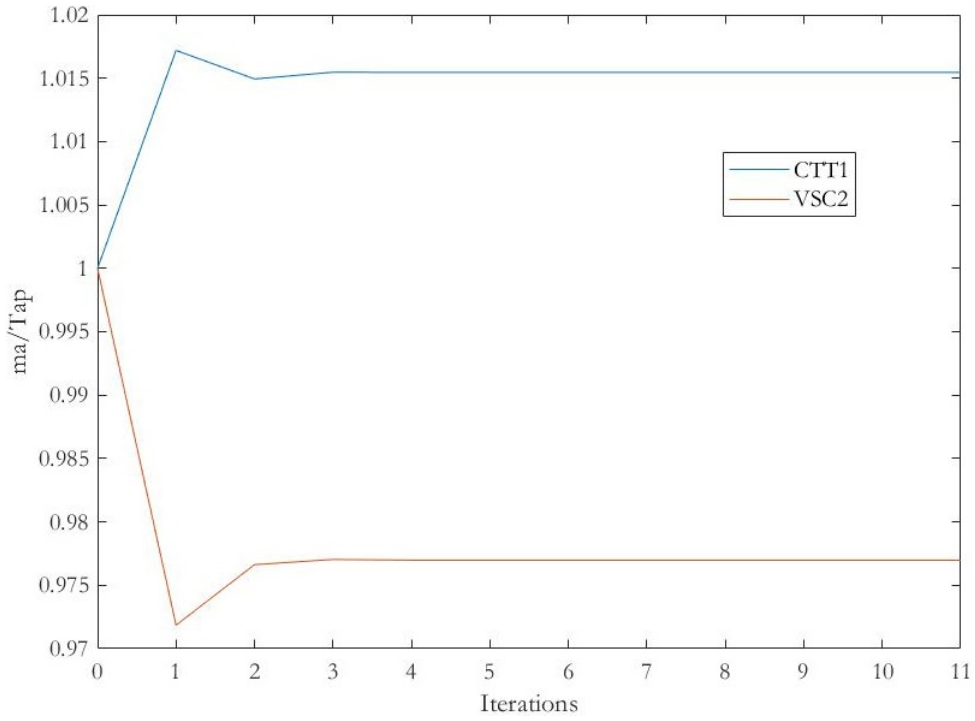

Figure 4.6: Modified IEEE 30 Modulation amplitude for Qt control

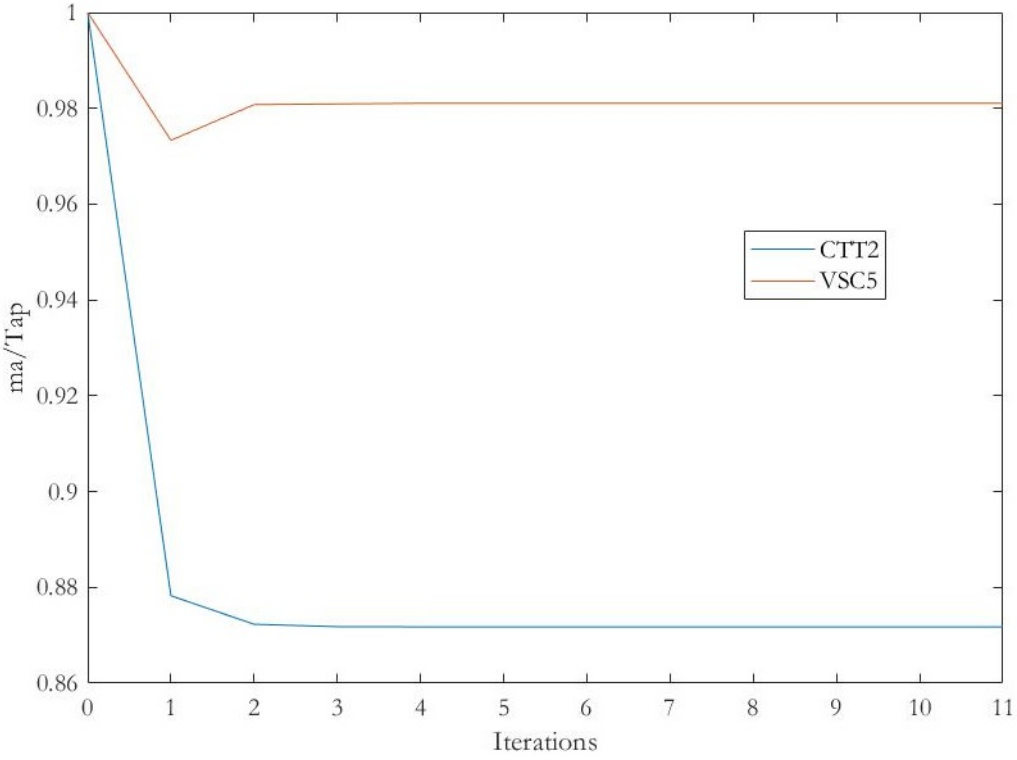

Figure 4.7: Modified IEEE 30 Modulation amplitude for Vt control

4.2.3 Case Study Modified PEGASE System

This case accurately represents the size and complexity of part of the European high voltage transmission network. It contains 1,354 buses, 260 generators, 1,991 branches and it operates at 380kV and 220kV. The data comes from the Pan European Grid Advanced Simulation and State Estimation (PEGASE) project [106] [107]. The original case has been modified to incorporate an HVDC Link and a MTDC grid as shown in Fig. 4.8. Both DC grids operate with a nominal voltage of 345kV and 500MVA rating. The HVDC link is set to operate as Voltage Droop Control strategy, and the MTDC grid is set for fixed Voltage regulation using a VSC type #II. Table 4.13 summarise the parameters of the DC grids, coupling transformers and VSCs . Additionally, the PST and the CTT between buses B7466-B3649 and B6153-B6807 have been changed from fixed control to automatic active power control and automatic tap changer for reactive power control respectively.

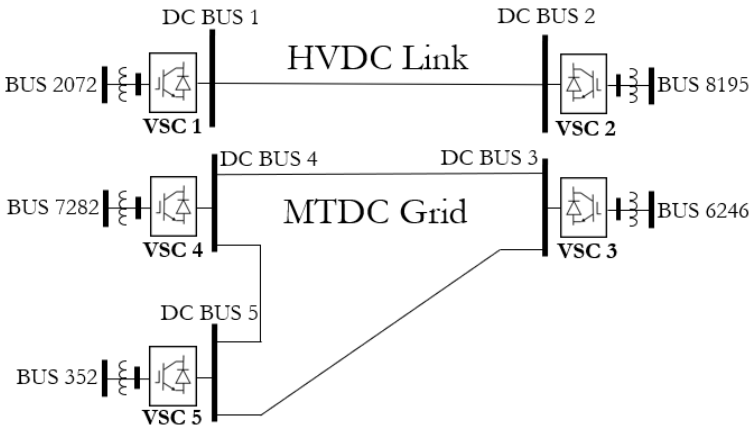

Figure 4.8: Modified PEGASE Project

Table 4.13: Converter and DC grid parameters

Parameter	Value	
Rating VSC / DC Voltage	1000MVA	345kV
Max / Min DC Voltage	1.1 p.u.	0.9 p.u.
Max / Min m_a	1.22	0.75
Coup. Transformer r_s / x_s	0.0001 p.u.	0.0105 p.u.
VSC (1,2) r_s / x_s	0.0002 p.u.	0.0250 p.u.
VSC (3,4,5) r_s / x_s	0.00015 p.u.	0.00305 p.u.
VSC (1,2) Loss Coefficient	$\alpha = 0.01, \beta = \gamma = 1x10^{-4}$	
VSC (3,4,5) Loss Coefficient	$\alpha = 0.001, \beta = \gamma = 1x10^{-5}$	
DC line r_s (HVDC Link)	0.0005 p.u.	
DC line r_s (MTDC Grid)	0.0007 p.u.	
VSC 2 Droop K_{dp}	5	
VSC 2 Droop P_f^{set}	1 [MW]	
VSC 2 Droop V_f^{set}	1.01 [pu]	

The AC node B4231 has been selected to be the voltage angle reference at zero degrees. All the AC and DC transmission elements of the case have been modelled using FUBM. Furthermore, all VSCs type #I have been set for reactive power compensation (*Zero constraint*). Table 4.14 contains the control settings for all VSCs, PSTs and CTTs. Notice even though all VSCs are operating in one of the explained control modes from Section 3.2.1, the control constraints are set individually within the FUBM. Therefore, the model is not restricted to them. As proof of this, the control constraint 2 of the VSC 5 has been left as a free variable.

Simulation Results and Discussion

The presented FPFA formulation for the FUBM has been successfully solved in 15 iterations and 45.03 seconds. The system voltages are initialised as 1 [pu] and zero degrees phase angles. Figure 4.9 shows the convergence in each iteration of the FPFA for all the mismatch equations of the EPS. Even though this case system is much larger than the modified IEEE30 bus system from Subsection 4.2.2, the mismatch

Table 4.14: Control Settings for VSC and Transformers

Converter	Type	Mode	Const. 1	Const. 2
VSC 1	I	1	Theta = 0	Vac=1.05
VSC 2	III	7	Vdc Droop	Vac=1.07
VSC 3	II	5	Vdc=1.00	Vac=1.06
VSC 4	I	3	Pf=-500	Vac=1.075
VSC 5	I	3	Pf=-450	Vac= free
Transformer	From	To	Control Constraint	
PST	B7466	B3649	Pf = -290	
CTT	B6153	B6807	Qt =1.95	

* Power is expressed in MW and Voltage in p.u.

equations have almost met the target from iteration number 5. This means that the FUBM formulation is scalable and it also maintains a relatively fast convergence rate as well. Similar to the test case from subsection 4.2.2. the rest of the iterations are just to match with the minimum tolerance ϵ.

Tables 4.15 and 4.16 present the DC grid voltages and the solution of the VSCs controls respectively. All the set controls have met their targets. It can be appreciated that the VSC 2 has delivered the appropriate active power according to the Voltage Droop Strategy. The control values for the state variables B_{eq}, θ_{sh} and m_a were obtained. The *Zero Constraint* compensated the reactive power in all VSC and thus there is only active power flowing though the DC grids. As it can be observed in this case the DC voltage angles are also maintained constant per DC grid. The results from the PST and the CTT are presented in Table 4.17.

Table 4.15: Modified PEGASE DC Grids Voltages Results

Bus ID	Vm [pu]	Va [deg]	Bus ID	Vm [pu]	Va [deg]
B001	1.0102	-17.3998	B003	1.0000	-7.4014
B002	1.0100	-17.3998	B004	1.0034	-7.4014
			B004	1.0033	-7.4014

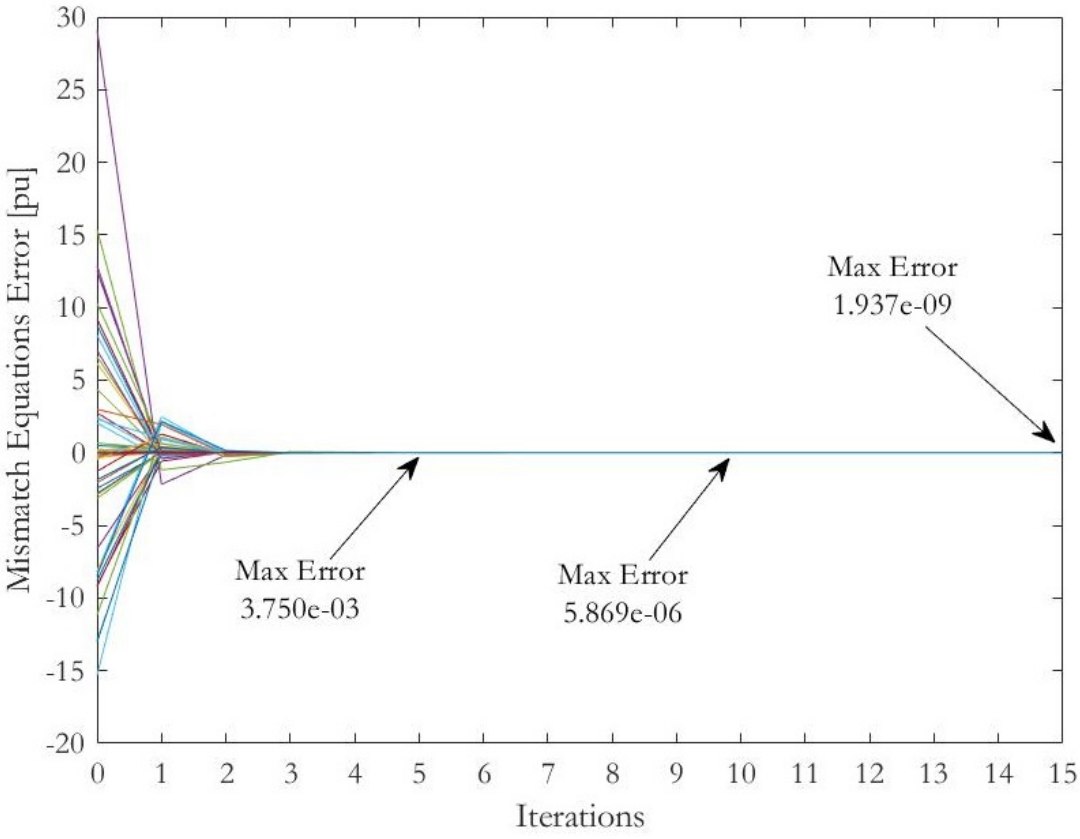

Figure 4.9: Modified Pegase Convergence for all State Variables

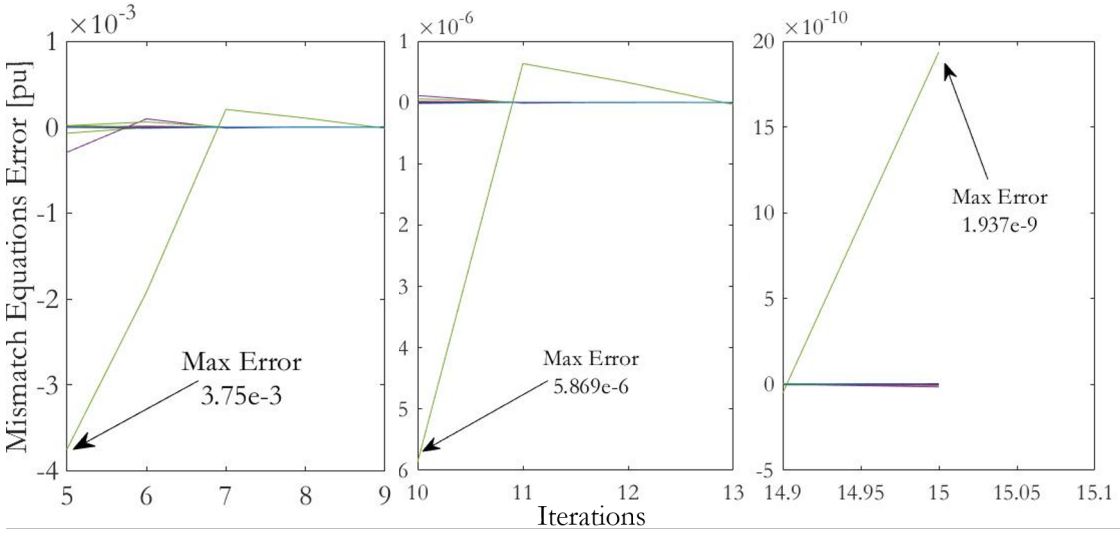

Figure 4.10: Modified Pegase Convergence for all State Variables (Zoom)

Table 4.16: Modified PEGASE VSC Control Results

VSC ID	P_f [MW]	Q_f [MVAr]	Q_t [MVAr]	θ_{sh} [deg]	B_{eq} [pu]	m_a [tap]
1	-50.0123	0	298.9929	0	-2.9907	1.0646
2	50.0000	0	-581.4818	0.3595	0.0200	0.7996
3	946.8592	0	-245.9472	0	3.9235	0.8263
4	-500.000	0	-123.5432	11.3586	1.8885	0.9113
5	-450.000	0	172.1516	7.9647	-0.8343	1.0000

Table 4.17: Modified PEGASE PSTs and CTTs Control Results

Transformer Type	Element No.	P_f [MW]	θ_{sh} [deg]	Q_t [MVAr]	m_a [tap]
PST	1	-290.0	0.0011	***	***
CTT	1	***	***	1.950	0.9822

From Fig. 4.11 it can be appreciated that from iteration 4 the modulation amplitude has almost reached convergence for voltage control and reactive power control in the AC side. Overall, with this simulation it is clear that the FUBM is capable to model several elements of the power system regardless of the size of the system and without sacrificing computational effort. Moreover the entire grid was calculated using just one reference angle in bus B4231. All the controls worked as expected. The FPFA has a fast convergence regardless of the amount of controls applied.

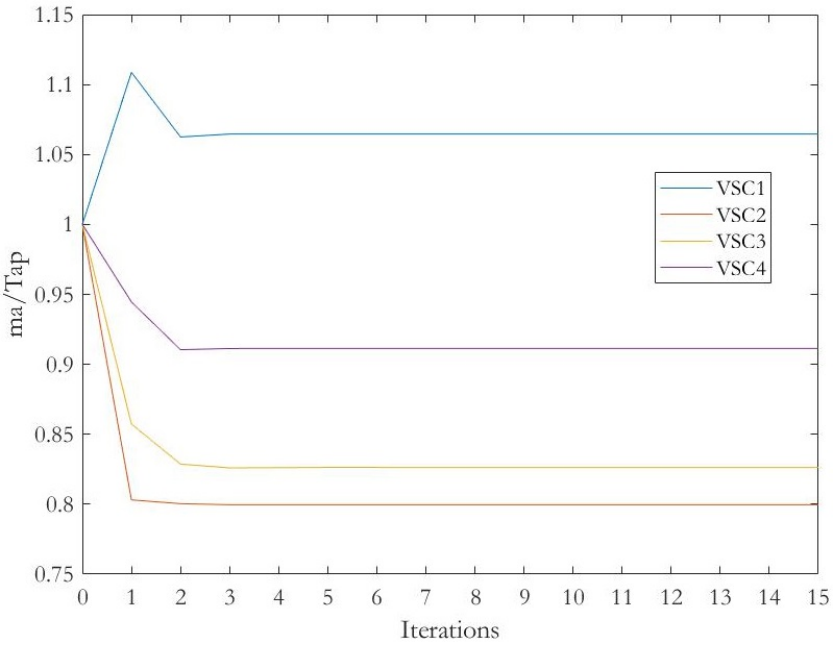

Figure 4.11: Modified PEGASE Modulation amplitude for Vt control

Chapter Summary

In this Chapter, the Power Flow Algorithm for the steady state solution of AC/DC EPS using FUBM has been presented. As seen in subsection 4.1.3, the proposed Power Flow Formulation takes advantage of all the extra variables that the FUBM model includes. Thus a fully flexible AC/DC grid could be accurately modelled and simulated. Accordingly, the extended mismatch equations for each one of the additional controls and constraints were presented in detail. Detailed formulation of the equations and the Jacobian partial derivative elements were also included. Additionally a Flowchart containing the step by step process of the FPFA has been presented. The FPFA using FUBM has been implemented in MATPOWER to create a fully flexible MATPOWER-FUBM power flow solver and showing the simplicity of its implementation. Three test cases were presented to show the capabilities of the FUBM in modelling a vast array of power system elements both for AC and DC networks and the FPFA for solving such systems seamlessly. The first test case was included to validate the FUBM model and FPFA algorithm. The second test case shows a highly modified test case to include as many control elements and MTDC

links as possible, and thus, show the performance of all the *in-models* working at the same time. Finally the last case tested the scalability of this new formulation by simulating a modified version of the PEGASE EPS. This test shows that there is no extra computational effort as the size of the problem gets increased. Moreover, the the amount of iterations to reach convergence between each test case was quite similar. The simulations results showed that there is no need to analyse the system equations grid by grid and thereby avoiding the inclusion of separate model libraries for each elements in the AC and DC grid. There is no need for introducing additional coupling constraints to maintain power balance between the AC and DC side of the grid. From a purely mathematical perspective, there is no distinction between AC and DC counterparts when the grid is modelled using FUBM. Thus, the same AC Power Flow equations can be used to solve the entire hybrid EPS whilst at the same time incorporating the extra levels of control and flexibility contained in such grids. In the proposed FPFA algorithm, voltage and power control are addressed per variable for all the elements. Simulation results demonstrate high speed quadratic convergence with full control over the grid solving AC/DC grids using AC-only equations. Such high flexibility of use as well as convergence characteristics, makes the FPFA algorithm alongside the FUBM model perfect candidates for solving Optimal Power Flows for hybrid AC/DC networks. This is shown in the next Chapter.

Chapter 5

Flexible AC/DC OPF using FUBM

Power Flow analysis tools are widely used on a daily basis by all TSOs around the world. In Chapter 4 the FUBM from Chapter 3 was used to propose a solution for conventional power flow analysis of hybrid AC/DC grids (the so-called FPFA). The FPFA is formulated such that it incorporates additional control variables and their associated constraints (in form of an expanded vector of state variables and accompanying mismatch constraints) for power system elements modelled through FUBM *in-models* for modelling and solving hybrid AC/DC networks that have extra degrees of control capabilities, and flexibility of operation. To this end, the FPFA coupled with FUBM modelling can be used to ascertain the state of a fully flexible system at each point in time. This can in principle therefore be used by the TSOs for planning network operation in advance of real-time for those systems where there are extra levels of flexibility promised by control devices such as PST/CTTs and VSCs.

Notwithstanding this, solving a conventional power flow problem - even with added level of control elements - for actual operational planning purposes may have drawbacks. More specifically there are two major disadvantages to using power flows for planning system operation namely, i) They do not consider any transmission or voltage limits for any of the elements in the EPS and ii) The power dispatch of all generation units has to be known beforehand. Typically in order to determine the power dispatch for all the committed generators in a system, an Economic Dispatch (ED) problem is solved. The premise of ED is to determine an *optimum*

schedule for power dispatch for all committed generators that would meet the system load profile for a specific planning timescale. The ED however does not take into account transmission losses in the network.

It may seem natural that by combining the power flow problem with the ED, an optimum power dispatch considering transmission losses can be determined, but unfortunately this is not the case. Even though both analyses are crucial for all TSOs in helping them determining the state of their system, neither the ED nor the power flow analysis consider the physical limitations of the elements in the EPS. Furthermore, by not including the transmission losses directly into the ED, it is highly likely the power dispatch will already be a sub-optimal solution. Thus, the results may not be realistic, or even feasible, especially for networks that does indeed exert extra levels of flexibility and control. Therefore, in order to address these shortcomings, the Optimal Power Flow (OPF) problem is the type of analysis that needs to be carried out. The OPF problem combines the ED with the power flow problem while considering all the physical limits of the EPS as well. The existence of the OPF analysis tools do not mean that the power flow or the ED analyses are not used in daily operational planning in power systems. They are practical tools that are widely used aimed at different planning timescales and/or applications. In fact, it is a common practice to use the power flow solution as the initial conditions for the OPF problem.

This chapter presents a formulation for solving OPFs problem for hybrid AC/DC grids using the FUBM from chapter 3 [1]. Just like the power flow formulation presented in chapter 4, the OPF-FUBM formulation also provides a direct link between the AC and DC parts of the grid. Thus, the entire network can be solved within a unified frame of reference. Therefore, conventional AC OPF equations are used to solve hybrid AC/DC grids. This formulation maintains the advantages of the FUBM formulation, such as its adaptability to simulate any network topology and diverse control elements. To this end, the OPF formulation accommodates extended opti-

[1] The flexible OPF formulation using FUBM as well as the some of the test cases and simulation results presented in this chapter have been published in the International Journal of Electrical Power and Energy Systems - ElSevier by the author of this thesis and his supervisors [28].

misation variables associated with all the control elements that are active over the course of the solution. Furthermore, the vector of constraints may be extended to accommodate any specific controls on power (e.g. scheduled power output of VSCs in a multi-terminal VSC-HVDC link) or on voltage (e.g. voltage control set points for a STATCOM) if deemed appropriate. As a result, the operation of a flexible and fully controllable AC/DC grid can be simulated without adding extra burden to the optimisation problem or any computational effort.

The remainder of this chapter is structured as follows: Section 5.1 describes the OPF formulation in detail. In this section, the extended optimisation variables, constraints and the full optimisation problem using FUBM are presented. Section 5.2 presents the creation of the Lagrangian function and its derivatives for all the traditional OPF variables and the extra FUBM optional variables. Similarly, derivatives for Objective function, Power balance equations and Branch Flow equations are also shown. Implementation of the FUBM-OPF for MATPOWER and AIMMS is presented in section 5.3. Test cases, Simulation results and analysis are presented in Section 5.4 for both implementations. Finally, a chapter summary is added.

5.1 Flexible OPF Formulation using FUBM

5.1.1 Introduction

Mathematically, in the OPF problem a chosen objective function is solved towards its optimum operating point subject to realistic technical and economical equality and inequality constraints of the power system [14, 15, 22]. More generally, the OPF problem is basically a constrained, non-linear, non-convex, optimisation problem, which for an actual EPS, contains a large number of non-linear constraints representing the equations required to accurately analyse the power transfer across the entire EPS (i.e. the power balance equations), the physical limitations of the actual system as well as the economic boundaries within which the system needs to operate [14]. The complexity and the growth of the number of constraints increases for a hybrid AC/DC EPS, and it grows even more if controls to improve the flexibility of operation of the network are included in the optimisation problem.

The formulation of the OPF using FUBM presented in this chapter ensures a computationally tractable and at the same time scalable solution for fully flexible and controllable hybrid AC/DC EPSs (i.e. it provides solutions to larger systems without significantly sacrificing computational time). Moreover, the OPF-FUBM solution properly reflects the intricacies of all the interactions of the control elements and capture enough detail to be a realistic representation of the actual hybrid system using a single frame of reference.

5.1.2 OPF-FUBM Formulation

This section presents the OPF formulation for solving hybrid AC/DC EPS when modelled using the FUBM. The presented formulation is the most complete since it includes the optional variables as well as the optional power and voltage controls that were described in Chapters 3 and 4. Just like in the FPFA-FUBM formulation of the preceding chapters, these optional controls can be activated or deactivated as needed. Therefore the formulation using FUBM can be used to solve OPF for AC, DC or hybrid AC/DC networks.

Extended Optimisation Variables

With the aim of optimising a fully controllable AC/DC grid, the traditional OPF equations and optimisation variables from section 2.2 are extended to include all the extra control variables that the FUBM can accommodate within its various *in-models*. Unlike the extended state variables for the FPFA formulation (presented in subsection 4.1.3), the extended optimisation variables do not need to be set as a balanced system where a one to one ratio between variables and constraints must be maintained. Therefore, in the optimisation problem, the formulation can have more variables than constraints. As a consequence, the extended optimisation variables does not have to be identified by their relationship with a specific constraint. Instead, they are identified by the element that posses the specific control to be modelled. For example, the variable θ_{sh} is active for the selected VSCs and PSTs because in these devices there can be provisions for active power control. For all the remaining elements present in the system that have no active power control, instead

of considering θ_{sh} as a variable, it is represented as a fixed parameter. Therefore, the extended state variables are now expressed as optimisation variables with different indices as presented in (5.1.1). It is worth to highlight that in contrast to the traditional formulation of the OPF presented in section 2.2, which identifies all the state and control variables of the full system as $\mathbf{x}_0$ and $\mathbf{u}_0$ respectively, for simplicity the OPF-FUBM formulation includes both vectors of variables in a single optimisation vector $\mathbf{x}$ as presented in (5.1.1).

$$\mathbf{x} = \begin{matrix}\text{Power Flow}\\ \text{State Variables}\end{matrix} \begin{bmatrix} \mathbf{V_a}^{\{i\}} & \forall i \in \boldsymbol{\mathcal{I}}_{pv} \cup \boldsymbol{\mathcal{I}}_{pq} \\ \mathbf{V_m}^{\{i\}} & \forall i \in \boldsymbol{\mathcal{I}}_{pq} \\ \boldsymbol{\theta}_{\mathbf{sh}}^{\{i\}} & \forall i \in \boldsymbol{\mathcal{I}}_{sh} \\ \mathbf{B_{eq}}^{\{i\}} & \forall i \in \boldsymbol{\mathcal{I}}_{Q_z} \\ \mathbf{B_{eq}}^{\{i\}} & \forall i \in \boldsymbol{\mathcal{I}}_{vscII} \\ \mathbf{m_a}^{\{i\}} & \forall i \in \boldsymbol{\mathcal{I}}_{V_t} \\ \mathbf{m_a}^{\{i\}} & \forall i \in \boldsymbol{\mathcal{I}}_{Q_t} \\ \boldsymbol{\theta}_{\mathbf{sh}}^{\{i\}} & \forall i \in \boldsymbol{\mathcal{I}}_{vscIII} \end{bmatrix} \longrightarrow \mathbf{x} = \begin{matrix}\text{Optimisation}\\ \text{Variables}\end{matrix} \begin{bmatrix} \mathbf{V_a}^{\{i\}} & \forall i \in \boldsymbol{\mathcal{I}}_{bus} \\ \mathbf{V_m}^{\{i\}} & \forall i \in \boldsymbol{\mathcal{I}}_{bus} \\ \mathbf{P_g}^{\{i\}} & \forall i \in \boldsymbol{\mathcal{I}}_{gen} \\ \mathbf{Q_g}^{\{i\}} & \forall i \in \boldsymbol{\mathcal{I}}_{gen} \\ \boldsymbol{\theta}_{\mathbf{sh}}^{\{i\}} & \forall i \in \boldsymbol{\mathcal{I}}_{sh} \\ \mathbf{B_{eq}}^{\{i\}} & \forall i \in \boldsymbol{\mathcal{I}}_{vsc} \\ \mathbf{m_a}^{\{i\}} & \forall i \in \boldsymbol{\mathcal{I}}_{ma} \end{bmatrix} \tag{5.1.1}$$

Notice that for the OPF formulation, there is no need to have PV nodes or PQ nodes as it was done for Power Flows. The index $\boldsymbol{\mathcal{I}}_{bus}$ identifies all the buses in the system, and the index $\boldsymbol{\mathcal{I}}_{ref}$ will be used for the node for which the voltage angle will be set as reference angle. Additionally, the active $\mathbf{P}_g$ and reactive $\mathbf{Q}_g$ generation now are optimisation variables, and they will be active for all the $\boldsymbol{\mathcal{I}}_{gen}$ generators in the EPS. Furthermore, the index $\boldsymbol{\mathcal{I}}_{sh}$ identifies the PSTs and VSCs that have θ_{sh} as an active variable. Similarly, the index $\boldsymbol{\mathcal{I}}_{ma}$ identifies the CTTs and VSCs with the tap/modulation amplitude as a variable. And finally the index $\boldsymbol{\mathcal{I}}_{vsc}$ identify all the VSCs in general.

Even though each element has the possibility to add their related optimisation variable, it does not mean that all the elements should have an active control variable. Thus, the selected elements within the index will have their respective

variables as active while the remaining ones will be just parameters. For example, the formulation can have some VSCs with a variable θ_{sh} and the remaining ones as a parameter. The only exception is the $\boldsymbol{\mathcal{I}}_{vsc}$ index, since the variable B_{eq} is active for all the VSCs for either *Zero Constraint* or Voltage regulation.

Each one of the optimisation variables in $\mathbf{x}$ can be limited using an upper and lower boundary to restrict its variation within certain limits. The upper and lower limits for each variable are set in the vectors $\mathbf{x}_{max}$ and $\mathbf{x}_{min}$ respectively. This limits are crucial since they represent realistic operational limits for all the elements in the power grid. For example, in the UK, the Grid Code of 2020 the CC.6.1.4 connection conditions states that the nodal voltage variation for 400kV should not be more than $\pm 5\%$ of their nominal operation value, thus the upper and lower boundaries for the voltage magnitude must be set as stated [108]. If a variable must be set to a specific value, the upper and lower boundaries will be set the same. Therefore, for a controlled voltage using the selected generators, VSCs, or CTTs, the maximum and minimum values for $\mathbf{x}$ are set as presented in (5.1.2)

$$\begin{aligned}
\mathbf{x}_{min}^{\{i\}} = \mathbf{x}_{max}^{\{i\}} = \mathbf{v}_{\mathbf{gen}}^{\mathbf{set}\ \{i\}} \quad \forall i \quad \text{gen nodes} \in \mathcal{I}_{v_{gen}} \\
\mathbf{x}_{min}^{\{i\}} = \mathbf{x}_{max}^{\{i\}} = \mathbf{v}_{\mathbf{t}}^{\mathbf{set}\{i\}} \quad \forall i \quad \text{“to” nodes} \in \mathcal{I}_{v_t} \\
\mathbf{x}_{min}^{\{i\}} = \mathbf{x}_{max}^{\{i\}} = \mathbf{v}_{\mathbf{dc}}^{\mathbf{set}\{i\}} \quad \forall i \quad \text{DC nodes} \in \boldsymbol{\mathcal{I}}_{v_{dc}}
\end{aligned} \tag{5.1.2}$$

where the index $\boldsymbol{\mathcal{I}}_{v_{gen}}$ identifies the AC voltage controlled nodes using generators. Similarly, the index $\boldsymbol{\mathcal{I}}_{v_t}$ identifies the CTTs and VSCs for voltage “to” control, and finally, the index $\boldsymbol{\mathcal{I}}_{v_{dc}}$, identifies the DC nodes for voltage regulation using VSCs.

The optimisation variables boundaries are not only to limit voltage variations, they are also used to restrict tap/m_a changes, generation limits, maximum reactive regulation from the VSCs and limits for θ_{sh} for PSTs and VSCs. Notice that the B_{eq}^{max} limit for reactive power regulation of the VSCs should be set as described in chapter 3 by equation (3.1.10).

Extended OPF Constraints

A general optimisation problem is typically subject to a set of $\mathbf{g}(\mathbf{x})$ equality and $\mathbf{h}(\mathbf{x})$ inequality constraints. As described in Chapter 2, the traditional OPF formulation

from section 2.2 only considers the real and reactive power balance equations as the equality constraints of the system. The FUBM-OPF formulation expands this set of equality constraints to include all the controls for all the *in-models* of the FUBM as shown in (5.1.3). The constraints are mainly focused on power exchange since fixed voltage regulation is limited by the optimisation variables as mentioned before.

$$\mathbf{g}(\mathbf{x}) = \underbrace{\begin{bmatrix} \mathbf{g}_{P_b}^{\{i\}}(\mathbf{x}) = 0 & \forall i \in \boldsymbol{\mathcal{I}}_{bus} \\ \mathbf{g}_{Q_b}^{\{i\}}(\mathbf{x}) = 0 & \forall i \in \boldsymbol{\mathcal{I}}_{bus} \end{bmatrix}}_{\substack{\text{Traditional OPF} \\ \text{Eq. Constraints}}} \longrightarrow \quad \mathbf{g}(\mathbf{x}) = \underbrace{\begin{bmatrix} \mathbf{g}_{P_b}^{\{i\}}(\mathbf{x}) = 0 & \forall i \in \boldsymbol{\mathcal{I}}_{bus} \\ \mathbf{g}_{Q_b}^{\{i\}}(\mathbf{x}) = 0 & \forall i \in \boldsymbol{\mathcal{I}}_{bus} \\ \mathbf{g}_{P_f}^{\{i\}}(\mathbf{x}) = 0 & \forall i \in \boldsymbol{\mathcal{I}}_{sh} \\ \mathbf{g}_{Q_z}^{\{i\}}(\mathbf{x}) = 0 & \forall i \in \boldsymbol{\mathcal{I}}_{Q_z} \\ \mathbf{g}_{Q_t}^{\{i\}}(\mathbf{x}) = 0 & \forall i \in \boldsymbol{\mathcal{I}}_{Q_t} \\ \mathbf{g}_{P_{dp}}^{\{i\}}(\mathbf{x}) = 0 & \forall i \in \boldsymbol{\mathcal{I}}_{vscIII} \\ \mathbf{g}_{G_{sw}}^{\{i\}}(\mathbf{x}) = 0 & \forall i \in \boldsymbol{\mathcal{I}}_{vsc} \end{bmatrix}}_{\substack{\text{Extended} \\ \text{FUBM-OPF} \\ \text{Eq. Constraints}}} \tag{5.1.3}$$

As it can be appreciated from (5.1.3), the extended equality constraints match perfectly with the extended mismatch equations from subsection 4.1.3. Thus, equations (4.1.8), (4.1.13), (4.1.16), (4.1.17), (4.1.20) and (4.1.21) from chapter 4 are also set as the equality constraints for the OPF formulation. Unlike the power flow (and the FPFA) mismatch constraints, for the OPF formulation, the power balance equations are calculated for all nodes instead of only for the PV and PQ nodes. Thus, the transmission losses, controls and interactions between all elements are considered during the optimisation process.

Additionally, just like in the FPFA, all the control constraints are optional. However, for the OPF-FUBM formulation, there is no need to have a one to one constraint-variable ratio. As a result, control variables can be optimised without the need to have a corresponding constraint. A clear example could be the θ_{sh} of a PST that could be optimised without specifying a specific power flow though the transformer. With that being said, the control constraints serve the purpose to accurately represent the settings for each element under specific operation strategies,

such as security reasons, control coordination, or as a result of contracts within the electricity market. Thus the constraints could be used to maintain a fixed power exchange between two areas (for example through an interconnector), represent the reactive power support from STATCOMs or control the reactive power using automatic tap changers.

The set of inequality constraints, $\mathbf{h}(\mathbf{x})$, represent the limits for the transmission lines (branch limits) for all *in-models* of the FUBM. The constraints are shown in (5.1.4) as one set of matrix equations and expanded in (5.1.5). They consist of two sets of n_l branch flow limits as nonlinear functions of the bus voltage angles and magnitudes, one for the from end and one for the to end of each branch. Notice that these equations also include the PQ-capability limit for all VSCs as seen in equation (3.1.7) in chapter 3. Finally, these equations will also use real and imaginary parts of the power injection equations (4.1.14) and (4.1.15) for their calculation.

$$\begin{aligned} \mathbf{h}_{S_f^2}(\mathbf{x}) \leq \mathbf{0} \quad &\rightarrow \quad |\mathbf{S}_f^2| - \mathbf{L}_{S_L^2} \leq \mathbf{0} \\ \mathbf{h}_{S_t^2}(\mathbf{x}) \leq \mathbf{0} \quad &\rightarrow \quad |\mathbf{S}_t^2| - \mathbf{L}_{S_L^2} \leq \mathbf{0} \end{aligned} \tag{5.1.4}$$

$$\begin{aligned} \left(\mathbf{P_f}^{\{i\}}(x)\right)^2 + \left(\mathbf{Q_f}^{\{i\}}(x)\right)^2 - \left(\mathbf{L}_{S_L}^{\{i\}}\right)^2 \leq \mathbf{0} \quad \forall i \in \mathcal{I}_{\text{FUBM}} \\ \left(\mathbf{P_t}^{\{i\}}(x)\right)^2 + \left(\mathbf{Q_t}^{\{i\}}(x)\right)^2 - \left(\mathbf{L}_{S_L}^{\{i\}}\right)^2 \leq \mathbf{0} \quad \forall i \in \mathcal{I}_{\text{FUBM}} \end{aligned} \tag{5.1.5}$$

Objective Function

The OPF objective function f can vary depending on the aim of the study. The OPF described in this Chapter, aims to minimise the total generation cost as it is a common practice in the industry. The cost function for each generator is typically quadratic. Therefore, f is defined as the summation of the individual polynomial cost functions for each generator as shown in (5.1.6).

$$f(\mathbf{x}) = \sum_{i=1}^{ng} f_P^{\{i\}}(P_g^{\{i\}}) + f_Q^{\{i\}}(Q_g^{\{i\}}) \tag{5.1.6}$$

Complete AC/DC FUBM-OPF Formulation

Considering the objective function, extended variables, and extended equality and inequality constraints from equations (5.1.1), (5.1.3), (5.1.5) and (5.1.6), the Hybrid

AC/DC OPF problem using FUBM can be compactly formulated as presented in equations (5.1.7) to (5.1.17). It is important to notice that the presented optimisation problem does not consider any discrete variables. Even though the transformers taps are not continuous, for this specific case, it has been proven that is good enough to consider them as continuous variables and once the optimal solution has been found they can be adjusted to their closest step/tap [74]. Not having any discrete variables, if it is not needed, will also help with convergence of the OPF as the problem need not have mixed integers which are mostly harder to solve computationally.

$$\begin{aligned} \min_{\mathbf{x}} \quad & f(\mathbf{x}) \end{aligned} \tag{5.1.7}$$

subject to:

$$\mathbf{g}_{S_b}(\mathbf{x}) = \mathbf{0} \tag{5.1.8}$$

$$\mathbf{g}_{P_f}(\mathbf{x}) = \mathbf{0} \tag{5.1.9}$$

$$\mathbf{g}_{Q_z}(\mathbf{x}) = \mathbf{0} \tag{5.1.10}$$

$$\mathbf{g}_{Q_t}(\mathbf{x}) = \mathbf{0} \tag{5.1.11}$$

$$\mathbf{g}_{Pv_{dp}}(\mathbf{x}) = \mathbf{0} \tag{5.1.12}$$

$$\mathbf{g}_{G_{sw}}(\mathbf{x}) = \mathbf{0} \tag{5.1.13}$$

$$\mathbf{h}_{S_f^2}(\mathbf{x}) \leq \mathbf{0} \tag{5.1.14}$$

$$\mathbf{h}_{S_t^2}(\mathbf{x}) \leq \mathbf{0} \tag{5.1.15}$$

where:

$$\mathbf{x} = [\mathbf{P_g}, \mathbf{Q_g}, \mathbf{V_a}, \mathbf{V_m}, \mathbf{B_{eq}}, \theta_{\mathbf{sh}}, \mathbf{m_a}, \mathbf{G_{sw}}]^\intercal \tag{5.1.16}$$

$$\mathbf{x}_{min} \leq \mathbf{x} \leq \mathbf{x}_{max} \tag{5.1.17}$$

After the construction of the full optimisation problem, it must be solved using an algorithm which is compatible with the characteristics of the problem. As seen in section 2.3, there are many algorithms for the solution of OPFs with different strategies to choose from. One of the most popular ones among deterministic algorithms relies on the construction and minimisation of the Lagrangian function.

5.2 FUBM-OPF Lagrangian and Derivatives

For convenience during the development of the Lagrangian and its derivatives, the full OPF-FUBM optimisation problem in (5.1.7) to (5.1.17) is expressed in a more general form as shown in (5.2.18) to (5.2.20).

$$\min_{\mathbf{x}} \quad f(\mathbf{x}) \tag{5.2.18}$$

subject to:

$$\mathbf{g}(\mathbf{x}) = \mathbf{0} \tag{5.2.19}$$

$$\mathbf{h}(\mathbf{x}) \leq \mathbf{0} \tag{5.2.20}$$

Where, all the equality constraints from equations (5.1.8) to (5.1.13) are represented by a single vector of equations $\mathbf{g}(\mathbf{x})$. Similarly, the loadability constraints (or thermal limits) from equations 5.1.14 and 5.1.15 for all FUBM elements are expressed by an inequality constraint vector $\mathbf{h}(\mathbf{x})$.

5.2.1 The Lagrangian function

As described in Section 2.2.1 the Lagrangian strategy aims to transform the constrained optimisation problem into an unconstrained problem to then find the critical points of the ensuing Lagrangian function and determine if it is a maximum or a minimum. The Lagrange theorem states that at any critical point of the function evaluated under the equality constraints, the gradient of the function (at that point) can be expressed as a linear combination of the gradients of the constraints (at that point), where the coefficients for the linear combination are the"Lagrange multipliers". Thus following the theory presented in chapter 2, the Lagrangian function for the FUBM-OPF formulation in (5.2.18) to (5.2.20), is presented as in (5.2.21).

$$\mathcal{L}(\mathbf{x}, \boldsymbol{\lambda}, \boldsymbol{\mu}) = f(\mathbf{x}) + \sum_{i=1}^{n_e} \lambda_i g_i(\mathbf{x}) + \sum_{j=1}^{n_i} \mu_j h_j(\mathbf{x}) \tag{5.2.21}$$

$$\mathcal{L}(\mathbf{x}, \boldsymbol{\lambda}, \boldsymbol{\mu}) = f(\mathbf{x}) + \boldsymbol{\lambda}^\top \mathbf{g}(\mathbf{x}) + \boldsymbol{\mu}^\top \mathbf{h}(\mathbf{x}) \tag{5.2.22}$$

The Lagrangian function can be expressed in matrix form as in (5.2.22). The vector variables λ and μ are the Lagrange multipliers for the of n_e and n_i equality and inequality constraints respectively.

5.2.2 Lagrangian Derivatives

Lagrangian First Order Partial Derivatives

Following the notation presented in subsection 2.4.3, the first order partial derivatives of the Lagrangian in (5.2.22) with respect to the vectors $\mathbf{x}$, $\boldsymbol{\lambda}$ and $\boldsymbol{\mu}$ are presented in equations (5.2.23), (5.2.24), (5.2.25).

$$\mathcal{L}_{\mathbf{x}}(\mathbf{x}, \lambda, \mu) = f_{\mathbf{x}} + \boldsymbol{\lambda}^{\top}\mathbf{g}_{\mathbf{x}} + \boldsymbol{\mu}^{\top}\mathbf{h}_{\mathbf{x}} \tag{5.2.23}$$

$$\mathcal{L}_{\boldsymbol{\lambda}}(\mathbf{x}, \lambda, \mu) = \mathbf{g}(\mathbf{x})^{\top} \tag{5.2.24}$$

$$\mathcal{L}_{\boldsymbol{\mu}}(\mathbf{x}, \lambda, \mu) = \mathbf{h}(\mathbf{x})^{\top} \tag{5.2.25}$$

Where the partial derivatives for the equality and inequality constraints are presented in (5.2.26), and (5.2.27) respectively.

$$\mathbf{g}_{\mathbf{x}} = \begin{bmatrix} \Re\{\mathbf{g}_{S_{b_{\mathbf{x}}}}\} & \Im\{\mathbf{g}_{S_{b_{\mathbf{x}}}}\} & \mathbf{g}_{P_{f_{\mathbf{x}}}} & \mathbf{g}_{Q_{z_{\mathbf{x}}}} & \mathbf{g}_{Q_{t_{\mathbf{x}}}} & \mathbf{g}_{Pv_{dp_{\mathbf{x}}}} & \mathbf{g}_{G_{sw_{\mathbf{x}}}} \end{bmatrix}^{\top} \tag{5.2.26}$$

$$\mathbf{h}_{\mathbf{x}} = \begin{bmatrix} \mathbf{h}_{S^2_{f_{\mathbf{x}}}} & \mathbf{h}_{S^2_{t_{\mathbf{x}}}} \end{bmatrix}^{\top} \tag{5.2.27}$$

Details of the first order partial derivatives of the objective function, the equality and inequality constraints inside $\mathbf{g}_{\mathbf{x}}$ and $\mathbf{h}_{\mathbf{x}}$ are described later in this subsection.

Lagrangian Second Order Partial Derivatives

The second order partial derivatives with respect to $\boldsymbol{\lambda}$ and $\boldsymbol{\mu}$ are zero. In the case of the optimisation vector, the Hessian of the Lagrangian with respect to $\mathbf{x}$ is given by (5.2.28).

$$\mathcal{L}_{\mathbf{xx}}(\mathbf{x}, \boldsymbol{\lambda}, \boldsymbol{\mu}) = f_{\mathbf{xx}} + \mathbf{g}_{\mathbf{xx}}(\boldsymbol{\lambda}) + \mathbf{h}_{\mathbf{xx}}(\boldsymbol{\mu}) \tag{5.2.28}$$

Where the hessian for the equality and inequality constraints are presented in (5.2.29), and (5.2.30) respectively.

$$\mathbf{g_{xx}} = \left[\mathbf{g}_{S_{b_{\mathbf{xx}}}} + \mathbf{g}_{P_{f_{\mathbf{xx}}}} + \mathbf{g}_{Q_{z_{\mathbf{xx}}}} + \mathbf{g}_{Q_{t_{\mathbf{xx}}}} + \mathbf{g}_{Pv_{dp_{\mathbf{xx}}}} + \mathbf{g}_{G_{sw_{\mathbf{xx}}}}\right] \tag{5.2.29}$$

$$\mathbf{h_x} = \left[\mathbf{h}_{S^2_{f_{\mathbf{x}}}} + \mathbf{h}_{S^2_{t\,\mathbf{x}}}\right] \tag{5.2.30}$$

Details of the second order partial derivatives of the objective function, the equality and inequality constraints inside $\mathbf{g_{xx}}$ and $\mathbf{h_{xx}}$ are described later in this subsection.

Objective Function derivatives

Details of the first and second order partial derivatives of the objective function from equations (5.2.23) and (5.2.28) are presented here. Considering equation (5.1.6), Let the vectors $\mathbf{f}_P$ and $\mathbf{f}_Q$ be the polynomial cost functions for the real and reactive power for generator i. The first partial derivatives with respect to $\mathbf{x}$ are shown in (5.2.31).

$$f_{\mathbf{x}} = \frac{\partial f}{\partial \mathbf{X}} = \begin{bmatrix} f_{\mathbf{V}_a} & f_{\mathbf{V}_m} & f_{\mathbf{P}_g} & f_{\mathbf{Q}_g} & f_{\mathbf{B}_{eq}} & f_{\boldsymbol{\theta}_{sh}} & f_{\mathbf{m}_a} & f_{\mathbf{G}_{sw}} \end{bmatrix} \tag{5.2.31}$$

$$f_{\mathbf{x}} = \begin{bmatrix} \mathbf{0} & \mathbf{0} & f_{\mathbf{P}_g} & f_{\mathbf{Q}_g} & \mathbf{0} & \mathbf{0} & \mathbf{0} & \mathbf{0} \end{bmatrix} \tag{5.2.32}$$

As noticed from equation (5.2.32) only the generator variables have non-zero partial derivatives, therefore, the second order partial derivatives of the objective function are expressed as:

$$f_{\mathbf{xx}} = \frac{\partial}{\partial \mathbf{X}}\left(f_{\mathbf{x}}^{\top}\right) = \begin{bmatrix} 0 & 0 & 0 & 0 & 0 & 0 & 0 & 0 \\ 0 & 0 & 0 & 0 & 0 & 0 & 0 & 0 \\ 0 & 0 & f_{P_gP_g} & 0 & 0 & 0 & 0 & 0 \\ 0 & 0 & 0 & f_{Q_gQ_g} & 0 & 0 & 0 & 0 \\ 0 & 0 & 0 & 0 & 0 & 0 & 0 & 0 \\ 0 & 0 & 0 & 0 & 0 & 0 & 0 & 0 \\ 0 & 0 & 0 & 0 & 0 & 0 & 0 & 0 \\ 0 & 0 & 0 & 0 & 0 & 0 & 0 & 0 \end{bmatrix} \tag{5.2.33}$$

Power Balance Derivatives

Details of the first and second order partial derivatives of the power balance equations from equations (5.2.23) and (5.2.28) are presented here. Considering equation (5.1.8) the first partial derivatives are shown in (5.2.35).

$$\mathbf{g}_{S_b\mathbf{x}} = \frac{\partial \mathbf{g}_{S_b}}{\partial \mathbf{x}} \tag{5.2.34}$$

$$= \begin{bmatrix} \mathbf{g}_{S_b\mathbf{V}_a} & \mathbf{g}_{S_b\mathbf{V}_m} & \mathbf{g}_{S_b\mathbf{P}_g} & \mathbf{g}_{S_b\mathbf{Q}_g} & \mathbf{g}_{S_b\mathbf{B}_{eq}} & \mathbf{g}_{S_b\boldsymbol{\theta}_{sh}} & \mathbf{g}_{S_b\mathbf{m}_a} & \mathbf{g}_{S_b\mathbf{G}_{sw}} \end{bmatrix} \tag{5.2.35}$$

$$\mathbf{g}_{S_b\mathbf{x}} = \begin{bmatrix} \mathbf{g}_{S_b\mathbf{V}_a} & \mathbf{g}_{S_b\mathbf{V}_m} & \mathbf{0} & \mathbf{0} & \mathbf{g}_{S_b\mathbf{B}_{eq}} & \mathbf{g}_{S_b\boldsymbol{\theta}_{sh}} & \mathbf{g}_{S_b\mathbf{m}_a} & \mathbf{g}_{S_b\mathbf{G}_{sw}} \end{bmatrix} \tag{5.2.36}$$

Contrary to the second derivatives of the objective function in (5.2.32), the second derivatives for the power balance equations do not have derivatives for the generation variables, but have for the voltage and FUBM variables. This can be appreciated in equation (5.2.37) where the hessian of the power balance equations is presented.

$$\mathbf{g}_{S_b\mathbf{xx}} = \frac{\partial}{\partial \mathbf{x}} \left(\mathbf{g}_{S_b\mathbf{x}}^{\top} \right) =$$

$$\begin{bmatrix}
\mathbf{g}_{S_b\mathbf{V}_a\mathbf{V}_a} & \mathbf{g}_{S_b\mathbf{V}_a\mathbf{V}_m} & 0 & 0 & \mathbf{g}_{S_b\mathbf{V}_a\mathbf{B}_{eq}} & \mathbf{g}_{S_b\mathbf{V}_a\boldsymbol{\theta}_{sh}} & \mathbf{g}_{S_b\mathbf{V}_a\mathbf{m}_a} & \mathbf{g}_{S_b\mathbf{V}_a\mathbf{G}_{sw}} \\
\mathbf{g}_{S_b\mathbf{V}_m\mathbf{V}_a} & \mathbf{g}_{S_b\mathbf{V}_m\mathbf{V}_m} & 0 & 0 & \mathbf{g}_{S_b\mathbf{V}_m\mathbf{B}_{eq}} & \mathbf{g}_{S_b\mathbf{V}_m\boldsymbol{\theta}_{sh}} & \mathbf{g}_{S_b\mathbf{V}_m\mathbf{m}_a} & \mathbf{g}_{S_b\mathbf{V}_m\mathbf{G}_{sw}} \\
0 & 0 & 0 & 0 & 0 & 0 & 0 & 0 \\
0 & 0 & 0 & 0 & 0 & 0 & 0 & 0 \\
\mathbf{g}_{S_b\mathbf{B}_{eq}\mathbf{V}_a} & \mathbf{g}_{S_b\mathbf{B}_{eq}\mathbf{V}_m} & 0 & 0 & \mathbf{g}_{S_b\mathbf{B}_{eq}\mathbf{B}_{eq}} & \mathbf{g}_{S_b\mathbf{B}_{eq}\boldsymbol{\theta}_{sh}} & \mathbf{g}_{S_b\mathbf{B}_{eq}\mathbf{m}_a} & \mathbf{g}_{S_b\mathbf{B}_{eq}\mathbf{G}_{sw}} \\
\mathbf{g}_{S_b\boldsymbol{\theta}_{sh}\mathbf{V}_a} & \mathbf{g}_{S_b\boldsymbol{\theta}_{sh}\mathbf{V}_m} & 0 & 0 & \mathbf{g}_{S_b\boldsymbol{\theta}_{sh}\mathbf{B}_{eq}} & \mathbf{g}_{S_b\boldsymbol{\theta}_{sh}\boldsymbol{\theta}_{sh}} & \mathbf{g}_{S_b\boldsymbol{\theta}_{sh}\mathbf{m}_a} & \mathbf{g}_{S_b\boldsymbol{\theta}_{sh}\mathbf{G}_{sw}} \\
\mathbf{g}_{S_b\mathbf{m}_a\mathbf{V}_a} & \mathbf{g}_{S_b\mathbf{m}_a\mathbf{V}_m} & 0 & 0 & \mathbf{g}_{S_b\mathbf{m}_a\mathbf{B}_{eq}} & \mathbf{g}_{S_b\mathbf{m}_a\boldsymbol{\theta}_{sh}} & \mathbf{g}_{S_b\mathbf{m}_a\mathbf{m}_a} & \mathbf{g}_{S_b\mathbf{m}_a\mathbf{G}_{sw}} \\
\mathbf{g}_{S_b\mathbf{G}_{sw}\mathbf{V}_a} & \mathbf{g}_{S_b\mathbf{G}_{sw}\mathbf{V}_m} & 0 & 0 & \mathbf{g}_{S_b\mathbf{G}_{sw}\mathbf{B}_{eq}} & \mathbf{g}_{S_b\mathbf{G}_{sw}\boldsymbol{\theta}_{sh}} & \mathbf{g}_{S_b\mathbf{G}_{sw}\mathbf{m}_a} & \mathbf{g}_{S_b\mathbf{g}_{sw}\mathbf{G}_{sw}}
\end{bmatrix} \tag{5.2.37}$$

Branch Flows Injections derivatives

From subsection 4.1.4 in chapter 4 it is clear that the branch power control constraints of the FUBM are based from the general Branch Flow Injection equations (4.1.14) and (4.1.15). Therefore equality constraints (5.1.9), (5.1.10), (5.1.11),

(5.1.12), (5.1.13) and inequality constraints in (5.1.14) and (5.1.15) share the same structure. Thus, the derivatives of the control constraints are the derivatives of S_f and S_t with some small variations. Therefore the first partial derivatives of S_f and S_t are shown in (5.2.38), and the specific derivatives for each constraint are extensively described in Appendix C. Also, notice that in (5.2.38) the derivatives with respect to the generator variables are Zero.

$$\mathbf{g}_{S_{br}\mathbf{x}} = \frac{\partial \mathbf{g}_{S_{br}}}{\partial \mathbf{x}} = \\ = \begin{bmatrix} \mathbf{g}_{S_{br}\mathbf{V}_a} & \mathbf{g}_{S_{br}\mathbf{V}_m} & \mathbf{0} & \mathbf{0} & \mathbf{g}_{S_{br}\mathbf{B}_{eq}} & \mathbf{g}_{S_{br}\boldsymbol{\theta}_{sh}} & \mathbf{g}_{S_{br}\mathbf{m}_a} & \mathbf{g}_{S_{br}\mathbf{G}_{sw}} \end{bmatrix} \quad (5.2.38)$$

Similarly to the second derivatives of the bus injections in (5.2.37), the second derivatives for the branch power injections do not have derivatives for the generation variables. Thus, the second derivatives are presented as in (5.2.39).

$$\mathbf{g}_{S_{br}\mathbf{xx}} = \frac{\partial}{\partial \mathbf{x}} \left(\mathbf{g}_{S_{br}\mathbf{x}}^{\top} \right) = \\ \begin{bmatrix} \mathbf{g}_{S_{br}\mathbf{V}_a\mathbf{V}_a} & \mathbf{g}_{S_{br}\mathbf{V}_a\mathbf{V}_m} & 0 & 0 & \mathbf{g}_{S_{br}\mathbf{V}_a\mathbf{B}_{eq}} & \mathbf{g}_{S_{br}\mathbf{V}_a\boldsymbol{\theta}_{sh}} & \mathbf{g}_{S_{br}\mathbf{V}_a\mathbf{m}_a} & \mathbf{g}_{S_{br}\mathbf{V}_a\mathbf{G}_{sw}} \\ \mathbf{g}_{S_{br}\mathbf{V}_m\mathbf{V}_a} & \mathbf{g}_{S_{br}\mathbf{V}_m\mathbf{V}_m} & 0 & 0 & \mathbf{g}_{S_{br}\mathbf{V}_m\mathbf{B}_{eq}} & \mathbf{g}_{S_{br}\mathbf{V}_m\boldsymbol{\theta}_{sh}} & \mathbf{g}_{S_{br}\mathbf{V}_m\mathbf{m}_a} & \mathbf{g}_{S_{br}\mathbf{V}_m\mathbf{G}_{sw}} \\ 0 & 0 & 0 & 0 & 0 & 0 & 0 & 0 \\ 0 & 0 & 0 & 0 & 0 & 0 & 0 & 0 \\ \mathbf{g}_{S_{br}\mathbf{B}_{eq}\mathbf{V}_a} & \mathbf{g}_{S_{br}\mathbf{B}_{eq}\mathbf{V}_m} & 0 & 0 & \mathbf{g}_{S_{br}\mathbf{B}_{eq}\mathbf{B}_{eq}} & \mathbf{g}_{S_b\mathbf{B}_{eq}\boldsymbol{\theta}_{sh}} & \mathbf{g}_{S_{br}\mathbf{B}_{eq}\mathbf{m}_a} & \mathbf{g}_{S_{br}\mathbf{B}_{eq}\mathbf{G}_{sw}} \\ \mathbf{g}_{S_{br}\boldsymbol{\theta}_{sh}\mathbf{V}_a} & \mathbf{g}_{S_{br}\boldsymbol{\theta}_{sh}\mathbf{V}_m} & 0 & 0 & \mathbf{g}_{S_{br}\boldsymbol{\theta}_{sh}\mathbf{B}_{eq}} & \mathbf{g}_{S_{br}\boldsymbol{\theta}_{sh}\boldsymbol{\theta}_{sh}} & \mathbf{g}_{S_{br}\boldsymbol{\theta}_{sh}\mathbf{m}_a} & \mathbf{g}_{S_{br}\boldsymbol{\theta}_{sh}\mathbf{G}_{sw}} \\ \mathbf{g}_{S_{br}\mathbf{m}_a\mathbf{V}_a} & \mathbf{g}_{S_{br}\mathbf{m}_a\mathbf{V}_m} & 0 & 0 & \mathbf{g}_{S_{br}\mathbf{m}_a\mathbf{B}_{eq}} & \mathbf{g}_{S_{br}\mathbf{m}_a\boldsymbol{\theta}_{sh}} & \mathbf{g}_{S_{br}\mathbf{m}_a\mathbf{m}_a} & \mathbf{g}_{S_{br}\mathbf{m}_a\mathbf{G}_{sw}} \\ \mathbf{g}_{S_{br}\mathbf{G}_{sw}\mathbf{V}_a} & \mathbf{g}_{S_{br}\mathbf{G}_{sw}\mathbf{V}_m} & 0 & 0 & \mathbf{g}_{S_{br}\mathbf{G}_{sw}\mathbf{B}_{eq}} & \mathbf{g}_{S_{br}\mathbf{G}_{sw}\boldsymbol{\theta}_{sh}} & \mathbf{g}_{S_{br}\mathbf{G}_{sw}\mathbf{m}_a} & \mathbf{g}_{S_{br}\mathbf{g}_{sw}\mathbf{G}_{sw}} \end{bmatrix} \quad (5.2.39)$$

Appendix C presents the full and detailed development of the FUBM Lagrangian in (5.2.22) and its derivatives, presented in equations (5.2.23) to (5.2.28). It also includes the extensively detailed derivatives for each constraint based on the derivatives presented in (5.2.31) to (5.2.39).

The Lagrangian function, its first and second order partial derivatives presented in this section can be used for the implementation of the FUBM if a deterministic algorithm is selected to solve OPF for the hybrid AC/DC system.

5.3 FUBM OPF Implementation

As mentioned in chapter 2, most commercial and open source software environment tailored for solving optimisation problems, like AIMMS, AMPL or MATLAB, support a variety of optimisation solvers and algorithms for solving both linear and non-linear optimisation problems. On the other hand, there are specialist modelling software like MATPOWER, which are tailored specifically for power systems, and they are designed to build the optimisation problem and call an internal or external solver. The OPF-FUBM formulation can be implemented in either an existing power system analysis tool (just like it was done for Power Flows in chapter 4), or into a general-purpose modelling software for optimisation. Each approach present advantages and disadvantages. If the FUBM is appropriately implemented, the model and formulation could be fully compatible with all the existing features that the power system analysis tool already possesses. However, such appropriate implementation of OPF-FUBM formulation into an existing power system specialist software such as . MATPOWER requires some additional modifications (in terms of coding) to the core components of the analysis tool. On the other hand, a more general approach would be to use a general-purpose modelling software (e.g. AIMMS) to implement and solve the FUBM-OPF formulation as a general mathematical optimisation (mathematical programming) problem. The latter approach obviously does not require modifications to any core components of the general-purpose modelling software. In AIMMS integrated development environment (IDE) the OPF-FUBM problem can be integrated as a mathematical programming model with all the data pertaining to the system being solved as well as all associated constraints included and presented. In this chapter, implementation of the OPF-FUBM formulation for solving fully controllable hybrid AC/DC grids is presented for both aforementioned approaches namely, implementing OPF-FUBM within an existing specialised power system analytical software, MATPOWER in this case, and as a mathematical programming problem in a general-purpose modelling software, which in this case is chosen to be AIMMS. For both approaches, fully controllable hybrid AC/DC grids are solved using a variety of optimisation algorithms, all of which were explained already in Chapter 2.

5.3.1 MATPOWER-FUBM OPF Implementation

Similar to the approach presented in Chapter 4 for formulating and solving the power flows using FUBM (FPFA-FUBM), in this section FUBM is implemented into the power systems simulation software MATPOWER for solving OPF problems. As it was mentioned, the core MATPOWER is not capable of modelling a fully controllable AC/DC grid. In fact, it can only solve AC grids. By adding the FUBM and building the optimisation model as presented in (5.1.7) to (5.1.17) with their respective Lagrangian derivatives , the OPF can be solved for a fully controllable AC/DC grid. This section will showcase the implementation of the FUBM into an existing power system analysis tool (i.e. MATPOWER).

It is worth noting that the FUBM implementation to MATPOWER for Power Flows (FPFA) and Optimal Power Flow (OPF) resulted in the publication of an alternative free open source software called "MATPOWER-FUBM". The MATPOWER-FUBM Software was released in collaboration with Dr Ray Zimmerman (Creator and principal developer of MATPOWER). The FUBM does not create any conflicts with the traditional usage of MATPOWER. Even though the MATPOWER-FUBM tool is designed to be fully compatible with MATPOWER, it has only been fully tested for Power Flow and OPF. The MATPOWER-FUBM tool uses MATLAB as the main platform, and currently modifications are being carried out for it to be compatible with Octave's platform as well. The original software of MATPOWER can be downloaded in [60] and the improved MATPOWER-FUBM for the solution of AC/DC grids using FUBM can be downloaded in [104]. This software implementation of the FUBM includes a technical note of the implementation and a user guide which are both downloaded with the software.

Figure 5.1 presents the general flow chart of the MATPOWER-FUBM OPF application. As it is observed, the FPFA from Chapter 4, can be used to initialise the OPF problem. Once the Optimisation model is constructed, the entire problem is solved by a specific solver. MATPOWER-FUBM has been coded to be compatible with each one of the following algorithms inlcuded below. They were described in detail in chapter 2.

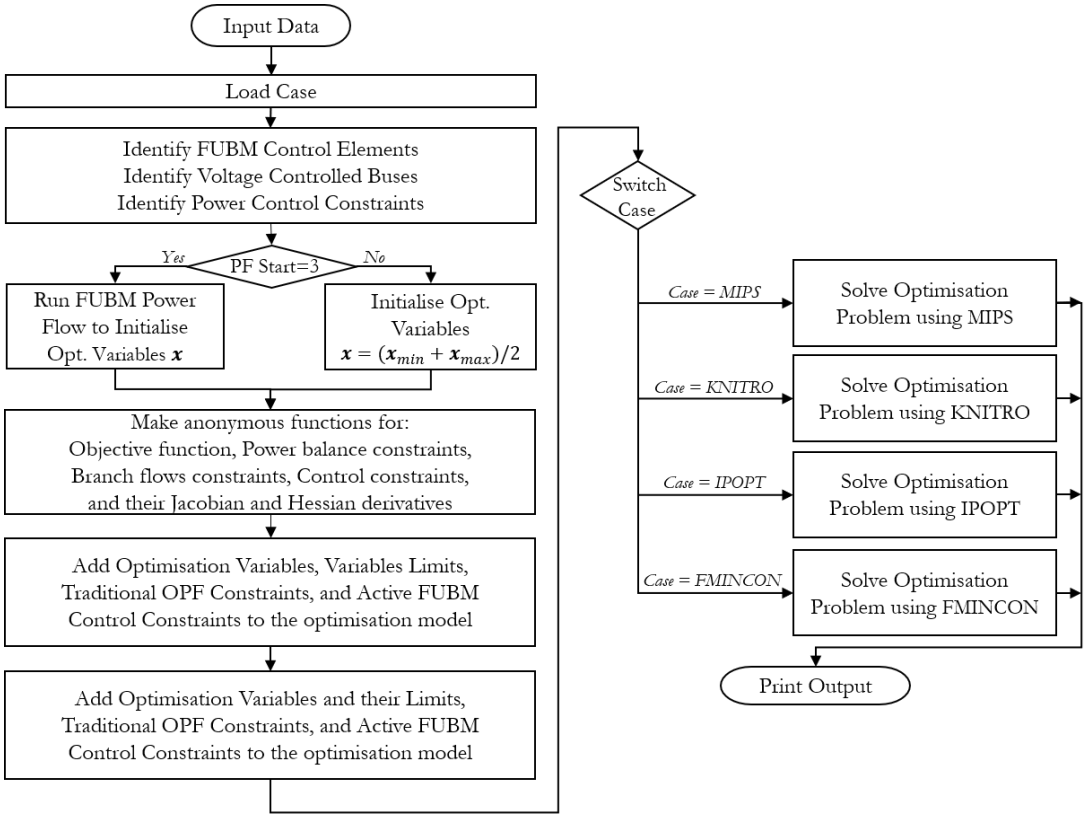

Figure 5.1: MATPOWER-FUBM General OPF Flux Diagram

- MIPS, MATPOWER Interior Point Solver, primal/dual interior point method.
- KNITRO, optimisation algorithm from Artelys
- IPOPT, Interior Point OPTimiser
- FMINCON, Matlab optimisation Toolbox

5.3.2 AIMMS-FUBM OPF Implementation

AIMMS is a general-purpose modelling software consisting of an integrated development environment (IDE), which integrates a state of the art modelling language to build the mathematical model for the problem with a suite of world class numerical solvers for linear, mixed-integer, and nonlinear programming such as baron, cplex, conopt, gurobi, knitro, path, snopt and xa. One of the most useful features of AIMMS is the capability of specifying and solving linear and nonlinear constraint-based op-

timisation models. In addition, AIMMS is able to manage stochastic programming and robust optimisation to include data uncertainty [80].

AIMMS environment allows for defining the full optimisation problem using a compact notation available for procedural statements and symbolic constraints. The OPF-FUBM formulation presented in equations (5.1.7) to (5.1.17) is directly implemented in AIMMS. Depending on which solver is selected, AIMMS transforms the optimisation model to match with the selected solver structure. Furthermore, the software also builds the Hessian and the Jacobian of the problem [81].

The following solvers are used for the implementation of the OPF-FUBM in AIMMS. Description of each one of the algorithms is presented in chapter 2.

- CONOPT 4.03, optimisation algorithm developed by ARKI Consulting.
- KNITRO 12.0, optimisation algorithm from Artelys
- IPOPT 3.11, Interior Point OPTimiser

5.4 Test Cases and OPF Simulations

To showcase the effectiveness of the FUBM for solving OPF for hybrid AC/DC EPS, this section presents a series of test cases which are solved using both the MATPOWER-FUBM and the AIMMS-FUBM implementation. All FUBM simulations have been solved using a PC with CPU Intel Core i7, 2.2GHz and 16GB RAM memory.

This section is structured as follows: Firstly validation of the FUBM formulation and both implementations is presented. Secondly, both implementations are used to run a two medium scale fully flexible hybrid AC/DC test cases using a variety of solvers as a confirmation of the versatility of the model. Thirdly a large scale system will be solved as a demonstration of its effectiveness against large scale systems when a series of diverse controls are active. The case also presents the convergence pattern with different solvers. Finally a series of AC and AC/DC cases are solved to compare the FUBM formulation against existent analysis tools to showcase the versatility and scalability of the FUBM without sacrificing computational efficiency.

5.4.1 Validation of the FUBM

The validation of the FUBM is carried out by simulating the test case of Fig. 5.2. The results are compared against the traditional approach for solving OPF in AC/DC grids, which are presented in [109] and [110]. The AC network data can be found in [111], and the DC network data along with VSCs parameters are presented in Table 5.1.

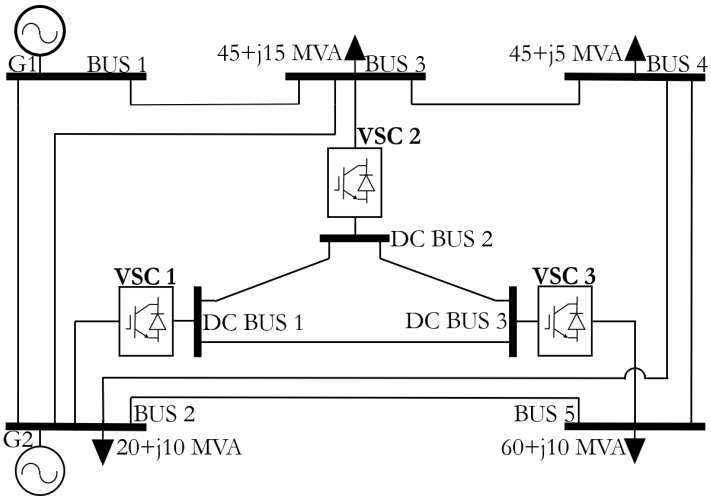

Figure 5.2: MTDC Stagg Test Case

The objective function of the OPF problem will be the total transmission losses of the test system [2]. They are calculated as shown in (5.4.40), where nl is the number of lines.

$$f(\mathbf{x}) = \sum_{i=1}^{nl} |P_f^{\{i\}} + P_t^{\{i\}}| \tag{5.4.40}$$

The case constraints are specified in Table 5.2. VSC 1 and 3 are selected as type I and VSC 2 will be regulating the DC voltage magnitude as type II. For all VSCs, the optional control variables of θ_{sh} and m_a are optimised.

[2]The default objective function of the downloadable version of the MATPOWER-FUBM implementation (available in [104]) is the total generation cost of the system, however only for this case the objective function is set to minimise the total transmission losses instead. This option is not currently available for the downloadable version, but it will be added in a future release.

Table 5.1: Converters and DC grid parameters

Parameter	Value
VSCs (1,2,3) r_s / x_s	0.0016 p.u. 0.2764 p.u.
VSCs Loss Coefficient	$\alpha = \beta = 0$, $\gamma = 0.01$
DC line r_s (1-2 and 2-3)	0.0260 p.u.
DC line r_s (3-1)	0.0365 p.u.
Max Reactive Power	100 MVAr

Table 5.2: MTDC Stagg Constraints

Bus ID	Vmin	Vmax	Element	Value [MVA]	
AC 1,2	1	1.02	P_{G1} Min/Max	10	250
AC 3,4,5	0.9	1.1	Q_{G1} Min/Max	-100	100
DC 2	1.01	1.01	P_{G2} Min/Max	-40	40
DC 1,3	0.9	1.1	Q_{G2} Min/Max	-40	40
AC Bus 1	$V_a = 0°$ (Reference)		Element	Value [p.u.]	
Lines Rate	1 MVA (AC & DC)		m_a Min/Max	0.75	1.22

All transmission elements of the test case were simulated using the FubM for both implementations (Matpower-FubM and Aimms-FubM). Convergence times, iterations, and minimised objective function are presented in table 5.3, where it can be appreciated that both implementations converged to the same objective function value of 4.14[MW] reported in [109].

Table 5.3: FubM Implementation Convergence

Implementation	Aimms-FubM	Matpower-FubM
OPF Solver	KNITRO 12.0	KNITRO 12.0
Iterations	13	11
Conv. Time [s]	0.06	1.05
Trans. Loss [MW]	4.14	4.14
Total Cost [$/hr]	365.4925	365.4925

Tables 5.4, 5.5 and 5.6 show a comparison of the simulation results between the Traditional and both FubM implementations for nodal voltages, Generation output

and VSC controls.

Table 5.4: Validation Voltage Comparison

	Vm [p.u.]			Va [°]		
Bus ID	Traditional Approach	AIMMS FUBM	MATPOWER FUBM	Traditional Approach	AIMMS FUBM	MATPOWER FUBM
AC 1	1.02	1.02	1.02	0	0	0
AC 2	1.006	1.006	1.006	-3.15	-3.15	-3.15
AC 3	0.992	0.992	0.992	-4.92	-4.92	-4.92
AC 4	0.991	0.991	0.991	-5.28	-5.28	-5.28
AC 5	0.991	0.991	0.991	-5.48	-5.48	-5.48
DC 1	1.015	1.015	1.015	***	-26.11	-26.11
DC 2	1.01	1.01	1.01	***	-26.11	-26.11
DC 3	1.008	1.008	1.008	***	-26.11	-26.11

Table 5.5: Validation Generation Comparison

	Pg [MW]			Qg[MVAr]		
Gen ID	Traditional Approach	AIMMS FUBM	MATPOWER FUBM	Traditional Approach	AIMMS FUBM	MATPOWER FUBM
G1	129.14	129.14	129.14	-8.37	-8.37	-8.37
G2	40	40	40	15.04	15.04	15.04

After the comparison presented in Tables 5.4 and 5.5, it is noticeable that all the voltage magnitudes, phase angles and generators' power outputs were optimised to the same value for both approaches. As expected, for the FUBM, the DC grid has an angle which is different from zero since the voltage angle reference is in the AC grid. Nevertheless, this angle remains constant through the entire DC grid. Thus, the flow of active power in the DC links is solely dictated by the DC nodal voltage magnitude difference (exactly as what it would be in a real DC link). Similarly, the obtained values for the DC grid and VSCs power comparison between the traditional and the FUBM approaches from Table 5.6 are practically the same. Moreover, the maximum error presented between the MATPOWER-FUBM and the AIMMS-FUBM

Table 5.6: VSC and DC Grid Comparison

	Traditional Approach			Matpower & Aimms FubM Implementations		
	VSC1	VSC2	VSC3	VSC1	VSC2	VSC3
P_f [MW]	-37.58	12.54	24.86	-37.55	12.47	24.86
P_t [MW]	37.90	-12.54	-24.86	37.79	-12.44	-24.79
Q_t [MVAr]	0	-9.07	-6.16	0	-9.04	-6.16
m_a	0.995	1.009	1.003	0.995	1.0087	1.0028
θ_{sh} [°]	***	***	***	-17.0771	-23.1389	-24.5510
B_{eq} [p.u.]	***	***	***	0.03811	0.09360	0.07827
DC Line from/to	DC 1-2	DC 2-3	DC 3-1	DC 1-2	DC 2-3	DC 3-1
P_f [MW]	19.17	6.61	-18.24	19.171	6.608	-18.266
P_t [MW]	-19.08	-6.6	18.36	-19.078	-6.597	18.386

implementations is $2.6 \times 10^{-4}\%$. Additionally for both FubM implementations, the values of θ_{sh} and B_{eq} are also obtained.

After analyzing the results obtained by both implementations of the FubM and its comparison with the traditional approach, the formulation of the FubM is considered as validated.

5.4.2 Medium Scale Fully Flexible hybrid AC/DC Grids

This subsection presents the solution of a medium scale fully flexible hybrid AC/DC test case to showcase the flexibility and versatility of the OPF-FubM formulation. The test case is solved using two types of initialisation, (i) Initialised by the FPFA developed in chapter 4 and (ii) Initialised using an average point between the upper and lower boundaries for all variables. Once initialised the test case is solved using both OPF-FubM implementations (the Matpower-FubM and the Aimms-FubM).

Modified IEEE 30 bus system

The description of this test case as well as its solution for Power Flows has been presented in 4.2.2 in chapter 4. In this chapter, the obtained results are used to initialise the OPF implementations of the FUBM for AIMMS and MATPOWER. Details in the control settings for all PSTs, CTTs, VSCs and STATCOM remain the same as the ones presented in Tables 4.8 and 4.9 in chapter 4. Full detailed data of the test case is available with the downloadable version of the MATPOWER-FUBM implementation in [104].

Simulation Results

The full hybrid AC/DC test case consist of 129 variables and 247 non-linear constraints. Convergence for both implementations is achieved using a variety of solvers. Table 5.7 presents the convergence times, iterations and optimised objective function. Figures 5.3 and 5.4 show graphically the minimisation of the total cost as well as the infeasibility[3] for all the mentioned solvers.

Table 5.7: Modified Case 30 OPF Convergence Results

Optimisation Solver	Total Iterations	Total Gen Cost [$/hr]	Convergence Time [s]
KNITRO 12.0*a	7	525.03	23.38
MIPS*a	13	525.03	34.12
FMINCON*a	6	525.03	25.15
IPOPT 3.0*a	12	525.03	35.39
CONOPT 4.0*b	7	525.03	1.13
KNITRO 12.0*b	7	525.03	1.09
IPOPT 3.0*b	12	525.03	1.43

*a: MATPOWER-FUBM Implementation
*b: AIMMS-FUBM Implementation

[3]Infeasibility: a measure that indicates how feasible the problem is. A problem is said to be infeasible if there is no solution that satisfies all the constraints. The smaller the infeasibility, the greater the likelihood that the solution (at that point) satisfies all the constraints.

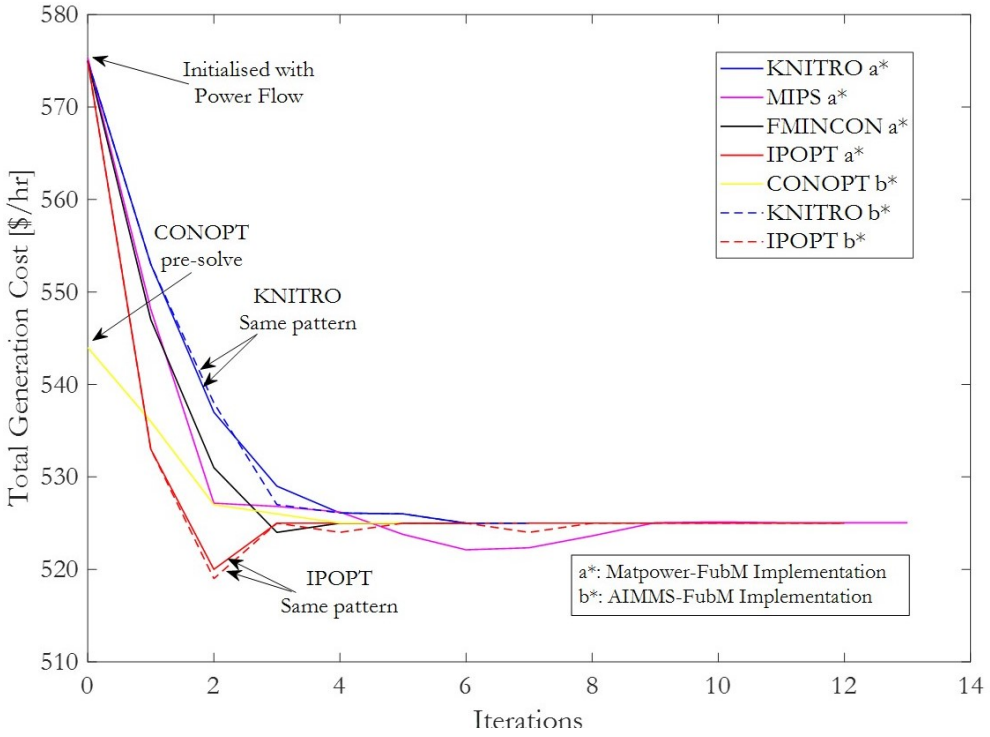

Figure 5.3: Modified Case 30 Convergence and Optimal Cost minimisation

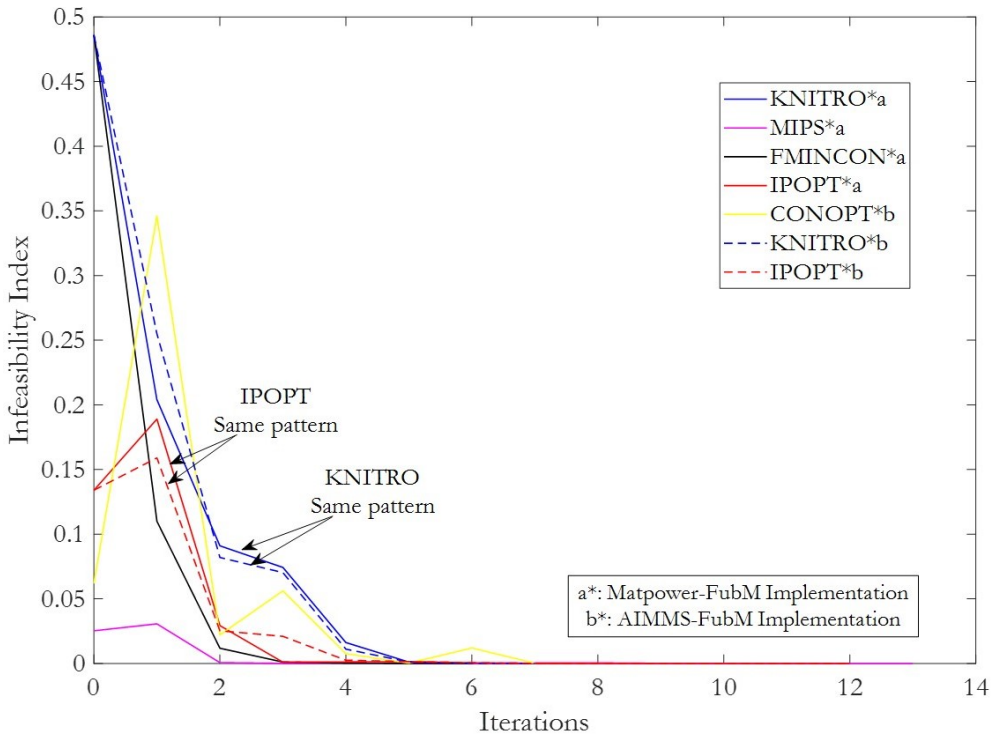

Figure 5.4: Modified Case 30 Infeasibility during OPF iterations

It can be appreciated from table 5.7 that all solvers minimised the total generation cost to the same point. The solvers KNITRO, FMINCON and CONOPT converged in almost half the number of iterations in comparison to the remaining solvers. However, the difference in the convergence times between the solvers within the same implementation is minimum.

It is also noticeable that the AIMMS-FUBM implementation converges faster than the MATPOWER-FUBM implementation. This is due to the way that MATPOWER is coded, when implementing the FUBM a recalculation of the Y_{bus} has to be done per node, and per iteration. This considerably impacts the computational time but not the number of iterations. This is clearly shown in figures 5.3 and 5.4 where both solutions follow practically the same pattern for the solvers that both implementations share (KNITRO and IPOPT). Therefore it is safe to conclude that when using the same solver, both implementations follow the same convergence pattern since both implementations have the same formulation. Thus, the results obtained with MATPOWER-FUBM are the same as the ones obtained with AIMMS-FUBM just slower. As proof of this, Tables 5.8, 5.9 and 5.10 present the optimised results of the simulation, to which all solvers converged with a maximum error of 1×10^{-6}.

After analysing the simulation results, it is clear that both implementations are able to solve medium scale fully controllable Hybrid AC/DC grids. Moreover, the formulation is compatible with a variety of optimisation solvers. Even though the MATPOWER-FUBM implementation is slower than the AIMMS-FUBM, both implementations follow the same convergence pattern and converge in the same number of iterations. Furthermore regardless of which the implementation is used the optimised results with either approach match.

Since AIMMS requires creating a complete new project for each case that is created or modified (in this case a different initialisation strategy), and since the MATPOWER-FUBM implementation is a more versatile tool (No modifications are needed to simulate a variety of test cases), the comparison for different initialisation options will be carried out using only the MATPOWER-FUBM implementation. It is expected that the AIMMS-FUBM implementation would have obtained the same results as the MATPOWER-FUBM implementation.

Table 5.8: Modified IEEE 30 DC Grids Voltages OPF Results

Bus ID	Vm [pu]	Va [deg]	Bus ID	Vm [pu]	Va [deg]	Bus ID	Vm [pu]	Va [deg]
B001	1.069	-4.411	B005	1.071	-0.562	B009	1.100	-3.540
B002	1.067	-4.411	B006	1.070	-0.562	B0010	1.043	-3.409
B003	1.068	-4.411	B007	1.077	-0.562	B0011	1.044	-3.409
B004	1.070	-0.562	B008	1.075	-0.562			

Table 5.9: Modified IEEE 30 VSCs Control OPF Results

VSC ID	P_f [MW]	Q_f [MVAr]	Q_t [MVAr]	θ_{sh} [deg]	B_{eq} [pu]	m_a [tap]
1	-2.59	0	0.01	-0.7211	0	1
2	4.48	0	-25.00	0	0.2103	0.9616
3	-1.89	0	-6.87	0.8875	0.0608	1
4	1.17	0	-10.00	0	0.0886	1
5	8.69	0	-6.59	0	0.0602	0.9904
6	15.00	0	-14.49	0.03173	0.1319	1
9	0.00	0	-20.45	0	0.1740	1
10	1.79	0	0.00	-0.1039	0	1
11	-1.79	0	-8.10	0	0.0753	1

Table 5.10: Modified IEEE 30 PSTs and CTTs Control OPF Results

Transformer Type	Element No.	P_f [MW]	θ_{sh} [deg]	V_t [pu]	Q_t [MVAr]	m_a [tap]
PST	1	3.5	0.3008	1.036	0.07	1
	2	7.5	-0.0434	1.013	1.51	1
CTT	1	5.36	0	1.017	3.0	1.0303
	2	0.72	0	1.010	-0.03	1.0222

For this comparison, the test case will be initialised using (i) the FPFA developed in chapter 4, and (ii) an average point in between the upper and lower boundaries for all variables. Table 5.11 presents the convergence times, objective function iteration

and infeasibility.

Table 5.11: OPF Convergence with Different Initial Points

Type of Initialisation	Number of Iterations	Total Gen Cost [$/hr]	Infeasibility Index	Total Time [s]
Power Flow	7	525.03	4.56E-08	22.38
Average Point	6	525.04	8.01E-07	21.74

Figure 5.5 shows the convergence of both approaches when different initial points are used, and Fig. 5.6 shows the infeasibility of the solution during the iterations.

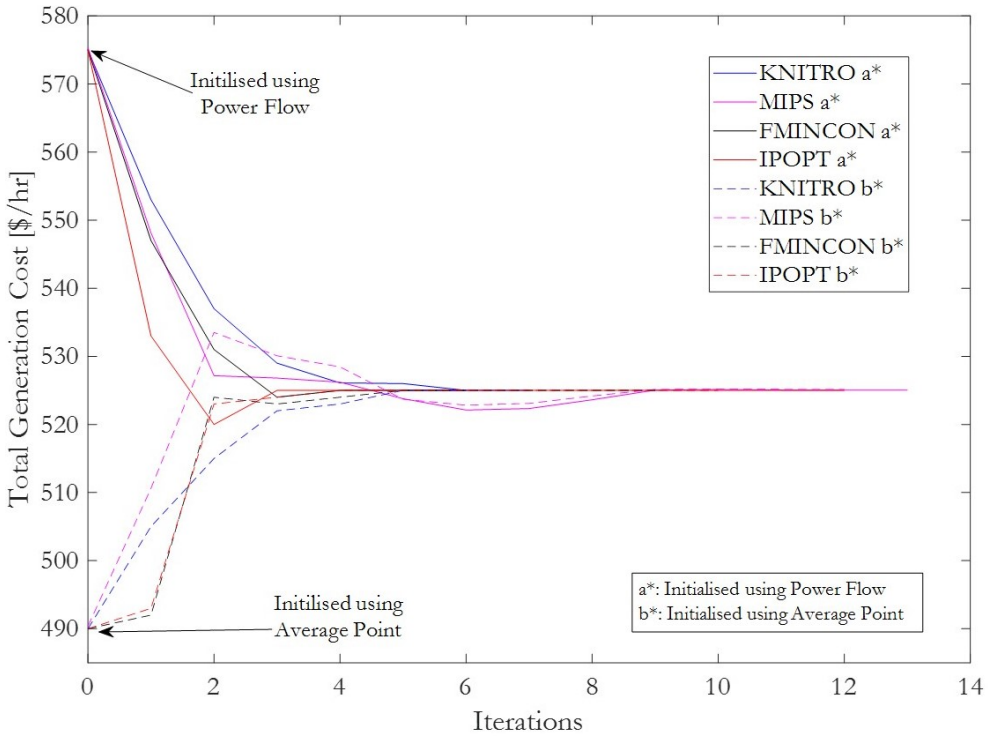

Figure 5.5: Modified Case 30 Convergence Two Different Initial Points

As it can be appreciated from 5.11, both OPF solutions converged to almost the same objective function with a maximum error of $9.63\times^{-3}$ where the power flow initialisation converged to a slightly better result. Even though the Average Point initialisation converged faster by one iteration, faster convergence results are expected when initialising the OPF using Power Flow if an ED is used to initialise the Power Flow generators, and then, the results of the Power Flow analysis are used

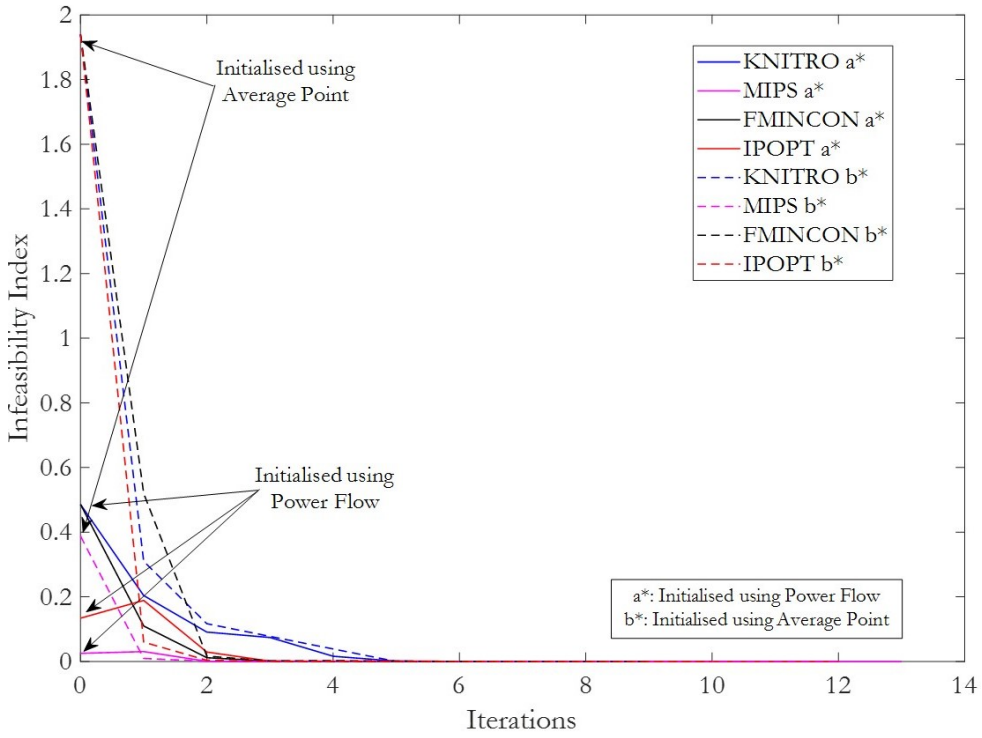

Figure 5.6: Modified Case 30 Infeasibility Two Different Initial Points

as a start point for the OPF. The ED analysis was out of the scope of this thesis, and therefore the improvements in the convergence speed when using Power Flow initialisation are not evident, however from Fig. 5.6 it is clear that the infeasibility index is improved.

5.4.3 Large Scale Fully Flexible hybrid AC/DC Grids

This subsection presents the solution of a Large scale fully flexible hybrid AC/DC test case to showcase the scalability of the OPF-FUBM formulation. The test case is solved using both OPF-FUBM implementations (the MATPOWER-FUBM and the AIMMS-FUBM). Then, analysis on the convergence for KNITRO, CONOPT and IPOPT is presented.

Modified Case PEGASE Project

This test case was introduced in subsection 4.2.3 in chapter 4, where the data and controls for the test case where specified. The control settings for all VSCs, PSTs

and CTTs presented in tables 4.13 and 4.14 will remain the same for the OPF. The full case data is available with the downloadable version of the MATPOWER-FUBM implementation in [104].

Simulation Results

The full Hybrid AC/DC test case optimisation problem consist of 44,728 Constraints and 41,250 Variables. An average between upper and lower boundaries has been used as initial conditions for all optimisation variables to show an objective convergence of both implementations and not a possible improved convergence due to a Power Flow initialisation. The OPF formulation using FUBM has successfully converged for both the MATPOWER-FUBM and the AIMMS-FUBM implementation. The case was simulated for MIPS and KNITRO 12.0 for the MATPOWER-FUBM implementation, and for KNITRO 12.0, CONOPT 4.03 and IPOPT 3.11, for the AIMMS-FUBM implementation. Tables 5.12 and 5.13 present the convergence times, iterations and the optimised value of the cost function.

Table 5.12: MATPOWER-FUBM Convergence Results

OPF Solver	KNITRO 12.0	MIPS
Infeasibility/minimisation	Infe. & Min.	Infe. & Min.
Iterations	55	37
Total Time [hr]	34.02	46.13
Total Gen. Cost [$/hr]	74038.3781	74038.3781

Table 5.13: AIMMS-FUBM Convergence Results

OPF Solver	CONOPT 4.03		KNITRO 12.0	IPOPT 3.11
Infeasibility/minimisation	Infe.	Min.	Infe. & Min.	Infe. & Min.
Iterations	116	27	56	134
Time [s]	19.01	7.23	25.69	271.36
Total Time [s]	26.24		25.69	271.36
Total Gen. Cost [$/hr]	74038.3781		74038.3781	74038.3781

From tables 5.12 and 5.13 it is observed that both implementations converged to the same optimal operating point. While MIPS converged in less iterations than all

the other solvers, the computational time was the highest in comparison to all the other solvers for both implementations. It is also noticeable that as expected KNITRO converges in almost the same amount of iterations for both implementations. The solver CONOPT preforms the optimisation in two steps to find the solution. First it ensures that the infeasibility index is small enough. If the problem is feasible, then it minimises the objective function while the infeasibility index continues decreasing. On the other hand, the solvers MIPS, KNITRO and IPOPT reduce infeasibility index while the objective function is minimised. The solvers KNITRO (AIMMS-FUBM) and CONOPT are faster solvers in comparison with the IPOPT, KNITRO (MATPOWER-FUBM) and MIPS methods. Nevertheless, the final results from the five solvers match for all the variables of the system with a maximum error of $2.48\times^{-4}$ in between solvers. It is also observed that the AIMMS-FUBM implementation is considerably faster than the MATPOWER-FUBM implementation. As mentioned, this is due to the way MATPOWER is coded, as the number of nodes increase, when implementing the FUBM, the computational time is increased too, therefore the MATPOWER-FUBM implementation is recommended to be used for small and medium size test cases (no more than 500 buses). The results presented by the AIMMS-FUBM implementation suggest that the MATPOWER-FUBM implementation can be improved to match the speed of the AIMMS-FUBM implementation since they both share the same formulation.

Table 5.14: AC and DC Voltages

Bus ID	Vm [pu]	Bus ID	Vm [pu]
VSC DC B1	1.00002	VSC AC B2072	1.08000
VSC DC B2	1.00000	VSC AC B8195	1.07500
VSC DC B3	1.01000	VSC AC B6246	1.06000
VSC DC B4	1.01334	VSC AC B7282	1.07000
VSC DC B5	1.01322	CCT AC B6807	1.10000

The optimisation results for the relevant AC and DC voltages are shown in Table 5.14. Furthermore, the active and reactive power flows through the control elements

and DC lines, as well as their optimised control variables are presented in Table 5.15. From both tables, it is shown that the results match with the control constraints from Table 4.14 in chapter 4. Additionally, all VSC have satisfactory meet the Zero Constraint for reactive power compensation. Furthermore, the optimal value of B_{eq} has been obtained. Finally, the variable θ_{sh} has been optimised for all active power controlled elements. It is clearly noticeable that a full power control has resulted in both DC grids.

Table 5.15: Optimised Variables and Power Control

Element ID	Pf [MW]	Theta [deg]	Beq [pu]	ma [tap]
VSC 1	-4.00007	0	-0.17288657	1.07337
VSC 2	3.99999	0	0.02220943	1.07585
VSC 3	946.92069	-52.0451219	0.49999995	1.00112
VSC 4	-500	-33.3258129	0.49999943	1.05951
VSC 5	-450	-36.465037	0.49999931	1.01408
PST	-173	-0.09532315	***	***
CTT	7.28653	***	***	1.04626
DC Line 1-2	4.00007	***	***	***
DC Line 3-4	-481.75773	***	***	***
DC Line 4-5	16.64963	***	***	***
DC Line 5-3	466.64775	***	***	***

Figure 5.7 presents the minimisation of the Cost for the five solvers. Notice that even though all of them are initialized in the same point, the start point varies. This is because the solver KNITRO runs a presolve before starting the optimisation (this presolve is more evident in this graph than it is in Fig. 5.5 for the Modified 30 bus system, where the presolve results were very similar to the starting point). Similarly, the solver CONOPT first solves for the infeasibility and then uses that final state as a starting point for the minimisation. Although the KNITRO solver selected a starting point quite far from the solution, the method is so effective that it manages to converge in less iterations than IPOPT and even CONOPT. It is

worth to highlight that even though it looks like CONOPT converged with the least amount of iterations, the iterations for the solution of the infeasibility have to be considered. Thus MIPS is the solver that converged in the least amount of iterations, and KNITRO(AIMMS-FUBM) remains the fastest as it was shown in Table 5.13.

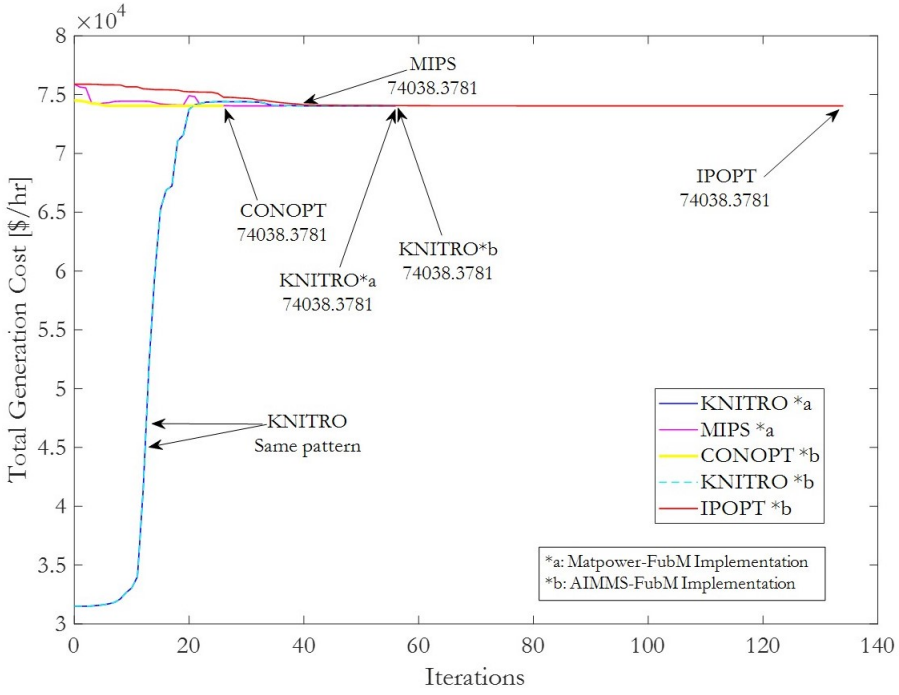

Figure 5.7: Convergence and Optimal Cost minimisation

Figure 5.8 shows the infeasibility value during the optimisation. For the IPOPT solver, the Primal infeasibility, indicates the maximum non-linear constraint violation, and the Dual infeasibility, is measured as the maximum deviation from complementary condition. The start infeasibility index for MIPS, KNITRO and IPOPT (Primal) was quite high in comparison with CONOPT. Nevertheless it can be seen that their values are dramatically reduced by iteration 6, 20 and 40 respectively.

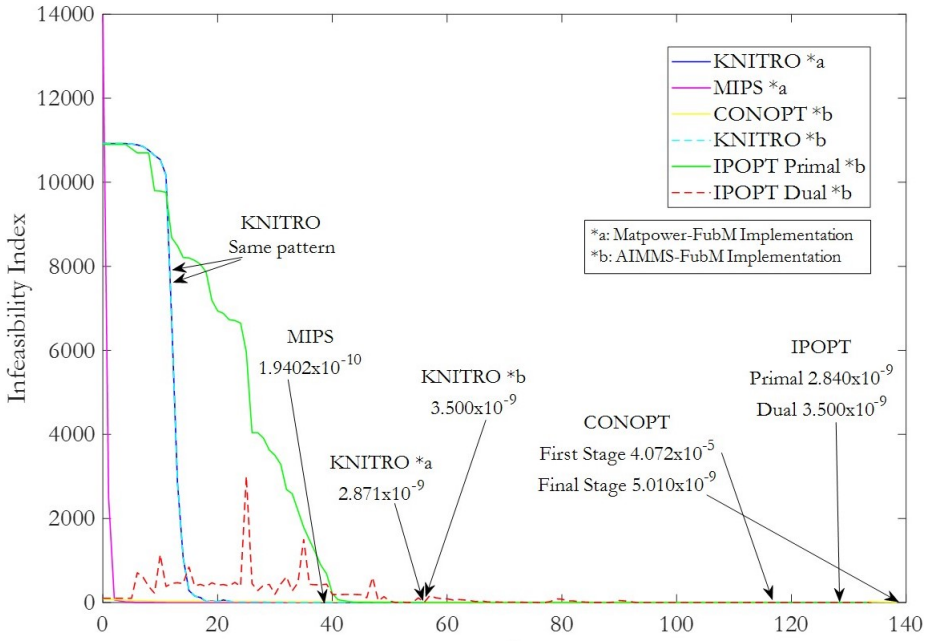

Figure 5.8: Infeasibility during OPF iterations

5.4.4 AC and AC/DC Cases for Scalability and Comparison

In this subsection, AC and AC/DC OPF studies are presented to further showcase the capabilities and versatility of applications of the FubM. AC cases serve as confirmation that the FubM optional variables do not create any extra computational effort for the AC OPF solution. The results compare both implementations against the original unmodified version of Matpower [24]. AC/DC cases compare the FubM OPF results with the results obtained in [32], where a Bus Incidence Model (BIM) for ACDC OPF is implemented as an extension of the 'PowerModels.jl' package [112], which is built on top of Julia/JuMP [113]. Both AC and AC/DC cases showcase the scalability and computational performance of the FubM formulation.

AC test Cases

For the AC OPF scalability and comparison, the IEEE 57 bus test case, and both the 89 and 1354 bus PEGASE cases are solved using both FubM implementations and compared against the results from Matpower (v7.0). All the data from the cases are taken from Matpower's library. Original Matpower software and test

cases data are available in [114].

Table 5.16 presents the AC OPF results of MATPOWER and AIMMS-FUBM, and Table 5.17 presents the AC OPF results of MATPOWER and MATPOWER-FUBM. In order to make a fair comparison, the cases are solved using the shared solvers KNITRO and IPOPT for both MATPOWER, MATPOWER-FUBM and AIMMS-FUBM. Additionally, CONOPT is also used for the AIMMS-FUBM implementation.

Table 5.16: AC OPF Results Comparison AIMMS-FUBM

	MATPOWER				AIMMS-FUBM					
AC	KNITRO 12.0		IPOPT 3.11		CONOPT 4.03		KNITRO 12.0		IPOPT 3.11	
Cases	Total Cost	Time	Total Cost	Time	Total Cost	Time	Total Cost	Time	Total Cost	Time
	[$/h]	[s]	[$/h]	[s]	[$/h]	[s]	[$/h]	[s]	[$/h]	[s]
Case 57	41737.77	0.87	41737.79	0.36	41737.79	0.05	41737.79	0.03	41737.79	0.09
Case 89	5819.81	0.39	5819.81	1.12	5814.86	0.19	5814.86	0.16	5814.86	0.41
Case 1354	74069.35	2.51	74069.35	2.96	74069.35	3.56	74069.35	4.28	74069.35	3.5

Table 5.17: AC OPF Results Comparison MATPOWER-FUBM

	MATPOWER				MATPOWER-FUBM			
AC	KNITRO 12.0		IPOPT 3.11		KNITRO 12.0		IPOPT 3.11	
Cases	Total Cost	Time	Total Cost	Time	Total Cost	Time	Total Cost	Time
	[$/h]	[s]	[$/h]	[s]	[$/h]	[s]	[$/h]	[s]
Case 57	41737.77	0.87	41737.79	0.36	41737.78	0.73	41737.78	0.42
Case 89	5819.81	0.39	5819.81	1.12	5814.86	0.51	5814.85	0.98
Case 1354	74069.35	2.51	74069.35	2.96	74069.35	3.02	74069.35	2.81

From Tables 5.16 and 5.17 it is observed that for all test cases the results of both implementations match with the expected solutions. Furthermore, the computational times are approximately the same for all solvers. While for the small and medium test cases the AIMMS-FUBM formulation is faster, in the large scale system there is a maximum time difference of 1.77[s] in the solution time. This is to be expected since the solution time in AIMMS includes the creation of the Jacobian and Hessian Matrices of partial derivatives, while for the MATPOWER approach and for the MATPOWER-FUBM implementation, the derivatives and their structure is predefined in the formulation. Nevertheless the time difference is too small to be considered.

Notice that regardless of the number of buses, the convergence time for the MATPOWER-FUBM implementation is as fast as the original MATPOWER, this is explained by the way the FUBM was implemented in MATPOWER. When simulating AC cases without any controls, the variables inside the FUBM remain constant (as explained in chapter 3), and thus no recalculation of the Y_{bus} is needed during the optimisation process. As a result, there is no impact in the computational time. If a single control, or an AC/DC grid is active, the variables inside the FUBM change during the optimisation process and a recalculation of the Y_{bus} is preformed. At this point, it is not significant if more controls or AC/DC grids are added since the recalculation will be preformed anyway. For this reason, the implementation of the MATPOWER-FUBM is only limited by the number of buses and not by the number of active controls.

AC/DC Test Cases

A small, a medium, and a large scale AC/DC test system are used to illustrate the scalability and performance of the FUBM formulation. Case-5-ACDC is a modified version of the IEEE 5 bus test system where a three node dc grid has been integrated using VSCs, the data can be found in [115]. Case 24-3 Zones is based on the two area IEEE 24 bus reliability test system which is extended to include a third asynchronous zone. The three areas are connected with two VSC MTDC grids with 3 and 4 DC nodes each one, data is reported in [25]. Finally the AC/DC 3120 bus case represents the Polish system with an interconnected 5 node MTDC grid. This modified large scale system has a total of 3125 buses, 3703 lines and 505 generators, full AC data can be found in [114] and the DC data in [116]. Case 5 and case 24-3 zones are solved using both FUBM implementations (MATPOWER-FUBM and AIMMS-FUBM), and the large scale case 3120 is only solved uding the AIMMS-FUBM implementation since the MATPOWER-FUBM is recommended for test cases with 500 buses or less. Table 5.18 presents a comparison of the simulation results reported in [32] for the BIM-JuMP approach, and the AIMMS-FUBM approach. Similarly, table 5.19 presents the comparison for the MATPOWER-FUBM implementation.

It is noticed from tables 5.18 and 5.19 that the OPF-FUBM formulation imple-

Table 5.18: AC/DC OPF Results Comparison AIMMS-FUBM

	BIM-JuMP		AIMMS-FUBM								
AC/DC	IPOPT		CONOPT 4.03			KNITRO 12.0			IPOPT 3.11		
Cases	Total Cost [$/h]	Time [s]	Total Cost [$/h]	Time [s]	Iter.	Total Cost [$/h]	Time [s]	Iter.	Total Cost [$/h]	Time [s]	Iter.
Case5	194.14	0.20	194.14	0.07	17	194.14	0.08	43	194.14	0.17	46
Case24-3z	150228.00	0.17	150227.09	0.14	42	150227.09	0.18	25	150227.09	0.23	26
Case 3120sp	2142635.0	122.7	2142635.0	50.01	157	2142635.0	118.23	60	2142634.9	298.7	479

Table 5.19: AC/DC OPF Results Comparison MATPOWER-FUBM

	BIM-JuMP		MATPOWER-FUBM					
AC/DC	IPOPT		KNITRO 12.0			IPOPT 3.11		
Cases	Total Cost [$/h]	Time [s]	Total Cost [$/h]	Time [s]	Iter.	Total Cost [$/h]	Time [s]	Iter.
Case5	194.14	0.20	194.14	1.02	41	194.14	1.31	46
Case24-3z	150228.00	0.17	150227.09	37.03	24	150227.09	42.15	26

mented in AIMMS and MATPOWER has been able to solve and converge to the same results from BIM-JuMP for all test cases. Even though the MATPOWER-FUBM implementation is slower than BIM-JuMP it managed to converge to the same optimal operating point while maintaining almost the same amount of iterations as the AIMMS-FUBM implementation. Regarding to the convergence time, it is clearly seen that the AIMMS-FUBM implementation using CONOPT as the solver has been the fastest for small, medium and large scale systems. For the large scale system (Case 3120sp), CONOPT is 72.69$[s]$ faster than BIM-IPOPT. The computational times between KNITRO (AIMMS-FUBM) and BIM-IPOPT are objectively similar for the three cases, with KNITRO (AIMMS-FUBM) slightly outperforming BIM-IPOPT for the largest scale system. The results for the small and medium cases using IPOPT(AIMMS-FUBM) are also objectively similar to BIM-IPOPT. On the other hand, for the 3120 case, even though the AIMMS-FUBM converged to a slightly better total cost, the BIM-IPOPT was faster, however it is worth noting that in both instances the convergence time is within the same order of magnitude.

Chapter Summary

In this Chapter, a steady-state FUBM model formulation for solving OPF for hybrid AC/DC EPS has been presented. With this formulation there is no need for introducing additional coupling constraints to maintain power balance between AC and DC parts of an hybrid EPS as the FUBM structure is configured in such a way that from a purely mathematical perspective, there is no distinction between AC and DC counterparts. Thus, the entire EPS is solved within a unified frame of reference. As a result, same AC OPF equations were be used to solve hybrid AC/DC EPS. The OPF-FUBM formulation maintained all the advantages of the FUBM, such as its adaptability to simulate a wide variety of elements with diverse controls. To this end the optional variables of the FUBM were also added as optional variables to the OPF formulation. The entire hybrid EPS is fully controllable thanks to the optional control constraints that were added to the formulation when needed depending on the network operational requirements. Meanwhile, realistic operational limits for all the elements in the EPS were included in the formulation. The Lagrangian function and its derivatives for the OPF-FUBM formulation were presented and described in detail. Two implementations for the OPF-FUBM formulation were presented, one in MATPOWER, and one in AIMMS. Both implementations were validated and compared against several test cases. Simulation results over the modified large scale Pegase system demonstrate full power and voltage control over several elements of the hybrid AC/DC grid whilst maintaining a good degree of convergence and accuracy of the solution. Finally, the FUBM has been successfully tested and compared with the traditional approaches for small, medium and large-scale AC and AC/DC systems, where the FUBM has proved to be working with a variety of optimisation solvers without sacrificing any computational effort, even presenting faster results in some cases. While the MATPOWER-FUBM implementation was limited to 500 buses, the results for small and medium scale test cases presents a good convergence rate and accurate results. Simulation results indicate that the FUBM model is flexible enough to be solved with a variety of solvers using general purpose model-based languages such as AIMMS. Considering that (i) All the components of the FUBM are either the same or an equivalent component for the Traditional models, and (ii)

The FUBM formulation solves OPF hybrid transmission AC/DC grids using traditional AC OPF equations, then, any convexification, linear approximation or robust optimisation applied to the AC OPF could be also applied as future research of the FUBM approach. The versatility and prowess of the FUBM plus its adaptability in modelling a variety of network elements both AC and DC makes it a suitable candidate and a formidable tool at the hands of the TSOs and network analysts for large-scale steady-state EPS studies without sacrificing computational efficiency and accuracy of the solution. Based on the results presented in this chapter the FUBM is a suitable candidate for SCOPF implementations.

Chapter 6

Flexible SCOPF for AC/DC grids using FUBM

In this chapter the developed FUBM that was implemented for Power Flows in chapter 4 and subsequently for OPF in chapter 5 is now implemented for solving Security Constrained Optimal Power Flow (SCOPF) for hybrid AC/DC networks. As presented from the developed OPF-FUBM implementation, the main aim of the OPF-FUBM problem is to obtain the optimal state variables for the system (e.g. Voltages, FUBM Controls and Generation output) for which a desired objective (e.g. total generation cost) is at its minimum when subject to realistic operational limitations (operational constraints) and control settings (control constraints) of each one of the elements involved. The SCOPF-FUBM adds another layer of analysis by considering not only the operation of the system under normal conditions but also its operation following the occurrence of disturbance (i.e. *contingency* scenarios) such as loss of generation or transmission line. It does this by considering contingency scenarios with a high severity index and/or a high probability of occurrence. These *binding* contingency scenarios are added to the formulation in the form of additional constraints. Thus, the SCOPF will obtain a pre-contingency optimal operating point of the system which will remain secure even under the occurrence of a contingency (post-contingency scenario). In keeping with the existing practice adopted by most TSOs, in this thesis, and for purposes of contingency analysis, an $N-1$ reliability criterion is chosen. The $N-1$ criterion is a condition which states

the system has to withstand the outage in any one single component.

As seen in section 2.2 in the SCOPF literature review, the post-contingency states can be either preventive secure or corrective secure depending on whether or not the control actions are allowed (or available) after a contingency. If no control actions take place following a contingency, the ensuing post-contingency states determined by the SCOPF are said to be preventive secure, whereas if there is any control action taken in response to a contingency (ensuring that all constraints are within bounds) the resulting post-contingency states are considered corrective secure. A more conservative approach is taken when preventive secure states are preferred, however the cost of operating in a preventive secure state is highly likely to be considerably higher than operating in an optimal point which allows corrective actions. Moreover, preventive secure post-contingency scenarios may not even be feasible if the constraints are too tight. On the other hand, corrective secure scenarios may allow the system to operate at an even more optimal operating point (e.g. a cheaper cost) whilst maintaining the security of the system. Traditional post-contingency corrective control actions may include slow response actions like network switching, connection of non-dispatched generators, and connection or disconnection of shunt compensation. The SCOPF-FUBM formulation uses the flexibility and extra variables of the FUBM to include the fast action control elements present in a hybrid AC/DC power system to take part in the preventive and corrective scenarios of the SCOPF (e.g. taps ratios of CTT, angles of PST and VSC controls) . Even though both fast and slow control actions are included as part of the SCOPF-FUBM formulation, in this thesis only the fast action control elements are included for the simulations since it is expected that most hybrid AC/DC networks contain elements capable of exerting fast action control responses (i.e. VSCs), as such simulations of slow action control actions are out of the scope of this thesis. However they are considered for future work.

Since the SCOPF-FUBM formulation could be considered as a generalisation of the OPF formulation presented in chapter 5, the SCOPF-FUBM formulation also provides a direct link between the AC and DC parts of the grid. Thus, the unified frame of reference which has been characteristic of the FUBM formulations is main-

tained. As a clear consequence, conventional AC SCOPF equations are used to solve fully controllable hybrid AC/DC grids. Just like the OPF-FUBM formulation, this formulation maintains the advantages of the FUBM, such as its adaptability to simulate any network topology and diverse control elements. The SCOPF-FUBM formulation accommodates optional optimisation variables associated with all the control elements that are active over the course of the solution for the pre-contingency scenario and all the post-contingency scenarios for all the c selected contingencies of the system.

The remainder of this chapter is structured as follows: Section 6.1 describes the SCOPF formulation in detail, in which the extended optimisation variables and constraints are presented for the pre- and post-contingency scenarios. Furthermore, the corrective actions using the fast action corrective controls from the VSCs, PSTs, CTTs and STATCOMs are included in the in the formulation. Additionally, a quick review of the contingency filter used for the SCOPF in this thesis is presented. The contingency filter takes into account both severity of the contingency and its probability of occurrence. The implementation of the AIMMS-FUBM for the SCOPF is described afterwards followed by Test Cases and Simulation Results. Finally a chapter summary containing the highlights of the chapter is presented.

6.1 Flexible SCOPF Formulation using FUBM

Following the OPF-FUBM formulation presented in equations (5.1.7) to (5.1.17) in chapter 5, the presented SCOPF-FUBM formulation can be presented as an extended optimisation problem in which both pre-contingency (normal operation) and c post-contingency (following a disturbance) binding constraints are included in the problem formulation to ensure a secure optimum operation for both pre- and post-contingency scenarios. The full hybrid AC/DC SCOPF-FUBM is thus formulated as a non-linear mathematical optimisation (mathematical programming) problem as presented in (6.1.1) to (6.1.9). Notice that in this case, contrary to the OPF-FUBM the optimisation variables are separated into two sets of vectors $\mathbf{x}$ and $\mathbf{u}$ containing the state variables and FUBM control variables respectively.

$$\begin{aligned} &min \qquad f_0(\mathbf{x}_0, \mathbf{u}_0) \\ &\mathbf{x}_0, \ldots, \mathbf{x}_c \\ &\mathbf{u}_0, \ldots, \mathbf{u}_c \end{aligned} \tag{6.1.1}$$

subject to:

$$\mathbf{g}_0(\mathbf{x}_0, \mathbf{u}_0) = \mathbf{0} \tag{6.1.2}$$

$$\mathbf{h}_0(\mathbf{x}_0, \mathbf{u}_0) \leq \mathbf{L_l} \tag{6.1.3}$$

$$\mathbf{g}_k{}^s(\mathbf{x}_k{}^s, \mathbf{u}_0) = \mathbf{0} \quad k = 1, \ldots, c \tag{6.1.4}$$

$$\mathbf{h}_k{}^s(\mathbf{x}_k{}^s, \mathbf{u}_0) \leq \mathbf{L_s} \quad k = 1, \ldots, c \tag{6.1.5}$$

$$\mathbf{g}_k(\mathbf{x}_k, \mathbf{u}_k) = \mathbf{0} \quad k = 1, \ldots, c \tag{6.1.6}$$

$$\mathbf{h}_k(\mathbf{x}_k, \mathbf{u}_k) \leq \mathbf{L_m} \quad k = 1, \ldots, c \tag{6.1.7}$$

$$|\mathbf{u}_k - \mathbf{u}_0| \leq \overline{\Delta \mathbf{u}_k} \quad k = 1, \ldots, c \tag{6.1.8}$$

$$\overline{\Delta \mathbf{u}_k} = T_k \tfrac{d\mathbf{u}_k}{dt} \tag{6.1.9}$$

The objective function in (6.1.1) depends on the aims of the study, and just like for the OPF-FUBM the SCOPF-FUBM main objective is to minimise the total generation cost as in (5.1.6). Equality constraints in (6.1.2), (6.1.4) and (6.1.6) correspond to the power balance constraints and the FUBM optional control constraints that were described in detail in chapter 5, however for the SCOPF-FUBM the first sub index (either 0 or k) will serve as an identifier for the pre- and post-contingency scenarios (both preventive and corrective) as presented in (6.1.10).

$$\mathbf{g}_i(\mathbf{x}_i, \mathbf{u}_j) = \begin{matrix} \mathbf{g}_{i_{S_b}}(\mathbf{x}_i, \mathbf{u}_j) = \mathbf{0} \\ \mathbf{g}_{P_f}(\mathbf{x}_i, \mathbf{u}_j) = \mathbf{0} \\ \mathbf{g}_{Q_z}(\mathbf{x}_i, \mathbf{u}_j) = \mathbf{0} \\ \mathbf{g}_{Q_t}(\mathbf{x}_i, \mathbf{u}_j) = \mathbf{0} \\ \mathbf{g}_{Pv_{dp}}(\mathbf{x}_i, \mathbf{u}_j) = \mathbf{0} \\ \mathbf{g}_{G_{sw}}(\mathbf{x}_i, \mathbf{u}_j) = \mathbf{0} \\ \mathbf{h}_{S_f^2}(\mathbf{x}_i, \mathbf{u}_j) \leq \mathbf{0} \\ \mathbf{h}_{S_t^2}(\mathbf{x}_i, \mathbf{u}_j) \leq \mathbf{0} \end{matrix} \quad \forall \quad \begin{cases} i = 0, j = 0, & \text{Pre-contingency,} \\ i = k, j = 0, & \text{Preventive Secure,} \\ i = k, j = k, & \text{Corrective Secure} \end{cases} \tag{6.1.10}$$

Similarly for the inequality constraints in (6.1.3), (6.1.5) and (6.1.7) which correspond to the thermal limit constraints (as described in chapter 5) have the same identifier as presented in (6.1.11).

$$\mathbf{h}_i(\mathbf{x}_i, \mathbf{u}_j) = \begin{matrix} \mathbf{h}_{i_{S_f^2}}(\mathbf{x}_i, \mathbf{u}_j) \leq \mathbf{0} \\ \mathbf{h}_{i_{S_t^2}}(\mathbf{x}_i, \mathbf{u}_j) \leq \mathbf{0} \end{matrix} \quad \forall \quad \begin{cases} i = 0, j = 0, & \text{Pre-contingency,} \\ i = k, j = 0, & \text{Preventive Secure,} \\ i = k, j = k, & \text{Corrective Secure} \end{cases} \tag{6.1.11}$$

where :

$$\begin{aligned} \mathbf{x}_i &= [\mathbf{P}_{\mathbf{g}i}, \mathbf{Q}_{\mathbf{g}i}, \mathbf{V}_{\mathbf{a}i}, \mathbf{V}_{\mathbf{m}i}]^\intercal \\ \mathbf{u}_i &= [\mathbf{B}_{\mathbf{eq}_i}, \boldsymbol{\theta}_{\mathbf{sh}i}, \mathbf{m}_{\mathbf{a}i}, \mathbf{G}_{\mathbf{sw}i}]^\intercal \\ \mathbf{x}_{mini} &\leq \mathbf{x}_i \leq \mathbf{x}_{maxi} \\ \mathbf{u}_{mini} &\leq \mathbf{u}_i \leq \mathbf{u}_{maxi} \end{aligned} \quad \forall \quad i = 0, 1, \ldots, c \tag{6.1.12}$$

From equations (6.1.1) to (6.1.12) it is clear that vectors $\mathbf{x_0}$ and $\mathbf{u_0}$ pertain to the state and control variables for the pre-contingency state. Post-contingency constraints given in equations (6.1.4) to (6.1.7), are defined for the k^{th} contingency with k ranging from 1 to the number of contingencies c, pertaining to each post-contingency state. Likewise, vectors $\mathbf{x}_k$ and $\mathbf{u}_k$ correspond to the state and FUBM control variables for post-contingency states.

Superscript s in (6.1.4) and (6.1.5) indicates "short-term time" relating to the time period in which TSOs cannot modify any control variable following a contingency. As such, the operational limits $\mathbf{L_s}$ are less restrictive, but the system cannot operate with those limits for long periods of time, after a certain period of time the equipment may get damaged. For corrective actions, equation (6.1.8) represents the maximum amount of adjustments to the control variables between the base case (i.e. $k = 0$) and the k^{th} post-contingency state in order to meet the constraints with "realistic" values. T_k is the interval of time available for corrective actions to ensure the feasibility of the post-contingency state and $d\mathbf{u}_k/dt$ is the rate of change of the control variables in response to a contingency. Finally $\mathbf{L}_s$, $\mathbf{L}_m$, and, $\mathbf{L}_l$ denote respectively the short-term (emergency), medium-term, and the long-term (normal) operating limits.

The SCOPF-FubM formulation presented above considers a set of c critical contingencies which are selected using the Reliability Contingency Filter described in detail in section 2.5 in chapter 2. Before describing the implementation of the SCOPF-FubM in Aimms a quick review of the Contingency Filter formulation is presented below.

6.2 Reliability Contingency Ranking

The formulation of the SCOPF-FubM is a general formulation which can include as many contingency scenarios as necessary. In practice a real EPS may contain millions of contingencies for which the vast majority are not critical and they will not be binding the solution of the problem. However if a contingency is excluded and it is binding, the solution may create security problems. Therefore an appropriate selection procedure for choosing the critical contingencies is crucial for the SCOPF. Typically, the TSOs select contingencies by first carrying out a thorough contingency analysis to identify contingencies and then filter the most critical ones, through a Contingency Filter (CF). The contingency analysis and filtering is normally predicated on a specific *reliability criterion*, which for most cases is the so-called $N-1$, which states that the system must continue to operate securely even after the outage in any one single component. However, most practical CFs only filter contingencies by their severity. The CF used in this thesis, on the other hand, ranks the contingencies in the EPS considering both the order of their severity (Severity Index [SI]) and by their respective probabilities of occurrence (using Reliability Rates), whilst adhering to the $N-1$ criterion. Thus, as shown in [88], the resulting ranking is more reliable than a filter which only relies on the SIs for their selection. Since this method has already been described in detail in section 2.5 in chapter 2 only the relevant equations for the SCOPF-FubM implementation are presented here for convenience.

The set of critical contingencies C_{RPI} are calculated as shown in (6.2.13) using the Reliability Performance Index (RPI).

$$C_{RPI} = \{C_{RPI_L} \cup C_{RPI_v}\} \tag{6.2.13}$$

where C_{RPI_L} and C_{RPI_v} are the set of contingencies which RPI is higher than a predefined limit κ for both the branch thermal limits and the voltage limits as shown in (6.2.14) and (6.2.15) respectively.

$$C_{RPI_L} = \{RPI_L | RPI_L > \kappa_L\} \tag{6.2.14}$$

$$C_{RPI_v} = \{RPI_v | RPI_v > \kappa_v\} \tag{6.2.15}$$

The RPIs is defined as a product of the SI and the probability of occurrence of a contingency, and for the branch thermal limits and voltage violations is calculated as presented in (6.2.16) and (6.2.17).

$$RPI_{L_i} = P_{S_i} \times PI_{L_i} \quad \forall i \in lines \tag{6.2.16}$$

$$RPI_{v_i} = P_{S_i} \times PI_{v_i} \quad \forall i \in lines \tag{6.2.17}$$

Details for both the Branch Probability States P_{S_i} and the PIs for branch thermal limits and voltage limits are also described in 2.5.

With the selected set of critical contingencies, the SCOPF-FUBM formulation for hybrid AC/DC grids can be implemented in AIMMS.

6.3 AIMMS-FUBM SCOPF Implementation

The SCOPF-FUBM formulation presented in (6.1.1) to (6.1.12) can be directly implemented into the graphical interface of AIMMS as the problem is already constructed as a mathematical optimisation problem. For the implementation, there will be a series of sets of equality and inequality constraints as presented in (6.1.10) and (6.1.11), one set of constraints for the pre-contingency case, and c sets for each one of the contingencies (selected using the described CF). Thus, the number of extra constraints will be the number of constraints for the case base multiplied by the number of contingencies. A similar case applies for the number of variables of

the system. It seems that the complexity of the SCOPF problem will be increasing linearly as the number of contingencies increase, however, this is not the case since the SCOPF must find an operational point which considers the interaction of all the constraints and variables, thus the problem complexity is even higher. Just like for the OPF-FUBM implementation from chapter 5, the hybrid AC/DC SCOPF problem using FUBM is solved using a variety of solvers. Since CONOPT 4.0 and KNITRO 12.0 had better performance out of all the tested solvers, they are selected as the main solvers for the SCOPF-FUBM implementation.

6.4 Test Cases and SCOPF Simulations

This section presents two main test cases which reflect the complexity of the SCOPF problem as well as their solution using the FUBM implementation in AIMMS. The first case aims to showcase the differences between the OPF solution, a solely preventive SCOPF solution, and a corrective SCOPF solution, all for Hybrid AC/DC grids. It also shows how the complexity of the optimisation problem escalates when the contingencies are introduced. The second test case presents a larger test case for which, the CF ranks and selects the critical contingencies, and then the SCOPF-FUBM implementation in AIMMS solves the problem for those contingencies. Fast action corrective actions for the most severe contingencies are shown. All FUBM simulations have been solved using a PC with CPU Intel Core i7, 2.2GHz and 16GB RAM memory.

6.4.1 Case 6 Bus - HVDC

This case accurately represents the increased complexity of a SCOPF problem in comparison to the OPF. This hybrid test case contains 6 buses, 2 generators, 4 transformers, 2 VSCs, 2 AC lines and 2 DC lines. Buses 1 and 6 operate at 138kV and buses 2, 3, 4 and 5 operate at 220kV. A single line diagram of the test case is shown in Fig. 6.1.

The VSC 1 in the HVDC link with double DC line is set to be type #II for fixed Voltage regulation of bus 3 at $V_m = 1.0$ [p.u.], and VSC 2 is set to be type #I with

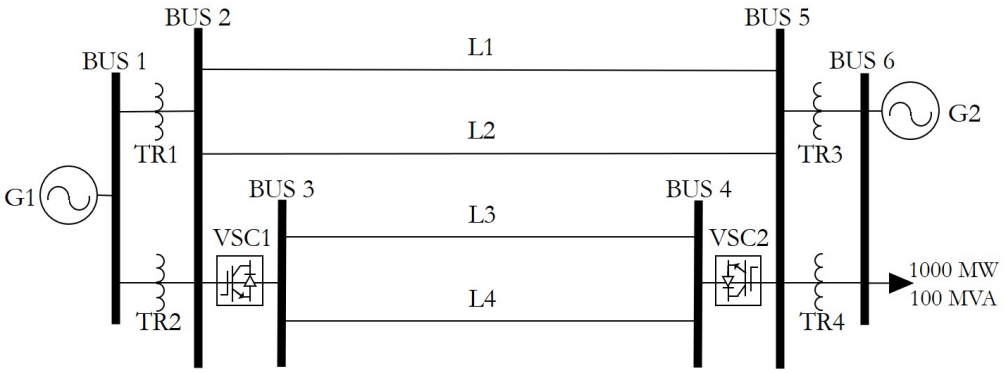

Figure 6.1: Case 6 Bus HVDC

control mode 1 and *zero constraint* control (see control modes in subsection 3.2.1). Parameters and operational limits of the test case are detailed in tables 6.1 and 6.2.

Table 6.1: Parameters of Case 6 HVDC

Variable	min	max	Element	Value [MVA]	
VSC 1 θ_{sh}	-50°	50°	P_{G1} Min/Max	0	1100
VSC 2 θ_{sh}	0°	0°	Q_{G1} Min/Max	-300	300
VSC 1 m_a	0.75	1	P_{G2} Min/Max	0	1100
VSC 2 m_a	0.75	1	Q_{G2} Min/Max	-300	300
Bus V_m^{min}/V_m^{max}	0.95 p.u.	1.05 p.u.	TR Rate	1100	
AC Bus 1 V_a	0°(Reference)		TR 1-4 r_s/x_s	5e-3 p.u.	0.05 p.u.
AC lines r_s/x_s	5e-3 p.u.	1.5e-2 p.u.	AC lines b_c/Rate	5e-3 p.u.	250 MVA

Simulation Results

The OPF, preventive SCOPF and corrective SCOPF problems are solved for the test case to obtain three optimal operating points of the grid. For the OPF no contingencies in the grid are considered. On the other hand, the SCOPF is solved considering the contingencies of lines 1 to 4. All three problems optimise the variables of the VSCs. In the preventive approach, no corrective actions are allowed, thus, the control variables are the same for the pre-contingency and the post-contingency scenarios. By contrast, the corrective approach takes advantage of the fast action controls of the VSCs and it is able to adjust the settings of them for all the post-contingency

Table 6.2: Converters and DC grid parameters

Parameter	Value
VSCs r_s / x_s	1e-5 p.u. 0.0015 p.u.
VSCs Loss Coefficient	$\alpha = \beta = \gamma = 0.001$
DC line r_s / Rate	0.001 p.u. 300 MVA
VSCs Rate	650 MVA

scenarios. Therefore, the maximum change allowed $\overline{\Delta \mathbf{u}_k}$ for the control variables from the pre-contingency state to the post contingency state in equation (6.1.8) is: (i) $\overline{\Delta \mathbf{u}_k} = 0$, for the preventive approach, and (ii) $\overline{\Delta \mathbf{u}_k} = |\mathbf{u_0^{max}} - \mathbf{u_0^{min}}| \times \mathbf{0.25}$, for the corrective approach, or in other words, the maximum change allowed will be 25% of the total range per variable for the corrective approach. This value was calculated considering a linear control ramp for all VSCs from equation (6.1.9).

The AIMMS-FUBM implementation converged for all the three problems using KNITRO 12.0 and CONOPT 4.0. Table 6.3 presents the size of each problem in terms of variables and constraints as well as the results of the simulations for OPF, Preventive SCOPF and Corrective SCOPF. Figures 6.2 and 6.3 show the convergence of the three problems for KNITRO and CONOPT respectively.

Table 6.3: OPF, Preventive SCOPF and Corrective SCOPF Comparison

Optimisation Prob.	OPF	SCOPF-Prev.	SCOPF-Corre.
No. Variables	295	1477	1477
No. Contraints	325	1623	1623
Solver	KNITRO 12.0		
Optimisation Prob.	OPF	SCOPF-Prev.	SCOPF-Corre.
Total Iterations	24	297	85
Total Cost [$/hr]	22631.61	31877.22	28047.74
Conv. Time [s]	0.25	1.46	0.51
Solver	CONOPT 4.0		
Optimisation Prob.	OPF	SCOPF-Prev.	SCOPF-Corre.
Iterations Infe./Min.	26 5	107 551	76 17
Total Iterations	31	658	93
Total Cost [$/hr]	22631.61	31877.22	28047.74
Conv. Time [s]	0.28	18.92	0.93

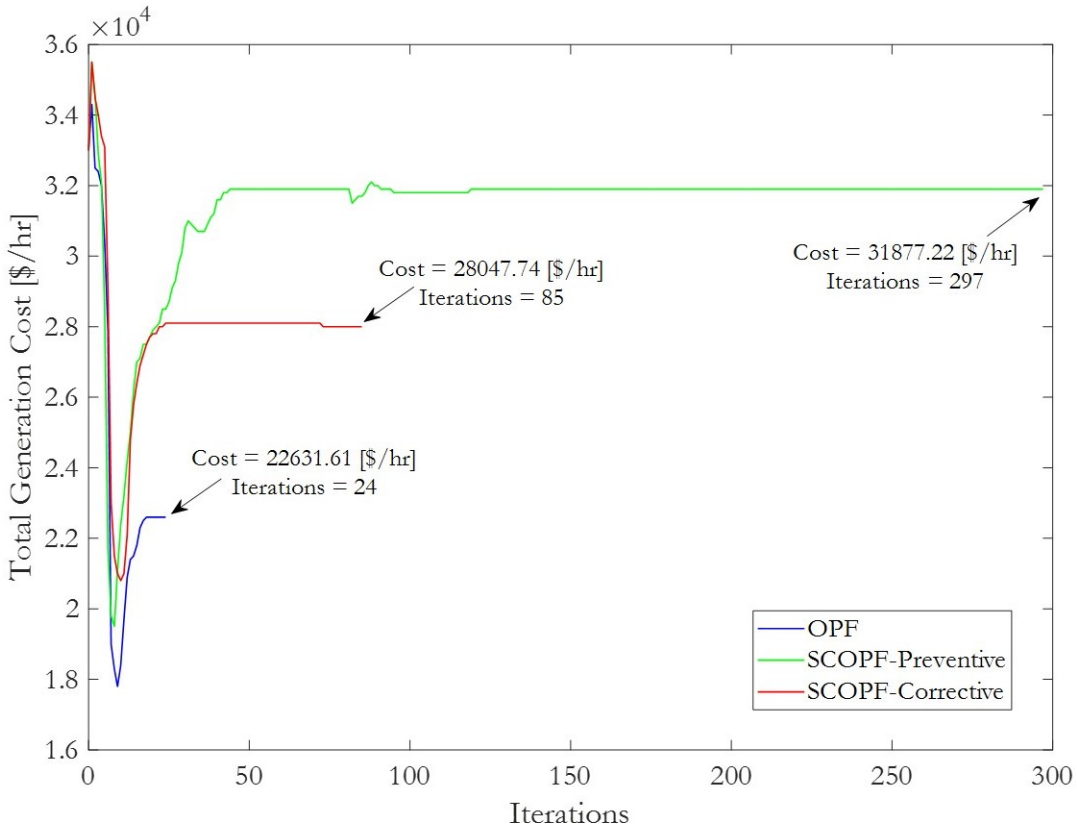

Figure 6.2: Case 6 Bus-HVDC Convergence using KNITRO

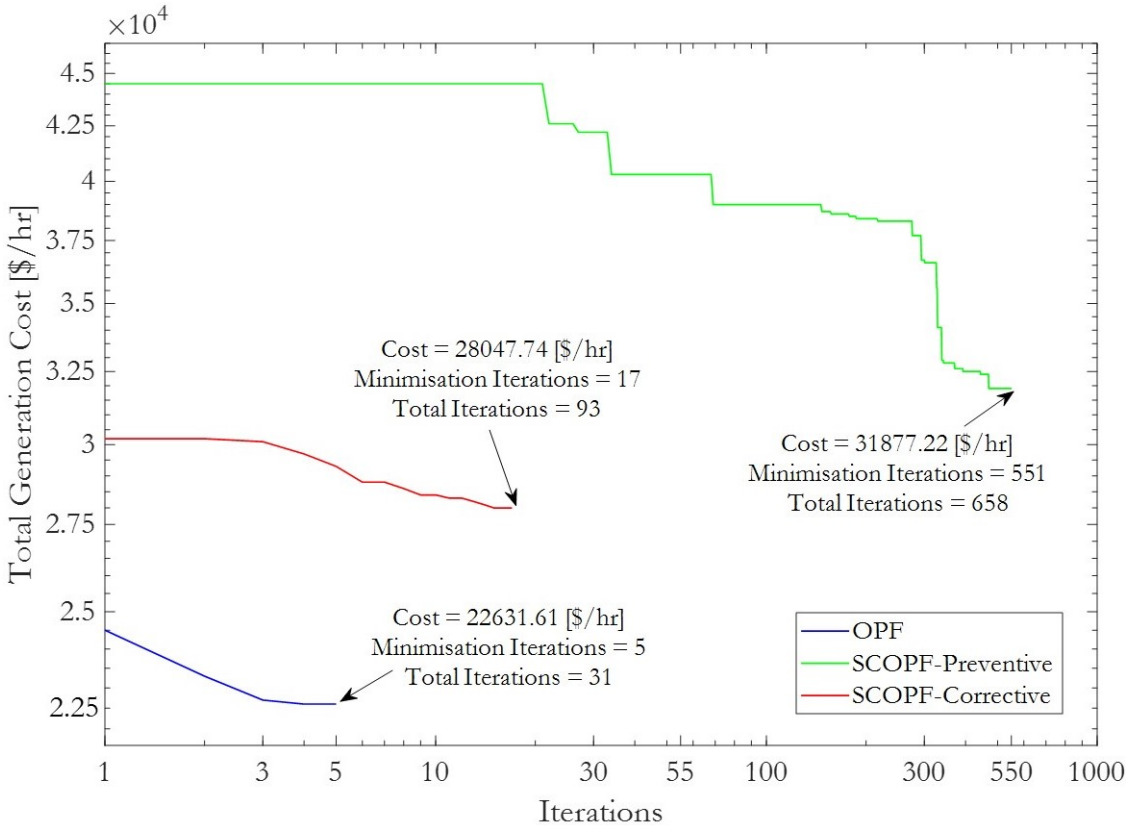

Figure 6.3: Case 6 Bus-HVDC Convergence using CONOPT

From Table 6.3 it is clear the three solvers converged to the same optimal operating point for each optimisation problem. It is noticeable that the number of constraints and variables increase drastically when contingencies are considered. Thus, even though the test case is considered relatively small from an OPF perspective, since the SCOPF problem considers contingencies the optimisation problem becomes 4 to 5 times more complicated than the OPF problem. Additionally, KNITRO appears to be faster than CONOPT since it achieved the optimal operating point in less time and in fewer iterations for all the optimisation problems. In particular, for the preventive case, KNITRO converges in half of the iterations and more than ten times faster than CONOPT.

In figures 6.2 and 6.3 its observed that the Preventive-SCOPF converges to a higher cost and in many more iterations than the Corrective-SCOPF even though they share the same amount of variables and constraints. This is because the fast action controls add flexibility to each post-contingency state and thus the overall

problem. As a result, the convergence time and even the cost is reduced dramatically. It can be concluded that the OPF obtains the best operational cost, but without considering the security of the system, the Preventive-SCOPF does consider the security of the system but at a much higher cost, and the Corrective-SCOPF adds flexibility degrees to each post-contingency stage and thus is able to obtain a cheaper generation cost that satisfies all the security constraints.

Table 6.4: Corrective SCOPF Optimised Variables

Variable	Pre-Cont	Cont. L1	Cont. L3
$P_{g_{G1}}$ [MW]	732.7	731.7	733.7
$P_{g_{G2}}$ [MW]	325.8	324.6	325.9
$Q_{g_{G1}}$ [MW]	-22.3	-20.1	-21.4
$Q_{g_{G2}}$ [MW]	181.4	191.4	191.4
$\theta_{sh_{VSC1}}$ [deg]	-1.526	-2.205	-1.276
$\theta_{sh_{VSC2}}$ [deg]	0	0	0
$m_{a_{VSC1}}$ [p.u.]	0.95	0.862	0.998
$m_{a_{VSC2}}$ [p.u.]	0.966	0.965	0.916

Table 6.4 shows the optimised variables for the Corrective-SCOPF. The Optimised values for contingencies L1 and L2 are the same, and similarly the optimised values for contingencies L3 and L4 are also the same in between them. Therefore only contingencies L1 and L3 are presented. It is observed that there is no significant change in the power output from the generators from the pre-contingency state to all the post-contingency states. This is a solid proof that even during a contingency the generation dispatch did not change, and therefore the power and voltage changes in the system are the result of the corrective actions from the VSCs fast action controls. Considering the pre-contingency state, it is clear that if no corrective actions were taken in the post-contingency states, the transmission lines would have reached their thermal limits. For example, if no corrective actions were taken and there was a contingency in Line 1, there will be an overload of Line 2. The power would not have been redistributed to the DC grid because the VSC controls would have remained fixed in the post contingency state, and thus the power flow though

the DC grid would have remained constant. However, since corrective actions are activated for θ_{sh} and m_a, their value is adjusted in the post contingency state, and the power is redistributed to meet the constraints. This can be appreciated in Fig. 6.4, where the redirection of the power is clear for each contingency. As a result, the optimal point selected by the Corrective SCOPF is operating at a cheaper cost in comparison with the preventive SCOPF whilst meeting all the security constraints.

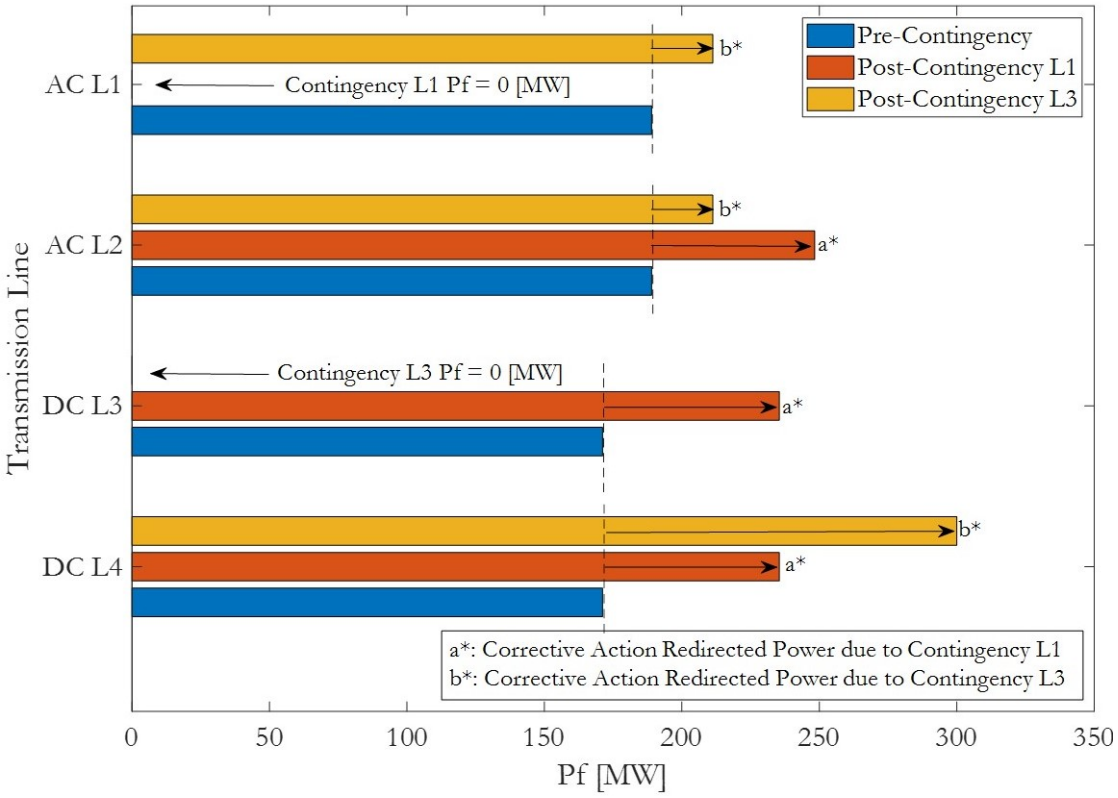

Figure 6.4: Redirection of the Power using Corrective Actions

6.4.2 Modified RTS-GMLC Test System

The IEEE reliability test system called RTS-GMLC was designed to serve as a platform to analyse power system operation strategies and issues, including UC, ED, Power Flows, and associated techno-economic impacts. This system was extensively modified by the National Renewable Energy Laboratory (NREL) in [117]. The modifications include additional sources of generation such as solar Photovoltaic, Concentrated Solar Power, Natural Gas, wind and storage units. The RTS-GMLC

layout has 73 buses distributed in three regions, 120 branches with lengths of circuits being 1128 km for 138 kV and 2125 km for 230 kV. It also consists of 74 conventional generation units, 20 hydro units, 25 PV farms, 31 RTPV, six winds stations, one storage unit and 16 transformers with 6400 MVA total rating capacity. Additionally, in this thesis the RTS-GMLC has been modified even more to simulate a highly complex and fully flexible AC/DC grid. Among the modifications, the DC line from bus 113 to 316 has been removed, branches 107 to 108, 207 to 208, and 307 to 308 have been duplicated to avoid Islands in the system. Furthermore a highly complex series of MTDC grids have been added on top of the AC layer of the system. This series of DC grids consist of 38 DC buses, 38 VSCs, 38 transformers and 45 DC Lines. Parameters of the DC grids are presented in 6.5. The AC layer of the system is shown in Fig. 6.5, and the DC layer of the system is shown in Fig. 6.6. Reliability indexes and weights for branches and buses is taken from [88].

Table 6.5: MTDC Grids Data for the Modified RTS-GMLC

Parameter	Value
VSCs r_s / x_s	1e-4 p.u. 0.01643 p.u.
VSCs Loss Coefficient	$\alpha = \beta = \gamma = 0.001$
DC line r_s / Rate	0.005 p.u. 250 MVA
VSCs Rate	250 MVA
Transformers r_s / x_s	1e-4 p.u. 0.01121 p.u.
Transformers Rate	250 MVA
DC Buses V_m^{min} / V_m^{max}	0.95 p.u. 1.05 p.u.

All modulation amplitudes m_a and shift angles θ_{sh} for all VSCs are set as free variables to be optimised. Voltage regulation is provided by VSCs 4, 12, 20, 25, 27, 29, 33 and 35 as they are set as type # II with a V_m^{set} of 1.0 [p.u.]. The remaining VSCs are set as type #I for *Zero Constraint* control.

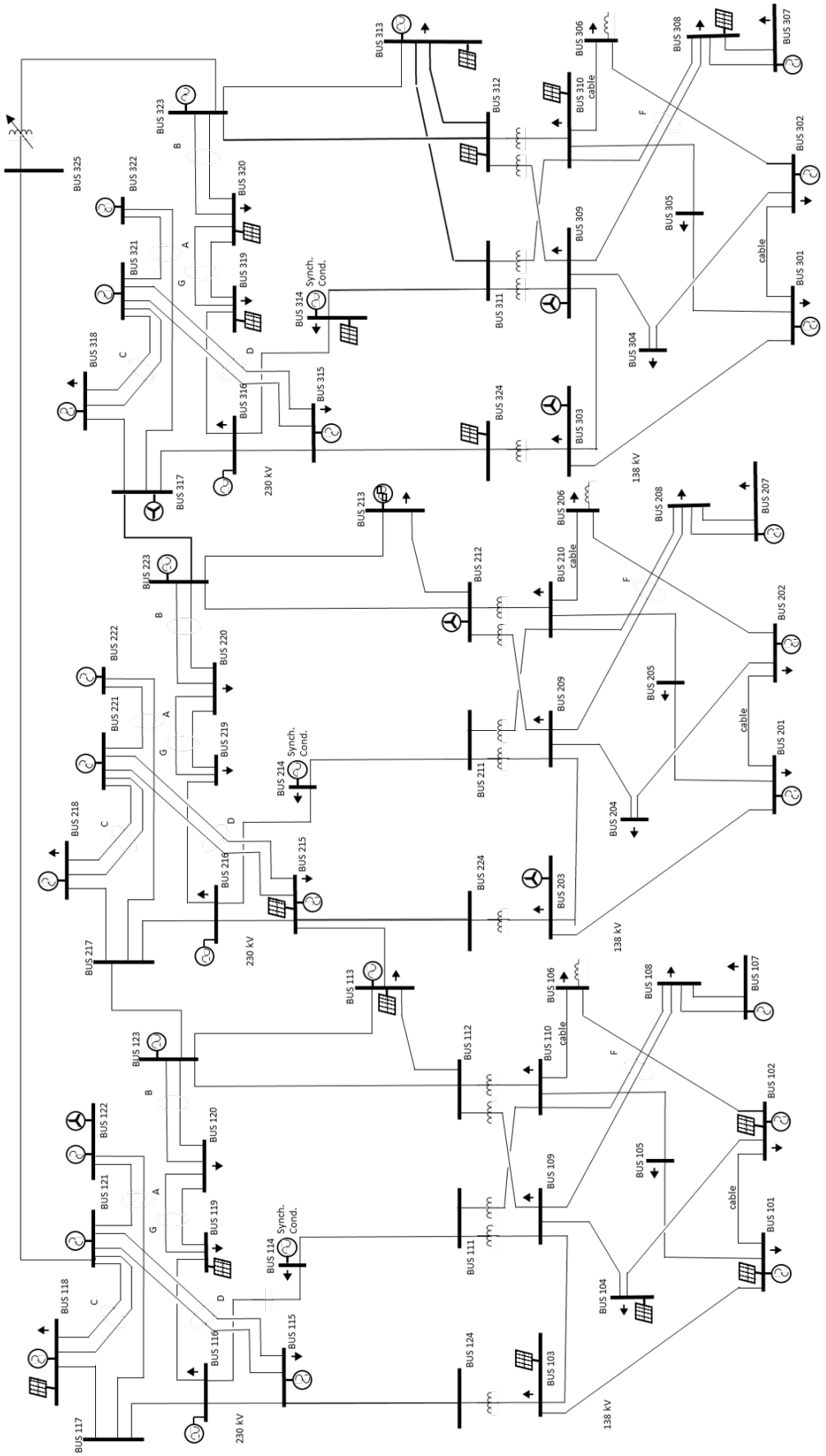

Figure 6.5: Modified RTS-GMLC Test System (AC grid only)

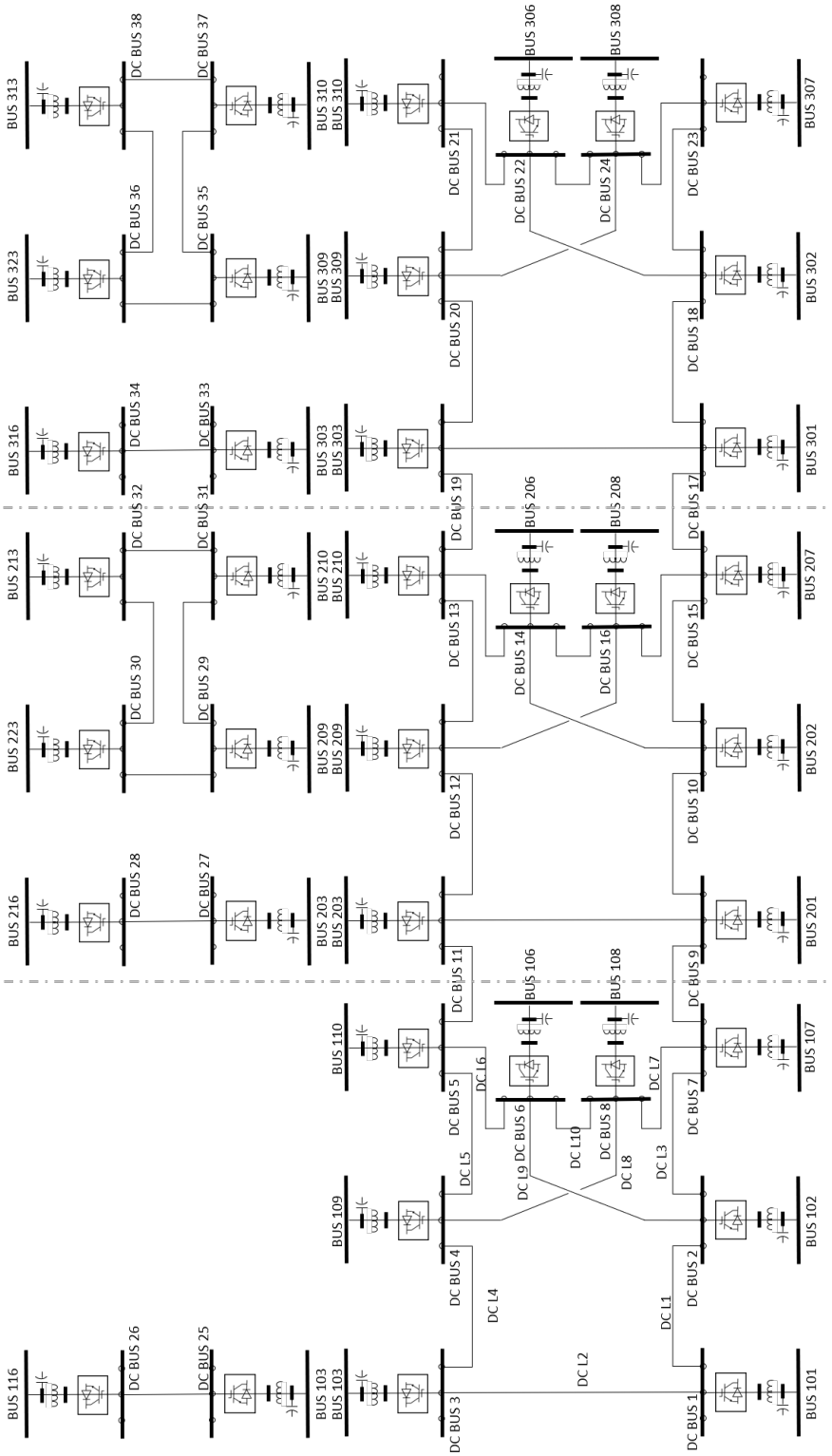

Figure 6.6: Modified RTS-GMLC Test System (DC grid only)

6.4.3 Contingency Ranking for the Modified RTS-GMLC

The contingency ranking plays an important role for the selection of the critical contingencies of the SCOPF. Using equations (6.2.13) to (6.2.17) in the Modified RTS-GMLC test system, the Reliability Performance index for voltages and branch thermal limits are obtained. Furthermore the combination of them will give a set of selected critical contingencies for the case. The value of κ_L is set to 1.5e-4, and the value for κ_v is set to 5e-4. The power flow calculations to obtain the RPI are done using the MATPOWER-FUBM implementation. Figure 6.7 shows the results obtained with the contingency filter. It can be appreciated that 27 critical branch contingencies were selected out of 240 transmission elements. Notice that due to the highly meshed DC grids no element of the DC grid presents critical contingencies. The selected contingencies will be implemented into AIMMS to build the complete optimisation case.

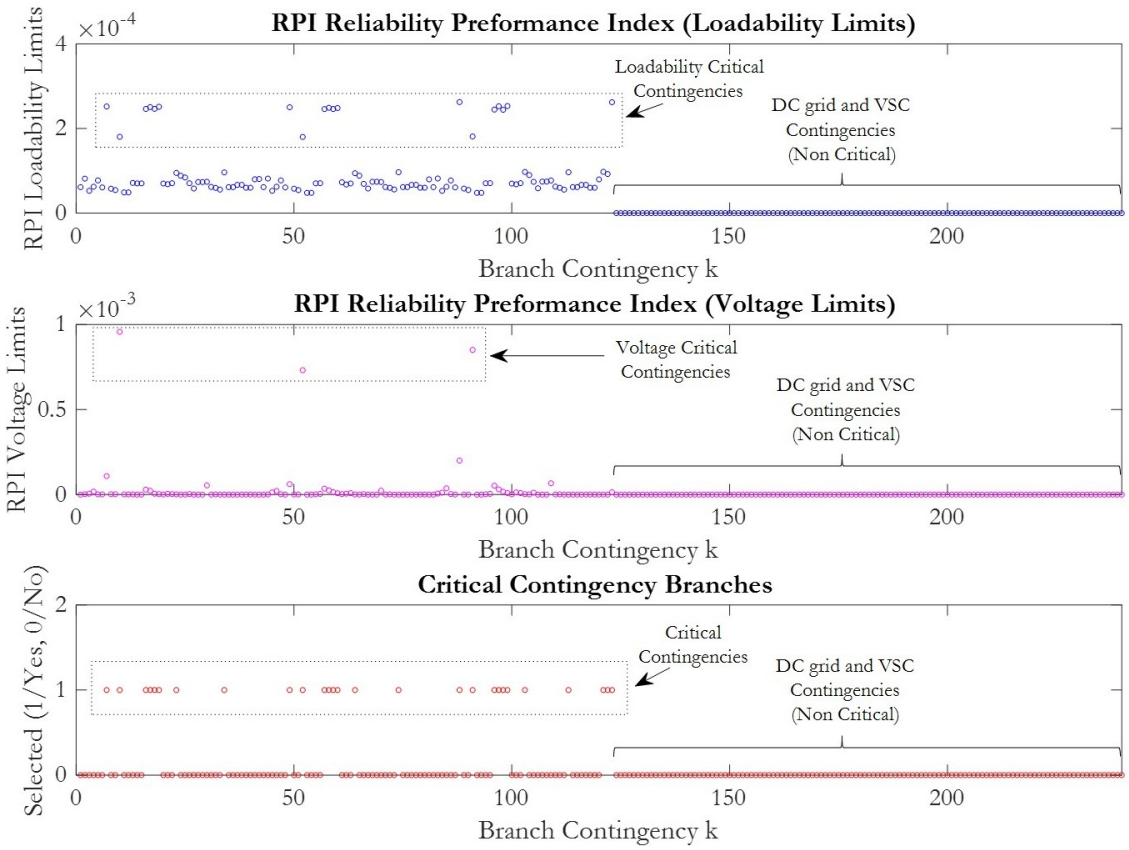

Figure 6.7: Critical Contingencies for the Modified Reliability Test System

6.4.4 Simulation Results

Just like it was done for Case 6 HVDC, for the modified RTS-GMLC the OPF, preventive SCOPF and corrective SCOPF problems are solved. The SCOPF however now is solved considering the 27 contingencies obtained from previous subsection. Table 6.6 present the list of these contingencies.

Table 6.6: Critical Contingencies

Line ID	From Bus	To Bus	Line ID	From Bus	To Bus
L7	103	124	L60	210	212
L10	106	110	L64	212	223
L16	109	111	L74	217	222
L17	109	112	L88	303	324
L18	110	111	L91	306	310
L19	110	112	L96	309	311
L23	112	123	L97	309	312
L34	117	122	L98	310	311
L49	203	224	L99	310	312
L52	206	210	L103	312	323
L57	209	211	L113	317	322
L58	209	212	L121	325	121
L59	210	211	L122	318	223
			L123	323	325

Again, for the three optimisation problems the control variables of the VSCs are optimised. The SCOPF preventive and corrective approach remain with the same considerations used for Case 6 HVDC. Thus, for the preventive approach, the control variables are locked to the same value for the pre-contingency and the post-contingency scenarios. And for the corrective approach the fast action controls of the VSCs are allowed to be active for all post-contingency states. Also, the maximum change allowed $\overline{\Delta \mathbf{u}_k}$ for the control variables from the pre-contingency state to the post contingency state in equation (6.1.8) are again: (i) $\overline{\Delta \mathbf{u}_k} = 0$, for the preventive approach, and (ii) $\overline{\Delta \mathbf{u}_k} = |\mathbf{u_0^{max}} - \mathbf{u_0^{min}}| \times \mathbf{0.25}$, for the corrective approach.

Table 6.7: OPF, Preventive SCOPF and Corrective SCOPF Comparison

Solver	KNITRO 12.0		
Optimisation Prob.	OPF	SCOPF-Prev.	SCOPF-Corre.
No. Variables	6637	164277	164277
No. Contraints	7385	182790	182790
Total Iterations	2039	1332*	2792
Total Cost [$/hr]	219214.50	251435.60*	219214.50
Conv. Time [hr]	0.57	0.76*	2.35

*: Infeasible Solution, solver stopped

Simulation results for the three optimisation problems are presented in Table 6.7. Again, the number of constraints and variables is drastically increased from the OPF problem to the SCOPF problem. From 6,637 variables and 7,385 constraints, to 164,277 variables and 182,790 constraints (More than 25 times bigger). The AIMMS-FUBM implementation converged in 2,039 iterations for the OPF problem. On the other hand, once the 27 contingencies are considered for the SCOPF problem, the solver determined that a Preventive solution of the test case is infeasible. For this, KNITRO evaluated the case for 1,332 iterations, and after 750 iterations without a change in either the infeasibility or the Total generation cost, is determined that there is no operating point that meets all the constraints.

In contrast, the Corrective SCOPF approach not only converges in a similar amount of iterations (2,792), but the resulting optimal operating point is the same as the one obtained with the basic OPF. A secure post contingency operating point is possible thanks to the fast action controls that "correct" the state of the system, thus meeting all the constraints. This means that the resulting operating point from the Corrective SCOPF approach is not only as costly effective as the optimal operating point obtained by OPF with a full grid, but it is also secure for all the $n-1$ contingencies of the system. Convergence for the OPF and both SCOPFs can be appreciated in detail in figures 6.8 and 6.9, where it is clear that the OPF and the corrective SCOPF solutions converge to the same operating point. Furthermore, the infeasibility of the preventive SCOPF for this test case is shown.

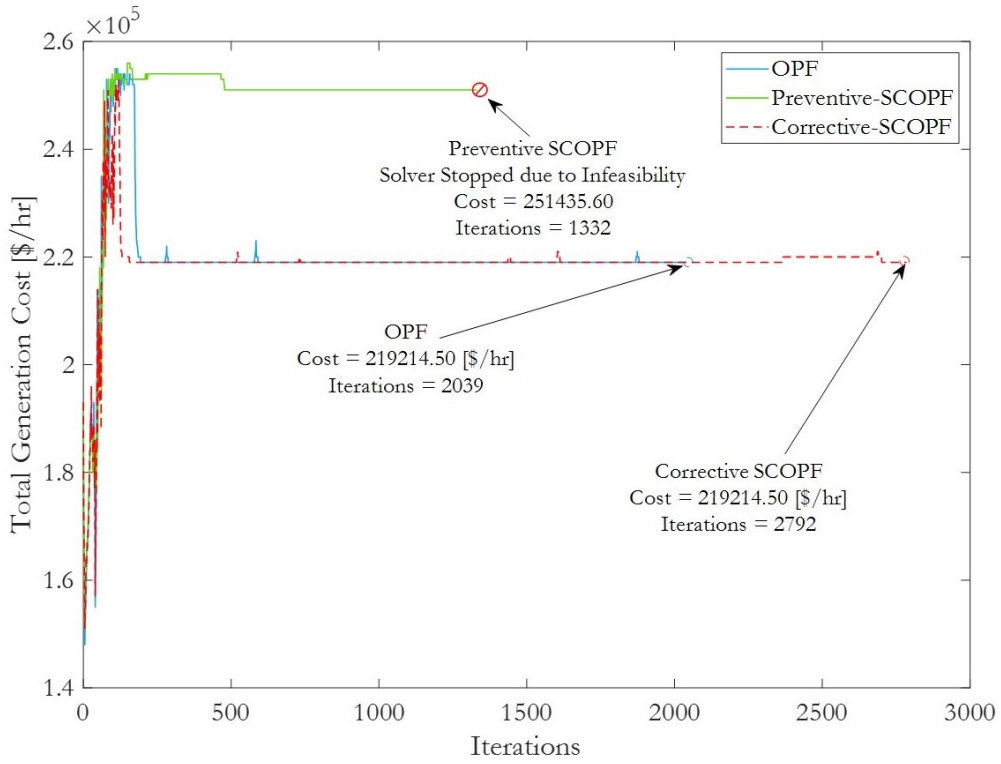

Figure 6.8: RTS-GMLC Convergence using KNITRO

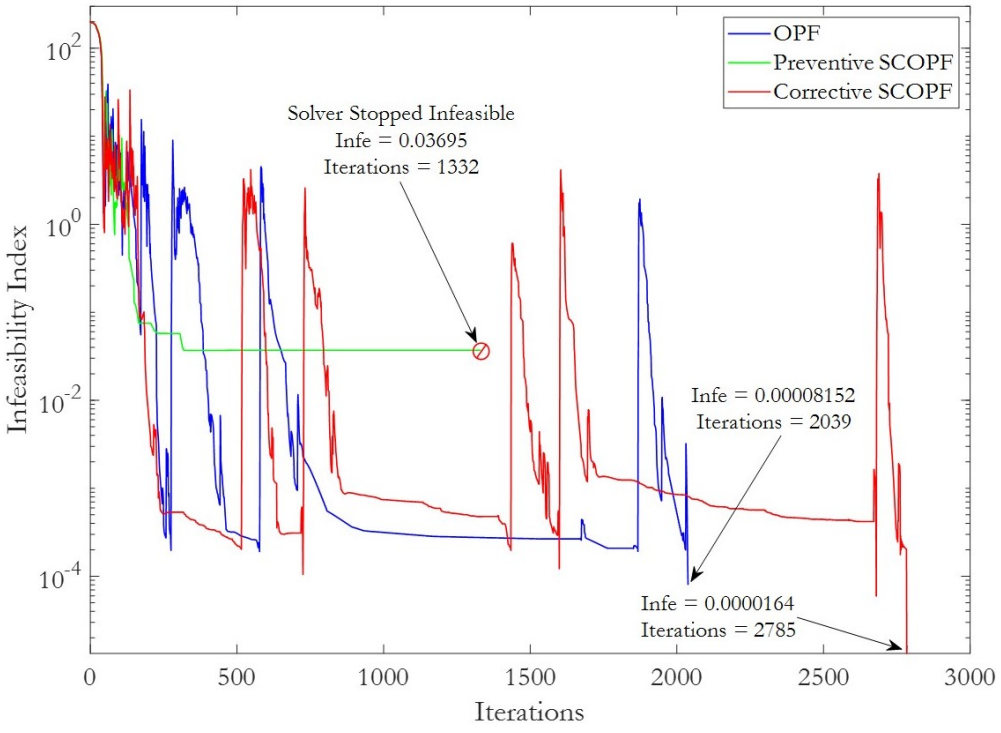

Figure 6.9: RTS-GMLC Infeasibility using KNITRO

Since the modified RTS-GMLC is widely meshed instead of observing the post-contingency power flow redistribution (for the corrective SCOPF), the changes in the control variables for all VSCs are plotted in figures 6.10 and 6.11. Notice that only the contingencies that required a larger change in the VSCs variables to achieve a corrective secure post contingency state are plotted. The contingencies that are not plotted had a smaller variation with respect to the pre-contingency state, thus their values are fairly similar.

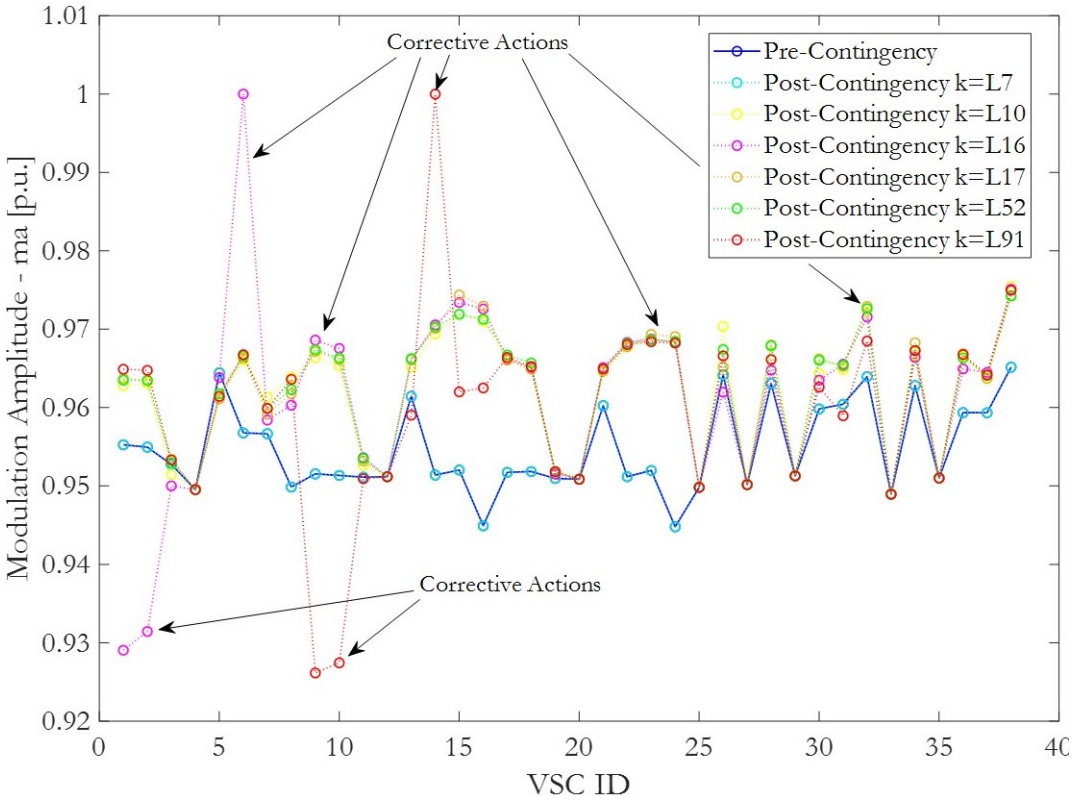

Figure 6.10: VSCs Corrective actions using m_a

Contingency of Line L16 will serve as a clear example of the effects that the corrective actions have in the post-contingency states. From Fig. 6.7, it is observed that the CF selected line L16 as critical since its contingency creates voltage problems as well as loadability problems. The voltage problems are clear by analysing the single line diagram of figure 6.5. Line 16 is a transformer in between buses 109 and 111 that connects the upper part of the system with the lower part of the system. When the contingency happens, a drastic undervoltage is present in bus 106,

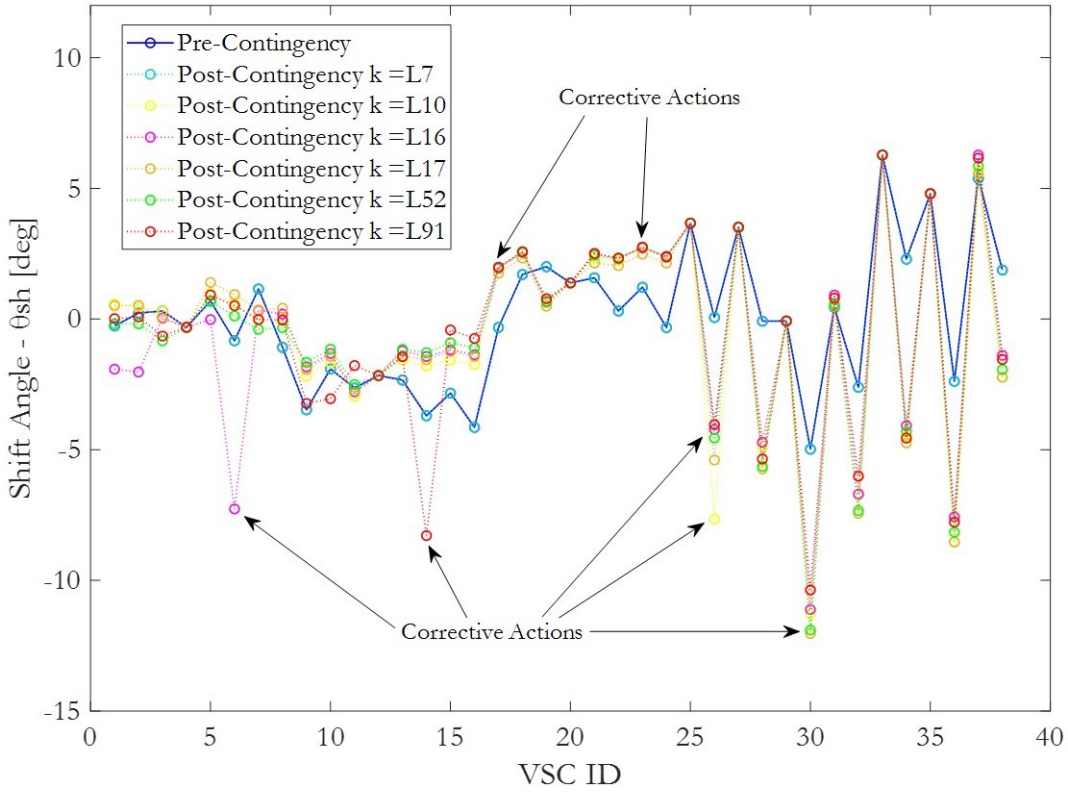

Figure 6.11: VSCs Corrective actions using θ_{sh}

and an overvoltage is presented in bus 101 due to the shunt reactor connected to bus 106 an the fixed reactive power output of the generator in bus 101. In response to this contingency, the fast active controls, change the modulation amplitude of VSCs 1 and 6 to reduce and increase their AC side voltage respectively, and thus "correct" the post-contingency state. This change is noticeable in Fig. 6.10. Also, for the same contingency, the loads in buses 103, 109 and 110 are mostly supplied with the generators of buses 101,102 and 107, since their power output cannot change drastically, a redirection of the power is necessary to satisfy the demand, thus, VSC 6 also changes its θ_{sh} to redirect the power though the DC grid. This change is shown in Fig. 6.11. Thus, just like the corrective actions for the contingency L16, all the 27 contingencies have their own corrective actions that counteract the contingency effects.

After analysing the simulation results for both the Case 6 HVDC, and the RTS-GMLC, it is clear that the SCOPF-FUBM formulation is able to solve hy-

brid AC/DC grids while considering the security constraints of the systems. The formulation of the FubM for steady state analysis has proven to be flexible enough to simulate highly complex EPS using one single model for all the transmission elements. Moreover, the FubM was also used to obtain the critical contingencies as shown in section 6.4.3. Furthermore, since the variables of the FubM are designed to be independent, they can be easily be fixed to a specific value (like it was done for the preventive SCOPF) or set as free variables to be optimised and even perform security corrective actions under contingencies (in the case of the corrective SCOPF).

Chapter summary

In this Chapter, a steady-state FubM model formulation for solving the SCOPF for hybrid AC/DC EPS has been presented. This formulation maintains the same advantages that the ones presented in 5 for the OPF-FubM formulation. The main difference is that this formulation is a more generalised optimisation problem that not only obtains an optimal operating point of the system, but also it considers the security constraints of the system. Control constraints were adding for each post contingency state, and a maximum variation in between the Pre-contingency state and the Post-contingency state for the FubM was included. The reliability Performance Index formulation was presented and used to select the most critical contingencies of any test case. Then the SCOPF-FubM formulation was implemented in Aimms while considering a powerful CF. Test cases and simulations were presented. Two main test cases were used to showcase the effectiveness of the SCOPF-FubM implementation in Aimms. Simulation results showed that the FubM is able to be used for the Preventive SCOPF and the corrective SCOPF thanks to the independent variables of the FubM. Finally the results from the test systems were discussed.

Chapter 7

Conclusions and Future Work

This final chapter draws the conclusion to the research as presented throughout the thesis. It outlines the key findings, highlights and contributions of this research in accordance with the aims and objectives stated in section 1.3 in Chapter 1. In addition, it lays out a path forward for ongoing and future work based and on this research.

7.1 Key Results

Overall, the main aim of this thesis has been to develop a Flexible Universal Branch Model (FUBM) and and its formulation for steady state operational analysis and optimisation (Power Flow, OPF and SCOPF) of fully controllable hybrid AC/DC grids through which, the global impact of the control actions of the system elements (hence its flexibility) can be thoroughly investigated.

As discussed throughout this thesis, existing power systems analysis tools currently require an extensive model library to be able to simulate and solve EPSs, particularly when using AC-only formulations for Power Flows and OPF/SCOPF. Each model has different parameters and features which corresponds to a very specific element. These features are particularly important because they will have an impact on how the problem is formulated. For this reason, not all the existing software (both commercial and open-source) have particularly diverse customisation and modification capabilities in terms of including new element models and/or expanding

formulations for accommodating extra controls. Notwithstanding this, the Electric Power Systems are undergoing a transformation from passive AC-only vertically oriented networks to a more active AC/DC hybrid system for maximising integration of renewable resources and generally a more efficient, and flexible operation of the power system under a variety of operating conditions. It is therefore necessary for system operators and analysts as well as the wider research community to be able to properly analyse the impact of flexibility in future hybrid AC/DC systems. Meanwhile, the problem formulation is rather more challenging in the case of hybrid AC/DC EPS. For solving those hybrid grids, the EPS is traditionally partitioned into their AC and DC grids. When this partition is used, there is a unique element (and therefore a special model) that will serve as an interface between both grids. The modelling of the interface between AC and DC sides is particularly important because it will have an impact on the formulation of the problem. Some approaches solve AC/DC hybrid girds sequentially, while other approaches take a more unified method for solving hybrid AC/DC grids. Even if a *standard* unified approach is used, the formulation still has to consider a wide variety of models, controls and coupling equations. This will be a challenge for all steady-state analysis models for solving Power Flows, OPFs and SCOPFs as they all share the same core equations (i.e. solving the power balance equations). The TSOs normally counter these inherent challenges by resorting to approximate formulations, for example solving a DC approximation (linear approximation) of the OPF/SCOPF. The DC approximation, while simpler to solve than the AC formulation of these problems, is not able to properly capture the impact of flexibility of operation for hybrid AC/DC networks. It also ignores important system characteristics, for example impact on voltage regulation and/or realistic physical boundaries on system elements such as VSCs.

It is therefore more ideal to be able to model all elements (AC and DC) using a *universal* approach for solving any system with any topology and complexity and with any number of elements (AC or DC) using simply AC-only formulations with minimum approximations.

In this thesis, a novel *universal* model, FUBM, was introduced to be able to

achieve this very premise of both flexibility in modelling a diverse pool of elements and simplicity of implementation and solving steady-state analysis problems for Power Flows, and OPF/SCOPF.

Following this quick overview of the problem statement (presented in detail in section 1.1), it can be observed there are many intricacies to be considered in the formulation of the Power Flow, OPF and the SCOPF problems for hybrid AC/DC EPS using a FUBM to simulate all its elements within. In achieving the main objectives as outlined in Section 1.3, a series of Research Challenge (RC) were identified and presented in Section 1.4 of this thesis. This section describes how each RC was addressed as well as the chapter or section of the thesis in which it was developed.

7.1.1 RC1: Development of the FUBM

In Chapter 3 the FUBM model for the steady state analysis of fully controllable hybrid AC/DC EPS has been developed. The proposed FUBM model provides a physical link between AC and DC parts of the grid, thus, there is no need to separate the EPS into its AC and DC counterparts. The FUBM has also been shown to be capable of modelling a variety of network elements, both AC and DC, ranging from standard AC transmission lines to more complex control elements including Phase Shifter Transformers (PSTs), Controlled Tap-Changing Transformerss (CTTs), and more importantly Voltage Source Converters (VSCs) and VSC-interfaced elements including point-to-point and multi-terminal HVDC links used to create hybrid AC/DC networks, and even STATCOMs. All model elements were realistically represented using internal models (*in-model*) within the FUBM, where all *in-models* share variables and parameters that may or may not be activated depending on the model and its controls. Control elements were represented explicitly by their associated control variables within the FUBM and constraints on the steady state problem formulation, thus, adding degrees of flexibility to the formulation. Moreover, the VSCs *in-model* within the FUBM considered a quadratic correction for the calculation of the switching losses. Meanwhile, realistic operational limits for each one of the presented *in-models* were also considered. Finally, thanks to its

ability of simulating all the aforementioned *in-models* there is no need to analyse the system equations model by model thereby from a software perspective reducing the need for developing separate model libraries for several network elements.

7.1.2 RC2: Flexible Steady State Formulation using FUBM

The flexible steady state formulations for Power Flow, OPF and SCOPF using FUBM (namely Power Flow-FUBM, OPF-FUBM, and SCOPF-FUBM) were developed in detail in Chapters 4, 5, and 6 respectively. These formulations allow for analysing a fully controllable AC/DC grid and thus the operational impact of the flexibility and security of those networks can be studied in detail and taking into account system's realistic operational boundaries. These three formulations were designed for the FUBM from chapter 3, consequently they were able to take advantages of the full control capabilities of the FUBM, and thus providing maximum flexibility for the solution. Meanwhile, when modelling AC/DC grids, there is no need for introducing additional coupling constraints to maintain power balance between AC and DC parts of the network as the FUBM model structure was configured in such a way that from a purely mathematical perspective, there is no distinction between AC and DC counterparts. Thus, same AC equations were used to solve the entire hybrid EPS while capturing any interactions between the interconnected grids. Moreover, the three formulations were able to solve entire AC/DC grids within a unified frame of reference. All the variables of the FUBM are added to the formulation as optional state variables (or optimisation variables for the OPF and the SCOPF formulation) and similarly their respective controls were added as optional constraints (or mismatch equations for the Power Flow formulation), thus their impact over the flexibility of the grid can be analysed . Furthermore, first and second order partial derivatives of the formulation were also developed in detail. Simulation results validated the formulations and prove their effectiveness and efficiency in comparison with their traditional counterparts.

7.1.3 RC3: Implementation of the FUBM

In Chapters 4, 5, and 6 the Power Flow-FUBM,OPF-FUBM, and SCOPF-FUBM formulations were implemented in two analytical software packages namely, the open-source power systems steady-state analytical package, MATPOWER, which runs in MATLAB, and in the commercially available general-purpose optimisation software, AIMMS. These implementations showed that the FUBM steady state formulations can be easily implemented in either a mathematical optimisation software or into an existing power systems software without making major modifications to the original code and core components of either software. Both the MATPOWER-FUBM and the AIMMS-FUBM implementations were validated and compared against the traditional approaches for several cases. For the Power flow implementation, the simulation results demonstrated high speed and quadratic convergence with full control over the grid. Moreover its results were used to initialise the OPF implementations, which proved to be working with a variety of optimisation solvers without sacrificing any computational effort, even presenting faster results than traditional approaches in some cases. Simulation results showed that the FUBM implementation is able to be used for the Preventive SCOPF and the Corrective SCOPF thanks to the independent variables of the FUBM. Finally, the three implementations have proven to be scalable and maintain computational tractability for small, medium and large scale systems.

7.1.4 RC4: Flexibility of the System

Chapters 4, 5, and 6 address the flexibility of the system by analysing the simulation results from several test cases. It was clear that the implementations allow for having optional control variables, and optional control constraints which had a direct impact over the flexibility of the system. It was observed that if more controls were set as active, the infeasibility index decreases since more degrees of freedom are added. On the other hand as the number of constraints is increased the feasibility is decreased. This was particularly clear for the SCOPF simulations, where it shows that the Preventive SCOPF by having their controls fixed for their post-contingency

states, was not able to match the minimised total generation cost presented by the Corrective SCOPF. This is to be expected since the corrective SCOPF does allow corrective actions in its post-contingency states, therefore its feasible region is larger than the restricted Preventive SCOPF. This is a clear example of how the flexibility of the system is increased as the number of control variables increase. This same idea applies for the three formulations in both implementations.

7.1.5 Contributions

The main contributions of the thesis can be enlisted as follows:

1. The Flexible Universal Branch Model (FUBM)

   One of the mayor contributions of this thesis was the development of the FUBM. This model combines fundamental traditional models into one single model for AC and DC grids. Furthermore, the model has shown unique control features which makes it a particularly flexible for modelling.

   (a) The FUBM in-models

   The model has proven to be capable of seamlessly modelling several of network elements using its unique *in-models* ranging from conventional AC and DC branches, CTTs, PSTs, STATCOMs and VSCs. Furthermore thanks to the individual control variables of the FUBM, it can also model additional combined elements like the Unified Power Flow Controller (UPFC) and the Bidirectional DC Converter.

   (b) The FUBM Flexible Control

   A flexible and individual control of the FUBM variables is also included in addition to the *in-models*. The way the variables of the FUBM can be set allow the user to set the desired element to be modelled with unique controls that may be restricted if other traditional models are used. (e.g. the FUBM allow an individual control of the variables and thus the *VSC in-model* is not restricted by the control modes presented in table 3.4 in Chapter 3)

2. The steady state FUBM formulations

   Three steady state formulations for the solution of fully controllable AC/DC grids were developed, namely the Power Flow, the OPF, and the SCOPF. These formulations allow the system to be analysed in one single frame of reference and thus, there is no need to separate hybrid grids into their AC and DC parts. Furthermore, since the FUBM does not make a distinction between AC and DC elements, the developed formulation can be used to solve AC, DC and hybrid grids.

   (a) The Power Flow - FUBM formulation

   For this formulation, a special Flexible AC/DC Power Flow Algorithm (FPFA) was developed. This algorithm provides quadratic convergence, and it allows the introduction of control constraints which are related to each one of the *in-models*.

   (b) The OPF - FUBM formulation

   This formulation allows to selectively optimise each one of the extra variables of the FUBM to provide extra degrees of freedom to the optimisation problem. Also, it has the option to include voltage and power control to the optimisation problem. The formulation allows the optimisation of fully controllable hybrid AC/DC grids, and thus analyse the flexibility of the systems.

   (c) The SCOPF - FUBM formulation

   This formulation is a generalisation of the OPF-FUBM formulation to consider the security limitations of the system when contingencies are considered. This formulation not only obtains an optimal operating point, but it ensures that the system will remain secure even in the event of a contingency. This formulation took advantage of the control features of the FUBM to individually correct the post contingency states of the system and therefore, it allows the system to operate at a cheaper cost while considering the security of the EPS (in comparison with the preventive approach).

3. The Flexible Universal Branch Model (FUBM) Implementations

   These implementations showed how easily an existent AC software can be improved for the solution of hybrid AC/DC grids by using the FUBM. They also show that the FUBM formulations can be implemented as a mathematical optimisation problem to be solved by an optimisation software. MATPOWER and AIMMS were used as the platforms for the implementation of the FUBM.

   (a) The MATPOWER-FUBM Implementation

   This implementation was done for both the Power Flow-FUBM formulation and the OPF-FUBM formulation. With this implementation both formulations were validated, and simulation results show reliable results and a fast convergence rate (for 500 buses or less).

   (b) The AIMMS-FUBM Implementation

   This implementation was done for both the OPF-FUBM formulation and the SCOPF-FUBM formulation. This implementation was compared against existent power system software tools for several cases. The simulation results show fast and accurate convergence for small, medium, and large scale systems. Furthermore, for some cases, this implementation out-preformed the traditional implementations.

4. Conference Paper

   The developed FPFA and first stage of the FUBM were published at the IEEE International Conference of Electrical Engineering 2018 for Energy systems in Europe (EEEIC/I&CPS Europe) [103].

5. Journal Paper

   This paper presents the results of the final stage of the FUBM as well as the OPF-FUBM formulation in AIMMS. This paper was published at the International Journal of Electrical Power Energy Systems ElSevier [28].

6. MATPOWER-FUBM Software Release

   The results of the implementation of the FUBM in MATPOWER for Power flows and OPFs resulted in an official extension to the original MATPOWER

analytical software with direct collaboration with MATPOWER's creator and lead developer, Dr Ray Zimmerman. This software release came along with test cases, technical notes and user guide all specially for the FUBM implementation. The software is open source and its available for the public in [104].

7.2 Future Work

Future Collaborations

As mentioned in section 1.6, due to the interest garnered from the power systems research community as a result of the publications in this thesis , the author and supervisors of this thesis have been contacted to collaborate in the development of the next generation universal analysis tools. Table 1.2 summarises the projects that are currently planned to be spun out of this thesis. This table has also been added below for convenience.

Table 7.1: Future Research Collaborations

Project:	MATPOWER MP Element-FUBM
Lead Researcher:	Ray Zimmerman
Development of the next generation of the worldwide known tool MATPOWER. This project combines the ideas developed in the FUBM with the MPelement to create a unique and fully controllable class element to simulate all the elements of the power system for generation, transmission and distribution systems for hybrid AC/DC grids and Smart Grids. This MPelement-FUBM will require a novel formulation to solve the transmission positive sequence equations and the unbalanced distribution three phase equations will be developed in a unified approach.	
Project:	GridCal-FUBM
Lead Developer:	Santiago Peñate Vera
GridCal is an open source power systems calculation software with a well developed graphical user interface (GUI). The project aims to include the FUBM and its formulation to Gridcal. This project will be mainly developed in Python. At the end of the project a new version of the software (GridCal-FUBM) will be released.	
Project:	AIMMS-FUBM
Lead Developer:	AIMMS Optimisation Software Company
Writing a Book and designing video tutorials for the power/energy research community of advanced optimisation of AC/DC hybrid grids in AIMMS e-learning platform.	

Future Research Topics and Improvements

In addition to future collaborations, a list of improvements and possible research topics is included below.

- Improvement of the MATPOWER-FUBM: The simulation results presented by the MATPOWER-FUBM and the AIMMS-FUBM implementations, suggest that the MATPOWER implementation can improve its convergence times to match the results presented by the AIMMS implementation. As mentioned,

this limitation is due to the way MATPOWER core components are coded. A possible solution would be to avoid the recalculation of the full Y_{bus} per node and per iteration, and consider to update only the relevant values. This approach is going to be explored in form of a follow-up research proposal which the thesis author and supervisors are currently exploring.

- Implementation of the SCOPF in MATPOWER: So far MATPOWER only includes the basic DC-SCOPF which does not consider any reactive power and voltage variations for solving the SCOPF. Since the AIMMS-FUBM implementation has proven to be able to solve hybrid AC/DC SCOPF problems, implementing it to MATPOWER would be an important addition to this already powerful open source software.

- Research the Convexification of the FUBM Formulation: So far the FUBM formulation has proven to be very powerful for the optimal solution of Hybrid AC/DC grids. Nevertheless, since the convergence time for both the traditional OPF formulation and the FUBM formulation is still slightly considerable, efforts to convexify the traditional approach have been carried out. Therefore, convexification of the FUBM Formulation could be of interest.

- Research Robust Optimisation for the FUBM Formulation: In this thesis only traditional optimisation has been considered for the solution of hybrid AC/DC grids using FUBM. Future works opens a new path to solve the FUBM formulation considering robust optimisation. This approach is going to be explored in form of a follow-up research proposal which the thesis author and supervisors are currently exploring.

- Machine Learning solutions for hybrid AC/DC grids using FUBM. Artificial intelligence has been recently applied for the solution of power systems optimisation. The promising results presented by this trend make it a strong choice for the solution of hybrid AC/DC grids using FUBM. This approach is going to be explored in form of a follow-up research proposal which the thesis author and supervisors are currently exploring.

Bibliography

[1] Hong Chen. *Power Grid Operation in a Market Environment:Economic Efficiency and Risk Mitigation*. Wiley-IEEE Press, New Jersey, USA, first edition, 2017.

[2] United Nations. Report of the Conference of the Parties on its 21^{st} session. *Framework Convention on Climate Change, Conference of the Parties*, December 2015.

[3] National Grid. Future energy scenareos, system operator. *National Grid Reports*, July 2018.

[4] Menlo Energy Economics. EEnergy informer, the international energy newsletter. *EEnergy Informer*, January 2019.

[5] ENTSO-e. Ten-year network development plan (tyndp) 2020, 2020. URL https://tyndp.entsoe.eu/documents/.

[6] National Grid. Future energy scenareos, system operator. *National Grid Reports*, July 2020.

[7] Rodrigo Teixeira Pinto, Alejandro Christian Leon-Ramirez, Monica Argues-Penalba, Andreas Sumper, and Elmer Sorrentino. A fast methodology for solving power flows in hybrid AC/DC networks: The european north sea supergrid case study. In *PCIM Europe 2016*, Nuremberg, Germany, May 2016.

[8] ENTSO-e. Value of timely implementation of "better projects", May 2019. URL https://www.entsoe.eu/2019/05/20/value-of-timely-implementation-of-better-projects/.

[9] ENTSO-e. Improving hvdc system reliability, December 2018. URL https://www.entsoe.eu/2018/12/10/improving-hvdc-system-reliability/.

[10] Ettore Bompard, Gianluca Fulli, Mircea Ardelean, and Marcelo Masera. It's a bird it's a plane it's a...Supergrid!: Evolution opportunities and critical issues for Pan-European transmission. *IEEE Power and Energy Magazine*, 12(2): 40–50, February 2014.

[11] ENTSO-e. R and i roadmap 2017–2026, April 2019. URL https://www.entsoe.eu/publications/research-and-development/.

[12] Roni Irnawan. *Planning and Control of Expandable Multi-Terminal VSC-HVDC Transmission Systems*. Springer Nature, Aalborg University, Aalborg Denmark, first edition, 2019.

[13] ENTSO-e. Operational limits and conditions for frequency coupling, February 2020. URL https://www.entsoe.eu/publications/system-operations-reports/.

[14] Enrique Acha, Pedro Roncero-Sánchez, Antonio de la Villa-Jaen, Luis M. Castro, and Behzad Kazemtabrizi. *VSC-FACTS-HVDC: Analysis, Modelling and Simulation in Power Grids*. Wiley, Laboratory of Electrical Energy Engineering, Tampere University of Technology, Finland, 2019.

[15] A.J. Wood, B.F. Wollenberg, and G.B. Sheblé. *Power generation operation and control*. Wiley-IEEE Press, New Jersey, USA, third edition, 2014.

[16] Yunfeng Wen, Junpeng Zhan, C.Y. Chung, and Wenyuan Li. Frequency stability enhancement of integrated AC/VSC-MTDC systems with massive infeed of offshore wind generation. *IEEE Transactions on Power Systems*, pages 1–10, January 2018.

[17] Wang Feng, Anh Le Tuan, Lina Bertling Tjernberg, Anders Mannikoff, and Anders Bergman. A new approach for benefit evaluation of multiterminal VSC–HVDC using a proposed mixed AC/DC optimal power flow. *IEEE Transactions on Power Delivery*, pages 432–443, July 2013.

[18] Zhuo di Wang, Ke-Jun Li, Jing guo Ren, Li-Jun Sun, Jian-Guo Zhao, Yong-Liang Liang, Wei-Jen Lee, and Zhao hao Ding. A coordination control strategy of voltage-source-converter-based MTDC for offshore wind farms. *IEEE Transactions on Industry Applications*, pages 2743–2752, February 2015.

[19] Jef Beerten and Ronnie Belmans. A comprehensive modeling framework for dynamic and steady state analysis of voltage droop control strategies in HVDC grids. *International Journal of Electrical Power and Energy Systems*, 73, December 2015.

[20] Zhifang Yang, Haiwang Zhong, Anjan Bose, Qing Xia, and Chongqing Kang. Optimal power flow in ACDC grids with discrete control devices. *IEEE Transactions Power Systems*, 33, March 2018.

[21] Jizhong Zhu. *Optimization of Power System Operation*. Wiley-IEEE Press, Piscataway, NJ, USA, second edition, 2015.

[22] B. Stott, O. Alsac, and A.J. Monticelli. Security analysis and optimization. *IEEE Transactions on Power Systems*, 12(1):1623–1644, February 1987.

[23] A. Monticelli, M.V.F. Pereira, and S. Granville. Security-Constrained Optimal Power Flow with Post-contingency Corrective Rescheduling. *IEEE Transactions on Power Systems*, PWRS-2(1):175–180, February 1987.

[24] R. D. Zimmerman, C. E. Murillo-Sánchez, , and R. J. Thomas. MATPOWER: Steady-state operations, planning and analysis tools for power systems research and education. *Power Systems, IEEE Transactions on*, 26(1):12–19, February 2011.

[25] Jef Beerten and Ronnie Belmans. Development of an open source power flow software for high voltage direct current grids and hybrid ACDC systems MATACDC. *IET Generation Transmission Distribution*, 9(10):966 – 974, June 2015.

[26] SIEMENS. *PSS®E Transmission Planning and Operations Software for the*

Power Industry. SIEMENS Energy Management Division, Freyeslebenstrasse 1 91058 Erlangen, Germany, 2019.

[27] DIgSILENT. *Power Factory-Power system analysis software*. DIgSILENT, Heinrich-Hertz-Straße 9 72810 Gomaringen, Germany, 2020.

[28] Abraham Alvarez-Bustos, Behzad Kazemtabrizi, Mahmoud Shahbazi, and Enrique Acha-Daza. Universal branch model for the solution of optimal power flows in hybrid ac/dc grids. *International Journal of Electrical Power & Energy Systems*, 126:106543, 2021. doi: https://doi.org/10.1016/j.ijepes.2020.106543.

[29] T. LEVERINGHAUS, T. BREITHAUPT, S. GARSKE, and L. HOFMANN. Modelling of sequential optimal power flow by piecewise linear convexificated quadratic approximations. In *2018 International Conference on Power System Technology (POWERCON)*, pages 87–92, 2018.

[30] W. Wei, J. Wang, N. Li, and S. Mei. Optimal power flow of radial networks and its variations: A sequential convex optimization approach. *IEEE Transactions on Smart Grid*, 8(6):2974–2987, 2017.

[31] I. M. Nejdawi, K. A. Clements, and P. W. Davis. An efficient interior point method for sequential quadratic programming based optimal power flow. *IEEE Transactions on Power Systems*, 15(4):1179–1183, 2000.

[32] H. Ergun, J. Dave, D. Van Hertem, and F. Geth. Optimal power flow for ac–dc grids: Formulation, convex relaxation, linear approximation, and implementation. *IEEE Transactions on Power Systems*, 34(4):2980–2990, 2019.

[33] M. Hotz and W. Utschick. hynet: An optimal power flow framework for hybrid ac/dc power systems. *IEEE Transactions on Power Systems*, 35(2):1036–1047, 2020.

[34] J.Carpentier. Contribution a l'etude du dispaching economique. *Bulletin de la Societe Francaise des Electriciens*, 3(8):431–447, August 1962.

[35] J.A. Momoh, R.J. Koessler, M.S. Bond, B. Stott, D. Sun, A. Papalexopoulos, and P. Ristanovic. Challenges to optimal power flow. *IEEE Transactions on Power Systems*, 12(1):444–455, February 1997.

[36] A. Papalexopoulos. Challenges To On-line OPF Implementation. *IEEE Transactions on Power Systems*, 12(1):449–451, February 1997.

[37] North American Electric Reliability Corporation (NERC). Glossary of Terms. *NERC Reliability Standards*, pages 1–55, July 2017.

[38] R. Bacher. *Power system models, objectives and constraints in optimal power flow calculations*. Physica Verlag (Springer), Heidelberg, Germany, first edition, 1993.

[39] F. Capitanescu, J.L. Martinez Ramos, P. Panciatici, D. Kirschen, A. Marano Marcolini, L. Platbrood, and L. Wehenkel. State-of-the-art, challenges, and future trends in security constrained optimal power flow. *El Sevier - Electric Power Systems Research*, 81(8):1731–1741, August 2011.

[40] W.F. Tinney, J.M. Bright, K.D. Demaree, and B.A. Hughes. Some Deficiencies in Optimal Power Flow. *IEEE Transactions on Power Systems*, 3(2):676 – 683, May 1988.

[41] D. Thukaram S.A. Soman, K. Parthasarathy. Curtailed number and reduced controller movement optimization algorithms for real time voltage/reactive power control. *IEEE Transactions on Power Systems*, 9(4):2035 – 2041, November 1994.

[42] W.-H. Edwin Liu and X. Gupa. Fuzzy constraint enforcement and control action curtailment in an optimal power flow. In *IEEE Power Industry Computer Application Conference*, Salt Lake City, UT, USA, May 1995.

[43] L. Wehenkel F. Capitanescu, W. Rosehart. Optimal power flow computations with constraints limiting the number of control actions. In *Power Tech Conference*, Bucharest, Romania, June 2009.

[44] J.L. Martinez Ramos (task leader), A. Marano Marcolini, F. Capitanescu, L. Wehenkel, D. Kirschen, M. Ortega-Vazquez, P. Panciatici, S. Fliscounakis, Y. Hassaine, H. Crisciu, and L. Platbrood. Deliverable D3.1 (Part II): Description of the State of the Art in OPF and the Requirements for European Transmission Network Optimization Problems. *PEGASE Project, http://www.fp7-pegase.eu/*, 2009.

[45] O. Alsac, J. Bright, M. Prais, and B. Stott. Further developments in LP-based optimal power flow. *IEEE Transactions on Power Systems*, 5(3):697–711, October 1900.

[46] F. Capitanescua, M. Glavic, D. Ernst, and L. Wehenkel. Contingency filtering techniques for preventive security-constrained optimal power flow. *IEEE Transactions on Power Systems*, 22(4):1690–1697, October 2007.

[47] F. Capitanescu and L. Wehenkel. A new iterative approach to the corrective security-constrained optimal power flow problem. *IEEE Transactions on Power Systems*, 23(4):1533–1541, November 2008.

[48] M. Rodrigues, O.R. Saavedra, and A. Monticelli. Asynchronous programming model for the concurrent solution of the security constrained optimal power flow problem. *IEEE Transactions on Power Systems*, 9(4):2021 – 2027, November 1994.

[49] E. Liu, A.D. Papalexopoulos, and W.F. Tinney. Discrete shunt controls in a Newton optimal power flow. *IEEE Transactions on Power Systems*, 7(2): 1509–1518, November 1992.

[50] S.Y. Lin, Y.C. Ho, and C.H. Lin. An ordinal optimization theory-based algorithm for solving optimal power flow problem with discrete control variables. *IEEE Transactions on Power Systems*, 19(1):276–286, February 2004.

[51] L. Liu, X. Wang, X. Ding, and H. Chen. A robust approach to optimal power flow with discrete variables. *IEEE Transactions on Power Systems*, 24(3): 1182–1190, February 2009.

[52] F. Capitanescu and L. Wehenkel. Sensitivity-based approaches for handling discrete variables in optimal power flow computations. *IEEE Transactions on Power Systems*, 25(4):1780–1789, November 2010.

[53] A.G. Bakirtzis, P.N. Biskas, C.E. Zoumas, and V. Petridis. Optimal power flow by enhanced genetic algorithm. *IEEE Transactions on Power Systems*, 17(1):229–236, November 2002.

[54] L. Chen, H. Suzuki, and K. Katou. Mean-field theory for optimal power flow. *IEEE Transactions on Power Systems*, 12(4):1481–1486, November 1997.

[55] W. Yan, F. Liu, C.Y. Chung, and K.P. Wong. A hybrid genetic algorithm-interior point method for optimal reactive power flow. *IEEE Transactions on Power Systems*, 21(3):1163–1169, November 2006.

[56] James Jamal Thomas and Santiago Grijalva. Flexible Security-Constrained Optimal Power Flow. *IEEE Transactions on Power Systems*, 30(3):1195–1202, May 2015.

[57] Power World Corporation. *Power World electric power system analysis software*. Power World Corporation, S1st St Champaign, IL 61820, USA, 2020.

[58] Carleton Coffrin and Advanced Network Science Initiative at Los Alamos National Laboratory. PowerModels.jl: a JuliaJuMP package for Steady-State Power Network Optimization, 2020. URL https://github.com/lanl-ansi/PowerModels.jl.

[59] Santiago Penate Vera. GridCal: Research Oriented Power Systems Software, 2020. URL https://github.com/SanPen/GridCal.

[60] R. D. Zimmerman, C. E. Murillo-Sánchez, , and R. J. Thomas. MATPOWER: Steady-state operations, planning and analysis tools for power systems research and education, 2020. URL https://matpower.org/download/,https://github.com/MATPOWER/matpower.

[61] Jose Carlos Fernandez Perez, Francisco M. Echavarren, and Luis Rouco. On the convergence of the sequential power flow for multiterminal VSC AC/DC systems. *IEEE Transactions on Power Systems*, PP(99):1–8, June 2017.

[62] Runze Chai, Baohui Zhang, Jingming Dou, Zhiguo Hao, and Tao Zheng. Unified power flow algorithm based on the NR method for hybrid AC/DC grids incorporating VSCs. *IEEE Transactions on Power Systems*, 31(6):4310 – 4318, November 2016.

[63] Jef Beerten, Stijn Cole, and Ronnie Belmans. Generalized steady-state VSC MTDC model for sequential AC/DC power flow algorithms. *IEEE Transactions on Power Systems*, 27(2):821–829, May 2012.

[64] M. Baradar, M. Ghandhari, and D. Van Hertem. The modeling multi-terminal vsc-hvdc in power flow calculation using unified methodology. In *2011 2nd IEEE PES International Conference and Exhibition on Innovative Smart Grid Technologies*, pages 1–6, 2011. doi: 10.1109/ISGTEurope.2011.6162666.

[65] Jingting Lei, Ting An, Zhengchun Du, and Zheng Yuan. A general unified AC/DC power flow algorithm with MTDC. *IEEE Transactions on Power Systems*, 32(4):2837 – 2846, July 2017.

[66] P. E. Wiernes, J. Priebe, S. Pleines, and A. Moser. Performance comparision of integrated ac/dc power flow calculation methodologies. In *2016 IEEE International Energy Conference (ENERGYCON)*, pages 1–6, 2016. doi: 10.1109/ENERGYCON.2016.7514053.

[67] Norris M. Peterson and W. Scott Meyer. Automatic adjustment of transformer and phase-shifter taps in the Newton power flow. *IEEE Transactions on Power Apparatus and Systems*, 90(1):103–108, January 1971.

[68] William. F. Tinney, , and Clifford E. Hart. Power flow solution by Newton's method. *IEEE Transactions on Power Apparatus and Systems*, 86(11):1449–1460, November 1967.

[69] Enrique Acha, Behzad Kazemtabrizi, and Luis M. Castro. A new VSC-HVDC model for power flows using the Newton-Raphson method. *IEEE Transactions on Power Systems*, 28(3):2602–2612, August 2013.

[70] O. Alsac and B. Stott. Optimal Load Flow with Steady-State Security. *IEEE Transactions on Power Systems*, (1):745–751, February 1974.

[71] Narayan S. Rau. *Optimization Principles:Practical Applications to the Operation and Markets of the Electric Power Industry*. Wiley-IEEE Press, Piscataway, NJ, USA, first edition, 2003.

[72] Dimitri P. Bertsekas. *Constrained Optimization and Lagrange Multiplier Methods*. Athena Scientific, Belmont, Massachusetts, USA, first edition, 1996.

[73] Morgridge Institute for Research MIR. Neos guide, 2017. URL https://neos-guide.org/terms-of-use.

[74] Robert J. Thomas, Carlos E. Murillo-Sanchez, and Ray D. Zimmerman. An advanced security constrained OPF that produces correct market based pricing. In *Power and Energy Society General Meeting Conversion and Delivery of Electrical Energy in the 21st Century*, Detroit, MI, USA, July 2008.

[75] Luenberger DG. *Introduction to Linear and Nonlinear Programming*. Addison-wesley, New York, USA, first edition, 1973.

[76] Kennedy J and Eberhart R. Particle swarm optimization. In *IEEE International Conference*, Perth, Australia, June 1995.

[77] Rainer Bacher Hans Glavitsch. *Control and Dynamic Systems - Optimal Power Flow Algorithms*. Academic Press, Swiss Federal Institute of Technology, first edition, 1991.

[78] Bruxe A. Murtagh and Michael A. Saunders. *MINOS 5.5 user guide*. Systems Optimisation Laboratory Department of Operations Research Stanford University, Stanford University, California, USA, first edition, 1993.

[79] Chunjie Li, Huiru Zhao, and Tao Chen. The Hybrid Differential Evolution Algorithm for Optimal Power Flow Based on Simulated Annealing and Tabu Search. In *Management and Service Science (MASS), 2010 International Conference on*, Wuhan, China, August 2010.

[80] Marcel Roelofs and Johannes Bisschop. *AIMMS, The user's guide*. AIMMS Inc., Haarlem, The Netherlands, third edition, 2020.

[81] Marcel Roelofs and Johannes Bisschop. *AIMMS, The Functions Reference*. AIMMS Inc., Haarlem, The Netherlands, second edition, 2020.

[82] Arne Drud and ARKI Consulting Development. Conopt a solver for large scale nonlinear optimization, 2020. URL http://www.conopt.com.

[83] The General Algebraic Modelling System GAMS. Conopt for gams, 2020. URL https://www.gams.com/latest/docs/S-CONOPT.html.

[84] Richard H. Byrd, Jorge Nocedal, and Richard A. Waltz. *Knitro: An Integrated Package for Nonlinear Optimization*. Springer US, Boston, MA, 2006.

[85] Artelys. Knitro algorithms, 2020. URL https://www.artelys.com/docs/knitro/2-userGuide/algorithms.html.

[86] A. J. Wathen. *Preconditioning*. Mathematical Institute, University of Oxford, Woodstock Road, Oxford, UK, 2020.

[87] A. Wächter. *An Interior Point Algorithm for Large-Scale Nonlinear Optimization with Applications in Process Engineering, PhD Thesis*. Carnegie Mellon University, Pittsburgh, PA, USA, 2002.

[88] C. J. Ferrandon Cervantes, B. Kazemtabrizi, and M. C. M. Troffaes. Contingency ranking in power systems via reliability rates. In *2018 IEEE International Conference on Environment and Electrical Engineering and 2018 IEEE Industrial and Commercial Power Systems Europe (EEEIC / I CPS Europe)*, pages 1–6, 2018. doi: 10.1109/EEEIC.2018.8493853.

[89] Ebrahim Vaahedi. *Practical Power System Operation*. IEEE Press-Wiley, 2014.

[90] W. S. Tan and M. Shaaban. Ranking of power system contingencies based on a risk quantification criterion. In *2015 IEEE Student Conference on Research and Development (SCOReD)*, pages 356–361, Dec 2015. doi: 10.1109/SCORED.2015.7449355.

[91] J. McCalley, S. Asgarpoor, L. Bertling, R. Billinton, H. Chao, J. Chen, J. Endrenyi, R. Fletcher, A. Ford, C. Grigg, G. Hamoud, D. Logan, A. P. Meliopoulos, M. Ni, N. Rau, L. Salvaderi, M. Schilling, Y. Schlumberger, A. Schneider, and C. Singh. Probabilistic security assessment for power system operations. In *IEEE Power Engineering Society General Meeting, 2004.*, pages 212–220 Vol.1, June 2004. doi: 10.1109/PES.2004.1372788.

[92] Wenyuan Li. *Risk Assessment of Power Systems*. IEEE Press-Wiley, 2014.

[93] Sakis Meliopoulos, David Taylor, Chanan Singh, Fang Yang, Sun Wook Kang, and George Stefopoulos. *Comprehensive Power System Reliability Assessment Final Project report*. Power Systems Engineering Research Center, 2005.

[94] Roy Billinton and Ronald N. Allan. *Reliability Evaluation of Engineering Systems*. Springer, 1992.

[95] International Electrotechnical Commission (IEC). IEC 62751-2 Power losses in voltage sourced converter (VSC) valves for high-voltage direct current (HVDC) systems - Part 2 Modular multilevel converters. *IEC International Standard*, August 2014.

[96] S.G. Johansson, G. Asplund, E. Jansson, and R. Rudervall. Power system stability benefits with VSC DC-transmission systems. In *in Proc. CIGRE 2004 Session*, Paris, France, 2004.

[97] W. Feng, L. A. Tuan, L. B. Tjernberg, A. Mannikoff, and A. Bergman. A new approach for benefit evaluation of multiterminal vsc–hvdc using a proposed

mixed ac/dc optimal power flow. *IEEE Transactions on Power Delivery*, 29 (1):432–443, 2014.

[98] Behzad Kazemtabrizi and Enrique Acha. An advanced STATCOM model for optimal power flows using Newton's method. *IEEE Transactions on Power Systems*, 29, March 2014.

[99] L. Gyugyi, C. D. Schauder, S. L. Williams, T. R. Rietman, D. R. Torgerson, and A. Edris. The unified power flow controller: a new approach to power transmission control. *IEEE Transactions on Power Delivery*, 10(2):1085–1097, 1995.

[100] L. Liu, P. Zhu, Y. Kang, and J. Chen. Power-flow control performance analysis of a unified power-flow controller in a novel control scheme. *IEEE Transactions on Power Delivery*, 22(3):1613–1619, 2007.

[101] D. Jovcic. Bidirectional, high-power dc transformer. *IEEE Transactions on Power Delivery*, 24(4):2276–2283, 2009.

[102] Til Kristian Vranaa, Jef Beertenb, Ronnie Belmans, and Olav Bjarte Fosso. A classification of DC node voltage control methods for HVDC grids. *Electric Power Systems Research*, pages 137–144, October 2013.

[103] Abraham Alvarez-Bustos, Behzad Kazemtabrizi, and Mahmoud Shahbazi. Flexible general branch model unified power flow algorithm for future flexible AC/DC networks. In *2018 IEEE International Conference on Environment and Electrical Engineering (EEEIC / I&CPS Europe)*, Palermo, Italy, June 2018.

[104] Abraham Alvarez-Bustos, Behzad Kazemtabrizi, and Mahmoud Shahbazi. MATPOWER-FUBM: Steady-state operations, planning and analysis tools for AC/DC power systems research and education, 2020. URL https://github.com/AbrahamAlvarezB/matpower-fubm.

[105] Zhicheng Li, Jinghan He, Yin Xu, and Xiaojun Wang. An optimal power flow algorithm for AC/DC hybrid power systems with VSC-Based MTDC

considering converter power losses and voltage-droop control strategy. *IEEJ Transactions on electrical and electronic engineering*, June 2018.

[106] S. Fliscounakis, P. Panciatici, F. Capitanescu, and L. Wehenkel. Contingency ranking with respect to overloads in very large power systems taking into account uncertainty, preventive and corrective actions. *IEEE Transactions Power Systems*, 28, November 2013.

[107] C. Josz, S. Fliscounakis, J. Maeght, and P. Panciatici. Ac power flow data in matpower and qcqp format: itesla, rte snapshots, and pegase, 2013. URL https://arxiv.org/abs/1603.01533.

[108] National Grid Electricity System Operator. The Grid Code. *National Grid Documents*, 5, June 2020.

[109] JavierRenedo, Ahmad A. Ibrahim, Behzad Kazemtabrizi, Aurelio García-Cerrada, Luis Rouco, Quanyu Zhao, and Javier García-González. A simplified algorithm to solve optimal power flows in hybrid VSC-based ACDC systems. *International Journal of Electrical Power and Energy Systems - El Sevier*, 110, 2019.

[110] Q. Zhao, J. Garcia-Gonzalez, O. Gomis-Bellmunt, E. Prieto-Araujo, and F. M. Echavarren. Impact of converter losses on the optimal power flow solution of hybrid networks based on VSC-MTDC. *Electric Power Systems Research*, 151: 395–403, 2017.

[111] Glenn W. Stagg and Ahmed H. El-Abiad. *Computer Methods in Power System Analysis*. McGraw-Hill, New York, 9th edition, 1971.

[112] C. Coffrin, R. Bent, K. Sundar, Y. Ng, and M. Lubin. Powermodels.jl: An open-source framework for exploring power flow formulations. *in Proc. Power Syst. Comput. Conf.*, 20, 2018.

[113] I. Dunning, J. Huchette, , and M. Lubin. Jump: A modeling language for mathematical optimization. *SIAM Rev.*, 59(2):295–320, 2017.

[114] R. D. Zimmerman and C. E. Murillo-Sanchez. Matpower software version 7.0, 2020. URL https://matpower.org.

[115] J. Beerten, D. Van Hertem, and R. Belmans. Vsc mtdc systems with a distributed dc voltage control - a power flow approach. In *2011 IEEE Trondheim PowerTech*, pages 1–6, 2011.

[116] J. Rimez and R. Belmans. A combined ac/dc optimal power flow algorithm for meshed ac and dc networks linked by vsc converters. *Int. Trans. Elect. Energy Syst*, 25(10):2024–2035, 2015.

[117] C. Barrows, A. Bloom, A. Ehlen, J. Ikäheimo, J. Jorgenson, D. Krishnamurthy, J. Lau, B. McBennett, M. O'Connell, E. Preston, A. Staid, G. Stephen, and J. Watson. The ieee reliability test system: A proposed 2019 update. *IEEE Transactions on Power Systems*, 35(1):119–127, 2020. doi: 10.1109/TPWRS.2019.2925557.

[118] S. Boyd and L. Vandenberghe. *Convex Optimization*. Cambridge University Press, University Printing House, Cambridge, UK, 2004.

Appendix A

Barrier Method

Before describing the optimisation methods this subsection will describe a widely used method to transform inequality constraints into equality constraints by using a log barrier function. Even though not all optimisation methods transform the inequality constraints into equality constraints, some of they do, and this subsection is added for the sake of completeness.

Consider the optimisation problem in (A.0.1),

$$\begin{aligned} min \quad & f(\mathbf{x}) \\ \text{subject to} \quad & \mathbf{h}(\mathbf{x}) \leq \mathbf{0} \\ & \mathbf{A}\mathbf{x} = \mathbf{b} \end{aligned} \tag{A.0.1}$$

Where f and $\mathbf{h}$ are both twice differentiable convex functions, and it is assumed that the problem is solvable (an optimal $\mathbf{x}^*$ exists), and also it is strictly feasible (there is an $\mathbf{x}$ that satisfies all the constraints). Then, by re-writing the problem in (A.0.1) to implicitly include the $\mathbf{h}$ inequality constraints into the objective function, then the problem can be re-written as in (A.0.5).

$$\begin{aligned} min \quad & f(\mathbf{x}) + \sum_{i=0}^{ni} D\left(h_i(\mathbf{x})\right) \\ \text{subject to} \quad & \mathbf{A}\mathbf{x} = \mathbf{b}, \end{aligned} \tag{A.0.2}$$

Where D is a function to indicate the non-positive reals as in (A.0.3).

$$D(w) = \begin{cases} 0 & w \leq 0 \\ \infty & w \geq 0 \end{cases} \tag{A.0.3}$$

The problem in (A.0.5) has no inequality constraints. However, the new objective function to minimise cannot be differentiable, therefore some optimisation methods cannot be applied. To solve this problem the "Logarithmic barrier method" is used. The main idea is to approximate the indicator function D as shown in (A.0.4).

$$\hat{D}(w) = -(1/\zeta)log(-w), \quad \mathbf{dom}\hat{D} = -\mathbb{R}_{++}, \tag{A.0.4}$$

The new function $\hat{D}(w)$ is differentiable, and in (A.0.4), the parameter ζ will set the accuracy of the approximation. Figure A.1 shows the original D function as well as the approximation function $\hat{D}$ for different values of ζ.

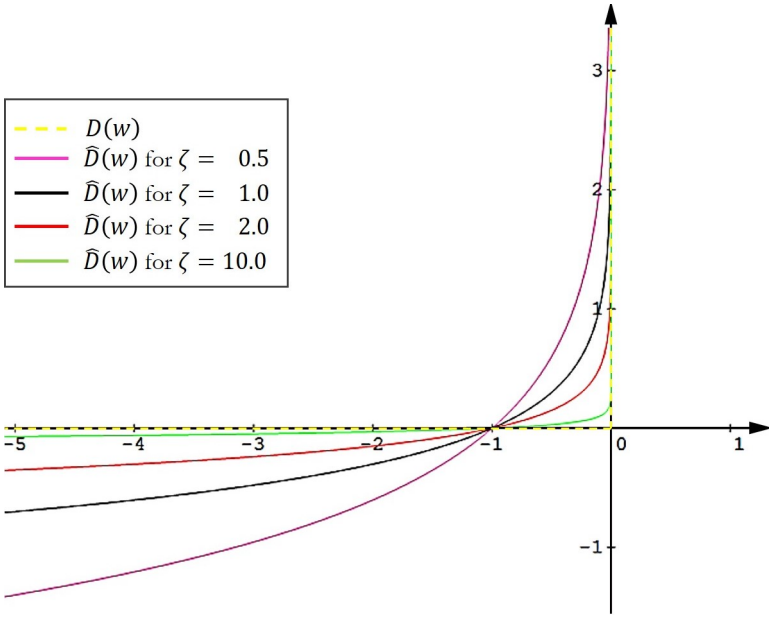

Figure A.1: Indicator D and approximation $\hat{D}$ functions for different values of ζ

Substituting $\hat{D}$ for D in (A.0.5) the approximation to the problem is a convex problem of the form:

$$\begin{aligned} min \qquad & f(\mathbf{x}) + \sum_{i=0}^{ni} -(1/\zeta)\, log\left(-h_i(\mathbf{x})\right) \\ \text{subject to} \qquad & \mathbf{Ax} = \mathbf{b}, \end{aligned} \tag{A.0.5}$$

Therefore the *logarithmic barrier* function for the problem in (A.0.1) is defined as in (A.0.6).

$$\phi(\mathbf{x}) = -\sum_{i=0}^{ni} log\left(-h_i(\mathbf{x})\right)) \tag{A.0.6}$$

$$\text{with, } \mathbf{dom}\phi = \{\mathbf{x} \in \mathbb{R}^n | h_i(\mathbf{x}) < \mathbf{0}, \quad \mathbf{i} = \mathbf{1}, \ldots, \mathbf{ni}\} \tag{A.0.7}$$

The function domain is the set of points that satisfy the inequality constraints of the original problem. The quality of the approximation improves as the parameter ζ grows. A common practice is to increase the value of ζ at each step [118].

Appendix B

Detailed Equations

B.1 FUBM Branch Power Flow in Real and Imaginary Parts

From the Euler representation of the voltage in (B.1.1),

$$V = V_m e^{jV_a} \tag{B.1.1}$$

and substituting (B.1.1) in (3.1.14):

$$\begin{aligned} S_f &= [v_{m_f} e^{jv_{a_f}}][y_{ff} v_{m_f} e^{jv_{a_f}} + y_{ft} v_{m_t} e^{jv_{a_t}}]^* \\ S_t &= [v_{m_t} e^{jv_{a_t}}][y_{ft} v_{m_f} e^{jv_{a_f}} + y_{tt} v_{m_t} e^{jv_{a_t}}]^* \end{aligned} \tag{B.1.2}$$

or

$$\begin{aligned} S_f &= [v_{m_f} e^{jv_{a_f}}][y^*_{ff} v_{m_f} e^{-jv_{a_f}} + y^*_{ft} v_{m_t} e^{-jv_{a_t}}] \\ S_t &= [v_{m_t} e^{jv_{a_t}}][y^*_{ft} v_{m_f} e^{-jv_{a_f}} + y^*_{tt} v_{m_t} e^{-jv_{a_t}}] \end{aligned} \tag{B.1.3}$$

and simplifying:

$$\begin{aligned} S_f &= y^*_{ff} v^2_{m_f} + y^*_{ft} v_{m_f} v_{m_t} e^{j\left(v_{a_f} - v_{a_t}\right)} \\ S_t &= y^*_{tt} v^2_{m_t} + y^*_{tf} v_{m_t} v_{m_f} e^{j\left(v_{a_t} - v_{a_f}\right)} \end{aligned} \tag{B.1.4}$$

Now, using Euler's identity,

$$\begin{aligned} S_f &= y_{ff}^* v_{m_f}^2 + y_{ft}^* v_{m_f} v_{m_t} \left(\cos\left(v_{a_f} - v_{a_t}\right) + j \sin\left(v_{a_f} - v_{a_t}\right)\right) \\ S_t &= y_{tt}^* v_{m_t}^2 + y_{tf}^* v_{m_t} v_{m_f} \left(\cos\left(v_{a_t} - v_{a_f}\right) + j \sin\left(v_{a_t} - v_{a_f}\right)\right) \end{aligned} \tag{B.1.5}$$

and simplifying

$$\begin{aligned} S_f &= y_{ff}^* v_{m_f}^2 + y_{ft}^* v_{m_f} v_{m_t} \cos\left(v_{a_f} - v_{a_t}\right) + j y_{ft}^* v_{m_f} v_{m_t} \sin\left(v_{a_f} - v_{a_t}\right) \\ S_t &= y_{tt}^* v_{m_t}^2 + y_{tf}^* v_{m_t} v_{m_f} \cos\left(v_{a_t} - v_{a_f}\right) + j y_{tf}^* v_{m_t} v_{m_f} \sin\left(v_{a_t} - v_{a_f}\right) \end{aligned} \tag{B.1.6}$$

Considering $R_{y_{ff}}$, $R_{y_{ft}}$, $R_{y_{tf}}$, $R_{y_{tt}}$ and $I_{y_{ff}}$, $I_{y_{ft}}$, $I_{y_{tf}}$, $I_{y_{tt}}$ the real and imaginary part of y_{ff}, y_{ft}, y_{tf}, y_{tt} respectively, then:

$$\begin{aligned} S_f = &\left(R_{y_{ff}} - jI_{y_{ff}}\right) v_{m_f}^2 + \\ &\left(R_{y_{ft}} - jI_{y_{ft}}\right) v_{m_f} v_{m_t} \cos\left(v_{a_f} - v_{a_t}\right) + \\ &j\left(R_{y_{ft}} - jI_{y_{ft}}\right) v_{m_f} v_{m_t} \sin\left(v_{a_f} - v_{a_t}\right) \end{aligned} \tag{B.1.7}$$

$$\begin{aligned} S_t = &\left(R_{y_{tt}} - jI_{y_{tt}}\right) v_{m_t}^2 + \\ &\left(R_{y_{tf}} - jI_{y_{tf}}\right) v_{m_t} v_{m_f} \cos\left(v_{a_t} - v_{a_f}\right) + \\ &j\left(R_{y_{tf}} - jI_{y_{tf}}\right) v_{m_t} v_{m_f} \sin\left(v_{a_t} - v_{a_f}\right) \end{aligned} \tag{B.1.8}$$

then expanding them both,

$$\begin{aligned} S_f = &\left(R_{y_{ff}} v_{m_f}^2 - jI_{y_{ff}} v_{m_f}^2\right) + \\ &\left(R_{y_{ft}} v_{m_f} v_{m_t} \cos\left(v_{a_f} - v_{a_t}\right) - jI_{y_{ft}} v_{m_f} v_{m_t} \cos\left(v_{a_f} - v_{a_t}\right)\right) + \\ &j\left(R_{y_{ft}} v_{m_f} v_{m_t} \sin\left(v_{a_f} - v_{a_t}\right) - jI_{y_{ft}} v_{m_f} v_{m_t} \sin\left(v_{a_f} - v_{a_t}\right)\right) \end{aligned} \tag{B.1.9}$$

$$\begin{aligned} S_t = &\left(R_{y_{tt}} v_{m_t}^2 - jI_{y_{tt}} v_{m_t}^2\right) + \\ &\left(R_{y_{tf}} v_{m_t} v_{m_f} \cos\left(v_{a_t} - v_{a_f}\right) - jI_{y_{tf}} v_{m_t} v_{m_f} \cos\left(v_{a_t} - v_{a_f}\right)\right) + \\ &j\left(R_{y_{tf}} v_{m_t} v_{m_f} \sin\left(v_{a_t} - v_{a_f}\right) - jI_{y_{tf}} v_{m_t} v_{m_f} \sin\left(v_{a_t} - v_{a_f}\right)\right) \end{aligned} \tag{B.1.10}$$

and reorganising,

$$\begin{aligned} S_f =& R_{y_{ff}} v_{m_f}^2 - jI_{y_{ff}} v_{m_f}^2 + \\ & R_{y_{ft}} v_{m_f} v_{m_t} \cos\left(v_{a_f} - v_{a_t}\right) - jI_{y_{ft}} v_{m_f} v_{m_t} \cos\left(v_{a_f} - v_{a_t}\right) + \\ & jR_{y_{ft}} v_{m_f} v_{m_t} \sin\left(v_{a_f} - v_{a_t}\right) + I_{y_{ft}} v_{m_f} v_{m_t} \sin\left(v_{a_f} - v_{a_t}\right) \end{aligned} \tag{B.1.11}$$

$$\begin{aligned} S_t =& R_{y_{tt}} v_{m_t}^2 - jI_{y_{tt}} v_{m_t}^2 + \\ & R_{y_{tf}} v_{m_t} v_{m_f} \cos\left(v_{a_t} - v_{a_f}\right) - jI_{y_{tf}} v_{m_t} v_{m_f} \cos\left(v_{a_t} - v_{a_f}\right) + \\ & jR_{y_{tf}} v_{m_t} v_{m_f} \sin\left(v_{a_t} - v_{a_f}\right) + I_{y_{tf}} v_{m_t} v_{m_f} \sin\left(v_{a_t} - v_{a_f}\right) \end{aligned} \tag{B.1.12}$$

and finally, since $S = P + jQ$ by grouping the Real and Imaginary parts of (B.1.11) and (B.1.12), the P_f, P_t, Q_f, and Q_t are obtained

$$\begin{aligned} P_f =& R_{y_{ff}} v_{m_f}^2 + \\ & R_{y_{ft}} v_{m_f} v_{m_t} \cos\left(v_{a_f} - v_{a_t}\right) + \\ & I_{y_{ft}} v_{m_f} v_{m_t} \sin\left(v_{a_f} - v_{a_t}\right) \end{aligned} \tag{B.1.13}$$

$$\begin{aligned} P_t =& R_{y_{tt}} v_{m_t}^2 + \\ & R_{y_{tf}} v_{m_t} v_{m_f} \cos\left(v_{a_t} - v_{a_f}\right) + \\ & I_{y_{tf}} v_{m_t} v_{m_f} \sin\left(v_{a_t} - v_{a_f}\right) \end{aligned} \tag{B.1.14}$$

$$\begin{aligned} Q_f =& I_{y_{ff}} v_{m_f}^2 + \\ & - I_{y_{ft}} v_{m_f} v_{m_t} \cos\left(v_{a_f} - v_{a_t}\right) + \\ & R_{y_{ft}} v_{m_f} v_{m_t} \sin\left(v_{a_f} - v_{a_t}\right) \end{aligned} \tag{B.1.15}$$

$$\begin{aligned} Q_t =& - I_{y_{tt}} v_{m_t}^2 + \\ & - I_{y_{tf}} v_{m_t} v_{m_f} \cos\left(v_{a_t} - v_{a_f}\right) + \\ & R_{y_{tf}} v_{m_t} v_{m_f} \sin\left(v_{a_t} - v_{a_f}\right) \end{aligned} \tag{B.1.16}$$

Appendix C

FUBM Equations and Derivatives

C.1 Useful Equations and Derivatives

C.1.1 Optimisation Variables

$$X = \begin{bmatrix} V_a & V_m & P_g & Q_g & B_{eq} & \theta_{sh} & m_a & G_{sw} \end{bmatrix}^\top \tag{C.1.1}$$

C.1.2 Voltage Equations

$$V = V_m e^{jV_a} \tag{C.1.2}$$

Voltage First Derivatives

$$\frac{\partial V}{\partial V_a} = j\left[V_m e^{jV_a}\right] = j[V] \tag{C.1.3}$$

$$\frac{\partial V}{\partial V_m} = \left[1 e^{jV_a}\right] \tag{C.1.4}$$

Voltage Second Derivatives

$$\frac{\partial^2 V}{\partial^2 V_a} = -\left[V_m e^{jV_a}\right] = -[V] \tag{C.1.5}$$

$$\frac{\partial^2 V}{\partial V_m \partial V_a} = \left[j e^{jV_a}\right] \tag{C.1.6}$$

$$\frac{\partial^2 V}{\partial V_a \partial V_m} = \frac{\partial^2 V}{\partial V_m \partial V_a}^\top \tag{C.1.7}$$

$$\frac{\partial V^2}{\partial^2 V_m} = \left[0\right] \tag{C.1.8}$$

C.1.3 Admittance Equations

$$\begin{bmatrix} i_f \\ i_t \end{bmatrix} = \begin{bmatrix} Y_{ff} & Y_{ft} \\ Y_{tf} & Y_{tt} \end{bmatrix} \begin{bmatrix} v_f \\ v_t \end{bmatrix} = \begin{bmatrix} Y_{br} \end{bmatrix} \begin{bmatrix} v_f \\ v_t \end{bmatrix} \tag{C.1.9}$$

$$Y_{br} = \begin{bmatrix} G_{sw} + (y_s + j\frac{b_c}{2} + jB_{eq})\frac{1}{{m'_a}^2} & \frac{-y_s}{m'_a e^{-j\theta_{\text{sh}}}} \\ \frac{-y_s}{m'_a e^{j\theta_{\text{sh}}}} & y_s + j\frac{b_c}{2} \end{bmatrix} \tag{C.1.10}$$

$$Y_f = [Y_{ff}]C_f + [Y_{ft}]C_t \tag{C.1.11}$$

$$Y_t = [Y_{tf}]C_f + [Y_{tt}]C_t \tag{C.1.12}$$

$$Y_{bus} = C_f^\top Y_f + C_t^\top Y_t + [Y_{sh}] \tag{C.1.13}$$

Admittance First Derivatives

$$\frac{\partial Y_{bus}}{\partial B_{eq}} = C_f^\top \frac{\partial Y_f}{\partial B_{eq}} + C_t^\top \frac{\partial Y_t}{\partial B_{eq}} \tag{C.1.14}$$

$$\frac{\partial Y_{bus}}{\partial \theta_{sh}} = C_f^\top \frac{\partial Y_f}{\partial \theta_{sh}} + C_t^\top \frac{\partial Y_t}{\partial \theta_{sh}} \tag{C.1.15}$$

$$\frac{\partial Y_{bus}}{\partial m_a} = C_f^\top \frac{\partial Y_f}{\partial m_a} + C_t^\top \frac{\partial Y_t}{\partial m_a} \tag{C.1.16}$$

$$\frac{\partial Y_{bus}}{\partial G_{sw}} = C_f^\top \frac{\partial Y_f}{\partial G_{sw}} + C_t^\top \frac{\partial Y_t}{\partial G_{sw}} \tag{C.1.17}$$

$$\frac{\partial Y_f}{\partial B_{eq}} = \left[\frac{\partial Y_{ff}}{\partial B_{eq}}\right] C_f + \left[\frac{\partial Y_{ft}}{\partial B_{eq}}\right] C_t \tag{C.1.18}$$

$$\frac{\partial Y_f}{\partial \theta_{sh}} = \left[\frac{\partial Y_{ff}}{\partial \theta_{sh}}\right] C_f + \left[\frac{\partial Y_{ft}}{\partial \theta_{sh}}\right] C_t \tag{C.1.19}$$

$$\frac{\partial Y_f}{\partial m_a} = \left[\frac{\partial Y_{ff}}{\partial m_a}\right] C_f + \left[\frac{\partial Y_{ft}}{\partial m_a}\right] C_t \tag{C.1.20}$$

$$\frac{\partial Y_f}{\partial G_{sw}} = \left[\frac{\partial Y_{ff}}{\partial G_{sw}}\right] C_f + \left[\frac{\partial Y_{ft}}{\partial G_{sw}}\right] C_t \tag{C.1.21}$$

$$\frac{\partial Y_t}{\partial B_{eq}} = \left[\frac{\partial Y_{tf}}{\partial B_{eq}}\right] C_f + \left[\frac{\partial Y_{tt}}{\partial B_{eq}}\right] C_t \tag{C.1.22}$$

$$\frac{\partial Y_t}{\partial \theta_{sh}} = \left[\frac{\partial Y_{tf}}{\partial \theta_{sh}}\right] C_f + \left[\frac{\partial Y_{tt}}{\partial \theta_{sh}}\right] C_t \tag{C.1.23}$$

$$\frac{\partial Y_t}{\partial m_a} = \left[\frac{\partial Y_{tf}}{\partial m_a}\right] C_f + \left[\frac{\partial Y_{tt}}{\partial m_a}\right] C_t \tag{C.1.24}$$

$$\frac{\partial Y_t}{\partial G_{sw}} = \left[\frac{\partial Y_{tf}}{\partial G_{sw}}\right] C_f + \left[\frac{\partial Y_{tt}}{\partial G_{sw}}\right] C_t \tag{C.1.25}$$

$$\frac{\partial Y_{ff}}{\partial B_{eq}} = \frac{j}{\left(k_2 m_a\right)^2} \tag{C.1.26}$$

$$\frac{\partial Y_{ft}}{\partial B_{eq}} = 0 \tag{C.1.27}$$

$$\frac{\partial Y_{tf}}{\partial B_{eq}} = 0 \tag{C.1.28}$$

$$\frac{\partial Y_{tt}}{\partial B_{eq}} = 0 \tag{C.1.29}$$

$$\frac{\partial Y_{ff}}{\partial \theta_{sh}} = 0 \tag{C.1.30}$$

$$\frac{\partial Y_{ft}}{\partial \theta_{sh}} = \frac{-j y_s}{k_2 m_a e^{-j\theta_{sh}}} \tag{C.1.31}$$

$$\frac{\partial Y_{tf}}{\partial \theta_{sh}} = \frac{j y_s}{k_2 m_a e^{j\theta_{sh}}} \tag{C.1.32}$$

$$\frac{\partial Y_{tt}}{\partial \theta_{sh}} = 0 \tag{C.1.33}$$

$$\frac{\partial Y_{ff}}{\partial m_a} = \frac{-2\left(y_s + j\frac{b_c}{2} + jB_{eq}\right)}{k_2^2 m_a^3} \tag{C.1.34}$$

$$\frac{\partial Y_{ft}}{\partial m_a} = \frac{y_s}{k_2 m_a^2 e^{-j\theta_{sh}}} \tag{C.1.35}$$

$$\frac{\partial Y_{tf}}{\partial m_a} = \frac{y_s}{k_2 m_a^2 e^{j\theta_{sh}}} \tag{C.1.36}$$

$$\frac{\partial Y_{tt}}{\partial m_a} = 0 \tag{C.1.37}$$

$$\frac{\partial Y_{ff}}{\partial G_{sw}} = 1 \tag{C.1.38}$$

$$\frac{\partial Y_{ft}}{\partial G_{sw}} = 0 \tag{C.1.39}$$

$$\frac{\partial Y_{tf}}{\partial G_{sw}} = 0 \tag{C.1.40}$$

$$\frac{\partial Y_{tt}}{\partial G_{sw}} = 0 \tag{C.1.41}$$

Admittance Second Derivatives

$$\frac{\partial^2 Y_{bus}}{\partial B_{eq} \partial \theta_{sh}} = C_f^\top \frac{\partial^2 Y_f}{\partial B_{eq} \partial \theta_{sh}} + C_t^\top \frac{\partial^2 Y_t}{\partial B_{eq} \partial \theta_{sh}} \tag{C.1.42}$$

$$\frac{\partial^2 Y_{bus}}{\partial B_{eq} \partial m_a} = C_f^\top \frac{\partial^2 Y_f}{\partial B_{eq} \partial m_a} + C_t^\top \frac{\partial^2 Y_t}{\partial B_{eq} \partial m_a} \tag{C.1.43}$$

$$\frac{\partial^2 Y_{bus}}{\partial^2 B_{eq}} = C_f^\top \frac{\partial^2 Y_f}{\partial^2 B_{eq}} + C_t^\top \frac{\partial^2 Y_t}{\partial^2 B_{eq}} \tag{C.1.44}$$

$$\frac{\partial^2 Y_{bus}}{\partial B_{eq} \partial m_a} = C_f^\top \frac{\partial^2 Y_f}{\partial B_{eq} \partial G_{sw}} + C_t^\top \frac{\partial^2 Y_t}{\partial B_{eq} \partial G_{sw}} \tag{C.1.45}$$

$$\frac{\partial^2 Y_f}{\partial B_{eq} \partial \theta_{sh}} = \left[\frac{\partial^2 Y_{ff}}{\partial B_{eq} \partial \theta_{sh}}\right] C_f + \left[\frac{\partial^2 Y_{ft}}{\partial B_{eq} \partial \theta_{sh}}\right] C_t \tag{C.1.46}$$

$$\frac{\partial^2 Y_f}{\partial B_{eq} \partial m_a} = \left[\frac{\partial^2 Y_{ff}}{\partial B_{eq} \partial m_a}\right] C_f + \left[\frac{\partial^2 Y_{ft}}{\partial B_{eq} \partial m_a}\right] C_t \tag{C.1.47}$$

$$\frac{\partial^2 Y_f}{\partial^2 B_{eq}} = \left[\frac{\partial^2 Y_{ff}}{\partial^2 B_{eq}}\right] C_f + \left[\frac{\partial^2 Y_{ft}}{\partial^2 B_{eq}}\right] C_t \tag{C.1.48}$$

$$\frac{\partial^2 Y_f}{\partial B_{eq}\partial G_{sw}} = \left[\frac{\partial^2 Y_{ff}}{\partial B_{eq}\partial G_{sw}}\right] C_f + \left[\frac{\partial^2 Y_{ft}}{\partial B_{eq}\partial G_{sw}}\right] C_t \tag{C.1.49}$$

$$\frac{\partial^2 Y_t}{\partial B_{eq}\partial \theta_{sh}} = \left[\frac{\partial^2 Y_{tf}}{\partial B_{eq}\partial \theta_{sh}}\right] C_f + \left[\frac{\partial^2 Y_{tt}}{\partial B_{eq}\partial \theta_{sh}}\right] C_t \tag{C.1.50}$$

$$\frac{\partial^2 Y_t}{\partial B_{eq}\partial m_a} = \left[\frac{\partial^2 Y_{tf}}{\partial B_{eq}\partial m_a}\right] C_f + \left[\frac{\partial^2 Y_{tt}}{\partial B_{eq}\partial m_a}\right] C_t \tag{C.1.51}$$

$$\frac{\partial^2 Y_t}{\partial^2 B_{eq}} = \left[\frac{\partial^2 Y_{tf}}{\partial^2 B_{eq}}\right] C_f + \left[\frac{\partial^2 Y_{tt}}{\partial^2 B_{eq}}\right] C_t \tag{C.1.52}$$

$$\frac{\partial^2 Y_t}{\partial B_{eq}\partial G_{sw}} = \left[\frac{\partial^2 Y_{tf}}{\partial B_{eq}\partial G_{sw}}\right] C_f + \left[\frac{\partial^2 Y_{tt}}{\partial B_{eq}\partial G_{sw}}\right] C_t \tag{C.1.53}$$

2nd Derivatives of Y_{ff}

$$\frac{\partial^2 Y_{ff}}{\partial^2 B_{eq}} = 0 \tag{C.1.54}$$

$$\frac{\partial^2 Y_{ff}}{\partial^2 \theta_{sh}} = 0 \tag{C.1.55}$$

$$\frac{\partial^2 Y_{ff}}{\partial^2 m_a} = \frac{6\left(y_s + j\frac{b_c}{2} + jB_{eq}\right)}{k_2^2 m_a^4} \tag{C.1.56}$$

$$\frac{\partial^2 Y_{ff}}{\partial^2 G_{sw}} = 0 \tag{C.1.57}$$

$$\frac{\partial^2 Y_{ff}}{\partial B_{eq}\partial \theta_{sh}} = \frac{\partial^2 Y_{ff}}{\partial \theta_{sh}\partial B_{eq}} = 0 \tag{C.1.58}$$

$$\frac{\partial^2 Y_{ff}}{\partial B_{eq}\partial m_a} = \frac{\partial^2 Y_{ff}}{\partial m_a\partial B_{eq}} = \frac{-2j}{k_2^2 m_a^3} \tag{C.1.59}$$

$$\frac{\partial^2 Y_{ff}}{\partial B_{eq}\partial G_{sw}} = \frac{\partial^2 Y_{ff}}{\partial G_{sw}\partial B_{eq}} = 0 \tag{C.1.60}$$

$$\frac{\partial^2 Y_{ff}}{\partial \theta_{sh}\partial m_a} = \frac{\partial^2 Y_{ff}}{\partial m_a\partial \theta_{sh}} = 0 \tag{C.1.61}$$

$$\frac{\partial^2 Y_{ff}}{\partial \theta_{sh} \partial G_{sw}} = \frac{\partial^2 Y_{ff}}{\partial G_{sw} \partial \theta_{sh}} = 0 \tag{C.1.62}$$

$$\frac{\partial^2 Y_{ff}}{\partial m_a \partial G_{sw}} = \frac{\partial^2 Y_{ff}}{\partial G_{sw} \partial m_a} = 0 \tag{C.1.63}$$

2nd Derivatives of Y_{ft}

$$\frac{\partial^2 Y_{ft}}{\partial^2 B_{eq}} = 0 \tag{C.1.64}$$

$$\frac{\partial^2 Y_{ft}}{\partial^2 \theta_{sh}} = \frac{y_s}{k_2 m_a e^{-j\theta_{sh}}} \tag{C.1.65}$$

$$\frac{\partial^2 Y_{ft}}{\partial^2 m_a} = \frac{-2y_s}{k_2 m_a^3 e^{-j\theta_{sh}}} \tag{C.1.66}$$

$$\frac{\partial^2 Y_{ft}}{\partial^2 G_{sw}} = 0 \tag{C.1.67}$$

$$\frac{\partial^2 Y_{ft}}{\partial B_{eq} \partial \theta_{sh}} = \frac{\partial^2 Y_{ft}}{\partial \theta_{sh} \partial B_{eq}} = 0 \tag{C.1.68}$$

$$\frac{\partial^2 Y_{ft}}{\partial B_{eq} \partial m_a} = \frac{\partial^2 Y_{ft}}{\partial m_a \partial B_{eq}} = 0 \tag{C.1.69}$$

$$\frac{\partial^2 Y_{ft}}{\partial B_{eq} \partial G_{sw}} = \frac{\partial^2 Y_{ft}}{\partial G_{sw} \partial B_{eq}} = 0 \tag{C.1.70}$$

$$\frac{\partial^2 Y_{ft}}{\partial \theta_{sh} \partial m_a} = \frac{\partial^2 Y_{ft}}{\partial m_a \partial \theta_{sh}} = \frac{j y_s}{k_2 m_a^2 e^{-j\theta_{sh}}} \tag{C.1.71}$$

$$\frac{\partial^2 Y_{ft}}{\partial \theta_{sh} \partial G_{sw}} = \frac{\partial^2 Y_{ft}}{\partial G_{sw} \partial \theta_{sh}} = 0 \tag{C.1.72}$$

$$\frac{\partial^2 Y_{ft}}{\partial m_a \partial G_{sw}} = \frac{\partial^2 Y_{ft}}{\partial G_{sw} \partial m_a} = 0 \tag{C.1.73}$$

2nd Derivatives of Y_{tf}

$$\frac{\partial^2 Y_{tf}}{\partial^2 B_{eq}} = 0 \tag{C.1.74}$$

$$\frac{\partial^2 Y_{tf}}{\partial^2 \theta_{sh}} = \frac{y_s}{k_2 m_a e^{j\theta_{sh}}} \tag{C.1.75}$$

$$\frac{\partial^2 Y_{tf}}{\partial^2 m_a} = \frac{-2y_s}{k_2 m_a^3 e^{j\theta_{sh}}} \tag{C.1.76}$$

$$\frac{\partial^2 Y_{tf}}{\partial^2 G_{sw}} = 0 \tag{C.1.77}$$

$$\frac{\partial^2 Y_{tf}}{\partial B_{eq}\partial \theta_{sh}} = \frac{\partial^2 Y_{tf}}{\partial \theta_{sh}\partial B_{eq}} = 0 \tag{C.1.78}$$

$$\frac{\partial^2 Y_{tf}}{\partial B_{eq}\partial m_a} = \frac{\partial^2 Y_{tf}}{\partial m_a \partial B_{eq}} = 0 \tag{C.1.79}$$

$$\frac{\partial^2 Y_{tf}}{\partial B_{eq}\partial G_{sw}} = \frac{\partial^2 Y_{tf}}{\partial G_{sw}\partial B_{eq}} = 0 \tag{C.1.80}$$

$$\frac{\partial^2 Y_{tf}}{\partial \theta_{sh}\partial m_a} = \frac{\partial^2 Y_{tf}}{\partial m_a \partial \theta_{sh}} = \frac{-jy_s}{k_2 m_a^2 e^{j\theta_{sh}}} \tag{C.1.81}$$

$$\frac{\partial^2 Y_{tf}}{\partial \theta_{sh}\partial G_{sw}} = \frac{\partial^2 Y_{tf}}{\partial G_{sw}\partial \theta_{sh}} = 0 \tag{C.1.82}$$

$$\frac{\partial^2 Y_{tf}}{\partial m_a \partial G_{sw}} = \frac{\partial^2 Y_{tf}}{\partial G_{sw}\partial m_a} = 0 \tag{C.1.83}$$

2nd Derivatives of Y_{tt}

$$\frac{\partial^2 Y_{tt}}{\partial^2 B_{eq}} = 0 \tag{C.1.84}$$

$$\frac{\partial^2 Y_{tt}}{\partial^2 \theta_{sh}} = 0 \tag{C.1.85}$$

$$\frac{\partial^2 Y_{tt}}{\partial^2 m_a} = 0 \tag{C.1.86}$$

$$\frac{\partial^2 Y_{tt}}{\partial^2 G_{sw}} = 0 \tag{C.1.87}$$

$$\frac{\partial^2 Y_{tt}}{\partial B_{eq} \partial \theta_{sh}} = \frac{\partial^2 Y_{tt}}{\partial \theta_{sh} \partial B_{eq}} = 0 \tag{C.1.88}$$

$$\frac{\partial^2 Y_{tt}}{\partial B_{eq} \partial m_a} = \frac{\partial^2 Y_{tt}}{\partial m_a \partial B_{eq}} = 0 \tag{C.1.89}$$

$$\frac{\partial^2 Y_{tt}}{\partial B_{eq} \partial G_{sw}} = \frac{\partial^2 Y_{tt}}{\partial G_{sw} \partial B_{eq}} = 0 \tag{C.1.90}$$

$$\frac{\partial^2 Y_{tt}}{\partial \theta_{sh} \partial m_a} = \frac{\partial^2 Y_{tt}}{\partial m_a \partial \theta_{sh}} = 0 \tag{C.1.91}$$

$$\frac{\partial^2 Y_{tt}}{\partial \theta_{sh} \partial G_{sw}} = \frac{\partial^2 Y_{tt}}{\partial G_{sw} \partial \theta_{sh}} = 0 \tag{C.1.92}$$

$$\frac{\partial^2 Y_{tt}}{\partial m_a \partial G_{sw}} = \frac{\partial^2 Y_{tt}}{\partial G_{sw} \partial m_a} = 0 \tag{C.1.93}$$

C.2 Bus Injections

Consider the power balance equation $G^s(X) = 0$, where:

$$G^s(X) = S^{bus} + S_d - C_g S_g \tag{C.2.94}$$

and

$$S^{bus} = \left[V\right] I^{bus} = \left[V\right] \left(Y_{bus} V\right)^* \tag{C.2.95}$$

C.2.1 First Derivatives

$$\begin{aligned} \tilde{G^s_X} &= \frac{\partial G^s}{\partial X} \\ &= \begin{bmatrix} G^s_{V_a} & G^s_{V_m} & G^s_{P_g} & G^s_{Q_g} & G^s_{B_{eq}} & G^s_{\theta_{sh}} & G^s_{m_a} & G^s_{G_{sw}} \end{bmatrix} \end{aligned} \tag{C.2.96}$$

where:

$$\begin{aligned} G^{\tilde{s}}_{V_a} &= \frac{\partial S^{bus}}{\partial V_a} \\ &= \frac{\partial V}{\partial V_a}\left(Y_{bus}V\right)^* + [V]\left(Y_{bus}\frac{\partial V}{\partial V_a}\right)^* \end{aligned} \tag{C.2.97}$$

$$\begin{aligned} G^{\tilde{s}}_{V_m} &= \frac{\partial S^{bus}}{\partial V_m} \\ &= \frac{\partial V}{\partial V_m}\left(Y_{bus}V\right)^* + [V]\left(Y_{bus}\frac{\partial V}{\partial V_m}\right)^* \end{aligned} \tag{C.2.98}$$

$$G^{s}_{P_g} = \frac{\partial S^{bus}}{\partial P_g} = -C_g \tag{C.2.99}$$

$$G^{s}_{Q_g} = \frac{\partial S^{bus}}{\partial Q_g} = -jC_g \tag{C.2.100}$$

$$G^{s}_{B_{eq}} = \frac{\partial S^{bus}}{\partial B_{eq}} = [V]\left(\frac{\partial Y_{bus}}{\partial B_{eq}}V\right)^* \tag{C.2.101}$$

$$G^{s}_{\theta_{sh}} = \frac{\partial S^{bus}}{\partial \theta_{sh}} = [V]\left(\frac{\partial Y_{bus}}{\partial B_{eq}\theta_{sh}}V\right)^* \tag{C.2.102}$$

$$G^{s}_{m_a} = \frac{\partial S^{bus}}{\partial m_a} = [V]\left(\frac{\partial Y_{bus}}{\partial m_a}V\right)^* \tag{C.2.103}$$

$$G^{s}_{G_{sw}} = \frac{\partial S^{bus}}{\partial G_{sw}} = [V]\left(\frac{\partial Y_{bus}}{\partial G_{sw}}V\right)^* \tag{C.2.104}$$

C.2.2 Second Derivatives

$$G^s_{XX}(\lambda) = \frac{\partial}{\partial X}\left(G^s_X{}^{\top}\lambda\right) = \tag{C.2.105}$$

$$\begin{bmatrix}
G^s_{V_aV_a}(\lambda) & G^s_{V_aV_m}(\lambda) & G^s_{V_aP_g}(\lambda) & G^s_{V_aQ_g}(\lambda) & G^s_{V_aB_{eqz}}(\lambda) & G^s_{V_aB_{eqv}}(\lambda) & G^s_{V_a\theta_{sh}}(\lambda) & G^s_{V_aqtm_a}(\lambda) & G^s_{V_avtm_a}(\lambda) & G^s_{V_aG_{sw}}(\lambda) \\
G^s_{V_mV_a}(\lambda) & G^s_{V_mV_m}(\lambda) & G^s_{V_mP_g}(\lambda) & G^s_{V_mQ_g}(\lambda) & G^s_{V_mB_{eqz}}(\lambda) & G^s_{V_mB_{eqv}}(\lambda) & G^s_{V_m\theta_{sh}}(\lambda) & G^s_{V_mqtm_a}(\lambda) & G^s_{V_mvtm_a}(\lambda) & G^s_{V_mG_{sw}}(\lambda) \\
G^s_{P_gV_a}(\lambda) & G^s_{P_gV_m}(\lambda) & G^s_{P_gP_g}(\lambda) & G^s_{P_gQ_g}(\lambda) & G^s_{P_gB_{eqz}}(\lambda) & G^s_{P_gB_{eqv}}(\lambda) & G^s_{P_g\theta_{sh}}(\lambda) & G^s_{P_gqtm_a}(\lambda) & G^s_{P_gvtm_a}(\lambda) & G^s_{P_gG_{sw}}(\lambda) \\
G^s_{Q_gV_a}(\lambda) & G^s_{Q_gV_m}(\lambda) & G^s_{Q_gP_g}(\lambda) & G^s_{Q_gQ_g}(\lambda) & G^s_{Q_gB_{eqz}}(\lambda) & G^s_{Q_gB_{eqv}}(\lambda) & G^s_{Q_g\theta_{sh}}(\lambda) & G^s_{Q_gqtm_a}(\lambda) & G^s_{Q_gvtm_a}(\lambda) & G^s_{Q_gG_{sw}}(\lambda) \\
G^s_{B_{eqz}V_a}(\lambda) & G^s_{B_{eqz}V_m}(\lambda) & G^s_{B_{eqz}P_g}(\lambda) & G^s_{B_{eqz}Q_g}(\lambda) & G^s_{B_{eqz}B_{eqz}}(\lambda) & G^s_{B_{eqz}B_{eqv}}(\lambda) & G^s_{B_{eqz}\theta_{sh}}(\lambda) & G^s_{B_{eqz}qtm_a}(\lambda) & G^s_{B_{eqz}vtm_a}(\lambda) & G^s_{B_{eqz}G_{sw}}(\lambda) \\
G^s_{B_{eqv}V_a}(\lambda) & G^s_{B_{eqv}V_m}(\lambda) & G^s_{B_{eqv}P_g}(\lambda) & G^s_{B_{eqv}Q_g}(\lambda) & G^s_{B_{eqv}B_{eqz}}(\lambda) & G^s_{B_{eqv}B_{eqv}}(\lambda) & G^s_{B_{eqv}\theta_{sh}}(\lambda) & G^s_{B_{eqv}qtm_a}(\lambda) & G^s_{B_{eqv}vtm_a}(\lambda) & G^s_{B_{eqv}G_{sw}}(\lambda) \\
G^s_{\theta_{sh}V_a}(\lambda) & G^s_{\theta_{sh}V_m}(\lambda) & G^s_{\theta_{sh}P_g}(\lambda) & G^s_{\theta_{sh}Q_g}(\lambda) & G^s_{\theta_{sh}B_{eqz}}(\lambda) & G^s_{\theta_{sh}B_{eqv}}(\lambda) & G^s_{\theta_{sh}\theta_{sh}}(\lambda) & G^s_{\theta_{sh}qtm_a}(\lambda) & G^s_{\theta_{sh}vtm_a}(\lambda) & G^s_{\theta_{sh}G_{sw}}(\lambda) \\
G^s_{qtm_aV_a}(\lambda) & G^s_{qtm_aV_m}(\lambda) & G^s_{qtm_aP_g}(\lambda) & G^s_{qtm_aQ_g}(\lambda) & G^s_{qtm_aB_{eqz}}(\lambda) & G^s_{qtm_aB_{eqv}}(\lambda) & G^s_{qtm_a\theta_{sh}}(\lambda) & G^s_{qtm_aqtm_a}(\lambda) & G^s_{qtm_avtm_a}(\lambda) & G^s_{qtm_aG_{sw}}(\lambda) \\
G^s_{vtm_aV_a}(\lambda) & G^s_{vtm_aV_m}(\lambda) & G^s_{vtm_aP_g}(\lambda) & G^s_{vtm_aQ_g}(\lambda) & G^s_{vtm_aB_{eqz}}(\lambda) & G^s_{vtm_aB_{eqv}}(\lambda) & G^s_{vtm_a\theta_{sh}}(\lambda) & G^s_{vtm_aqtm_a}(\lambda) & G^s_{vtm_avtm_a}(\lambda) & G^s_{vtm_aG_{sw}}(\lambda) \\
G^s_{G_{sw}V_a}(\lambda) & G^s_{G_{sw}V_m}(\lambda) & G^s_{G_{sw}P_g}(\lambda) & G^s_{G_{sw}Q_g}(\lambda) & G^s_{G_{sw}B_{eqz}}(\lambda) & G^s_{G_{sw}B_{eqv}}(\lambda) & G^s_{G_{sw}\theta_{sh}}(\lambda) & G^s_{G_{sw}qtm_a}(\lambda) & G^s_{G_{sw}vtm_a}(\lambda) & G^s_{G_{sw}G_{sw}}(\lambda)
\end{bmatrix} \tag{C.2.106}$$

$$
\begin{bmatrix}
G^s_{V_aV_a}(\lambda) & G^s_{V_aV_m}(\lambda) & 0 & 0 & G^s_{V_aB_{eqz}}(\lambda) & G^s_{V_aB_{eqv}}(\lambda) & G^s_{V_a\theta_{sh}}(\lambda) & G^s_{V_aqtm_a}(\lambda) & G^s_{V_avtm_a}(\lambda) & G^s_{V_aG_{sw}}(\lambda) \\
G^s_{V_mV_a}(\lambda) & G^s_{V_mV_m}(\lambda) & 0 & 0 & G^s_{V_mB_{eqz}}(\lambda) & G^s_{V_mB_{eqv}}(\lambda) & G^s_{V_m\theta_{sh}}(\lambda) & G^s_{V_mqtm_a}(\lambda) & G^s_{V_mvtm_a}(\lambda) & G^s_{V_mG_{sw}}(\lambda) \\
0 & 0 & 0 & 0 & 0 & 0 & 0 & 0 & 0 & 0 \\
0 & 0 & 0 & 0 & 0 & 0 & 0 & 0 & 0 & 0 \\
G^s_{B_{eqz}V_a}(\lambda) & G^s_{B_{eqz}V_m}(\lambda) & 0 & 0 & G^s_{B_{eqz}B_{eqz}}(\lambda) & G^s_{B_{eqz}B_{eqv}}(\lambda) & G^s_{B_{eqz}\theta_{sh}}(\lambda) & G^s_{B_{eqz}qtm_a}(\lambda) & G^s_{B_{eqz}vtm_a}(\lambda) & G^s_{B_{eqz}G_{sw}}(\lambda) \\
G^s_{B_{eqv}V_a}(\lambda) & G^s_{B_{eqv}V_m}(\lambda) & 0 & 0 & G^s_{B_{eqv}B_{eqz}}(\lambda) & G^s_{B_{eqv}B_{eqv}}(\lambda) & G^s_{B_{eqv}\theta_{sh}}(\lambda) & G^s_{B_{eqv}qtm_a}(\lambda) & G^s_{B_{eqv}vtm_a}(\lambda) & G^s_{B_{eqv}G_{sw}}(\lambda) \\
G^s_{\theta_{sh}V_a}(\lambda) & G^s_{\theta_{sh}V_m}(\lambda) & 0 & 0 & G^s_{\theta_{sh}B_{eqz}}(\lambda) & G^s_{\theta_{sh}B_{eqv}}(\lambda) & G^s_{\theta_{sh}\theta_{sh}}(\lambda) & G^s_{\theta_{sh}qtm_a}(\lambda) & G^s_{\theta_{sh}vtm_a}(\lambda) & G^s_{\theta_{sh}G_{sw}}(\lambda) \\
G^s_{qtm_aV_a}(\lambda) & G^s_{qtm_aV_m}(\lambda) & 0 & 0 & G^s_{qtm_aB_{eqz}}(\lambda) & G^s_{qtm_aB_{eqv}}(\lambda) & G^s_{qtm_a\theta_{sh}}(\lambda) & G^s_{qtm_aqtm_a}(\lambda) & G^s_{qtm_avtm_a}(\lambda) & G^s_{qtm_aG_{sw}}(\lambda) \\
G^s_{vtm_aV_a}(\lambda) & G^s_{vtm_aV_m}(\lambda) & 0 & 0 & G^s_{vtm_aB_{eqz}}(\lambda) & G^s_{vtm_aB_{eqv}}(\lambda) & G^s_{vtm_a\theta_{sh}}(\lambda) & G^s_{vtm_aqtm_a}(\lambda) & G^s_{vtm_avtm_a}(\lambda) & G^s_{vtm_aG_{sw}}(\lambda) \\
G^s_{G_{sw}V_a}(\lambda) & G^s_{G_{sw}V_m}(\lambda) & 0 & 0 & G^s_{G_{sw}B_{eqz}}(\lambda) & G^s_{G_{sw}B_{eqv}}(\lambda) & G^s_{G_{sw}\theta_{sh}}(\lambda) & G^s_{G_{sw}qtm_a}(\lambda) & G^s_{G_{sw}vtm_a}(\lambda) & G^s_{G_{sw}G_{sw}}(\lambda)
\end{bmatrix} \tag{C.2.107}
$$

$$= \begin{bmatrix} G^s_{V_aV_a}(\lambda) & G^s_{V_aV_m}(\lambda) & 0 & 0 & G^s_{V_aB_{eq}}(\lambda) & G^s_{V_a\theta_{sh}}(\lambda) & G^s_{V_am_a}(\lambda) & G^s_{V_aG_{sw}}(\lambda) \\ G^s_{V_mV_a}(\lambda) & G^s_{V_mV_m}(\lambda) & 0 & 0 & G^s_{V_mB_{eq}}(\lambda) & G^s_{V_m\theta_{sh}}(\lambda) & G^s_{V_mm_a}(\lambda) & G^s_{V_mG_{sw}}(\lambda) \\ 0 & 0 & 0 & 0 & 0 & 0 & 0 & 0 \\ 0 & 0 & 0 & 0 & 0 & 0 & 0 & 0 \\ G^s_{B_{eq}V_a}(\lambda) & G^s_{B_{eq}V_m}(\lambda) & 0 & 0 & G^s_{B_{eq}B_{eq}}(\lambda) & G^s_{B_{eq}\theta_{sh}}(\lambda) & G^s_{B_{eq}m_a}(\lambda) & G^s_{B_{eq}G_{sw}}(\lambda) \\ G^s_{\theta_{sh}V_a}(\lambda) & G^s_{\theta_{sh}V_m}(\lambda) & 0 & 0 & G^s_{\theta_{sh}B_{eq}}(\lambda) & G^s_{\theta_{sh}\theta_{sh}}(\lambda) & G^s_{\theta_{sh}m_a}(\lambda) & G^s_{\theta_{sh}G_{sw}}(\lambda) \\ G^s_{m_aV_a}(\lambda) & G^s_{m_aV_m}(\lambda) & 0 & 0 & G^s_{m_aB_{eq}}(\lambda) & G^s_{m_a\theta_{sh}}(\lambda) & G^s_{m_am_a}(\lambda) & G^s_{m_aG_{sw}}(\lambda) \\ G^s_{G_{sw}V_a}(\lambda) & G^s_{G_{sw}V_m}(\lambda) & 0 & 0 & G^s_{G_{sw}B_{eq}}(\lambda) & G^s_{G_{sw}\theta_{sh}}(\lambda) & G^s_{G_{sw}m_a}(\lambda) & G^s_{G_{sw}G_{sw}}(\lambda) \end{bmatrix} \tag{C.2.108}$$

C.2.3 Bus Injection Detailed Hessian

$$G^s_{V_aV_a}(\lambda) = \frac{\partial}{\partial V_a}\left({G^s_{V_a}}^\top \lambda\right) \tag{C.2.109}$$

$$= \frac{\partial}{\partial V_a}\left(\left(\frac{\partial V}{\partial V_a}\left(Y_{bus}V\right)^* + [V]\left(Y_{bus}\frac{\partial V}{\partial V_a}\right)^*\right)^\top \lambda\right) \tag{C.2.110}$$

$$\begin{aligned} &= \left(\frac{\partial V}{\partial V_a}\left(Y_{bus}\frac{\partial V}{\partial V_a}\right)^* + \frac{\partial^2 V}{\partial^2 V_a}\left(Y_{bus}V\right)^* + \right. \\ &\left. \left[\frac{\partial V}{\partial V_a}\right]\left(Y_{bus}\frac{\partial V}{\partial V_a}\right)^* + [V]\left(Y_{bus}\frac{\partial^2 V}{\partial^2 V_a}\right)^*\right)^\top \lambda \end{aligned} \tag{C.2.111}$$

$$G^s_{V_mV_a}(\lambda) = \frac{\partial}{\partial V_a}\left({G^s_{V_m}}^\top \lambda\right) \tag{C.2.112}$$

$$= \frac{\partial V}{\partial V_a}\left(\left(\frac{\partial V}{\partial V_m}\left(Y_{bus}V\right)^* + [V]\left(Y_{bus}\frac{\partial V}{\partial V_m}\right)^*\right)^\top \lambda\right) \tag{C.2.113}$$

$$\begin{aligned} &= \left(\frac{\partial V}{\partial V_m}\left(Y_{bus}\frac{\partial V}{\partial V_a}\right)^* + \frac{\partial^2 V}{\partial V_m \partial V_a}\left(Y_{bus}V\right)^* + \right. \\ &\left. \left[\frac{\partial V}{\partial V_a}\right]\left(Y_{bus}\frac{\partial V}{\partial V_m}\right)^* + [V]\left(Y_{bus}\frac{\partial^2 V}{\partial V_m \partial V_a}\right)^*\right)^\top \lambda \end{aligned} \tag{C.2.114}$$

$$G^s_{P_gV_a}(\lambda) = \frac{\partial}{\partial V_a}\left({G^s_{P_g}}^\top \lambda\right) = 0 \tag{C.2.115}$$

$$G^s_{Q_gV_a}(\lambda) = \frac{\partial}{\partial V_a}\left({G^s_{Q_g}}^\top \lambda\right) = 0 \tag{C.2.116}$$

$$G^s_{B_{eqz}V_a}(\lambda) = \frac{\partial}{\partial V_a}\left({G^s_{B_{eqz}}}^\top \lambda\right) \tag{C.2.117}$$

$$= \left(\frac{\partial V}{\partial V_a} \left(\frac{\partial Y_{bus}}{\partial B_{eqz}} V \right)^* + [V] \left(\frac{\partial Y_{bus}}{\partial B_{eqz}} \frac{\partial V}{\partial V_a} \right)^* \right)^\top \lambda \tag{C.2.118}$$

$$G^s_{B_{eqv}V_a}(\lambda) = \frac{\partial}{\partial V_a} \left({G^s_{B_{eqv}}}^\top \lambda \right) \tag{C.2.119}$$

$$= \left(\frac{\partial V}{\partial V_a} \left(\frac{\partial Y_{bus}}{\partial B_{eqv}} V \right)^* + [V] \left(\frac{\partial Y_{bus}}{\partial B_{eqv}} \frac{\partial V}{\partial V_a} \right)^* \right)^\top \lambda \tag{C.2.120}$$

$$G^s_{\theta_{sh}V_a}(\lambda) = \frac{\partial}{\partial V_a} \left({G^s_{\theta_{sh}}}^\top \lambda \right) \tag{C.2.121}$$

$$= \left(\frac{\partial V}{\partial V_a} \left(\frac{\partial Y_{bus}}{\partial \theta_{sh}} V \right)^* + [V] \left(\frac{\partial Y_{bus}}{\partial \theta_{sh}} \frac{\partial V}{\partial V_a} \right)^* \right)^\top \lambda \tag{C.2.122}$$

$$G^s_{qtm_aV_a}(\lambda) = \frac{\partial}{\partial V_a} \left({G^s_{qtm_a}}^\top \lambda \right) \tag{C.2.123}$$

$$= \left(\frac{\partial V}{\partial V_a} \left(\frac{\partial Y_{bus}}{\partial qtm_a} V \right)^* + [V] \left(\frac{\partial Y_{bus}}{\partial qtm_a} \frac{\partial V}{\partial V_a} \right)^* \right)^\top \lambda \tag{C.2.124}$$

$$G^s_{vtm_aV_a}(\lambda) = \frac{\partial}{\partial V_a} \left({G^s_{vtm_a}}^\top \lambda \right) \tag{C.2.125}$$

$$= \left(\frac{\partial V}{\partial V_a} \left(\frac{\partial Y_{bus}}{\partial vtm_a} V \right)^* + [V] \left(\frac{\partial Y_{bus}}{\partial vtm_a} \frac{\partial V}{\partial V_a} \right)^* \right)^\top \lambda \tag{C.2.126}$$

$$G^s_{G_{sw}V_a}(\lambda) = \frac{\partial}{\partial V_a} \left({G^s_{G_{sw}}}^\top \lambda \right) \tag{C.2.127}$$

$$= \left(\frac{\partial V}{\partial V_a} \left(\frac{\partial Y_{bus}}{\partial G_{sw}} V \right)^* + [V] \left(\frac{\partial Y_{bus}}{\partial G_{sw}} \frac{\partial V}{\partial V_a} \right)^* \right)^\top \lambda \tag{C.2.128}$$

$$G^s_{V_aV_m}(\lambda) = \frac{\partial}{\partial V_m} \left({G^s_{V_a}}^\top \lambda \right) \tag{C.2.129}$$

$$= {G^s_{V_mV_a}}^\top(\lambda) \tag{C.2.130}$$

$$G^s_{V_mV_m}(\lambda) = \frac{\partial}{\partial V_m} \left({G^s_{V_m}}^\top \lambda \right) \tag{C.2.131}$$

$$= \frac{\partial}{\partial V_m} \left(\left(\frac{\partial V}{\partial V_m} \left(Y_{bus} V \right)^* + [V] \left(Y_{bus} \frac{\partial V}{\partial V_m} \right)^* \right)^\top \lambda \right) \tag{C.2.132}$$

$$\begin{aligned} &= \left(\frac{\partial V}{\partial V_m} \left(Y_{bus} \frac{\partial V}{\partial V_m} \right)^* + \frac{\partial^2 V}{\partial^2 V_m} \left(Y_{bus} V \right)^* + \right. \\ &\left. \left[\frac{\partial V}{\partial V_m} \right] \left(Y_{bus} \frac{\partial V}{\partial V_m} \right)^* + [V] \left(Y_{bus} \frac{\partial^2 V}{\partial^2 V_m} \right)^* \right)^\top \lambda \end{aligned} \tag{C.2.133}$$

$$G^s_{P_g V_m}(\lambda) = \frac{\partial}{\partial V_m}\left({G^s_{P_g}}^\top \lambda\right) = 0 \tag{C.2.134}$$

$$G^s_{Q_g V_m}(\lambda) = \frac{\partial}{\partial V_m}\left({G^s_{Q_g}}^\top \lambda\right) = 0 \tag{C.2.135}$$

$$G^s_{B_{eqz} V_m}(\lambda) = \frac{\partial}{\partial V_m}\left({G^s_{B_{eqz}}}^\top \lambda\right) \tag{C.2.136}$$

$$= \left(\frac{\partial V}{\partial V_m}\left(\frac{\delta Y_{bus}}{\delta B_{eqz}} V\right)^* + [V]\left(\frac{\delta Y_{bus}}{\delta B_{eqz}} \frac{\partial V}{\partial V_m}\right)^*\right)^\top \lambda \tag{C.2.137}$$

$$G^s_{B_{eqv} V_m}(\lambda) = \frac{\partial}{\partial V_m}\left({G^s_{B_{eqv}}}^\top \lambda\right) \tag{C.2.138}$$

$$= \left(\frac{\partial V}{\partial V_m}\left(\frac{\delta Y_{bus}}{\delta B_{eqv}} V\right)^* + [V]\left(\frac{\delta Y_{bus}}{\delta B_{eqv}} \frac{\partial V}{\partial V_m}\right)^*\right)^\top \lambda \tag{C.2.139}$$

$$G^s_{\theta_{sh} V_m}(\lambda) = \frac{\partial}{\partial V_m}\left({G^s_{\theta_{sh}}}^\top \lambda\right) \tag{C.2.140}$$

$$= \left(\frac{\partial V}{\partial V_m}\left(\frac{\delta Y_{bus}}{\delta \theta_{sh}} V\right)^* + [V]\left(\frac{\delta Y_{bus}}{\delta \theta_{sh}} \frac{\partial V}{\partial V_m}\right)^*\right)^\top \lambda \tag{C.2.141}$$

$$G^s_{qtm_a V_m}(\lambda) = \frac{\partial}{\partial V_m}\left({G^s_{qtm_a}}^\top \lambda\right) \tag{C.2.142}$$

$$= \left(\frac{\partial V}{\partial V_m}\left(\frac{\delta Y_{bus}}{\delta qtm_a} V\right)^* + [V]\left(\frac{\delta Y_{bus}}{\delta qtm_a} \frac{\partial V}{\partial V_m}\right)^*\right)^\top \lambda \tag{C.2.143}$$

$$G^s_{vtm_a V_m}(\lambda) = \frac{\partial}{\partial V_m}\left({G^s_{vtm_a}}^\top \lambda\right) \tag{C.2.144}$$

$$= \left(\frac{\partial V}{\partial V_m}\left(\frac{\delta Y_{bus}}{\delta vtm_a} V\right)^* + [V]\left(\frac{\delta Y_{bus}}{\delta vtm_a} \frac{\partial V}{\partial V_m}\right)^*\right)^\top \lambda \tag{C.2.145}$$

$$G^s_{G_{sw} V_m}(\lambda) = \frac{\partial}{\partial V_m}\left({G^s_{G_{sw}}}^\top \lambda\right) \tag{C.2.146}$$

$$= \left(\frac{\partial V}{\partial V_m}\left(\frac{\partial Y_{bus}}{\partial G_{sw}} V\right)^* + [V]\left(\frac{\partial Y_{bus}}{\partial G_{sw}} \frac{\partial V}{\partial V_m}\right)^*\right)^\top \lambda \tag{C.2.147}$$

$$G^s_{V_a P_g}(\lambda) = \frac{\partial}{\partial P_g}\left({G^s_{V_a}}^\top \lambda\right) = 0 \tag{C.2.148}$$

$$G^s_{V_m P_g}(\lambda) = \frac{\partial}{\partial P_g}\left({G^s_{P_g}}^\top \lambda\right) = 0 \tag{C.2.149}$$

$$G^s_{P_g P_g}(\lambda) = \frac{\partial}{\partial P_g}\left({G^s_{P_g}}^\top \lambda\right) = 0 \tag{C.2.150}$$

$$G^s_{Q_g P_g}(\lambda) = \frac{\partial}{\partial P_g}\left({G^s_{Q_g}}^\top \lambda\right) = 0 \tag{C.2.151}$$

$$G^s_{B_{eqz} P_g}(\lambda) = \frac{\partial}{\partial P_g}\left({G^s_{B_{eqz}}}^\top \lambda\right) = 0 \tag{C.2.152}$$

$$G^s_{B_{eqv} P_g}(\lambda) = \frac{\partial}{\partial P_g}\left({G^s_{B_{eqv}}}^\top \lambda\right) = 0 \tag{C.2.153}$$

$$G^s_{\theta_{sh} P_g}(\lambda) = \frac{\partial}{\partial P_g}\left({G^s_{\theta_{sh}}}^\top \lambda\right) = 0 \tag{C.2.154}$$

$$G^s_{qtm_a P_g}(\lambda) = \frac{\partial}{\partial P_g}\left({G^s_{qtm_a}}^\top \lambda\right) = 0 \tag{C.2.155}$$

$$G^s_{vtm_a P_g}(\lambda) = \frac{\partial}{\partial P_g}\left({G^s_{vtm_a}}^\top \lambda\right) = 0 \tag{C.2.156}$$

$$G^s_{G_{sw} P_g}(\lambda) = \frac{\partial}{\partial P_g}\left({G^s_{G_{sw}}}^\top \lambda\right) = 0 \tag{C.2.157}$$

$$G^s_{V_a Q_g}(\lambda) = \frac{\partial}{\partial Q_g}\left({G^s_{V_a}}^\top \lambda\right) = 0 \tag{C.2.158}$$

$$G^s_{V_m Q_g}(\lambda) = \frac{\partial}{\partial Q_g}\left({G^s_{Q_g}}^\top \lambda\right) = 0 \tag{C.2.159}$$

$$G^s_{P_g Q_g}(\lambda) = \frac{\partial}{\partial Q_g}\left({G^s_{P_g}}^\top \lambda\right) = 0 \tag{C.2.160}$$

$$G^s_{Q_g Q_g}(\lambda) = \frac{\partial}{\partial Q_g}\left({G^s_{Q_g}}^\top \lambda\right) = 0 \tag{C.2.161}$$

$$G^s_{B_{eqz} Q_g}(\lambda) = \frac{\partial}{\partial Q_g}\left({G^s_{B_{eqz}}}^\top \lambda\right) = 0 \tag{C.2.162}$$

$$G^s_{B_{eqv}Q_g}(\lambda) = \frac{\partial}{\partial Q_g}\left({G^s_{B_{eqv}}}^\top \lambda\right) = 0 \tag{C.2.163}$$

$$G^s_{\theta_{sh}Q_g}(\lambda) = \frac{\partial}{\partial Q_g}\left({G^s_{\theta_{sh}}}^\top \lambda\right) = 0 \tag{C.2.164}$$

$$G^s_{qtm_aQ_g}(\lambda) = \frac{\partial}{\partial Q_g}\left({G^s_{qtm_a}}^\top \lambda\right) = 0 \tag{C.2.165}$$

$$G^s_{vtm_aQ_g}(\lambda) = \frac{\partial}{\partial Q_g}\left({G^s_{vtm_a}}^\top \lambda\right) = 0 \tag{C.2.166}$$

$$G^s_{G_{sw}Q_g}(\lambda) = \frac{\partial}{\partial Q_g}\left({G^s_{G_{sw}}}^\top \lambda\right) = 0 \tag{C.2.167}$$

$$G^s_{V_aB_{eqz}}(\lambda) = \frac{\partial}{\partial B_{eqz}}\left({G^s_{V_a}}^\top \lambda\right) \tag{C.2.168}$$

$$= {G^s_{B_{eqz}V_a}}^\top(\lambda) \tag{C.2.169}$$

$$G^s_{V_mB_{eqz}}(\lambda) = \frac{\partial}{\partial B_{eqz}}\left({G^s_{V_m}}^\top \lambda\right) \tag{C.2.170}$$

$$G^s_{V_mB_{eqz}}(\lambda) = {G^s_{B_{eqz}V_m}}^\top(\lambda) \tag{C.2.171}$$

$$G^s_{P_gB_{eqz}}(\lambda) = \frac{\partial}{\partial B_{eqz}}\left({G^s_{P_g}}^\top \lambda\right) = 0 \tag{C.2.172}$$

$$G^s_{Q_gB_{eqz}}(\lambda) = \frac{\partial}{\partial B_{eqz}}\left({G^s_{Q_g}}^\top \lambda\right) = 0 \tag{C.2.173}$$

$$G^s_{B_{eqz}B_{eqz}}(\lambda) = \frac{\partial}{\partial B_{eqz}}\left({G^s_{B_{eqz}}}^\top \lambda\right) \tag{C.2.174}$$

$$= \left([V]\left(\frac{\partial^2 Y_{bus}}{\partial^2 B_{eqz}}V\right)^*\right)^\top \lambda \tag{C.2.175}$$

$$G^s_{B_{eqv}B_{eqz}}(\lambda) = \frac{\partial}{\partial B_{eqz}}\left({G^s_{B_{eqv}}}^\top \lambda\right) \tag{C.2.176}$$

$$= \left([V]\left(\frac{\partial^2 Y_{bus}}{\partial B_{eqv}B_{eqz}}V\right)^*\right)^\top \lambda \tag{C.2.177}$$

$$G^s_{\theta_{sh}B_{eqz}}(\lambda) = \frac{\partial}{\partial B_{eqz}}\left({G^s_{\theta_{sh}}}^\top \lambda\right) \tag{C.2.178}$$

$$= \left([V]\left(\frac{\partial^2 Y_{bus}}{\partial \theta_{sh} B_{eqz}} V\right)^*\right)^\top \lambda \tag{C.2.179}$$

$$G^s_{qtm_a B_{eqz}}(\lambda) = \frac{\partial}{\partial B_{eqz}}\left({G^s_{qtm_a}}^\top \lambda\right) \tag{C.2.180}$$

$$= \left([V]\left(\frac{\partial^2 Y_{bus}}{\partial qtm_a B_{eqz}} V\right)^*\right)^\top \lambda \tag{C.2.181}$$

$$G^s_{vtm_a B_{eqz}}(\lambda) = \frac{\partial}{\partial B_{eqz}}\left({G^s_{vtm_a}}^\top \lambda\right) \tag{C.2.182}$$

$$= \left([V]\left(\frac{\partial^2 Y_{bus}}{\partial vtm_a B_{eqz}} V\right)^*\right)^\top \lambda \tag{C.2.183}$$

$$G^s_{G_{sw}B_{eqz}}(\lambda) = \frac{\partial}{\partial B_{eqz}}\left({G^s_{G_{sw}}}^\top \lambda\right) \tag{C.2.184}$$

$$= \left([V]\left(\frac{\partial^2 Y_{bus}}{\partial G_{sw} B_{eqz}} V\right)^*\right)^\top \lambda \tag{C.2.185}$$

$$G^s_{V_a B_{eqv}}(\lambda) = \frac{\partial}{\partial B_{eqv}}\left({G^s_{V_a}}^\top \lambda\right) \tag{C.2.186}$$

$$= {G^s_{B_{eqv}V_a}}^\top(\lambda) \tag{C.2.187}$$

$$G^s_{V_m B_{eqv}}(\lambda) = \frac{\partial}{\partial B_{eqv}}\left({G^s_{P_g}}^\top \lambda\right) \tag{C.2.188}$$

$$= {G^s_{B_{eqv}V_m}}^\top(\lambda) \tag{C.2.189}$$

$$G^s_{P_g B_{eqv}}(\lambda) = \frac{\partial}{\partial B_{eqv}}\left({G^s_{P_g}}^\top \lambda\right) = 0 \tag{C.2.190}$$

$$G^s_{Q_g B_{eqv}}(\lambda) = \frac{\partial}{\partial B_{eqv}}\left({G^s_{Q_g}}^\top \lambda\right) = 0 \tag{C.2.191}$$

$$G^s_{B_{eqz}B_{eqv}}(\lambda) = \frac{\partial}{\partial B_{eqv}}\left({G^s_{B_{eqz}}}^\top \lambda\right) \tag{C.2.192}$$

$$= {G^s_{B_{eqv}B_{eqz}}}^\top(\lambda) \tag{C.2.193}$$

$$G^s_{B_{eqv}B_{eqv}}(\lambda) = \frac{\partial}{\partial B_{eqv}}\left({G^s_{B_{eqv}}}^\top \lambda\right) \tag{C.2.194}$$

$$= \left([V]\left(\frac{\partial^2 Y_{bus}}{\partial^2 B_{eqv}} V\right)^*\right)^\top \lambda \tag{C.2.195}$$

$$G^s_{\theta_{sh}B_{eqv}}(\lambda) = \frac{\partial}{\partial B_{eqv}}\left({G^s_{\theta_{sh}}}^\top \lambda\right) \tag{C.2.196}$$

$$= \left([V]\left(\frac{\partial^2 Y_{bus}}{\partial \theta_{sh} B_{eqv}} V\right)^*\right)^\top \lambda \tag{C.2.197}$$

$$G^s_{qtm_a B_{eqv}}(\lambda) = \frac{\partial}{\partial B_{eqv}}\left({G^s_{qtm_a}}^\top \lambda\right) \tag{C.2.198}$$

$$= \left([V]\left(\frac{\partial^2 Y_{bus}}{\partial qtm_a B_{eqz}} V\right)^*\right)^\top \lambda \tag{C.2.199}$$

$$G^s_{vtm_a B_{eqv}}(\lambda) = \frac{\partial}{\partial B_{eqv}}\left({G^s_{vtm_a}}^\top \lambda\right) \tag{C.2.200}$$

$$= \left([V]\left(\frac{\partial^2 Y_{bus}}{\partial vtm_a B_{eqz}} V\right)^*\right)^\top \lambda \tag{C.2.201}$$

$$G^s_{G_{sw}B_{eqv}}(\lambda) = \frac{\partial}{\partial B_{eqv}}\left({G^s_{G_{sw}}}^\top \lambda\right) \tag{C.2.202}$$

$$= \left([V]\left(\frac{\partial^2 Y_{bus}}{\partial G_{sw} B_{eqz}} V\right)^*\right)^\top \lambda \tag{C.2.203}$$

$$G^s_{V_a\theta_{sh}}(\lambda) = \frac{\partial}{\partial \theta_{sh}}\left({G^s_{V_a}}^\top \lambda\right) \tag{C.2.204}$$

$$= {G^s_{\theta_{sh}V_a}}^\top(\lambda) \tag{C.2.205}$$

$$G^s_{V_m\theta_{sh}}(\lambda) = \frac{\partial}{\partial \theta_{sh}}\left({G^s_{P_g}}^\top \lambda\right) \tag{C.2.206}$$

$$= G^s_{\theta_{sh}V_m}(\lambda)^\top(\lambda) \tag{C.2.207}$$

$$G^s_{P_g\theta_{sh}}(\lambda) = \frac{\partial}{\partial \theta_{sh}}\left({G^s_{P_g}}^\top \lambda\right) = 0 \tag{C.2.208}$$

$$G^s_{Q_g\theta_{sh}}(\lambda) = \frac{\partial}{\partial \theta_{sh}}\left({G^s_{Q_g}}^\top \lambda\right) = 0 \tag{C.2.209}$$

$$G^s_{B_{eqz}\theta_{sh}}(\lambda) = \frac{\partial}{\partial \theta_{sh}} \left({G^s_{B_{eqz}}}^\top \lambda \right) \tag{C.2.210}$$

$$= {G^s_{\theta_{sh} B_{eqz}}}^\top (\lambda) \tag{C.2.211}$$

$$G^s_{B_{eqv}\theta_{sh}}(\lambda) = \frac{\partial}{\partial \theta_{sh}} \left({G^s_{B_{eqv}}}^\top \lambda \right) \tag{C.2.212}$$

$$= {G^s_{\theta_{sh} B_{eqv}}}^\top (\lambda) \tag{C.2.213}$$

$$G^s_{\theta_{sh}\theta_{sh}}(\lambda) = \frac{\partial}{\partial \theta_{sh}} \left({G^s_{\theta_{sh}}}^\top \lambda \right) \tag{C.2.214}$$

$$= \left([V] \left(\frac{\partial^2 Y_{bus}}{\partial^2 \theta_{sh}} V \right)^* \right)^\top \lambda \tag{C.2.215}$$

$$G^s_{qtm_a\theta_{sh}}(\lambda) = \frac{\partial}{\partial \theta_{sh}} \left({G^s_{qtm_a}}^\top \lambda \right) \tag{C.2.216}$$

$$= \left([V] \left(\frac{\partial^2 Y_{bus}}{\partial qtm_a \theta_{sh}} V \right)^* \right)^\top \lambda \tag{C.2.217}$$

$$G^s_{vtm_a\theta_{sh}}(\lambda) = \frac{\partial}{\partial \theta_{sh}} \left({G^s_{vtm_a}}^\top \lambda \right) \tag{C.2.218}$$

$$= \left([V] \left(\frac{\partial^2 Y_{bus}}{\partial vtm_a \theta_{sh}} V \right)^* \right)^\top \lambda \tag{C.2.219}$$

$$G^s_{G_{sw}\theta_{sh}}(\lambda) = \frac{\partial}{\partial \theta_{sh}} \left({G^s_{G_{sw}}}^\top \lambda \right) \tag{C.2.220}$$

$$= \left([V] \left(\frac{\partial^2 Y_{bus}}{\partial G_{sw} \theta_{sh}} V \right)^* \right)^\top \lambda \tag{C.2.221}$$

$$G^s_{V_a qtm_a}(\lambda) = \frac{\partial}{\partial qtm_a} \left({G^s_{V_a}}^\top \lambda \right) \tag{C.2.222}$$

$$= {G^s_{qtm_a V_a}}^\top (\lambda) \tag{C.2.223}$$

$$G^s_{V_m qtm_a}(\lambda) = \frac{\partial}{\partial qtm_a} \left({G^s_{P_g}}^\top \lambda \right) \tag{C.2.224}$$

$$= {G^s_{qtm_a V_m}}^\top (\lambda) \tag{C.2.225}$$

$$G^s_{P_g qtm_a}(\lambda) = \frac{\partial}{\partial qtm_a} \left({G^s_{P_g}}^\top \lambda \right) = 0 \tag{C.2.226}$$

$$G^s_{Q_g qtm_a}(\lambda) = \frac{\partial}{\partial qtm_a}\left({G^s_{Q_g}}^\top \lambda\right) \tag{C.2.227}$$

$$G^s_{B_{eqz} qtm_a}(\lambda) = \frac{\partial}{\partial qtm_a}\left({G^s_{B_{eqz}}}^\top \lambda\right) \tag{C.2.228}$$

$$= {G^s_{qtm_a B_{eqz}}}^\top(\lambda) \tag{C.2.229}$$

$$G^s_{B_{eqv} qtm_a}(\lambda) = \frac{\partial}{\partial qtm_a}\left({G^s_{B_{eqv}}}^\top \lambda\right) \tag{C.2.230}$$

$$= {G^s_{qtm_a B_{eqv}}}^\top(\lambda) \tag{C.2.231}$$

$$G^s_{\theta_{sh} qtm_a}(\lambda) = \frac{\partial}{\partial qtm_a}\left({G^s_{\theta_{sh}}}^\top \lambda\right) \tag{C.2.232}$$

$$= {G^s_{qtm_a \theta_{sh}}}^\top(\lambda) \tag{C.2.233}$$

$$G^s_{qtm_a qtm_a}(\lambda) = \frac{\partial}{\partial qtm_a}\left({G^s_{qtm_a}}^\top \lambda\right) \tag{C.2.234}$$

$$= \left([V]\left(\frac{\partial^2 Y_{bus}}{\partial^2 qtm_a} V\right)^*\right)^\top \lambda \tag{C.2.235}$$

$$G^s_{vtm_a qtm_a}(\lambda) = \frac{\partial}{\partial qtm_a}\left({G^s_{vtm_a}}^\top \lambda\right) \tag{C.2.236}$$

$$= \left([V]\left(\frac{\partial^2 Y_{bus}}{\partial vtm_a qtm_a} V\right)^*\right)^\top \lambda \tag{C.2.237}$$

$$G^s_{G_{sw} qtm_a}(\lambda) = \frac{\partial}{\partial qtm_a}\left({G^s_{G_{sw}}}^\top \lambda\right) \tag{C.2.238}$$

$$= \left([V]\left(\frac{\partial^2 Y_{bus}}{\partial G_{sw} qtm_a} V\right)^*\right)^\top \lambda \tag{C.2.239}$$

$$G^s_{V_a vtm_a}(\lambda) = \frac{\partial}{\partial vtm_a}\left({G^s_{V_a}}^\top \lambda\right) \tag{C.2.240}$$

$$= {G^s_{vtm_a V_a}}^\top(\lambda) \tag{C.2.241}$$

$$G^s_{V_m vtm_a}(\lambda) = \frac{\partial}{\partial vtm_a}\left({G^s_{P_g}}^\top \lambda\right) \tag{C.2.242}$$

$$= {G^s_{vtm_a V_m}}^\top(\lambda) \tag{C.2.243}$$

$$G^s_{P_g vtm_a}(\lambda) = \frac{\partial}{\partial vtm_a}\left({G^s_{P_g}}^\top \lambda\right) = 0 \tag{C.2.244}$$

$$G^s_{Q_g vtm_a}(\lambda) = \frac{\partial}{\partial vtm_a}\left({G^s_{Q_g}}^\top \lambda\right) \tag{C.2.245}$$

$$G^s_{B_{eqz} vtm_a}(\lambda) = \frac{\partial}{\partial vtm_a}\left({G^s_{B_{eqz}}}^\top \lambda\right) \tag{C.2.246}$$

$$= {G^s_{vtm_a B_{eqz}}}^\top(\lambda) \tag{C.2.247}$$

$$G^s_{B_{eqv} vtm_a}(\lambda) = \frac{\partial}{\partial vtm_a}\left({G^s_{B_{eqv}}}^\top \lambda\right) \tag{C.2.248}$$

$$= {G^s_{vtm_a B_{eqv}}}^\top(\lambda) \tag{C.2.249}$$

$$G^s_{\theta_{sh} vtm_a}(\lambda) = \frac{\partial}{\partial vtm_a}\left({G^s_{\theta_{sh}}}^\top \lambda\right) \tag{C.2.250}$$

$$= {G^s_{vtm_a \theta_{sh}}}^\top(\lambda) \tag{C.2.251}$$

$$G^s_{qtm_a vtm_a}(\lambda) = \frac{\partial}{\partial vtm_a}\left({G^s_{qtm_a}}^\top \lambda\right) \tag{C.2.252}$$

$$= {G^s_{vtm_a qtm_a}}^\top(\lambda) \tag{C.2.253}$$

$$G^s_{vtm_a vtm_a}(\lambda) = \frac{\partial}{\partial vtm_a}\left({G^s_{vtm_a}}^\top \lambda\right) \tag{C.2.254}$$

$$= \left([V]\left(\frac{\partial^2 Y_{bus}}{\partial^2 vtm_a} V\right)^*\right)^\top \lambda \tag{C.2.255}$$

$$G^s_{G_{sw} vtm_a}(\lambda) = \frac{\partial}{\partial vtm_a}\left({G^s_{G_{sw}}}^\top \lambda\right) \tag{C.2.256}$$

$$= \left([V]\left(\frac{\partial^2 Y_{bus}}{\partial G_{sw} \partial vtm_a} V\right)^*\right)^\top \lambda \tag{C.2.257}$$

C.3 Branch Flows

Consider the branch flow constraints for Loadability, Zero Constraint, Active power control and Reactive power Control of equations (C.3.258) to (C.3.262).

Branch Loadability

$$\begin{aligned} |F_f(X)| - F_{max} \leq 0 \\ |F_t(X)| - F_{max} \leq 0 \end{aligned} \tag{C.3.258}$$

where:

$$F_f(X) = \begin{cases} S_f & \text{apparent power} \\ P_f & \text{real power} \\ I_f & \text{current} \end{cases} \tag{C.3.259}$$

Zero Constraint

$$\Im\left(S_f\right) = 0 \tag{C.3.260}$$

Active Power Control

$$\Re\left(S_f\right) - P_{set} = 0 \tag{C.3.261}$$

$$\Im\left(S_f\right) - Q_{set} = 0 \tag{C.3.262}$$

Which are in function of S_f and S_t. Where:

$$\begin{aligned} S_f = C_f[V][Y_f V]^* \\ S_t = C_t[V][Y_t V]^* \end{aligned} \tag{C.3.263}$$

C.3.1 First Derivatives

$$S_X^f = \frac{\partial S^f}{\partial X} = \begin{bmatrix} S_{V_a}^f & S_{V_m}^f & S_{P_g}^f & S_{Q_g}^f & S_{B_{eq}}^f & S_{\theta_{sh}}^f & S_{m_a}^f & S_{G_{sw}}^f \end{bmatrix} \tag{C.3.264}$$

$$S_X^t = \frac{\partial S^t}{\partial X} =$$

$$\begin{bmatrix} S^t_{V_a} & S^t_{V_m} & S^t_{P_g} & S^t_{Q_g} & S^t_{B_{eq}} & S^t_{\theta_{sh}} & S^t_{m_a} & S^t_{G_{sw}} \end{bmatrix} \tag{C.3.265}$$

$$S^f_{V_a} = \frac{\partial S_f}{\partial V_a} = \left[C_f V\right]\left(Y_f \tfrac{\partial V}{\partial V_a}\right)^* + \left[C_f\right]\left[C_f \tfrac{\partial V}{\partial V_a}\right]\left(Y_f V\right)^* \tag{C.3.266}$$

$$S^t_{V_a} = \frac{\partial S_t}{\partial V_a} = \left[C_t V\right]\left(Y_t \tfrac{\partial V}{\partial V_a}\right)^* + \left[C_t\right]\left[C_t \tfrac{\partial V}{\partial V_a}\right]\left(Y_t V\right)^* \tag{C.3.267}$$

$$S^f_{V_m} = \frac{\partial S_f}{\partial V_m} = \left[C_f V\right]\left(Y_f \tfrac{\partial V}{\partial V_m}\right)^* + \left[C_f\right]\left[C_f \tfrac{\partial V}{\partial V_m}\right]\left(Y_f V\right)^* \tag{C.3.268}$$

$$S^t_{V_m} = \frac{\partial S_t}{\partial V_m} = \left[C_t V\right]\left(Y_t \tfrac{\partial V}{\partial V_m}\right)^* + \left[C_t\right]\left[C_t \tfrac{\partial V}{\partial V_m}\right]\left(Y_t V\right)^* \tag{C.3.269}$$

$$S^f_{P_g} = \frac{\partial S_f}{\partial P_g} = 0 \tag{C.3.270}$$

$$S^t_{P_g} = \frac{\partial S_t}{\partial P_g} = 0 \tag{C.3.271}$$

$$S^f_{Q_g} = \frac{\partial S_f}{\partial Q_g} = 0 \tag{C.3.272}$$

$$S^t_{Q_g} = \frac{\partial S_t}{\partial Q_g} = 0 \tag{C.3.273}$$

$$S^f_{B_{eq}} = \frac{\partial S_f}{\partial B_{eq}} = \left[C_f V\right]\left(\tfrac{\partial Y_f}{\partial B_{eq}} V\right)^* \tag{C.3.274}$$

$$S^t_{B_{eq}} = \frac{\partial S_t}{\partial B_{eq}} = \left[C_t V\right]\left(\tfrac{\partial Y_t}{\partial B_{eq}} V\right)^* \tag{C.3.275}$$

$$S^f_{\theta_{sh}} = \frac{\partial S_f}{\partial \theta_{sh}} = \Big[C_f V\Big] \left(\tfrac{\partial Y_f}{\partial \theta_{sh}} V\right)^* \tag{C.3.276}$$

$$S^t_{\theta_{sh}} = \frac{\partial S_t}{\partial \theta_{sh}} = \Big[C_t V\Big] \left(\tfrac{\partial Y_t}{\partial \theta_{sh}} V\right)^* \tag{C.3.277}$$

$$S^f_{m_a} = \frac{\partial S_f}{\partial m_a} = \Big[C_f V\Big] \left(\tfrac{\partial Y_f}{\partial m_a} V\right)^* \tag{C.3.278}$$

$$S^t_{m_a} = \frac{\partial S_t}{\partial m_a} = \Big[C_t V\Big] \left(\tfrac{\partial Y_t}{\partial m_a} V\right)^* \tag{C.3.279}$$

C.3.2 Second Derivatives

$$S^f_{XX}(\mu) = \frac{\partial}{\partial X}\left(S^f_X{}^\top \mu\right) = \tag{C.3.280}$$

$$\begin{bmatrix}
S^f_{V_aV_a}(\mu) & S^f_{V_aV_m}(\mu) & S^f_{V_aB_{eqz}}(\mu) & S^f_{V_aB_{eqv}}(\mu) & S^f_{V_a\theta_{sh}}(\mu) & S^f_{V_aqtm_a}(\mu) & S^f_{V_avtm_a}(\mu) & S^f_{V_aG_{sw}}(\mu) \\
S^f_{V_mV_a}(\mu) & S^f_{V_mV_m}(\mu) & S^f_{V_mB_{eqz}}(\mu) & S^f_{V_mB_{eqv}}(\mu) & S^f_{V_m\theta_{sh}}(\mu) & S^f_{V_mqtm_a}(\mu) & S^f_{V_mvtm_a}(\mu) & S^f_{V_mG_{sw}}(\mu) \\
S^f_{B_{eqz}V_a}(\mu) & S^f_{B_{eqz}V_m}(\mu) & S^f_{B_{eqz}B_{eqz}}(\mu) & S^f_{B_{eqz}B_{eqv}}(\mu) & S^f_{B_{eqz}\theta_{sh}}(\mu) & S^f_{B_{eqz}qtm_a}(\mu) & S^f_{B_{eqz}vtm_a}(\mu) & S^f_{B_{eqz}G_{sw}}(\mu) \\
S^f_{B_{eqv}V_a}(\mu) & S^f_{B_{eqv}V_m}(\mu) & S^f_{B_{eqv}B_{eqz}}(\mu) & S^f_{B_{eqv}B_{eqv}}(\mu) & S^f_{B_{eqv}\theta_{sh}}(\mu) & S^f_{B_{eqv}qtm_a}(\mu) & S^f_{B_{eqv}vtm_a}(\mu) & S^f_{B_{eqv}G_{sw}}(\mu) \\
S^f_{\theta_{sh}V_a}(\mu) & S^f_{\theta_{sh}V_m}(\mu) & S^f_{\theta_{sh}B_{eqz}}(\mu) & S^f_{\theta_{sh}B_{eqv}}(\mu) & S^f_{\theta_{sh}\theta_{sh}}(\mu) & S^f_{\theta_{sh}qtm_a}(\mu) & S^f_{\theta_{sh}vtm_a}(\mu) & S^f_{\theta_{sh}G_{sw}}(\mu) \\
S^f_{qtm_aV_a}(\mu) & S^f_{qtm_aV_m}(\mu) & S^f_{qtm_aB_{eqz}}(\mu) & S^f_{qtm_aB_{eqv}}(\mu) & S^f_{qtm_a\theta_{sh}}(\mu) & S^f_{qtm_aqtm_a}(\mu) & S^f_{qtm_avtm_a}(\mu) & S^f_{qtm_aG_{sw}}(\mu) \\
S^f_{vtm_aV_a}(\mu) & S^f_{vtm_aV_m}(\mu) & S^f_{vtm_aB_{eqz}}(\mu) & S^f_{vtm_aB_{eqv}}(\mu) & S^f_{vtm_a\theta_{sh}}(\mu) & S^f_{vtm_aqtm_a}(\mu) & S^f_{vtm_avtm_a}(\mu) & S^f_{vtm_aG_{sw}}(\mu) \\
S^f_{G_{sw}V_a}(\mu) & S^f_{G_{sw}V_m}(\mu) & S^f_{G_{sw}B_{eqz}}(\mu) & S^f_{G_{sw}B_{eqv}}(\mu) & S^f_{G_{sw}\theta_{sh}}(\mu) & S^f_{G_{sw}qtm_a}(\mu) & S^f_{G_{sw}vtm_a}(\mu) & S^f_{G_{sw}G_{sw}}(\mu)
\end{bmatrix} \tag{C.3.281}$$

$$= \begin{bmatrix}
S^f_{V_aV_a}(\mu) & S^f_{V_aV_m}(\mu) & S^f_{V_aB_{eq}}(\mu) & S^f_{V_a\theta_{sh}}(\mu) & S^f_{V_am_a}(\mu) & S^f_{V_aG_{sw}}(\mu) \\
S^f_{V_mV_a}(\mu) & S^f_{V_mV_m}(\mu) & S^f_{V_mB_{eq}}(\mu) & S^f_{V_m\theta_{sh}}(\mu) & S^f_{V_mm_a}(\mu) & S^f_{V_mG_{sw}}(\mu) \\
S^f_{B_{eq}V_a}(\mu) & S^f_{B_{eq}V_m}(\mu) & S^f_{B_{eq}B_{eq}}(\mu) & S^f_{B_{eq}\theta_{sh}}(\mu) & S^f_{B_{eq}m_a}(\mu) & S^f_{B_{eq}G_{sw}}(\mu) \\
S^f_{\theta_{sh}V_a}(\mu) & S^f_{\theta_{sh}V_m}(\mu) & S^f_{\theta_{sh}B_{eq}}(\mu) & S^f_{\theta_{sh}\theta_{sh}}(\mu) & S^f_{\theta_{sh}m_a}(\mu) & S^f_{\theta_{sh}G_{sw}}(\mu) \\
S^f_{m_aV_a}(\mu) & S^f_{m_aV_m}(\mu) & S^f_{m_aB_{eq}}(\mu) & S^f_{m_a\theta_{sh}}(\mu) & S^f_{m_am_a}(\mu) & S^f_{qtm_aG_{sw}}(\mu) \\
S^f_{G_{sw}V_a}(\mu) & S^f_{G_{sw}V_m}(\mu) & S^f_{G_{sw}B_{eq}}(\mu) & S^f_{G_{sw}\theta_{sh}}(\mu) & S^f_{G_{sw}m_a}(\mu) & S^f_{G_{sw}G_{sw}}(\mu)
\end{bmatrix} \tag{C.3.282}$$

C.3.3 Branch Flows Detailed Hessian

$$S^f_{V_aV_a}(\mu) = \frac{\partial}{\partial V_a}\left(S^f_{V_a}{}^\top \mu\right) \tag{C.3.283}$$

$$\begin{aligned} &= \Big(\left[C_f \tfrac{\partial V}{\partial V_a}\right] \left(Y_f \tfrac{\partial V}{\partial V_a}\right)^* + \left[C_f V\right] \left(Y_f \tfrac{\partial^2 V}{\partial^2 V_a}\right)^* + \\ &\left[C_f\right] \left[C_f \tfrac{\partial V}{\partial V_a}\right] \left(Y_f \tfrac{\partial V}{\partial V_a}\right)^* + \left[C_f\right] \left[C_f \tfrac{\partial^2 V}{\partial^2 V_a}\right] \left(Y_f V\right)^* \Big)^\top \lambda \end{aligned} \tag{C.3.284}$$

$$S^f_{V_mV_a}(\mu) = \frac{\partial}{\partial V_a}\left(S^f_{V_m}{}^\top \mu\right) \tag{C.3.285}$$

$$\begin{aligned} &= \Big(\left[C_f \tfrac{\partial V}{\partial V_a}\right] \left(Y_f \tfrac{\partial V}{\partial V_m}\right)^* + \left[C_f V\right] \left(Y_f \tfrac{\partial^2 V}{\partial V_m \partial V_a}\right)^* + \\ &\left[C_f\right] \left[C_f \tfrac{\partial V}{\partial V_m}\right] \left(Y_f \tfrac{\partial V}{\partial V_a}\right)^* + \left[C_f\right] \left[C_f \tfrac{\partial^2 V}{\partial V_m \partial V_a}\right] \left(Y_f V\right)^* \Big)^\top \mu \end{aligned} \tag{C.3.286}$$

$$S^f_{B_{eqz}V_a}(\mu) = \frac{\partial}{\partial V_a}\left(S^f_{B_{eqz}}{}^\top \mu\right) \tag{C.3.287}$$

$$= \frac{\partial}{\partial V_a}\left(\left[C_f V\right] \left(\tfrac{\partial Y_f}{\partial B_{eqz}} V\right)^{*\top} \mu\right) \tag{C.3.288}$$

$$= \Big(\left[C_f V\right] \left(\tfrac{\partial Y_f}{\partial B_{eqz}} \tfrac{\partial V}{\partial V_a}\right)^* + \left[C_f\right] \left[C_f \tfrac{\partial V}{\partial V_a}\right] \left(\tfrac{\partial Y_f}{\partial B_{eqz}} V\right)^* \Big)^\top (\mu) \tag{C.3.289}$$

$$S^f_{B_{eqv}V_a}(\mu) = \frac{\partial}{\partial V_a}\left(S^f_{B_{eqv}}{}^\top \mu\right) \tag{C.3.290}$$

$$= \frac{\partial}{\partial V_a}\left(\left[C_f V\right] \left(\tfrac{\partial Y_f}{\partial B_{eqv}} V\right)^{*\top} \mu\right) \tag{C.3.291}$$

$$= \Big(\left[C_f V\right] \left(\tfrac{\partial Y_f}{\partial B_{eqv}} \tfrac{\partial V}{\partial V_a}\right)^* + \left[C_f\right] \left[C_f \tfrac{\partial V}{\partial V_a}\right] \left(\tfrac{\partial Y_f}{\partial B_{eqv}} V\right)^* \Big)^\top (\mu) \tag{C.3.292}$$

$$S^f_{\theta_{sh}V_a}(\mu) = \frac{\partial}{\partial V_a}\left(S^f_{\theta_{sh}}{}^\top \mu\right) \tag{C.3.293}$$

$$= \Big(\left[C_f V\right] \left(\tfrac{\partial Y_f}{\partial \theta_{sh}} \tfrac{\partial V}{\partial V_a}\right)^* + \left[C_f\right] \left[C_f \tfrac{\partial V}{\partial V_a}\right] \left(\tfrac{\partial Y_f}{\partial \theta_{sh}} V\right)^* \Big)^\top (\mu) \tag{C.3.294}$$

$$S^f_{qtm_aV_a}(\mu) = \frac{\partial}{\partial V_a}\left(S^f_{qtm_a}{}^\top \mu\right) \tag{C.3.295}$$

$$= \Big(\left[C_f V\right] \left(\tfrac{\partial Y_f}{\partial qtm_a} \tfrac{\partial V}{\partial V_a}\right)^* + \left[C_f\right] \left[C_f \tfrac{\partial V}{\partial V_a}\right] \left(\tfrac{\partial Y_f}{\partial qtm_a} V\right)^* \Big)^\top (\mu) \tag{C.3.296}$$

$$S^f_{vtm_aV_a}(\mu) = \frac{\partial}{\partial V_a}\left(S^f_{vtm_a}{}^\top \mu\right) \tag{C.3.297}$$

$$= \Big(\left[C_f V\right] \left(\tfrac{\partial Y_f}{\partial vtm_a} \tfrac{\partial V}{\partial V_a}\right)^* + \left[C_f\right] \left[C_f \tfrac{\partial V}{\partial V_a}\right] \left(\tfrac{\partial Y_f}{\partial vtm_a} V\right)^* \Big)^\top (\mu) \tag{C.3.298}$$

$$S^f_{G_{sw}V_a}(\mu) = \frac{\partial}{\partial V_a}\left(S^f_{G_{sw}}{}^\top \mu\right) \tag{C.3.299}$$

$$= \left(\left[C_f V\right] \left(\frac{\partial Y_f}{\partial G_{sw}} \frac{\partial V}{\partial V_a}\right)^* + \left[C_f\right] \left[C_f \frac{\partial V}{\partial V_a}\right] \left(\frac{\partial Y_f}{\partial G_{sw}} V\right)^* \right)^\top (\mu) \tag{C.3.300}$$

$$S^f_{V_a V_m}(\mu) = \frac{\partial}{\partial V_m}\left(S^f_{V_a}{}^\top \mu\right) \tag{C.3.301}$$

$$= S^f_{V_a V_m}{}^\top (\mu) \tag{C.3.302}$$

$$S^f_{V_m V_m}(\mu) = \frac{\partial}{\partial V_m}\left(S^f_{V_m}{}^\top \mu\right) \tag{C.3.303}$$

$$\begin{aligned} = \frac{\partial}{\partial V_m}\Big(&\left[C_f \frac{\partial V}{\partial V_m}\right] \left(Y_f \frac{\partial V}{\partial V_m}\right)^* + \left[C_f V\right] \left(Y_f \frac{\partial^2 V}{\partial^2 V_m}\right)^* + \\ &\left[C_f\right] \left[C_f \frac{\partial V}{\partial V_m}\right] \left(Y_f \frac{\partial V}{\partial V_m}\right)^* + \left[C_f\right] \left[C_f \frac{\partial^2 V}{\partial^2 V_m}\right] \left(Y_f V\right)^* \Big)^\top \mu \end{aligned} \tag{C.3.304}$$

$$S^f_{B_{eqz}V_m}(\mu) = \frac{\partial}{\partial V_m}\left(S^f_{B_{eqz}}{}^\top \mu\right) \tag{C.3.305}$$

$$= \left(\left[C_f V\right] \left(\frac{\partial Y_f}{\partial B_{eqz}} \frac{\partial V}{\partial V_m}\right)^* + \left[C_f\right] \left[C_f \frac{\partial V}{\partial V_m}\right] \left(\frac{\partial Y_f}{\partial B_{eqz}} V\right)^* \right)^\top (\mu) \tag{C.3.306}$$

$$S^f_{B_{eqv}V_m}(\mu) = \frac{\partial}{\partial V_m}\left(S^f_{B_{eqv}}{}^\top \mu\right) \tag{C.3.307}$$

$$= \left(\left[C_f V\right] \left(\frac{\partial Y_f}{\partial B_{eqv}} \frac{\partial V}{\partial V_m}\right)^* + \left[C_f\right] \left[C_f \frac{\partial V}{\partial V_m}\right] \left(\frac{\partial Y_f}{\partial B_{eqv}} V\right)^* \right)^\top (\mu) \tag{C.3.308}$$

$$S^f_{\theta_{sh}V_m}(\mu) = \frac{\partial}{\partial V_m}\left(S^f_{\theta_{sh}}{}^\top \mu\right) \tag{C.3.309}$$

$$= \left(\left[C_f V\right] \left(\frac{\partial Y_f}{\partial \theta_{sh}} \frac{\partial V}{\partial V_m}\right)^* + \left[C_f\right] \left[C_f \frac{\partial V}{\partial V_m}\right] \left(\frac{\partial Y_f}{\partial \theta_{sh}} V\right)^* \right)^\top (\mu) \tag{C.3.310}$$

$$S^f_{qtm_a V_m}(\mu) = \frac{\partial}{\partial V_m}\left(S^f_{qtm_a}{}^\top \mu\right) \tag{C.3.311}$$

$$= \left(\left[C_f V\right] \left(\frac{\partial Y_f}{\partial qtm_a} \frac{\partial V}{\partial V_m}\right)^* + \left[C_f\right] \left[C_f \frac{\partial V}{\partial V_m}\right] \right)^\top (\mu) \left(\frac{\partial Y_f}{\partial qtm_a} V\right)^* \tag{C.3.312}$$

$$S^f_{vtm_a V_m}(\mu) = \frac{\partial}{\partial V_m}\left(S^f_{vtm_a}{}^\top \mu\right) \tag{C.3.313}$$

$$= \left(\left[C_f V\right] \left(\frac{\partial Y_f}{\partial vtm_a} \frac{\partial V}{\partial V_m}\right)^* + \left[C_f\right] \left[C_f \frac{\partial V}{\partial V_m}\right] \left(\frac{\partial Y_f}{\partial vtm_a} V\right)^* \right)^\top (\mu) \tag{C.3.314}$$

$$S^f_{G_{sw}V_m}(\mu) = \frac{\partial}{\partial V_m}\left(S^f_{G_{sw}}{}^\top \mu\right) \tag{C.3.315}$$

$$= \left(\left[C_f V\right]\left(\frac{\partial Y_f}{\partial G_{sw}}\frac{\partial V}{\partial V_m}\right)^* + \left[C_f\right]\left[C_f \frac{\partial V}{\partial V_m}\right]\left(\frac{\partial Y_f}{\partial G_{sw}}V\right)^*\right)^\top(\mu) \tag{C.3.316}$$

$$S^f_{V_a B_{eqz}}(\mu) = \frac{\partial}{\partial B_{eqz}}\left(S^f_{V_a}{}^\top \mu\right) \tag{C.3.317}$$

$$= S^f_{B_{eqz}V_a}{}^\top(\mu) \tag{C.3.318}$$

$$S^f_{V_m B_{eqz}}(\mu) = \frac{\partial}{\partial B_{eqz}}\left(S^f_{P_g}{}^\top \mu\right) \tag{C.3.319}$$

$$= S^f_{B_{eqz}V_m}{}^\top(\mu) \tag{C.3.320}$$

$$S^f_{B_{eqz}B_{eqz}}(\mu) = \frac{\partial}{\partial B_{eqz}}\left(S^f_{B_{eqz}}{}^\top \mu\right) \tag{C.3.321}$$

$$= \left(\left[C_f V\right]\left(\frac{\partial^2 Y_f}{\partial^2 B_{eqz}}V\right)^*\right)^\top(\mu) \tag{C.3.322}$$

$$S^f_{B_{eqv}B_{eqz}}(\mu) = \frac{\partial}{\partial B_{eqz}}\left(S^f_{B_{eqv}}{}^\top \mu\right) \tag{C.3.323}$$

$$= \left(\left[C_f V\right]\left(\frac{\partial^2 Y_f}{\partial B_{eqv}\partial B_{eqz}}V\right)^*\right)^\top(\mu) \tag{C.3.324}$$

$$S^f_{\theta_{sh}B_{eqz}}(\mu) = \frac{\partial}{\partial B_{eqz}}\left(S^f_{\theta_{sh}}{}^\top \mu\right) \tag{C.3.325}$$

$$= \left(\left[C_f V\right]\left(\frac{\partial^2 Y_f}{\partial \theta_{sh}\partial B_{eqz}}V\right)^*\right)^\top(\mu) \tag{C.3.326}$$

$$S^f_{qtm_a B_{eqz}}(\mu) = \frac{\partial}{\partial B_{eqz}}\left(S^f_{qtm_a}{}^\top \mu\right) \tag{C.3.327}$$

$$= \left(\left[C_f V\right]\left(\frac{\partial^2 Y_f}{\partial qtm_a \partial B_{eqz}}V\right)^*\right)^\top(\mu) \tag{C.3.328}$$

$$S^f_{vtm_a B_{eqz}}(\mu) = \frac{\partial}{\partial B_{eqz}}\left(S^f_{vtm_a}{}^\top \mu\right) \tag{C.3.329}$$

$$= \left(\left[C_f V\right]\left(\frac{\partial^2 Y_f}{\partial vtm_a \partial B_{eqz}}V\right)^*\right)^\top(\mu) \tag{C.3.330}$$

$$S^f_{G_{sw}B_{eqz}}(\mu) = \frac{\partial}{\partial B_{eqz}}\left(S^f_{G_{sw}}{}^\top \mu\right) \tag{C.3.331}$$

$$= \left(\left[C_f V\right]\left(\frac{\partial^2 Y_f}{\partial G_{sw}\partial B_{eqz}} V\right)^*\right)^\top (\mu) \tag{C.3.332}$$

$$S^f_{V_a B_{eqv}}(\mu) = \frac{\partial}{\partial B_{eqv}}\left(S^f_{V_a}{}^\top \mu\right) \tag{C.3.333}$$

$$= S^f_{B_{eqv}V_a}{}^\top (\mu) \tag{C.3.334}$$

$$S^f_{V_m B_{eqv}}(\mu) = \frac{\partial}{\partial B_{eqv}}\left(S^f_{P_g}{}^\top \mu\right) \tag{C.3.335}$$

$$= S^f_{B_{eqv}V_m}{}^\top (\mu) \tag{C.3.336}$$

$$S^f_{B_{eqz}B_{eqv}}(\mu) = \frac{\partial}{\partial B_{eqv}}\left(S^f_{B_{eqz}}{}^\top \mu\right) \tag{C.3.337}$$

$$= S^f_{B_{eqv}B_{eqz}}{}^\top (\mu) \tag{C.3.338}$$

$$S^f_{B_{eqv}B_{eqv}}(\mu) = \frac{\partial}{\partial B_{eqv}}\left(S^f_{B_{eqv}}{}^\top \mu\right) \tag{C.3.339}$$

$$= \left(\left[C_f V\right]\left(\frac{\partial^2 Y_f}{\partial^2 B_{eqv}} V\right)^*\right)^\top (\mu) \tag{C.3.340}$$

$$S^f_{\theta_{sh}B_{eqv}}(\mu) = \frac{\partial}{\partial B_{eqv}}\left(S^f_{\theta_{sh}}{}^\top \mu\right) \tag{C.3.341}$$

$$= \left(\left[C_f V\right]\left(\frac{\partial^2 Y_f}{\theta_{sh}\partial B_{eqv}} V\right)^*\right)^\top (\mu) \tag{C.3.342}$$

$$S^f_{qtm_a B_{eqv}}(\mu) = \frac{\partial}{\partial B_{eqv}}\left(S^f_{qtm_a}{}^\top \mu\right) \tag{C.3.343}$$

$$= \left(\left[C_f V\right]\left(\frac{\partial^2 Y_f}{qtm_a \partial B_{eqv}} V\right)^*\right)^\top (\mu) \tag{C.3.344}$$

$$S^f_{vtm_a B_{eqv}}(\mu) = \frac{\partial}{\partial B_{eqv}}\left(S^f_{vtm_a}{}^\top \mu\right) \tag{C.3.345}$$

$$= \left(\left[C_f V\right]\left(\frac{\partial^2 Y_f}{vtm_a \partial B_{eqv}} V\right)^*\right)^\top (\mu) \tag{C.3.346}$$

$$S^f_{G_{sw}B_{eqv}}(\mu) = \frac{\partial}{\partial B_{eqv}}\left(S^f_{G_{sw}}{}^\top \mu\right) \tag{C.3.347}$$

$$= \left(\left[C_f V\right]\left(\frac{\partial^2 Y_f}{G_{sw}\partial B_{eqv}} V\right)^*\right)^\top (\mu) \tag{C.3.348}$$

$$S^f_{V_a\theta_{sh}}(\mu) = \frac{\partial}{\partial \theta_{sh}}\left(S^f_{V_a}{}^\top \mu\right) \tag{C.3.349}$$

$$= S^f_{\theta_{sh}V_a}{}^\top (\mu) \tag{C.3.350}$$

$$S^f_{V_m\theta_{sh}}(\mu) = \frac{\partial}{\partial \theta_{sh}}\left(S^f_{P_g}{}^\top \mu\right) \tag{C.3.351}$$

$$= S^f_{\theta_{sh}V_m}{}^\top (\mu) \tag{C.3.352}$$

$$S^f_{B_{eqz}\theta_{sh}}(\mu) = \frac{\partial}{\partial \theta_{sh}}\left(S^f_{B_{eqz}}{}^\top \mu\right) \tag{C.3.353}$$

$$= S^f_{\theta_{sh}B_{eqz}}{}^\top (\mu) \tag{C.3.354}$$

$$S^f_{B_{eqv}\theta_{sh}}(\mu) = \frac{\partial}{\partial \theta_{sh}}\left(S^f_{B_{eqv}}{}^\top \mu\right) \tag{C.3.355}$$

$$= S^f_{\theta_{sh}B_{eqv}}{}^\top (\mu) \tag{C.3.356}$$

$$S^f_{\theta_{sh}\theta_{sh}}(\mu) = \frac{\partial}{\partial \theta_{sh}}\left(S^f_{\theta_{sh}}{}^\top \mu\right) \tag{C.3.357}$$

$$= \left(\left[C_f V\right]\left(\frac{\partial^2 Y_f}{\partial^2 \theta_{sh}} V\right)^*\right)^\top (\mu) \tag{C.3.358}$$

$$S^f_{qtm_a\theta_{sh}}(\mu) = \frac{\partial}{\partial \theta_{sh}}\left(S^f_{qtm_a}{}^\top \mu\right) \tag{C.3.359}$$

$$= \left(\left[C_f V\right]\left(\frac{\partial^2 Y_f}{\partial qtm_a\theta_{sh}} V\right)^*\right)^\top (\mu) \tag{C.3.360}$$

$$S^f_{vtm_a\theta_{sh}}(\mu) = \frac{\partial}{\partial \theta_{sh}}\left(S^f_{vtm_a}{}^\top \mu\right) \tag{C.3.361}$$

$$= \left(\left[C_f V\right]\left(\frac{\partial^2 Y_f}{\partial vtm_a\theta_{sh}} V\right)^*\right)^\top (\mu) \tag{C.3.362}$$

$$S^f_{G_{sw}\theta_{sh}}(\mu) = \frac{\partial}{\partial \theta_{sh}} \left({S^f_{G_{sw}}}^\top \mu \right) \tag{C.3.363}$$

$$= \left(\left[C_f V \right] \left(\tfrac{\partial^2 Y_f}{\partial G_{sw} \theta_{sh}} V \right)^* \right)^\top (\mu) \tag{C.3.364}$$

$$S^f_{V_a qtm_a}(\mu) = \frac{\partial}{\partial qtm_a} \left({S^f_{V_a}}^\top \mu \right) \tag{C.3.365}$$

$$= {S^f_{qtm_a V_a}}^\top (\mu) \tag{C.3.366}$$

$$S^f_{V_m qtm_a}(\mu) = \frac{\partial}{\partial qtm_a} \left({S^f_{P_g}}^\top \mu \right) \tag{C.3.367}$$

$$= {S^f_{qtm_a V_m}}^\top (\mu) \tag{C.3.368}$$

$$S^f_{B_{eqz} qtm_a}(\mu) = \frac{\partial}{\partial qtm_a} \left({S^f_{B_{eqz}}}^\top \mu \right) \tag{C.3.369}$$

$$= {S^f_{qtm_a B_{eqz}}}^\top (\mu) \tag{C.3.370}$$

$$S^f_{B_{eqv} qtm_a}(\mu) = \frac{\partial}{\partial qtm_a} \left({S^f_{B_{eqv}}}^\top \mu \right) \tag{C.3.371}$$

$$= {S^f_{qtm_a B_{eqv}}}^\top (\mu) \tag{C.3.372}$$

$$S^f_{\theta_{sh} qtm_a}(\mu) = \frac{\partial}{\partial qtm_a} \left({S^f_{\theta_{sh}}}^\top \mu \right) \tag{C.3.373}$$

$$= {S^f_{qtm_a \theta_{sh}}}^\top (\mu) \tag{C.3.374}$$

$$S^f_{qtm_a qtm_a}(\mu) = \frac{\partial}{\partial qtm_a} \left({S^f_{qtm_a}}^\top \mu \right) \tag{C.3.375}$$

$$= \left(\left[C_f V \right] \left(\tfrac{\partial^2 Y_f}{\partial^2 qtm_a} V \right)^* \right)^\top (\mu) \tag{C.3.376}$$

$$S^f_{vtm_a qtm_a}(\mu) = \frac{\partial}{\partial qtm_a} \left({S^f_{vtm_a}}^\top \mu \right) \tag{C.3.377}$$

$$= \left(\left[C_f V \right] \left(\tfrac{\partial^2 Y_f}{\partial vtm_a \partial qtm_a} V \right)^* \right)^\top (\mu) \tag{C.3.378}$$

$$S^f_{G_{sw}qtm_a}(\mu) = \frac{\partial}{\partial qtm_a}\left(S^f_{G_{sw}}{}^\top \mu\right) \tag{C.3.379}$$

$$= \left(\left[C_f V\right]\left(\tfrac{\partial^2 Y_f}{\partial G_{sw}\partial qtm_a} V\right)^*\right)^\top(\mu) \tag{C.3.380}$$

$$S^f_{V_a vtm_a}(\mu) = \frac{\partial}{\partial vtm_a}\left(S^f_{V_a}{}^\top \mu\right) \tag{C.3.381}$$

$$= S^f_{vtm_a V_a}{}^\top(\mu) \tag{C.3.382}$$

$$S^f_{V_m vtm_a}(\mu) = \frac{\partial}{\partial vtm_a}\left(S^f_{P_g}{}^\top \mu\right) \tag{C.3.383}$$

$$= S^f_{vtm_a V_m}{}^\top(\mu) \tag{C.3.384}$$

$$S^f_{B_{eqz}vtm_a}(\mu) = \frac{\partial}{\partial vtm_a}\left(S^f_{B_{eqz}}{}^\top \mu\right) \tag{C.3.385}$$

$$= S^f_{vtm_a B_{eqz}}{}^\top(\mu) \tag{C.3.386}$$

$$S^f_{B_{eqv}vtm_a}(\mu) = \frac{\partial}{\partial vtm_a}\left(S^f_{B_{eqv}}{}^\top \mu\right) \tag{C.3.387}$$

$$= S^f_{vtm_a B_{eqv}}{}^\top(\mu) \tag{C.3.388}$$

$$S^f_{\theta_{sh}vtm_a}(\mu) = \frac{\partial}{\partial vtm_a}\left(S^f_{\theta_{sh}}{}^\top \mu\right) \tag{C.3.389}$$

$$= S^f_{vtm_a \theta_{sh}}{}^\top(\mu) \tag{C.3.390}$$

$$S^f_{qtm_a vtm_a}(\mu) = \frac{\partial}{\partial vtm_a}\left(S^f_{qtm_a}{}^\top \mu\right) \tag{C.3.391}$$

$$= S^f_{vtm_a qtm_a}{}^\top(\mu) \tag{C.3.392}$$

$$S^f_{vtm_a vtm_a}(\mu) = \frac{\partial}{\partial vtm_a}\left(S^f_{vtm_a}{}^\top \mu\right) \tag{C.3.393}$$

$$= \left(\left[C_f V\right]\left(\tfrac{\partial^2 Y_f}{\partial^2 vtm_a} V\right)^*\right)^\top(\mu) \tag{C.3.394}$$

$$S^f_{G_{sw}vtm_a}(\mu) = \frac{\partial}{\partial vtm_a}\left(S^f_{G_{sw}}{}^\top \mu\right) \tag{C.3.395}$$

$$= \left(\left[C_f V \right] \left(\frac{\partial^2 Y_f}{\partial G_{sw} \partial v t m_a} V \right)^* \right)^\top (\mu) \tag{C.3.396}$$

$$S^f_{V_a G_{sw}}(\mu) = \frac{\partial}{\partial G_{sw}} \left({S^f_{V_a}}^\top \mu \right) \tag{C.3.397}$$

$$= {S^f_{G_{sw} V_a}}^\top (\mu) \tag{C.3.398}$$

$$S^f_{V_m G_{sw}}(\mu) = \frac{\partial}{\partial G_{sw}} \left({S^f_{P_g}}^\top \mu \right) \tag{C.3.399}$$

$$= {S^f_{G_{sw} V_m}}^\top (\mu) \tag{C.3.400}$$

$$S^f_{B_{eqz} G_{sw}}(\mu) = \frac{\partial}{\partial G_{sw}} \left({S^f_{B_{eqz}}}^\top \mu \right) \tag{C.3.401}$$

$$= {S^f_{G_{sw} B_{eqz}}}^\top (\mu) \tag{C.3.402}$$

$$S^f_{B_{eqv} G_{sw}}(\mu) = \frac{\partial}{\partial G_{sw}} \left({S^f_{B_{eqv}}}^\top \mu \right) \tag{C.3.403}$$

$$= {S^f_{G_{sw} B_{eqv}}}^\top (\mu) \tag{C.3.404}$$

$$S^f_{\theta_{sh} G_{sw}}(\mu) = \frac{\partial}{\partial G_{sw}} \left({S^f_{\theta_{sh}}}^\top \mu \right) \tag{C.3.405}$$

$$= {S^f_{G_{sw} \theta_{sh}}}^\top (\mu) \tag{C.3.406}$$

$$S^f_{q t m_a G_{sw}}(\mu) = \frac{\partial}{\partial G_{sw}} \left({S^f_{q t m_a}}^\top \mu \right) \tag{C.3.407}$$

$$= {S^f_{v t m_a G_{sw}}}^\top (\mu) \tag{C.3.408}$$

$$S^f_{v t m_a G_{sw}}(\mu) = \frac{\partial}{\partial G_{sw}} \left({S^f_{v t m_a}}^\top \mu \right) \tag{C.3.409}$$

$$= \left(\left[C_f V \right] \left(\frac{\partial^2 Y_f}{\partial v t m_a \partial G_{sw}} V \right)^* \right)^\top (\mu) \tag{C.3.410}$$

$$S^f_{G_{sw} G_{sw}}(\mu) = \frac{\partial}{\partial G_{sw}} \left({S^f_{G_{sw}}}^\top \mu \right) \tag{C.3.411}$$

$$= \left(\left[C_f V \right] \left(\frac{\partial^2 Y_f}{\partial^2 G_{sw}} V \right)^* \right)^\top (\mu) \tag{C.3.412}$$